NASA Contractor Report 3053

Aerodynamic Characteristics of Forebody and Nose Strakes Based on F-16 Wind Tunnel Test Experience

Volume I: Summary and Analysis

C. W. Smith, J. N. Ralston, and H. W. Mann

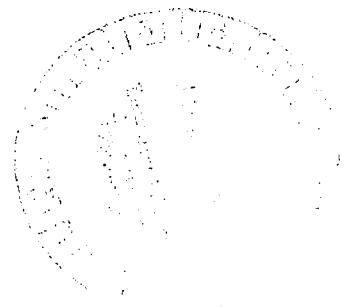NASA

NASA Contractor Report 3053

Aerodynamic Characteristics of Forebody and Nose Strakes Based on F-16 Wind Tunnel Test Experience

Volume I: Summary and Analysis

C. W. Smith, J. N. Ralston, and H. W. Mann
General Dynamics
Fort Worth, Texas

TABLE OF CONTENTS

LIST OF SYMBOLS, (Continued)

S_w	Wing theoretical planform area	$m^2 (ft^2)$
TEF	Trailing-edge-flap deflection angle	deg
WL	Water line of the full-scale airplane	cm (in.)
α	Angle of attack of the wing chord plane	deg
α_{break}	Angle of attack separating linear and non-linear lift curve regions	deg
β	Angle of sideslip or Prandtl-Glanert parameter, $\sqrt{1-M^2}$	deg, --
η_B	Non-dimensional span station separating inboard and outboard panels (See Figure 34)	--
$\Lambda_{c/4}$	Quarter-chord sweep angle	deg
Λ_{LE}	Wing leading-edge sweep angle	deg
Λ_{LE_i}	Strake leading-edge sweep angle	deg
Λ_{TE}	Wing trailing-edge sweep angle	
λ	Taper ratio of the theoretical wing planform	--

1. SUMMARY

The YF-16 and F-16 developmental wind tunnel test pro-
gram has been reviewed and all force data pertinent to the
design of forebody and nose strakes extracted. Volume I of
this study is reported herein and contains geometrical de-
scriptions, general comments, representative data, and the
initial efforts towards the development of design guides for
the application of strakes to future aircraft. Volume II of
this study contains a complete set of these data without
analysis and is reported in NASA CR-158922.

Longitudinal and lateral/directional data are presented
for low-speed and transonic Mach numbers for families of nose
and forebody strakes on several configurations that reflect
different stages in the F-16 development. Included are
simple wing-body configurations and highly blended wing-body-
strake configurations. All have 40-degree-leading-edge-sweep
wings with a nominal aspect ratio of 3.0.

It is concluded that the generation of incremental strake
lift is primarily dependent upon the area affected by the
strake vortex and that strake planform is of secondary impor-
tance below the angle of attack for which vortex breakdown
effects become significant. Forebody strakes can have bene-
ficial effects on lateral/directional stability if properly
designed. Nose strakes provide significant gains when added
to the forebody configurations of this study.

2. INTRODUCTION

Possibly the most distinguishing characteristic of the latest generation of fighter aircraft, the F-16 and F-18, is the utilization of forebody and nose strakes to provide significant increases in usable maneuver lift. These designs are the culmination of long and expensive design evolutions, which relied extensively on wind tunnel testing. This approach was required because no reliable aerodynamic prediction methods are available that address the highly complex flow field present at the moderate-to-high angles of attack under consideration. As a consequence, an extensive body of experimental aerodynamic data exists.

In particular, during the course of configuration development of the YF-16 Lightweight Fighter Prototype and the F-16 Air Combat fighter, General Dynamics wind-tunnel-tested many strake variations at subsonic and/or transonic speeds. Strake effects noted in these data can be generalized in the sense that both conventional and highly blended configurations were investigated early in the YF-16 development program. The effects of variations in strake size, strake planform, strake location relative to the nose, strake span relative to the span of the wing, and leading-edge-flap deflection received considerable interest. Additionally, several different types of strakes were investigated. These consisted of strakes that extended from the forebody to the wing leading edge (forebody strakes), strakes that started at the nose and extended only a short way back on the forebody (nose strakes), and relatively short strakes that were placed aft of the nose but did not extend to the wing leading edge (canard strakes).

The primary benefit attributed to the forebody strakes is a significant increase in usable lift at transonic speeds compared to a conventional wing configuration. During the development programs, General Dynamics found that significant interactions occur between the vortex flows generated by strakes, the wing and the empennage flow fields, and that the interactions can be favorable or unfavorable. While it is relatively simple to achieve a high maneuvering lift capability with forebody strakes, it is necessary to tailor the strake-wing-empennage combination to enhance the moderate-to-high-angle-of-attack lateral/directional stability characteristics and thus make the additional lift usable. Another major fact encountered in the development programs is that some strake-wing configurations result in a deep-stall

2

situation at angles of attack in the range from 35 to 60 degrees; therefore, it is also necessary to evaluate low-speed pitch-control effectiveness in this angle of attack range.

Forebody nose shape plays an important role in the high-angle-of-attack lateral/directional stability characteristics. The effects of nose shape can be minimized by employing nose strakes but, again, it is necessary to limit the nose-strake size to prevent adverse effects in pitch at high angles of attack.

The objective of this investigation is to conduct a detailed review of all of the YF-16 and F-16 developmental wind tunnel data, select the data pertinent to strake design, and present them in a useful form complete with detailed geometric data. Initial efforts have been conducted herein to coalesce the experimental aerodynamic characteristics of strakes into a set of generalized design guidelines for the application of forebody and nose strakes to future aircraft. Of particular interest are the geometric parameters that have the most significant effects on (1) the prevention of low-speed deep stall, (2) the development of lift capability at transonic speeds, and (3) the establishment of the limits on the usable angle of attack at transonic speeds that preserve satisfactory longitudinal and lateral/directional stability characteristics. The complete data base may be found in NASA CR-158922.

Northrop Corporation has been funded by the Air Force Flight Dynamics Lab to conduct a similar study dealing with the strake data obtained during the F-5 and YF-17 developments. The results of this work are published in AFFDL TR 78-94.

3. THE WIND TUNNEL
TEST PROGRAM

The YF-16 and F-16 aircraft are products of an extensive wind tunnel test developmental program. It was during the YF-16 test program that the many design features of the F-16 evolved. The resultant configuration is an integrated design incorporating:

o   Forebody strakes for controlled vortex flow

o   Automatically actuated leading-edge flaps

o   Relaxed static stability

o   Blended wing-body cross-section shape

o   Single engine fed by a simple underslung inlet

o   Single vertical tail

o   High-visibility canopy

The design evolution is discussed here to lay the groundwork for understanding the strake development and the impact of comparing strake effects from the multitude of configurations studied. Detailed descriptions of the strake geometry and summaries of the available wind tunnel test conditions pertinent to the evaluation of strake performance are also presented.

3.1 THE EVOLUTION OF FOREBODY STRAKES
ON THE F-16

A study of the YF-16 aerodynamic features began in 1968. After intensified analysis in 1970-71 and wind tunnel tests in 1971-72, detailed designs were finalized in 1972-73. Configuration refinement and growth modifications continued through wind-tunnel testing until the Full-Scale Development (FSD) aircraft, F-16A and F-16B, were finalized in 1975.

Early design studies set the basic features of two very different design approaches. One was a simple wing-body-empennage design with a single vertical tail (Configuration 785, shown in Figure 1). Later in the program this design

4

was also tested with a twin-tail arrangement (Configuration 786, Figure 2). The other approach was a highly blended wing-body with a wide lifting forebody and twin tails mounted on booms extending aft on either side of the engine exhaust nozzle. This design is known as Configuration 401F, an early version of which is shown in Figure 3 (Configuration 401F-2).

The best features of the two separate initial models were combined into one model and the resulting configuration refined through several tunnel entries to produce the final YF-16 design. Significant intermediate steps included the combination of the Configuration 785 afterbody with the Configuration 401F-2 forebody to obtain Configuration 401F-5, Figure 4, and the addition of afterbody shelves to which the horizontal tails were mated, Configuration 401F-10A, Figure 5. Minor modifications continued through Configuration 401F-16F, which is similar to the YF-16 prototype lines.

The aerodynamic design concept of obtaining high-lift coefficients at transonic speeds by the use of wide forebody shapes has been an integral feature of most General Dynamics fighter designs since before the FX (F-15) competition. The concept was initially wind-tunnel-tested in 1966. Sharp, narrow forebody strakes were also investigated briefly at that time; however, it was then considered an advantage to produce the lift with a blunt leading edge in order to maintain attached flow and greater leading-edge suction for lower drag.

The 401F-0 configuration was developed under that concept, and to accommodate the underslung single inlet, the forebody cross section was made elliptical (flattened on the lower surface), which blended into an upright triangular shape having rounded corners and finally blended into the wing. Available NASA test data on effects of body cross section on lift indicated that significant lift could be expected from the forebody. The first transonic test of the configuration verified these expectations.

However, the directional stability characteristics of the wing-vertical-tailed 401F-0 configuration exhibited a severe loss of directional stability at moderate-to-high angles of attack. In addition, the subsonic drag polar "breaks" occurred at lower lift coefficients than expected. Analysis of oil-flow-visualization photographs and force and moment test results utilizing FX and other research models (Reference 1) showed that forebody flow separations and the

interaction of the resulting vortices with the wing and vertical tail flow fields were major causes of the stability problem.

At this point, NASA/Langley Research Center aerodynamicists were consulted. They suggested that the lift of the wide forebody could be increased by sharpening the leading edge to strengthen the vortices rather than weaken them as our earlier attempts had done. The point was that forebody separation is inevitable at very high angle of attack; therefore, the lift advantages offered by sharp leading edges should be exploited. This also would allow the forebody vortices to dominate and stabilize the high-angle-of-attack flow field over the entire aircraft, even improving the flow over the outboard wing panels.

Two series of parametric forebody strake tests were initiated. A series of delta planform strakes were designed for testing on the conventional forebody aircraft Configurations 785 (single vertical tail) and 786 (twin vertical tail). The second series had curved planforms (gothic and ogee) and were designed for testing on the blended configuration, 401F-5. These two parametric transonic tests provided the basic data for all the other evolutionary forebody strake tests, which continued throughout the YF-16 and F-16 development as various design changes required re-evaluation of the strake effectiveness.

3.2 GEOMETRIC DESCRIPTIONS

All data presented herein were obtained with a 40-degree-leading-edge-sweep wing with a nominal aspect ratio of 3.0. The basic 26-square meter (280-square foot) wings, W3 and W3BB, were used on all of the YF-16 developmental configurations except Configurations 785 and 786, which used a 26-square -meter wing of different planform, W6. Later, F-16 versions utilized wings of 27.6 sq. m (297 sq. ft), W24, and 27.9 sq. m (300 sq. ft), W25. Each of these planforms is sketched in Figure 6.

A listing of all of the strakes and the configurations upon which they were tested is provided in Table 1. Also included are pertinent geometrical parameters, which consist of strake length, maximum width, exposed area and position on the forebody. Figures that provide sketches of the strakes on the appropriate forebodies are referenced in the table. After the initial strake tests on Configurations 785, 786, and 401F-2 through 401F-5, it became apparent that a forebody

6

strake would be part of the final configuration. As a consequence, forebody strake-off configurations were no longer tested. The subsequent configurations have variations in strake size, shape, and location but do not have definable strake geometry for the purpose of determining an explicit strake width and exposed area for Table 1.

Figures 7 to 20 present sketches of the strakes on the appropriate forebodies. Figure 7 shows the delta planform family, Z7-Z10, which was tested on the simple wing-body configurations, 785 and 786. Several canard-type strakes were tested early in the program on Configurations 401F-2 (Figure 8), 401F-4 (Figure 9), 401F-5 (Figure 10), and 401F-10A (Figure 11a). Also, a gothic planform, Z5, was tested on Configuration 401F-4 (Figure 9), and several ogee planforms in addition to a delta and gothic strake were tested on Configuration 401F-5 (Figure 10). Slotted strakes, Z22A and Z23, were also tested on Configuration 401F-5, as shown in Figure 10.

Later tests investigated small changes to blended strakes, generally ogee in shape (Figure 11b to 14). Low-speed tests were also conducted with a variety of small rotating (variable incidence) strakes that formed a piece of a basic ogee strake, Z33 (Figure 15). Larger sections of ogee planform strakes were also rotated, as shown in Figure 16. Nose strakes and additional canard strakes were also tested on the basic YF-16 configuration (Figure 17).

Initial designs for the trainer (two-place) version of the F-16 included fuselage stretches of 77.5 cm (30.5 in) and 113 cm (44.5 in). Numerous forebody strakes with ogee planforms of various width and length plus a few nose and canard strakes were tested on these configurations (Figure 18).

The FSD aircraft has two major modifications from the YF-16: a 25.4 cm (10 in) fuselage stretch and an increased wing area from 26 to 27.9 sq. m (280 to 300 sq. ft). Forebody-strake variations for this configuration are shown in Figure 19. Numerous nose strakes were also investigated as shown in Figure 20.

Several strake families have been selected for analysis purposes because they provide significant variations in strake geometry on the same basic configuration. Forebody-strake families that receive primary analysis are those of

7

Figure 7 (Z7-Z10, Configuration 785), Figure 10 (Z4, Z5, Z14-Z18, Configuration 401F-5), Figure 11b (Z24-Z27, Configuration 401F-10A), and Figure 18a (Z63-Z72, stretched YF-16). Nose-strake families of primary interest were tested on the F-16 FSD configuration and are shown in Figure 20 (Z110-Z117, Z123-Z128, Z131).

Several nose shapes were tested at low speed in conjunction with the nose strakes. Sketches of these noses are provided in Figure 21.

3.3 SCOPE OF STRAKE TESTING

A list of all of the YF-16 and F-16 force tests is provided in Table 2. These tests encompass the entire developmental program from the early configuration testing in 1971 to the recent FSD testing in 1977. Each of these tests has been surveyed for data applicable to strake design, resulting in the selection of the tests shown in Table 3. A complete set of the resultant data for the tests of Table 3 are provided in plotted form in Volume II of this study (NASA CR-158922). Test parameters for each strake configuration are summarized in Table 4. Figure numbers in Volume II for data for each strake configuration are also provided in Table 4. Selected data are shown in this volume.

During the initial development program, emphasis was placed on the aerodynamic and stability characteristics at specific transonic Mach numbers (.80 and 1.20). Later testing included additional Mach numbers for selected configurations. Very little low-speed testing was accomplished until the configuration had evolved to basically that of the YF-16 (Configuration 401F-16). Much of the low-speed effort was associated with the evolution of the two-place aircraft during the Air Combat Fighter (ACF) competition and, therefore, includes effects of stretching and modifying the forebody shapes. The nose strake testing also occurred at the time of the ACF competition and later during the FSD program.

All of the low-speed testing was conducted at a Reynolds number of 1.4 million per foot. The transonic tests were conducted with a Reynolds number range of 2 to 3 million per foot. Reynolds number effects on high-angle-of-attack aerodynamics may be significant; however, investigation of the effect of Reynolds number on the strake characteristics is beyond the scope of this document.

4. ANALYSIS AND DESIGN GUIDELINE DEVELOPMENT

This study makes the strake wind tunnel test data obtained during the F-16 development available for general use. This is accomplished through the geometrical descriptions of Section 3 and the complete set of plotted data provided in NASA CR-158922. Since a large amount of data was obtained during a development program containing numerous configuration changes, assimilation of the data is not a simple task. The intent of this section is to concisely extract and present the trends observed from the data, using representative data to illustrate and substantiate the conclusions. Where possible, initial steps have been taken to form general design guides. All deducements from the data must be tempered by the fact that high-angle-of-attack aerodynamics, and particularly lateral/directional stability characteristics, are strongly dependent upon the complete wing-body-empennage configuration. Assessments of the degree of general applicability of the conclusions reached, e.g., to configurations dissimilar to the F-16, have been attempted throughout the section.

4.1 LIFT AND DRAG

It is well-known that the addition of forebody strakes significantly increases the high-angle-of-attack lift and decreases the high-angle-of-attack drag of low- to medium-sweep wings. General observations as to the character and extent of these effects with respect to the strake geometry are presented in this subsection. The discussions are primarily concerned with strake effects on lift at moderate-to-high angles of attack. However, drag effects exhibit the same trends and will be shown to be a function of $C_L \tan \alpha$ as would be expected. A brief evaluation of an empirical prediction method for high-angle-of-attack lift has been made and the method found to be inadequate for strake configurations. This leads to empirical correlations of the strake lift and drag increments with the intent of producing design guides relating the aerodynamic effects to strake geometry. Results of these correlations are also discussed in this subsection.

4.1.1 General Discussion

Typical examples of the lift and drag benefits attributed to forebody strakes are shown in Figures 22 and 23. The family of delta planform strakes, Z7-Z10, on the simple wing-body configuration (785) yields lift and drag benefits beginning at approximately a 10-degree angle of attack (Figure 22). The most significant geometric parameter appears to be the area: the bigger the strake, the more the lift. The data shown in Figure 23 are representative of the later highly blended strake configurations (geometry of Figure 18a) and as such, there is no strake-off level for comparison. The strong effect of strake size is nonetheless again present at angles of attack above 17 degrees.

The effects of nose strakes on lift and drag are negligible for the size strakes tested in the F-16 program. A typical effect is that of nose strake Z124 tested in front of the F-16 forebody strake, Z120 (Figure 24). A sketch of Z124 was provided in Figure 20b. This negligible effect is undoubtably a result of the small size of the nose strakes. A contributing factor, however, is also that the vortex shed from the nose strake tends to flow over the forebody and does not interact with the wing flow field. Conversely, a vortex shed from a forebody strake passes over the strake and wing upper surface. Further evidence of this concept is present in Figure 25, which compares the lift effects of a nose strake and a small canard strake for the YF-16 forebody (Figure 17 shows geometry). The canard strake, although small, has a noticeable effect on the lift and drag, particularly at very high angles of attack. A vortex shed from this canard strake would pass over the forebody strake and wing, and tend to reinforce the existing forebody strake vortex.

The data of Figures 22 and 23 show significant beneficial effects of forebody strakes on the lift and drag of a wing with no leading-edge flap deflection. Wing leading-edge flap deflections can significantly reduce the incremental strake effects. For example, on configuration 401F-5 without a forebody strake, increasing the leading-edge flap deflection results in an orderly increase in lift with increasing angle of attack (Figure 26). However, the addition of a modified delta forebody strake, Z4, significantly reduces the effect of the leading edge flap (Figure 27). There is actually a reduction in lift with leading-edge flap deflection in the 15- to 23-degree angle-of-attack range for the configuration with strake Z4.

10

The result is that the effects of forebody strakes on the envelope lift and drag curves, which are representative of aircraft, such as the F-16, that have scheduled leading-edge-flap deflections, are significantly reduced from the no-leading-edge-flap case. Envelope curves (Figure 28) that result from a minimum-drag leading-edge-flap schedule illustrate this point. This effect is logical when the effect on the wing upper surface flow is considered. Without a leading-edge flap or a strake the flow over the F-16 wing, which is rather thin (t/c = .04), begins to exhibit significant separation (stall onset) at approximately a 10-degree angle-of-attack (Figure 22). A leading-edge flap delays this separation considerably and thus improves the lift and drag characteristics. A forebody strake accomplishes much the same effect at high angles of attack by passing high-energy vortex flow over the region of the wing that otherwise would have separated (stalled) airflow. These effects are not entirely additive, thus the strake benefit in the presence of leading-edge flaps is reduced from the no-flap case, Figure 28. In summary, the design of a forebody strake/wing leading-edge flap combination must consider the strong coupling effects.

The comparisons of Figure 28 are with a zero horizontal-tail deflection, i.e., untrimmed. Trim effects are generally favorable to the forebody strake configurations because of the linearization of the pitching moment curve, as will be discussed in Subsection 4.2.

Whenever additional exposed area, such as a strake, is added to a configuration to improve the high-angle-of-attack characteristics, the question of the effect on cruise and dash performance must be addressed. Figures 29 and 30 illustrate the typical low-lift drag penalty for forebody strakes at .80 and 1.20 Mach number, respectively. The predicted skin friction drag (Reference 2) for the largest strake shown, Z7, is .0007 at wind tunnel Reynolds number and .80 Mach number. It can be seen in Figure 29 that the data for all of the strakes fall within this band at the lift coefficient for minimum drag, indicating that the drag penalty is of the same order as the friction drag prediction at .80 Mach number. The penalty remains relatively constant up to typical optimum-altitude cruise lift coefficients for the F-16 ($C_L \approx .3$). Figure 30 shows that at 1.20 Mach number some strakes produce a small drag reduction at low lift. It is probable (based on area distributions from similar configurations) that for this unblended configuration (785) the strake is filling the area curve immediately forward of the wing, thus improving the airplane's 1.2 Mach area distribution.

11

The majority of the transonic strake parametric data is at Mach numbers of .80 and 1.20. Limited configuration comparisons are available at .90 Mach. Although the strake effects on lift and drag are, in general, consistent between .80 and .90 Mach, the effects are greatly reduced at the higher Mach number. Figures 31 and 32 illustrate this effect for a series of blended forebody strakes on Configuration 401F-10A.

The effect on lift and drag of fairing the strake into the forebody is shown in Figure 33. The basic Z4 strake is a flat plate added to Configuration 401F-5. This strake was first tested with the upper surface faired, Z4A, and then the upper and lower surfaces faired, Z4B (geometry in Figure 10). There are only very small effects on the lift and drag.

Of primary importance in this subsection is the effect of forebody strake size and shape on lift and drag and the associated interaction of the strake and leading-edge flap. These items are therefore considered in more detail in the following subsections.

4.1.2 Evaluation of Existing Prediction Techniques

If an existing method would adequately predict lift and drag effects of forebody strakes, it would be a considerable aid to the definition of the important geometrical relationships and associated development of design guides. To this end, a typical existing method has been evaluated. The method selected for consideration is an empirical method developed at General Dynamics under a USAF contract (WINSTAN) and documented in Reference 3. The contract task was to develop methods to predict the aerodynamic characteristics of double delta, cranked, and curved leading-edge wings. The particular aspect of interest herein is the method developed to predict the nonlinear lift of double-delta planforms.

The method is based on a correlation at constant angle of attack of the parameters $(C_L/C_{L_\alpha})(AR_i/\eta_B)$ and $\beta \tan \Lambda_{LE_i}$ for available experimental data for double-delta planforms. These parameters are defined as follows:

C_L - lift coefficient, lift/qS_{REF}

C_{L_α} - linear lift curve slope

AR_i — aspect ratio of inboard panel, b_i^2/S_i

η_B — nondimensional span station of intersection of inboard and outboard panels

β — Prandtl-Glauert parameter, $\sqrt{1 - M^2}$

Λ_{LE_i} — leading-edge-sweep angle of inboard panel

The resultant correlation, taken from Reference 3, is shown in Figure 34.

To apply this method to predict the incremental effects due to strakes, it is necessary to predict both the strake-on and strake-off configurations. The strake-on case is predicted as if it were a conventional double-delta planform. The strake-off case is predicted by assuming that a double delta planform approaches the wing-fuselage combination as a limiting case. It is noted in Figure 34 that as the sweep of the inboard panel approaches $90°$, the parameter (C_L/C_{L_α}) (AR_i/η_B) approaches an asymptotic value. The strake-off case is predicted by use of this asymptotic value as representative of a wing-body combination with the fuselage forward of the wing trailing edge defined as the inboard panel.

The family of delta planform strakes shown in Figure 7 has been selected for the test-prediction comparison because of its configuration simplicity. These strakes are not blended into the fuselage, thus the definition of each configuration component is straightforward. These strakes also form a consistent family, not involving several different planform shapes.

The predicted increment between strake on and off is shown in Figure 35. Obviously the increment predicted in this manner does not adequately model the increment obtained from the test data. It is noted that the strake does not produce a substantial lift increment within the range of angles of attack normally considered to be characterized by linear (or nearly linear in the case of the F-16 aspect ratio 3.0 wing) variations in lift. An attempt has been made to account for this region by predicting the α_{break} between the linear and nonlinear lift regions and utilizing the increment above this point to predict the strake effects.

A correlation of α_{break} and leading-edge-sweep angle of the inboard panel is presented in Reference 3 for an

13

uncambered wing. The effect of wing camber on α_{break} is estimated by use of an empirical correlation found in Reference 4 and repeated below.

$$\alpha_{break} = (12.05 - 4.1 \, M \cos \, \Lambda_{c/4}) \, (\frac{c_{\ell_d}}{\cos \, \Lambda_{c/4}})$$

The strake-on and -off predictions are collapsed at the value of α_{break} predicted by the above method, and the increment above this point used to predict the strake effects, as shown in Figure 36. This is an adaptation of the double-delta method, which is similar in approach to the adaptation used in Reference 3 for cranked wings.

Prediction using this technique is shown in Figure 37. This adaptation of the double-delta correlations predicts the order of magnitude of the strake lift, although the effects of angle of attack and strake geometry are not always predicted correctly.

The apparent failure of the double-delta method of Reference 3 to adequately model the incremental strake effects does not discredit the method with respect to its original intended use. The method is based on correlations of conventional double-delta planforms of relatively high sweep and low aspect ratio. The outboard wing panel of the configurations within the present study have in all cases a moderate sweep angle (40°) and aspect ratio (3.0). In addition, the incremental values used for comparison are dependent upon the ability to predict the strake-off levels at high angles of attack - a purpose for which the methods of Reference 3 were not originally intended.

Some of the more recently developed computerized methods show promise for evaluating the longitudinal aerodynamic characteristics of wing-body-strake configurations. For example, an adaptation of the Polhamus suction analogy concept is shown to reasonably predict forebody strake effects on a basic wing-body research model in Reference 5.

4.1.3 Correlation of Incremental Lift and Drag

Due to the lack of a fully adequate method to predict the strake incremental effects, attempts have been made to

14

correlate the effects with appropriate geometrical parameters. This effort is difficult due to the lack of a consistent baseline from which to increment. As discussed previously, most of the configurations with strakes are highly blended strake-wing-body combinations, and a true strake-off configuration does not always exist for incremental purposes. For these cases, the incremental values studied represent the effect of modifying an existing strake and not the total strake effect per se. Furthermore, not enough consistent families of strakes exist to systematically define the effect of a particular geometric variation. However, within the context of these limiting factors, correlations can be made that lead to several interesting conclusions concerning the general effects of forebody strake geometry.

Initial observations noted in Subsection 4.1 indicated a strong effect of strake area on the incremental lift. If indeed area is the dominating factor, it would be helpful to remove this effect from the data so that effects that are perhaps secondary can be identified. A first attempt at this consisted of referencing the strake incremental lift to the exposed area of the strake, thereby obtaining a pure strake lift coefficient. Results showed that the exposed area was much too small to collapse the data. At this point it was hypothesized that the strake incremental lift would be a direct function of the total area affected, or energized, by the strake vortex. This is similar in concept to the augmented vortex method developed by Lamar (Reference 6). Due to the lack of diagnostic data to determine the area being influenced by the strakes, a geometrical definition of an area considered to be representative was necessary. The definition of such an area is illustrated in Figures 38 and 39. For conventional strake-wing-body-combinations, the definition is simply the exposed strake area plus the wing planform area that falls within the projected strake exposed area, as shown in Figure 38. For the highly blended configurations, which do not have well-defined strake planforms, the definition was not as straightforward. For these configurations, the blended area between the strake and body was included with the strake exposed area as illustrated in Figure 39.

Four families of strakes were tested for which a definite strake-off baseline exists. The incremental lift data referenced to the theoretical wing area (26 square meters, 280 square feet) for these families are shown in Figures 40 through 43. Strake geometry was shown in Figures 7, 10 and

15

11b. The lift increments referenced to the strake-wing effective area, as defined in Figures 38 and 39, are shown in Figures 44 through 47. The lift increments tend to collapse to a single curve for a fixed value of wing leading-edge-flap deflection.

This is an important fact. It says that for a given configuration the overriding factor in determining the strake lift is the area affected by the strake generated vortex for the angle of attack range tested. Shape effects should become more pronounced in the 30 degree angle of attack range where vortex bursting will occur over the lifting surface.

An exception to the area correlation is the ogee family of data (Figure 46) at angles of attack greater than 18 degrees. Strakes Z16, Z18, and Z17 intersect the wing at increasing semi-spans. It can be speculated that for the larger span strakes (Z17 for example) the effective area needs to be redefined to include less of the inboard part of the wing, as shown in Figure 48. This would tend to further collapse the data of Z16, Z17, and Z18 in Figure 46 at high angles of attack. Strake Z14 is the least effective of those shown in Figure 46, which may indicate that it is too narrow to generate as strong a vortex as, say, Z18 (which has the same span).

Divergence of the effective area-based data at the higher angles of attack can also be caused by the sweeping of the strake vortex outboard over the wing. Typically, below about 20 degrees angle of attack the vortex passes across the wing in a streamwise direction for the F-16 configuration. However, at higher angles of attack (depending on leading edge flap deflection) the path of the vortex begins to curve spanwise over the wing. Obviously, the effective area definition would have to be modified to represent this effect.

Average fairings representing the collapsed data of Figures 44 through 47 are shown in Figure 49 for each family. Variations in strake shape are of only secondary importance to the generation of lift, as shown by the 10-degree flap data on Configuration 401F-5 for delta (Z4), ogee (Z14, Z16-Z18), and gothic (Z5) planforms. Figure 49 also shows that the incremental lift decreases for the more highly blended configurations. Configuration 401F-10A is the most highly blended configuration shown in Figure 49 and has the lowest incremental strake lift. Configurations 785 (simple wing body) and 401F-5 (blended) show approximately

the same level of strake lift to 18 degrees angle of attack. This is fortuitous, however, because the strakes of Configuration 785 have a nominal negative 2 degrees of incidence at the leading edge relative to those of Configuration 401F-5. The strakes on the simple wing body would be more effective at high angles of attack if they were at the same incidence as those of Configuration 401F-5.

A definite dependence on wing leading-edge-flap deflection can be noted in the lift increments of Figure 49. Deflecting the leading-edge flap delays the beneficial strake effects to a higher angle of attack as discussed previously in Subsection 4.1.1.

A substantial amount of strake data is available that cannot be analyzed in the preceding manner due to the lack of a true strake-off baseline. This is the case for many of the highly blended strake-wing-body configurations. For these configurations, the strake of smallest exposed area was selected as the baseline for all force increments. The incremental lift for two such families of strakes is shown in Figure 50 referenced to the wing area (26 sq. m, 280 sq. ft) and in Figure 51 referenced to the change in strake effective area from the baseline strake configuration. There is a tendency for these increments to collapse, although it is not as definite as noted in the previous comparisons. The strakes with the smallest changes in area from the baseline (Z64 and Z71), and thus the smallest lift increments (Figure 50), correspond to those curves in Figure 51 that fall the furthest away from the main body of data. Here small increments are being referenced to small areas, and a sensitivity factor may be involved. Or it may be that extension of the strake forward, Z63 to Z64, is a relatively efficient method (it takes less area) to increase the lift in the 20- to 30-degree angle of attack range because it provides a longer growth time for the vortex. More data is required to isolate this effect.

Since the forebody strakes tested on the F-16 are of high sweep and have sharp leading edges, it is expected that the drag, ΔC_D, due to the strake lift, ΔC_L, would be close to the no-suction value, $\Delta C_L \tan \alpha$. This has been evaluated in terms of incremental strake lift and drag in Figure 52 for several strakes with zero leading-edge flap

deflection. Since strakes Z7-Z10 have leading-edge inci-
dences of nominally 2 degrees, the angle of attack has been
appropriately modified. The data are reasonably approxi-
mated by an adaptation of the Reference 3 methodology for
double delta wings;

$$\Delta C_D = .95 \; \Delta C_L \tan (\alpha + i)$$

Some data scatter is apparent at the lower angles of attack,
but the data generally fall within $\pm$ 2 percent of the total
strakeoff configuration drag.

4.2 LONGITUDINAL STABILITY

The addition of strakes, particularly forebody strakes,
to a wing-body configuration produces changes in airplane
longitudinal characteristics. The purpose of this portion
of the investigation, therefore, is to examine the available
wind tunnel data in order to define pertinent strake design
factors, such as strake shape, area, location, etc., that
have significant effects on longitudinal stability.

Proper strake design and location can result in a
beneficial influence in maneuver lift, directional stability,
and/or longitudinal stability at high angles of attack. In
the longitudinal case, strakes can yield improved linearity
of pitching moment characteristics, particularly in the
transonic regime where wing stall usually results in a large
stable break of the pitching moment curve. It was observed
early in the analysis that available nose strakes had a small
effect on the longitudinal characteristics (presumably because
of their relatively small exposed area with respect to wing
area) and were, therfore, not included in this longitudinal
analysis. Forebody strakes, on the other hand, do affect
longitudinal characteristics and in some cases introduce
nonlinearities. These will be identified and reviewed.

The nature of the strake's effectiveness, its vortex
generation, and effects on the wing and forebody, is highly
dependent on the general configuration of the aircraft. Iso-
lation of these effects (particularly in regard to stability
characteristics) is difficult considering that nearly every
family of strakes as tested was on a different forebody con-
figuration, making overall correlation difficult. Additional
limitations are imposed on the low-speed analysis, since
relatively few forebody strakes were tested in this flight
regime, and, of those that were, no corresponding strake-off
condition was available. 18

4.2.1 Selected Low Speed Data and Discussion

For both subsonic and transonic cases it is apparent from References 7 and 8 and the data of the present study that the major influences on the forward shift of aerodynamic center due to the strake are the strake's exposed area and its location ahead of the wing. The faired ogee-shaped strakes of Figure 18a are the only forebody strake family that was tested at low speed, but no strake-off case was tested. However, the variation of geometries within this family provided information as to trends due to certain design factors.

Within the linear C_L region at 0.2 Mach number, it is apparent that the primary strake characteristic influencing the change in the a.c. is its area directly ahead of the wing. For example, strakes Z63 and Z64, which have similar planforms, except that Z64 extends approximately 102 cm (40 in.) further forward on the nose, have essentially the same a.c. location (Figure 53). Configurations Z65 and Z66, both of which retain the extension forward and the basic shape of Z64 but increase the areas in the region in front of the wing, yield proportional decreases in pitch stability. These data indicate that either the more powerful vortex produced by the larger area in front of the wing or the effect of the basic wing upwash, or both, tend to make this portion of the strake highly effective in influencing the overall a.c. location in the linear region of lift. Insufficient low-speed strake data precluded exact determination of shape effects.

The region above the linear C_L is crucial from a strake design standpoint, primarily because of the effect of the strake on the airplane stall and post-stall characteristics. The addition of forebody strakes enable the wing-strake combination to continue lifting to angles of attack of 30 to 40 degrees, whereupon the combination stalls. The pitching moment curve, linear up to stall in most cases, tends to break erratically stable or unstable after stall, depending on the configuration (see Figure 53). The nature of the pitching moment break after stall is extremely important to the prevention of a deep (unrecoverable) stall. As in the lower-angle-of-attack region, strake area has a major influence, the larger strake (Z66) exhibiting the most unstable break (Figure 53). No guidelines as to area requirements could be formulated from the available data because of the geometrical limitations discussed above.

19

In this region, the stall characteristics are also sensitive to the forward extension of the strake. In Figure 54, strakes Z63, Z64, and Z72 all have basically the same shape and are approximately the same size, but the narrow area extension increases with strake number. Post-stall stability is degraded with forward extension. This destabilizing effect indicates that the highly swept leading-edge extension, with the area further forward, produces lift beyond stall, and the adverse effects after stall are a consequence of the resulting moment.

Finally, forebody configuration has significance in stall behavior. The group of strakes Z68 through Z70 are identical to strakes Z64 through Z66, with the exception of being mounted on an extended forebody (35.6 cm. full scale) and the strake leading edge extended accordingly. This modification results in a considerable degradation of the stall characteristics when compared to strakes Z64 through Z66 (Figure 55). Whether this is dependent on forebody extension, strake extension, or (most likely) both could not be accurately established.

The control effectiveness of the horizontal tail beyond stall seems to be affected by the same strake factors influencing stall behavior. In Figure 56, strake Z63 displays a marked change from a stable to unstable stall break with a horizontal-tail deflection of 25 degrees, resulting in diminished control effectiveness at the post-stall angles of attack. In comparison to strake Z63, the larger strake Z66, with a 25-degree tail deflection, shows a more adverse break after stall, to the extent that the pitching moment almost falls on the corresponding zero-degree tail deflection curve, indicating little nose-down pitch control authority at these angles of attack. Strake extension forward on the nose and lengthening the forebody also tend to reduce nose down control effectiveness at post stall angles of attack. Careful attention to the available post stall pitching moment is an important part of the strake design process and may well be a driving factor in selecting the strake size and shape.

4.2.2 Selected Transonic Data and Discussion

A large array of forebody strake configurations were tested transonically, thus allowing considerably more analysis and correlation work to be performed. Several approaches

20

were followed. As mentioned earlier, the addition of strake
area ahead of the wing would be expected to produce a destab-
ilizing effect on longitudinal stability, essentially propor-
tional to the strake size and its positioning ahead of the
wing.

The a.c. shift has been correlated with pertinent strake
parameters. On the basis of the results of the lift incre-
ment analysis of Subsection 4.1.3, the strake is assumed to
be a low-aspect-ratio wing spanning from the body/strake
juncture to the wing-leading-edge/strake intersection and
inclusive of the portion of the wing directly aft of the
strake (the shaded areas in Figures 38 and 39). Geometrical
data for the resulting strake/wing inboard panel for several
strake configurations are given in Table 5. Representative
leading-edge sweeps were selected for the curved strakes as
shown in Table 5. The strake lift curve slopes, $C_{L_{\alpha_s}}$, and
the non-dimensional distance from the aerodynamic center of
the constructed strake area to the aerodynamic center of the
basic wing alone, $\ell_s/\overline{c}$, are predicted by the methods of
Reference 9 and 10, respectively. The predicted values are
presented in Table 6 with corresponding parameters

$$\frac{\ell_s A_{EFF}}{\overline{c} S_{REF}} \text{ and } \frac{\ell_s A_{EFF}}{\overline{c} S_{REF}} C_{L_{\alpha_s}}.$$ The relation between the change

in the a.c. in the linear C_L region (less than 10 degrees angle
of attack) due to the strake (ΔAC_1) and the parameter

$$\frac{\ell_s A_{EFF}}{\overline{c} S_{REF}} C_{L_{\alpha_s}}$$ is shown in Figure 57 for the various families

noted. For all of the strakes investigated, regardless of
shape, flap deflection, or fuselage configuration (785 and
401F-5), a linear relationship of a.c. with

$$\frac{\ell_s A_{EFF}}{\overline{c} S_{REF}} C_{L_{\alpha_s}}$$ was essentially obtained. Only strake Z17

falls considerably off the correlating line. This is
believed to be a result of the affected area definition for
large span strakes, as described in Subsection 4.1.3. A
similar linear relationship is shown in Figure 58 for the
strakes tested at Mach 1.2. Such a relationship of a.c.

with $\dfrac{\ell_s A_{EFF}}{\overline{c} S_{REF}} C_{L_{\alpha_s}}$ suggests the stability change in the linear

lift region due to the addition of the forebody strake is a
function of the lift produced by the strake and its influenced

area on the wing, and it shows promise for the development of a semi-empirical prediction method for strakes similar to the Paniszczyn a.c. prediction method for cranked wings of Reference 3. At this time, estimation of the strake effect on aerodynamic center in the linear lift region can be roughly determined by use of the relationship established in Figures 57 and 58.

$$\Delta AC_1 = 0.483 \; \frac{\ell_s A_{EFF}}{\bar{c} S_{REF}} \; C_{L_{\alpha_s}} \quad \text{at 0.80 Mach number}$$

$$\Delta AC_1 = 0.296 \; \frac{\ell_s A_{EFF}}{\bar{c} S_{REF}} \; C_{L_{\alpha_s}} \quad \text{at 1.20 Mach number}$$

Efforts to establish the change in a.c. due to strakes in the nonlinear lift region beyond the initiation of wing stall (nominally 10 degrees angle of attack) provided the results shown in Figure 59. For this nonlinear lift region the stability change (ΔAC_2) is correlated with the parameter $\frac{\ell_s A_{EFF}}{\bar{c} S_{REF}}$. Note that the lift curve slope term is omitted, primarily because of the characteristic nonlinear lift variation of low-aspect-ratio wings at high angles-of attack. All strake configurations exhibited essentially the same linear variation in a.c. with the parameter $\frac{\ell_s A_{EFF}}{\bar{c} S_{REF}}$ for given leading-edge-flap deflections. Deflecting the leading-edge flap in the nonlinear lift region reduces the shift due to the strake (as expected, based on the reduced lift, Figure 49). For strake configuration Z4 and a flap deflection of 25 degrees, there is a noticable change in stability over the strake-off configuration, although for this flap deflection the increment in lift due to the strake is small (Figures 26a and 27a). Thus strakes can provide beneficial linearization of the pitching moment even when the flap effects reduce the increment in lift due to the strakes.

An additional lateral shift between Configuration 785 and 401F-5 is shown in Figure 59. This is probably due to the fuselage blending of 401F-5, which results in further forward strake-off a.c. location and a smaller overall shift in a.c. due to the strake.

22

Examination of the data contained in Tables 5 and 6 indicate that the strake shapes tested seem to evidence negligible effects longitudinally at transonic speeds. The strake shape is, however, of considerable importance in the lateral directional case, as will be discussed in the following subsection

4.3 LATERAL/DIRECTIONAL STABILITY

Maintaining directional stability to maximum usable lift is of major importance in the design of high-performance maneuvering aircraft. Generally progressive deterioration in static directional stability begins at moderate-to-high angles of attack for most conventional configurations and, consequently, limits the maximum usable lift. Strakes, both nose and forebody, have proven effective in extending the usable lift range. Herein, families of nose strakes and forebody strakes are systematically reviewed to establish their effectiveness on lateral/directional characteristics in order to formulate a strake design guide toward extending the usable lift range.

The adverse effects on lateral/directional stability due to vortex flow shed by the fuselage nose and wing-body juncture, and the associated destablizing flow field on the fuselage afterbody and at the vertical tail, have been investigated and reported in References 7 and 8. Addition of strakes, both nose and forebody, were found to produce improvements in lateral/directional characteristics, particularly at high angles of attack by altering the generated vortex flow patterns.

A survey of catalogued strake lateral/directional data revealed a lack of systematic strake geometry variation. Consequently, practical considerations result in different investigation techniques based upon the kind and amount of strake data available. In contrast to developing quantitative results, the strake lateral/directional analyses are qualitative in nature on the basis of the available data. Several reasons are addressed in support of a qualitative analysis. First, strakes are predominantly effective at high angles of attack within a region in which vortex and separated flow are extremely complex and directly dependent upon numerous aircraft variables (e.g., forebody configuration, wing sweep, vertical-tail geometry, etc.). Analysis is complicated further by the numerous fuselages on which the strakes were tested and the large nonparametric variation in the combinations of strakes, tails, and forebodies.

23

Additional complications arose in that most nose strakes were
tested subsonically while the forebody strakes were primarily
tested transonically (one family series was tested subsoni-
cally).

4.3.1 Selected Low-Speed Data and
Discussion

Especially at low speed and moderate to high angles-of-
attack nose strakes have a pronounced effect on lateral/
directional stability characteristics. Improvement in
lateral/directional stability is influenced by the size
(length and width) of the nose strake. Each baseline con-
figuration used in the nose-strake evaluations had an inte-
grated forebody strake. In all cases, the improvement in
lateral/directional stability due to the nose strake over
the baseline forebody strake case is significant. Typical
results are displayed in Figure 60 for nose strake Z124
applied to forebody strake Configuration Z120 (faired ogee).
The strake width and extension aft are the most significant
design parameters. A typical example of the effect of nose
strake extension for a family of truncated strakes is shown
in Figure 61. The wider nose strakes also result in better
lateral/directional characteristics (Z112 vs Z114 in Figure 62).
Actual strake shape seems to be of little consequence; how-
ever, truncation of the strake (e.g., Z112, Z114) improves
stability, especially laterally, compared to the same strakes
faired back into the fuselage (Z110, Z113 in Figure 62).

Slight inclination of the strake with respect to the
aircraft waterline is of minor consequence. This is shown
in Figure 63 in which strake Z128 is rotated 5 degrees up
with respect to strake Z124 (both have same planform).

As mentioned earlier, the forebody strakes were not
found to be as effective lateral/directionally as the nose
strakes for the wing-body-strake configurations tested in
the F-16 program. Actual measurement of the forebody strake's
effectiveness over the strake-off configuration was not possi-
ble since no strake-off configurations were tested at low
speed. The variation of strake geometric parameters (leading-
edge extensions and width) in the one family tested (Z63-Z70)
displays few predictable trends since the data become quite
erratic at higher angle of attack (Figure 64). The extended
strake/forebody configurations (Z67-Z70 in Figure 65) are
noticeably less stable than the corresponding shorter fore-

body combinations (Z63 - Z66 shown in Figure 64). All configurations incorporating this family of strakes became directionally unstable beyond an angle of attack of 32 degrees.

The significant difference in effectivenss between the two types of strakes leads to the following postulation for the F-16 type configuration. Without nose strakes the shed vortices from the forebody emanate from variable locations along the nose depending on the angle of attack, sideslip, configuration, etc. With nose strakes applied, especially the truncated nose strakes, the location of vortex initiation is fixed and the vortex is directed along the fuselage afterbody and vertical tail in a more symmetrical manner resulting in improved lateral/directional behavior. The effectiveness of forebody strakes on directional stability is not as significant as the effectiveness of nose strakes since the forebody strakes tend to be located behind the initiation point of forebody vortices, plus the probability that their vortices are affected by the flow field surrounding the wing. However, it must be stressed that the effects of both nose and forebody strakes and their interactions are extremely configuration oriented and the results from this set of data are not necessarily representative of other configurations.

4.3.2 Selected Transonic Data and Discussion

The nose strakes tested at transonic speeds were limited to a small number of configurations. The few that were tested again exhibited an improvement in the lateral-directional stability compared to the forebody-strake-alone case, for example nose strake Z100 (Figure 66). The first three families of forebody strakes tested offer the best comparative basis for the effects of changes to the strake geometry.

The delta-shaped family of strakes displayed rather small effects with respect to directional stability but large changes laterally with the leading-edge flap deflection set at zero (Figure 67). In this case, the largest strake of the family, Z7, exhibited an extremely destabilizing increment in dihedral effect. This family of strakes has significant anhedral, (see in Figure 7) which may contribute to this effect. Subsequent leading-edge-flap deflections decreased the over-all effects exhibited by strakes Z7 and Z10 (Figure 68).

25

The second family, strakes Z4 (modified delta) and Z5 (gothic) exhibited improved directional stability behavior over the strake-off case (Figures 69 and 70). The change in lateral characteristics with leading-edge-flap deflection is not as great for this family (Figures 69 and 70) as for the delta-shaped strakes (Figures 67 and 68).

The third family, Z14 and Z16 - Z18 (ogee) show improvement in directional stability with adverse effects laterally with the leading-edge flap deflected 10 degrees (Figure 71). Because this was the only flap condition tested, flap effects could not be determined.

These results support some general conclusions. Adjustment of the forebody strake shape has definite effects on the lateral/directional stability, regardless of leading-edge-flap deflections. The most pertinent geometric parameters tend to be the extension of the strake forward on the nose and the width of the strake at this point. These trends are supported by the improved characteristics of the strakes Z4 and Z5 (Figures 69 and 70). Of the first three families, Z4 and Z5 extend furthest forward with the greatest width in the forward region. This conclusion is further supported by the relative stability within the fourth (Z24 - Z27) and fifth families (Z28 - Z33). For each family, the strake that extends furthest with the greatest width toward the nose (strakes Z25 and Z28, respectively) show the greatest improvement over the strake-off case (Figures 72 and 73). The reasoning behind this behavior agrees with the demonstrated subsonic stability improvements of the nose strakes compared to forebody strakes. For both cases, the obvious area of effectiveness lies forward on the nose. In that forebody strakes usually lie behind the shed point of the forebody nose vortices, their effect on lateral directional stability tends to be much less than properly positioned nose strakes. Only for cases in which the forebody strakes extend considerably forward on the nose do they show significant stability improvements. A contributing factor to the improved stability for some forebody strakes is the formation of a stronger, more stable vortex. This vortex, when sufficiently strong, provides a stabilizing influence on the wing flow field and in the afterbody region.

Obviously, the lateral/directional benefits attained through the use of strakes are of primary concern to any aircraft design. It is suggested that in configuration development well-structured testing be performed to thoroughly determine the influence of strakes on stability. In addition, care must be taken when combining nose and forebody strakes because the interactions can become significant and effects noted from separate testing are most likely not linearly additive.

4.4 DESIGN GUIDELINES

The analysis and resulting conclusions presented in the preceding sections have been qualified by the configurational dependence of high-angle-of-attack aerodynamics. However, some initial design guidelines have been developed that are believed to be valid for rather general application (at least to configurations with outboard wing panels and single vertical tails similar to the F-16). These are summarized in this subsection.

In addition to increased wing-body lift, one of the primary purposes for adding a forebody strake to a configuration is the linearization of the pitching moment curve at high angles of attack. Elimination of the typical strong stable break results in significant improvements in trim drag, which results in additional positive increments in maneuver lift.

Estimation of the aerodynamic-center shift in the linear lift region due to strakes can be made with the relations shown in Figures 57 and 58:

$$\Delta AC_1 = .483 \frac{\ell_s A_{EFF}}{\bar{c} S_{REF}} C_{L\alpha_S} \text{ at .80 Mach number}$$

and

$$\Delta AC_1 = .296 \frac{\ell_s A_{EFF}}{\bar{c} S_{REF}} C_{L\alpha_S} \text{ at 1.20 Mach number}$$

27

The strake lift curve slope, $C_{L_{\alpha_S}}$, and moment arm, ℓ_s, are estimated by the methods of References 9 and 10, as described in Section 4.2. The effective strake area, A_{EFF}, is defined as shown in Figures 38 and 39.

The aerodynamic-center shift above the linear region can be estimated from Figure 59. Since all configuration leading-edge-flap combinations have the same slope $\left(\dfrac{\ell_s A_{EFF}}{\bar{c} S_{REF}} \text{ versus } \Delta AC_2 \right)$, the effects of variations in strake size can easily be estimated for a particular configuration. Thus, Figure 59 can be used to size a forebody strake to provide a linear pitching moment curve.

The incremental lift effects of forebody strakes are primarily a function of the affected area, as defined in Figures 38 and 39. This means that given a particular strake, leading-edge flap, and body configuration, the lift increments that can be obtained by modifying the strake (e.g., to the strake area required for a linear pitching moment curve) are easily estimated up to the angle of attack for vortex breakdown (which may vary for different strake planforms).

$$\left(\Delta C_{L_{STRAKE}} \right)_2 = \left(\Delta C_{L_{STRAKE}} \right)_1 \times \frac{(A_{EFF})_2}{(A_{EFF})_1}$$

Furthermore, incremental lift and the stability shift due to adding a strake to a simple wing-body configuration or a blended configuration can be estimated to the first order with the curves of Figures 49 and 59 by simply selecting a similar configuration. The incremental drag resulting from the strake lift can also be obtained by use of the relation derived from the correlation shown in Figure 52:

$$\Delta C_D = .95 \; \Delta C_L \; \tan (\alpha + i)$$

At this time general design guides have not been developed for lateral/directional stability or low-speed stall characteristics because of the large configuration-dependence of these items and the lack of parametric information. Additional, well structured, testing is required to properly isolate the effects of strake geometry on these phenomena.

However, several general comments are appropriate. Care should be taken in the design of strakes to maintain adequate control capability in the post-stall region. This is a function of strake size and shape as well as tail size. Based on the data presented herein the effects of forebody strakes on lateral/directional stability become more pronounced when the strake is extended far forward on the nose.

Nose strakes strongly influence directional stability at high angle of attack. Results from the present study imply they should be truncated for best lateral characteristics. Additional important geometric parameters are the width and length. Caution is required when combining nose and forebody strake stability effects because the interactions can become significant and the effects noted from separate testing are most likely not linearly additive.

5. C O N C L U S I O N S   A N D
R E C O M M E N D A T I O N S

Nose strakes offer significantly improved lateral/
directional performance with a minimum increase in wetted
area and little effect on longitudinal characteristics.
Forebody strakes provide beneficial linearlization of the
pitching moment curve, improved maneuver lift, and in some
cases, improved lateral/directional characteristics. Al-
though the application of the strakes is highly configura-
tion-dependent and optimization will undoubtedly require tun-
nel testing, initial design guidelines have been developed
and several recommendations can be forwarded.

Design guidelines have been developed that allow fore-
body strakes to be sized to obtain a linear pitching moment
curve and the resulting lift and drag increments to be esti-
mated. The incremental lift effects have been shown to be
primarily a function of the area affected by the strake
induced vortex. Forebody-strake-planform shape is of sec-
ondary importance to lift generation below vortex breakdown
but has a significant effect on lateral/directional charac-
teristics.

The shape of nose strakes for lateral/directional
stability seems to be of minor importance. The major posi-
tive influences are found to be the width of the strake and
the truncation of the surface, that is, cutting it off rather
than fairing it back into the fuselage. The nose strakes
analyzed have little effect on longitudinal stability; how-
ever, increasing surface widths, and consequently area, may
lead to possible adverse effects in the subsonic high-angle-
of-attack region.

Forebody strake effects on lateral-directional stability
are most pronounced with no leading-edge flap deflection.
The lateral-directional effects appear to increase as the
strake is extended forward on the forebody. The extension
forward on the nose, however, becomes undesirable from the
standpoint of subsonic longitudinal stability at high angles-
of-attack.

A need has been identified for further well-structured
parametric testing designed to isolate the effects of strake
geometry on, in particular, the lateral/directional-stability

and low-speed-stall characteristics. It is recommended that systematic families of forebody and nose strakes be designed for a simple wing-body configuration with single and twin vertical tails and these definitive tests conducted. These data will also serve to verify and/or expand the initial design guidelines that have been developed for longitudinal effects.

REFERENCES

1. J. D. McAllister, D. B. Benepe, P. D. Whitten, and
    G. Kaftan, Wing Roll Control Devices for Transonic High
    Lift Conditions, Part 1 - Fixed Wing Configuration,
    Volume 1 - General Configuration, Devices, Test Results,
    Conclusions, AFFDL-TR-69-124 Part 1 Volume 1, January
    1970.

2. White, F. M., and Christoph, G. H., A Simple New Analysis
    of Compressible Turbulent Two-Dimensional Skin Friction
    Under Arbitrary Conditions, AFFDL-TR-70-133, February
    1971.

3. Benepe, David B., Kouri, Bobby G. and Webb, J. Bert,
    et al., Aerodynamic Characteristics of Non-Straight-
    Taper Wings, AFFDL-TR-66-73, October 1966.

4. Schemensky, R. T., Development of an Empirically Based
    Computer Program to Predict the Aerodynamic Character-
    istics of Aircraft, AFFDL-TR-73-144, November 1973.

5. Luckring, J. M., Theoretical and Experimental Aero-
    dynamics of Strake-Wing Interactions up to High Angle-
    of-Attack, AIAA Paper No. 78-1202, July 1978, AIAA 11th
    Fluid and Plasma Dynamics Conference, Seattle Washington.

6. Lamar, J. E., Some Recent Applications of the Suction
    Analogy to Vortex - Lift Estimates, NASA TM X-72785, 1976.

7. Polhamus, Edward C., and Spreemann, Kenneth P., Effect
    at High Subsonic Speeds of Fuselage Forebody Strakes on
    the Static Stability and Vertical-Tail-Load Character-
    istics of a Complete Model Having a Delta Wing, NACA
    RM L57K15a, 1958.

8. Sleeman, William C., Jr., Investigation at High Subsonic
    Speeds of the Effects of Various Horizontal Fuselage
    Forebody Fins on the Directional and Longitudinal Sta-
    bility of a Complete Model Having a 45° Sweptback Wing,
    NACA RM L56J25, 1957.

9. Falkner, V.M., The Solution of Lifting Plane Problems
    by Vortex-Lattice Theory, R. & M. No. 2591, British A.R.C.,
    1953.

REFERENCES (Continued)

10. <u>USAF Stability and Control DATCOM</u>, Air Force Flight
     Dynamics Laboratory, October 1960 (Revised August 1968).

Table 1 STRAKE GEOMETRY

NO.	CONFIG.	LENGTH cm (in)	MAXIMUM*** WIDTH cm (in)	A_{exp}/SIDE cm² (in²)	L.E. POSITION			TYPE	FIGURE
					F.S. cm(in)	W.L.* cm(in)	CANT		
Z1	401F-2	124.0 (48.8)	29.5 (11.6)	1806.4 (280)	292.1 (115)	236.2 (93)	0	canard (flat delta)	8
Z1A	401F-2,-5, -10A	124.0 (48.8)	29.5 (11.6)	1806.4 (280)	381.0 (150)	269.2 (106)	0	canard (flat delta)	8,10,11a
Z1B	401F-5,-4	124.0 (48.8)	29.5 (11.6)	1806.4 (280)	381.0 (150)	243.8 (96)	$-1^{\circ}55'$	canard (flat delta)	9,10
Z1D	YF-16 +30.5 stretch	124.0 (48.8)	29.5 (11.6)	1806.4 (280)	129.5 (51)	228.6 (90)	0	canard (flat delta)	18b
Z2	401F-2	124.0 (48.8)	29.5 (11.6)	1806.4 (280)	472.4 (186)	256.8 (101.1)	$-3^{\circ}15'$	canard (flat delta)	8
Z3	401F-4	215.9 (85.0)	18.0 (7.1)	2980.6 (462)	292.1 (115)	240.0 (94.5)	$-1^{\circ}55'$	canard (flat rect.)	9
Z3	401F-5	215.9 (85.0)	18.0 (7.1)	2832.3 (439)	292.1 (115)	240.0 (94.5)	$-1^{\circ}55'$	canard (flat rect.)	10
Z4+	401F-5	430.5 (169.5)	36.8 (14.5)	7851.6 (1217)	254.0 (100)	231.6 (91.2)	0	forebody (flat mod. delta)	10
Z4A +	401F-5	430.5 (169.5)	36.8 (14.5)	7851.6 (1217)	254.0 (100)	231.6 (91.2)	0	forebody (U.S. faired)	10
Z4B +	401F-5	430.5 (169.5)	36.8 (14.5)	7851.6 (1217)	254.0 (100)	231.6 (91.2)	0	forebody (U.& L.S. faired)	10
Z5	401F-4	494.0 (194.5)	50.3 (19.8)	14129.0 (2190)	190.5 (75)	237.5 (93.5)	$-1^{\circ}55'$	forebody (flat gothic)	9
Z5 +	401F-5	494.0 (194.5)	50.3 (19.8)	13806.4 (2140)	190.5 (75.0)	231.6 (91.2)	$-1^{\circ}55'$	forebody (flat gothic)	10
Z7 +	785,786	497.8 (196.0)	69.3 (27.3)	12645.1 (1960)	158.8 (62.5)	232.9 (91.7)	$-4^{\circ}01'$	forebody (flat delta)	7
Z8 +	785	345.4 (136.0)	50.3 (19.8)	9812.9 (1521)	311.2 (122.5)	247.9 (97.6)	$-4^{\circ}01'$	forebody (flat delta)	7

Table 1 (Continued)

NO.	CONFIG.	LENGTH cm (in)	MAXIMUM WIDTH cm (in)	A_{exp}/SIDE cm^2(in^2)	L.E. POSITION			TYPE	FIGURE
					F.S. cm(in)	W.L.* cm(in)	CANT		
Z9 +	785	332.7 (131.0)	40.9 (16.1)	7761.3 (1203)	311.2 (122.5)	247.9 (97.6)	-4°01'	forebody (flat delta)	7
Z10+	785	189.2 (74.5)	30.5 (12.0)	2567.7 (398)	433.1 (170.5)	256.5 (101.0)	-4°01'	forebody (flat delta)	7
Z14 +	401F-5	494.0 194.5	6.9 (2.7)	3625.8 (562)	190.5 (75)	231.6 (91.2)	0	forebody (flat ogee)	10
Z16 +	401F-5	452.1 (178.0)	21.6 (8.5)	5735.5 (889)	190.5 (75)	231.6 (91.2)	0	forebody (flat ogee)	10
Z17 +	401F-5	535.9 (211.0)	36.1 (14.2)	9870.9 (1530)	190.5 (75)	231.6 (91.2)	0	forebody (flat ogee)	10
Z18 +	401F-5	494.0 (194.5)	30.0 (11.8)	7754.8 (1202)	190.5 (75)	231.6 (91.2)	0	forebody (flat ogee)	10
Z20	401F-10A	642.6 (253)	**	**	55.9 (22)	231.6 (91.2)	0	forebody (faired)	11
Z21	401F-10A	508.0 (200)	**	**	190.5 (75)	218.2 (85.9)	0	forebody (faired)	11a
Z22	401F-5	632.5 (249.0)	22.9 (9.0)	8012.9 (1242)	52.1 (20.5)	231.6 (91.2)	0	forebody (flat ogee)	10
Z22A	401F-5	632.5 (249.0)	22.9 (9.0)	8012.9 (1242)	52.1 (20.5)	231.6 (91.2)	0	slotted Z22 (flat ogee)	10
Z23	401F-5	430.5 (169.5)	36.8 (14.5)	7103.2 (1101)	254.0 (100)	231.6 (91.2)	0	forebody (flat mod.delta)	10
Z24 +	401F-10A	190.5 (75)	**	**	190.5 (75.0)	231.6 (91.2)	0	forebody (faired)	11b
Z25+	401F-10A	325.1 (128)	**	**	55.9 (22)	231.6 (91.2)	0	forebody (faired)	11b
Z26+	401F-10A	505.5 (199)	**	**	190.5 (75.0)	231.6 (91.2)	0	forebody (faired)	11b

35

Table 1 (Continued)

NO.	CONFIG.	LENGTH cm (in)	MAXIMUM WIDTH cm (in)	A_{exp}/SIDE cm^2(in^2)	L.E.POSITION			TYPE	FIGURE
					F.S. cm(in)	W.L. cm(in)	CANT		
Z27 +	401F-10A	654.1 (257.5)	**	**	55.9 (22)	231.6 (91.2)	0	forebody (faired)	11b
Z28 +	401F-16	657.9 (259)	**	**	55.9 (22)	231.1 (91)	fwd of F.S. 381(150) down 1°27'	forebody (faired ogee)	12
Z29 +	401F-16	649.0 (255.5)	**	**	55.9 (22)	231.1 (91.0)	fwd of F.S. 381(150) down 1°27'	forebody (faired ogee)	12
Z29A'	401F-16	175.3 (69)	30.5 (12)	2621.0 (414)	523.2 (206)	231.1 (91)	var.	rotating (part of Z29)	15a
Z29A	401F-16	649.0 (255.5)	**	**	55.9 (22)	231.1 (91)	fwd of F.S. 381 (150) down 1°27'	slotted Z29	12
Z30+	401F-16	521.5 (205.3)	**	**	190.5 (75.0)	231.1 (91.0)	fwd of F.S. 381 (150) down 1°27'	forebody (faired delta)	12
Z31 +	401F-16	440.7 (173.5)	**	**	254.0 (100.0)	231.1 (91.0)	fwd of F.S. 381 (150) down 1°27'	forebody (faired delta)	12
Z32	401F-16	638.8 (251.5)	**	**	55.9 (22)	231.1 (91.0)	fwd of F.S. 381 (150) down 1°27'	forebody (mod. faired ogee)	12
Z33	401F-16	450.9 (177.5)	**	**	254.0 (100)	231.1 (91)	fwd of F.S. 381 (150) down 1°27'	forebody (faired ogee)	12
Z33A	401F-16	175.3 (69)	30.5 (12)	2671.0 (414)	523.2 (206)	231.1 (91)	var.	rotating (contoured)	15a
Z33A'	401F-16	175.3 (69)	30.5 (12)	2671.0 (414)	523.2 (206)	231.1 (91)	var.	rotating (flat)	15a
Z33B	401F-16	122.9 (48.4)	21.8 (8.6)	1400.0 (217)	538.5 (212)	231.1 (91)	var.	rotating (contoured)	15a

Table 1   (Continued)

NO.	CONFIG.	LENGTH cm(in)	MAXIMUM WIDTH cm(in)	A_{exp}/SIDE cm^2(in^2)	L.E. POSITION			TYPE	FIGURE
					F.S. cm(in)	W.L. cm(in)	CANT		
Z33B'	401F-16	121.4 (47.8)	32.4 (8.8)	2252.9 (349.2)	542.5 (213.6)	231.1 (91)	variable	rotating (flat)	15a
Z33C	401F-16	130.3 (51.3)	23.9 (9.4)	1664.5 (258)	534.9 (210.6)	231.1 (91)	variable	rotating (contoured)	15a
Z33D	401F-16	76.2 (30)	16.8 (6.6)	580.6 (90)	523.2 (206)	231.1 (91)	variable	rotating (contoured)	15b
Z33E	401F-16	77.0 (30.3)	15.2 (6.0)	464.5 (72)	523.2 (206)	231.1 (91)	variable	rotating (contoured)	15b
Z33F	401F-16	75.7 (29.8)	11.2 (4.4)	129.0 (20)	417.1 (164.2)	231.1 (91)	variable	rotating (contoured)	15b
Z33G	401F-16	69.1 (27.2)	14.2 (5.6)	309.7 (48)	427.2 (168.2)	231.1 (91)	variable	rotating (contoured)	15b
Z33H	401F-16	76.2 (30)	16.8 (6.6)	929.0 (144)	521.0 (205.1)	231.1 (91)	variable	rotating (contoured)	15a
Z33I	401F-16	--	--	--	--	--	--	rotating Z33C removed	15a
Z48	401F-16E	449.6 (177)	**	**	221.0 (87.0)	231.1 (91)	fwd of F.S. 381 (150) Down 1°27'	forebody (faired ogee)	13
Z49	401F-16E	511.8 (201.5)	**	**	158.8 (62.5)	231.1 (91)	fwd of F.S. 381(150) Down 1°27'	forebody (faired ogee)	13
Z50	401F-16E	511.8 (201.5)	**	**	158.8 (62.5)	231.1 (91)	fwd of F.S. 381(150) Down 1°27'	forebody (modified faired delta)	13
Z55	YF-16	383.5 (151)	**	**	254.0 (100)	231.1 (91)	fwd of F.S. 444.5(175) Down 45'	forebody (faired)	14
Z56	YF-16	383.5 (151)	**	**	254.0 (100)	231.1 (91)	fwd of F.S. 444.5(175) Down 45'	forebody (faired ogee)	14
Z57	YF-16	302.3 (119)	48.3 (19)	11367.7 (1762)	368.3 (145)	231.1 (91)	variable	rotating (faired gothic)	16
Z58	YF-16	233.7 (92)	48.3 (19)	7387.1 (1145)	436.9 (172)	231.1 (91)	variable	rotating (faired ogee)	16

Table 1 (Continued)

NO.	CONFIG.	LENGTH cm(in)	MAXIMUM WIDTH cm (in)	A_{exp}/SIDE cm^2(in^2)	L.E. POSITION			TYPE	FIGURE
					F.S. cm(in)	W.L. cm(in)	CANT		
Z63+	YF-16 + 30.5 Stretch	416.6 (164)	**	**	254.0 (100.0)	231.1 (91.0)	fwd of F.S. 381 (150) Down 1°	forebody (faired ogee)	18
Z64+	YF-16 + 30.5 Stretch	495.3 (195)	**	**	176.5 (69.5)	231.1 (91.0)	fwd of F.S. 381 (150) Down 1°	forebody (faired ogee)	18a
Z65+	YF-16 + 30.5 Stretch	495.3 (195)	**	**	176.5 (69.5)	231.1 (91.0)	fwd of F.S. 381 (150) Down 1°	forebody (faired ogee)	18a
Z66+	YF-16 + 30.5 Stretch	495.3 (195)	**	**	176.5 (69.5)	231.1 (91.0)	fwd of F.S. 381 (150) Down 1°	forebody (faired ogee)	18a
Z67+	YF-16 + 44.5 Stretch	416.6 (164.0)	**	**	254.0 (100.0)	231.1 (91.0)	fwd of F.S. 381 (150) Down 1°	forebody (faired ogee)	18a
Z68+	YF-16 + 44.5 Stretch	530.9 (209.0)	**	**	141.0 (55.5)	231.1 (91.0)	fwd of F.S. 381 (150) Down 1°	forebody (faired ogee)	18a
Z69+	YF-16 + 44.5 Stretch	530.9 (209)	**	**	141.0 (55.5)	231.1 (91.0)	fwd of F.S. 381 (150) Down 1°	forebody (faired ogee)	18a
Z70+	YF-16 + 44.5 Stretch	530.9 (209)	**	**	141.0 (55.5)	231.1 (91.0)	fwd of F S. 381 (150) Down 1°	forebody (faired ogee)	18a
Z71+	YF-16 + 30.5 Stretch	495.3 (195)	**	**	176.5 (69.5)	231.1 (91.0)	fwd of F.S. 381 (150) Down 1°	forebody (faired ogee)	18a
Z72+	YF-16 + 30.5 Stretch	571.2 (224.9)	**	**	99.6 (39.2)	231.1 (91.0)	fwd of F.S. 381 (150) Down 1°	forebody (faired ogee)	18a
Z73	YF-16 + 30.5 Stretch	54.6 (21.5)	4.1 (1.6)	193.5 (30)	-77.5 (-30.5)	209.3 (82.4)	0	nose	18b
Z74	YF-16 + 30.5 Stretch	54.6 (21.5)	7.9 (3.1)	387.1 (60)	-77.5 (-30.5)	209.3 (82.4)	0	nose	18b
Z75+	YF-16 + 30.5 Stretch	571.2 (224.9)	**	**	99.6 (39.2)	231.1 (91)	fwd of F.S. 381 (150) Down 1°	forebody (faired ogee)	18
Z76+	YF-16	57.2 (22.5)	8.4 (3.3)	451.6 (70)	20.3 (8)	217.7 (85.7)	-3°30'	nose	17
Z77	YF-16	123.7 (48.7)	9.4 (3.7)	1058.1 (164)	20.3 (8)	217.7 (85.7)	-3°30'	nose	17

Table 1 (Continued)

NO.	CONFIG.	LENGTH cm(in)	MAXIMUM WIDTH cm(in)	A_{exp}/SIDE cm²(in²)	L.E. POSITION			TYPE	FIGURE
					F.S. cm (in)	W.L. cm(in)	CANT		
Z79	YF-16	116.1 (45.7)	26.7 (10.5)	1567.7 (243)	144.0 (56.7)	225.3 (88.7)	-1°	canard (flat delta)	17
Z80+	YF-16 + 30.5 Stretch	571.2 (224.9)	**	**	99.6 (39.2)	231.1 (91)	fwd of F.S. 381 (150) Down 1°	forebody (faired ogee)	18
Z81	YF-16 + 30.5 Stretch	58.4 (23.0)	15.7 (6.2)	922.6 (143)	129.5 (51)	228.6 (90)	0	canard (flat delta)	18b
Z82	YF-16	104.9 (41.3)	15.2 (6.0)	735.5 (114)	144.0 (56.7)	225.3 (88.7)	-1°	canard (flat delta)	17
Z84	YF-16 + 30.5 Stretch	129.0 (50.8)	28.4 (11.2)	1806.4 (280)	131.6 (51.8)	228.6 (90)	0	canard (flat delta)	18b
Z86+	YF-16	62.0 (24.4)	26.7 (10.5)	858.1 (133)	198.1 (78.0)	226.1 (89)	-1°	canard (flat delta)	17
Z87	YF-16 + 30.5 Stretch	416.6 (164.0)	**	**	254.0 (100.0)	231.1 (91)	fwd of F.S. 381 (150) Down 1°	forebody (faired ogee)	18b
Z88	YF-16 + 30.5 Stretch	416.6 (164.0)	**	**	254.0 (100)	231.1 (91)	fwd of F.S. 381 (150) Down 1°	forebody (faired ogee)	18b
Z89	YF-16 + 30.5 Stretch	391.2 (154)	**	**	279.4 (110)	231.1 (91)	fwd of F.S. 381 (150) Down 1°	forebody (faired ogee)	18b
Z100+	F16	81.3 (32.0)	8.3 (3.25)	483.9 (75)	-49.8 (-19.6)	209.3 (82.4)	-2°30'	nose	20a
Z101	YF-16 + 30.5 Stretch	391.2 (154.0)	**	**	279.4 (110)	231.1 (91)	fwd of F.S. 381 (150) Down 1°	forebody (faired ogee)	18b
Z102	YF-16	416.0 (164.0)	**	**	254.0 (100)	231.1 (91)	fwd of F.S. 444.5(175) Down 1°	forebody (faired ogee)	19 (same planform as Z104)
Z103 +	F-16	416.6 (164.0)	**	**	254.0 (100)	231.1 (91)	fwd of F.S. 419.1(165) Down 1°	forebody (faired ogee)	19
Z104	F-16	430.0 (169.3)	**	**	240.5 (94.7)	231.1 (91)	fwd of F.S. 419.1(165) Down 1°	forebody (faired ogee)	19

39

Table 1 (Continued)

NO.	CONFIG.	LENGTH cm(in)	MAXIMUM WIDTH cm(in)	A_{exp}/SIDE cm²(in²)	L.E. POSITION F.S. cm(in)	W.L. cm(in)	CANT	TYPE	FIGURE
Z105	F-16	442.0 (174.0)	**	**	228.6 (90)	231.1 (91)	fwd of F.S. 419.1(165) Down 1°	forebody (faired ogee)	19
Z106	YF-16 + 30.5 Stretch	533.4 (210)	**	**	137.2 (54)	231.1 (91)	fwd of F.S. 381(150) Down 1°	forebody (faired ogee)	18b
Z107	F-16	378.5 (149)	**	**	292.1 (115)	231.1 (91)	fwd of F.S. 419.1(165) Down 1°	forebody (faired ogee)	19
Z108	F-16	340.4 (134)	**	**	330.2 (130)	231.1 (91)	fwd of F.S. 419.1(165) Down 1°	forebody (faired ogee)	19
Z109	F-16	340.4 (134)	**	**	330.2 (130)	231.1 (91)	fwd of F.S. 419.1(165) Down 1°	forebody (faired ogee)	19
Z110 +	F-16	238.0 (93.7)	7.9 (3.1)	1200.0 (186.0)	-66.8 (-26.3)	209.3 (82.4)	-2°30'	nose	20a
Z111 +	F-16	225.3 (88.7)	7.9 (3.1)	1083.9 (168.0)	-51.3 (-20.2)	209.3 (82.4)	-2°30'	nose	20a
Z112 +	F-16	99.1 (39.0)	8.4 (3.3)	667.7 (103.5)	-66.9 (-26.35)	209.3 (82.4)	-2°30'	nose	20a
Z113 +	F-16	194.3 (76.5)	5.3 (2.1)	696.8 (108.0)	-51.8 (-20.4)	209.3 (82.4)	-2°30'	nose	20a
Z114 +	F-16	83.8 (33.0)	5.0 (1.95)	343.2 (53.2)	-49.0 (-19.3)	209.3 (82.4)	-2°30'	nose	20a
Z115 +	F-16	96.5 (38.0)	6.1 (2.4)	327.7 (50.8)	-52.5 (-20.65)	209.3 (82.4)	-2°30'	nose	20a
Z117	F-16	81.3 (32.0)	8.3 (3.25)	483.9 (75)	-49.8 (-19.6)	209.3 (82.4)	-2°30';aft 35.6(14) +2°30'	nose	20a
Z120 +	F-16 (F-16A Production Strake)	430.5 (169.5)	**	**	240.0 (94.5)	231.1 (91)	fwd of F.S. 419.1(165) down 1°	forebody	19
Z121	F-16	378.5 (149)	**	**	292.1 (115)	231.1 (91)	fwd of F.S. 419.1(165) Down 1°	forebody	19
Z123	F-16	55.4 (21.8)	7.9 (3.1)	417.4 (64.7)	-10.9 (-4.3)	209.3 (82.4)	-2°30'	nose	20b

Table 1   (Continued)

NO.	CONFIG.	LENGTH cm(in)	MAXIMUM WIDTH cm (in)	A_{exp}/SIDE cm^2(in^2)	L.E. POSITION			TYPE	FIGURE
					F.S. cm(in)	W.L. cm(in)	CANT		
Z124 +	F-16	89.4 (35.2)	7.6 (3.0)	572.3 (88.7)	-45.2 (-17.8)	209.3 (82.4)	-2°30'	nose	20b
Z125	F-16	66.0 (26.0)	6.6 (2.6)	324.0 (51)	-21.6 (-8.5)	209.3 (82.4)	-2°30'	nose	20b
Z126	F-16	55.3 (21.78)	7.4 (2.9)	283.9 (44)	-39.9 (-15.71)	209.3 (82.4)	-2°30'	nose	20b
Z127	F-16	66.0 (26.0)	3.8 (1.5)	238.7 (37)	-21.6 (-8.5)	209.3 (82.4)	-2°30'	nose	20b
Z128 +	F-16	89.4 (35.2)	7.6 (3.0)	572.3 (88.7)	-45.2 (-17.8)	209.3 (82.4)	+2°30'	nose	20b
Z131 +	F-16	84.3 (33.2)	7.1 (2.8)	557.4 (86.4)	-39.9 (-15.7)	209.3 (82.4)	-2°30'	nose	20c
Z131A +	F-16	71.6 (28.2)	7.1 (2.8)	461.9 (71.6)	-39.9 (-15.7)	209.3 (82.4)	-2°30'	nose	20c
Z131B +	F-16	39.9 (15.7)	7.1 (2.8)	205.8 (31.9)	-39.9 (-15.7)	209.3 (82.4)	-2°30'	nose	20c
Z132	F-16	33.5 (13.2)	6.1 (2.4)	128.4 (19.9)	-33.5 (-13.2)	209.3 (82.4)	-2°30'	nose	20c
Z133	F-16	77.5 (30.5)	2.5 (1.0)	23.2 (3.6)	-33.0 (-13.0)	209.3 (82.4)	-2°30'	nose	20c

+ Data presented in this volume.
* Leading edge when all of strake is canted, position of horizontal portion when nose is canted up or down.
** Blended configuration, A_{exp} and width are not defined.
*** Maximum exposed width per side.

Table 2   YF-16 & F-16 DEVELOPMENTAL FORCE TESTS

Model	Tunnel/Test No.	Dates	Hours	General Dynamics Report
1/15 ADF 401F -1	CAL T03-153	8/3-8/12/71	76.0	FZT-205
1/15 ADF 401F	GDLST 594-0	8/19-8/21/71	22.5	FZT-200
1/15 ADF 401F	GDHST 319-0	8/23-8/26/71	16.3	FZT-202
1/15 ADF 401F -2, -3	CAL T03-163	9/10-9/15/71	71.0	FZT-206
1/15 ADF 785/786	CAL T03-173	9/15-9/20/71	70.25	FZT-208
1/15 ADF 401F -2	CAL T03-183	9/23-9/25/71	40.0	FZT-206
1/15 ADF 401F-4	CAL T03-193	10/6-10/11/71	39.5	FZT-209
1/15 ADF 401F-5	CAL T03-193	10/13-10/19/71	37.5	FZT-210
1/15 ADF 785	CAL T03-193	10/19-10/21/71	33.5	FZT-208
1/15 ADF 401FS-3	CAL T03-203	10/21-10/25/71	29.25	FZT-207
1/15 ADF 786	CAL T03-203	10/29-10/29/71	13.0	FZT-208
1/15 ADF 401F-5	CAL T03-213	11/12-11/15/71	24.0	FZT-210
1/15 ADF 401F-10A,5A	CAL T03-213	11/17-11/23/71	92.5	FZT-211
1/15 ADF 401F-16	CAL T03-223	12/7-12/13/71	78.0	FZT-212
1/15 ADF 401F-16,5A	GDLST 594-1	12/14-12/30/71	122.0	FZT-228
	GDLST 594-2		8.0	FZT-228
	GDHST 319-2		53.0	FZT-227
1/15 ADF 401F-16	CAL T03-233	1/3-1/7/72	69.5	FZT-212
1/15 ADF 401F-16	GDLST 594-3	1/11-1/18/72	80.0	FZT-228
	GDHST 319-3		14.0	FZT-227
1/15 ADF 401F-16E	CAL T03-253	1/27-2/3/72 2/5-2/7/72	127.0	FZT-224
1/15 ADF 401F-16	CAL T03-243	2/3-2/5/72	22.0	FZT-225
1/15 ADF 401F-16E	ARC 11-652-1	2/25-2/29/72	50.0	FZT-401-003
1/15 ADF 401F-16E	GDHST 319-4	5/2-5/9/72	34.0	FZT-401-012
1/15 ADF 401F-16E	GDLST 613-0	5/10-5/12/72	54.0	FZT-401-013
1/15 ADF 401F-16E	CAL T03-273	5/16-5/19/72	34.0	FZT-401-004
1/15 YF-16	CAL T03-283	7/12-7/17/72	35.0	FZT-401-010
1/15 YF-16	CAL T03-293	7/17-7/20/72	61.75	FZT-401-011

Table 2   (Continued)

Model	Tunnel/Test No.	Dates	Hours	General Dynamics Report
1/15 YF-16	LRC 4-996	8/14-8/25/72	75.0	FZT-401-016
1/15 YF-16	CAL T03-303	9/14-9/18/72	24.0	FZT-401-014
1/15 YF-16	CAL T03-313	9/18-9/19/72	8.0	FZT-233
1/15 YF-16	ARC 66-638-1	10/9-10/23/72	232.0	FZT-401-022
1/9 YF-16	ARC 12-680	10/16-10/26/72	100.0	FZT-401-021
1/15 YF-16 (SCW)	LRC 8-623	10/24-11/8/72	200.0	FZT-229
1/15 YF-16	ARC 66-628-2	11/15-11/22/72	76.0	FZT-401-022
1/9 YF-16	ARC-11-678-3	11/6-11/10/72	80.0	FZT-235
1/9 YF-16	ARC-11-688	11/13-11/23/72	210.0	FZT-401-015
1/15 YF-16 (SCW)	LRC-8-628	12/4-12/15/72	150.0	FZT-229
1/9 YF-16	GDLST 624	12/11-12/19/72	91.0	FZT-401-019
1/9 YF-16	GDLST 625	12/13-12/15/72	30.0	FZT-234
1/9 YF-16	CAL T03-323	12/27-12/29/72	24.0	FZT-401-020
1/15 YF-16	ARC-66-638-3	1/22-2/7/73	100.0	FZT-401-022
1/15 YF-16 (SCW)	LRC 4-1024	2/26-3/2/73	40.0	FZT 242
1/15 YF-16 (Stores)	GDLST 648	1/4-1/7/74	25.5	FZT-401-025
1/9 YF-16	GDLST 641-1	1/11/74	5.0	FZT-620-001
1/9 YF-16 (Ground Board)	GDLST 650	1/31-2/4/74	29.5	FZT-401-026
1/15 YF-16 (Stores)	CAL T03-333	2/21-2/27/74	54.5	FZT-401-027
1/15 YF-16 (Stores)	CAL T03-343	2/27-3/1/74	27.0	FZT-401-027
1/15 YF-16 + 30.5 Stretch, + 44.5 Stretch	GDLST 662-0	7/23-7/30/74	53.5	FZT-401-040
1/15 YF-16 + 30.5 Stretch	CAL T03-363	8/9-8/21/74	102.5	FZT-401-032
1/9 YF-16 + 30.5 Stretch	GDLST 664	8/26-8/30/74	51.5	FZT-401-041
1/15 YF-16 + 30.5 Stretch	GDHST 375-0	9/5-9/12/74	47.3	FZT-401-039

Table 2 (Continued)

Model	Tunnel/Test No.	Dates	Hours	General Dynamics Report
1/15 YF-16 + 30.5 Stretch	CAL T03-373	9/18-9/19/74	33.0	FZT-401-032
1/15 YF-16(Wing-lets)	CAL T03-383	9/20/74	11.75	FZT-401-032
1/15 YF-16(Bicon-vex)	CAL T03-393	9/21/74	13.25	FZT-401-032
1/15 YF-16 + 30.5 Stretch	AEDC TF-357	10/12-10/30/74	122.7	FZT-401-038
1/15 YF-16 + 30.5 Stretch, F-16	GDLST 677-0	2/10-2/13/75	58.0	16PR029
1/15 YF-16, F-16	CAL T03-403	2/18-2/22/75	44.75	16PR029
1/15 F-16	GDLST 677-1	2/24-2/25/75	25.5	16PR029
1/15 F-16	GDHST 385-0	2/25-2/28/75	23.5	16PR029
1/9 F-16	GDLST 681-0	4/25-4/27/75	22.5	16PR047
1/9 F-16	AEDC TF-380	5/1-5/14/75	153.7	16PR048
1/9 F-16	AEDC SF-175	5/15-5/18/75	43.7	16PR048
1/9 F-16	ARC 12-082-1	5/27-6/4/75	77.75	None
1/9 F-16	GDLST 681-1	6/6-6/26/75	135.5	16PR137
1/15 F-16	GDHST 385-1	7/7-7/11/75	19.6	16PR082
1/15 F-16	GDLST 677-2	7/18-7/21/75	20.0	16PR082
1/9 F-16	AEDC TF-390	8/21-9/9/75	224.0	16PR134
1/15 YF-16 (AIM 7)	LTV VSD 564	10/16-10/20/75	50.0	FZT-272
1/9 F-16	AEDC SF-177	10/27-11/4/75	67.5	16PR134
1/15 F-16(Stores)	CAL T03-443	11/4-11/15/75	131.5	FZT-271
	CAL T03-453			
1/15 F-16	LRC 4-1140	12/3-12/14/75	128.1	FZT-276
1/9 F-16	GDLST 690-0	1/20-1/30/76	51.0	16PR222
1/9 F-16	GDLST 690-1	2/13-2/20/76	48.0	FZT-280

Table 2   (Continued)

Model	Tunnel/Test No.	Dates	Hours	General Dynamics Report
1/9 F-16(AIM 7)	GDLST 690-2	2/25-2/26/76	9.5	FZT-280
1/15 F-16(AIM 7)	LRC 4-1146	3/8-3/19/76	96.0	FZT-282
1/15 F-16(AIM 7)	CAL T03-483	3/15-4/5/76	66.0	FZT-285
1/9 F-16	GDLST 695-0	4/19-4/23/76	33.5	16PR299
1/9 F-16 (Stores)	AEDC TF-406	5/7-5/29/76	234.1	16PR331
1/15 F-16 (Stores)	LRC 4-1172	11/4-11/17/76	54.0	FZT-293
1/15 F-16	LRC 4-1174	11/12/76	9.0	FZT-293
1/15YF-16,F-16	LRC 4-1180	12/6-12/10/76	46.0	FZT-294
1/9 F-16 (Stores)	AEDC TF-451	4/29-5/11/77	108.6	16PR814
1/9 F-16(AIM 7)	GDLST 721-0	7/11-7/12/77	18.0	FZT-318
1/9 F-16(Pave Penny)	GDLST 709-0	7/13-7/15/77	24.0	16PR761
1/9 F-16(Drag Chute)	GDLST 708-0	7/18-7/19/77	20.0	16PR761
1/9 F-16(Spin Chute)	GDLST 724-0	7/19-7/20/77	9.0	16PR761
1/15 F-16	LRC 4-1216	8/22-8/26/77	32.0	FZT-309

Table 3   WIND TUNNEL TESTS USED FOR STRAKE ANALYSIS

SPEED	TUNNEL	TEST	TEST CODE FOR PLOTS	STRAKES
Low	GDLST	594-1	5941	Z22,Z22A,Z29,Z29A,Z31,Z33,Z33A',Z33B'
		594-3	5943	Z29,Z33,Z33A-Z33I
		613-0	6130	Z33,Z50
		625-0	6250	Z55,Z56,Z57,Z58
		662	6620	Z33,Z63-Z66,Z67-Z70
		664	6640	Z63,Z64,Z72,Z74-Z77,Z79,Z80,Z82,Z84,Z86-Z89
		677-0	6770	Z63,Z87,Z100-Z106
		677-1	6771	Z103,Z107-Z115,Z117
		677-2 *	6672	Z124
		681-1 *	6811	Z79,Z120,Z123-Z128
		690-1 *	6901	Z131,Z131A,Z131B,Z132,Z133
Transonic	CALSPAN	T03-163	1630	Z1
		T03-173	1730	OFF
		T03-183	1830	Z1A,Z2
		T03-193	1930	Z1B,Z3,Z5
		T03-193	1931	Z7,Z8,Z9,Z10
		T03-193	1932	Z1A,Z1B,Z3,Z4,Z4A,Z4B,Z5,Z14,Z16,Z17,Z18
		T03-203	2031	Z7
		T03-213	2130	Z1A,Z22,Z23
		T03-213	2131	Z1A,Z20,Z21,Z22,Z24,Z25,Z26,Z27
		T03-223	2230	Z28,Z29,Z30,Z31,Z32
		T03-233	2330	Z31,Z33
		T03-253	2530	Z33,Z48,Z49,Z50
		T03-273	2730	Z33,Z50
		T03-363	3630	Z1D,Z63-Z66,Z71-Z75,Z80,Z81
		T03-403	4030	Z100,Z102,Z103,Z108,Z109
		T03-443 *	4430	Z124
	AEDC 16T	TF-390 *	3900	Z128
Supersonic	HST	375-0	3750	Z63,Z64,Z87,Z88
	LRC	4-1140 *	1140	Z124

* contains data for F-16 production strake/wing/fuselage
configuration

Table 4   TEST PARAMETERS

STRAKE	WING	CONFIGURATION (1) (2)	LS PITCH LEF 0	LEF 15	LEF 25	LEF 35	HT OFF	HT -25	HT -20	HT -10	HT 0	HT 25	LS SIDESLIP LEF 0	LEF 25	HT 0	TR PITCH LEF 0	LEF 5	LEF 10	LEF 15	LEF 25	HT -30	HT -20	HT -10	HT 0	MACH .6	.8	.9	1.2	1.6	2.0	TR SIDESLIP LEF 0	LEF 5	LEF 10	LEF 15	LEF 25	HT 0	MACH .8	.9	1.2	2.0	NASA CR-158922 FIGURE NUMBERS
Z1	W3	401F-2(TV)																	x					x	x										x	x	x					3-1, 4-1
Z1A	W3	401F-5	x					x					x											x	x		x				x			x	x	x			x		3-2,3-3,3-4,3-12,3-13, 3-40,3-41,4-7,4-8,4-9, 4-10,4-15,4-16
		401F-2(TV@15°)	x										x											x	x		x				x				x	x	x		x		3-5,3-7,4-4,4-5
		401F-2											x											x	x										x	x	x				3-6,4-6
		401F-2(TV@7.5)											x																		x				x	x	x		x		4-2,4-3
		401F-10A	x					x					x											x	x		x							x		x	x				3-36,3-37,3-38,4-34
Z1B	W3	401F-5	x										x											x	x		x				x	x			x	x		x		3-12,3-13,4-15,4-16
		401F-4(TV)	x										x																		x				x	x		x		4-12,4-14
Z1D	W3BB	YF-16+30.5Str.	x							x			x						x	x	x			x	x		x				x			x	x		x		3-74,3-75,3-76,3-77,4-51, 4-52
Z2	W3	401F-2(TV)	x										x											x	x		x								x	x				3-8,4-11
Z3	W3	401F-4(TV)	x										x							x	x	x			x		x				x			x	x	x	x		3-9,3-10,3-11,4-12,4-13, 4-14
		401F-5	x										x											x	x		x				x	x			x	x		x		3-12,3-13,4-15,4-16
Z4	W3	401F-5	x					x	x	x			x											x	x		x				x		x	x	x	x	x		x		3-14,3-16,3-17,3-18,3-19, 3-20,3-21,3-22,3-23,4-17, 4-18,4-19,4-20,4-21
Z4A	W3	401F-5	x						x				x											x	x		x							x		x	x				3-18,3-19,3-20,4-17
Z4B	W3	401F-5	x						x				x											x	x		x							x		x	x				3-18,3-19,3-20,4-17
Z5	W3	401F-5	x					x					x											x	x		x				x			x		x	x		x		3-21,3-22,3-23,4-18,4-19
	W3	401F-4(TV)											x																		x				x	x		x		4-22,4-23
Z7	W6	785	x	x		x		x	x	x	x		x						x	x	x			x	x		x				x	x	x	x		x	x		x		3-24,3-25,3-26,3-27,3-28, 3-30,4-24,4-25,4-26,4-27, 4-28
		786(TV)	x	x	x	x							x						x	x	x			x	x		x				x	x	x	x		x	x		x		3-31,3-32,3-33,3-34,3-29, 4-30,4-31,4-32,4-58
Z8	W6	785	x										x											x	x		x				x				x	x		x		3-24,3-25,4-24,4-25
Z9	W6	785	x										x											x	x		x				x				x	x		x		3-24,3-25,4-24,4-25
Z10	W6	785	x	x		x							x						x	x	x			x	x		x				x	x	x	x		x	x		x		3-24,3-25,3-26,3-27,4-24, 4-25,4-26,4-27,4-28
Z14	W3	401F-5		x									x		x									x	x						x				x	x				3-35,4-33
Z16	W3	401F-5		x									x		x									x	x						x				x	x				3-35,4-33
Z17	W3	401F-5		x									x		x									x	x						x				x	x				3-35,4-33
Z18	W3	401F-5		x									x		x									x	x						x				x	x				3-35,4-33
Z20	W3	401F-10A	x	x		x							x		x		x							x	x						x		x	x	x				3-36,3-37,3-38,3-39,4-34, 4-35
Z21	W3	401F-10A	x	x		x							x		x		x							x	x						x		x	x	x				3-36,3-37,3-38,3-39,4-34, 4-35

47

Table 4 (Continued)

STRAKE	WING	CONFIGURATION	LS PITCH LEF 0	LS PITCH LEF 15	LS PITCH LEF 25	LS PITCH LEF 35	LS PITCH HT OFF	LS PITCH HT -25	LS PITCH HT -20	LS PITCH HT -10	LS PITCH HT 0	LS PITCH HT 25	LS SIDESLIP LEF 0	LS SIDESLIP LEF 25	LS SIDESLIP HT 0	TR PITCH LEF 0	TR PITCH LEF 5	TR PITCH LEF 10	TR PITCH LEF 15	TR PITCH LEF 25	TR PITCH HT -30	TR PITCH HT -20	TR PITCH HT -10	TR PITCH HT 0	TR PITCH MACH .6	TR PITCH MACH .8	TR PITCH MACH .9	TR PITCH MACH 1.2	TR PITCH MACH 1.6	TR PITCH MACH 2.0	TR SIDESLIP LEF 0	TR SIDESLIP LEF 5	TR SIDESLIP LEF 10	TR SIDESLIP LEF 15	TR SIDESLIP LEF 25	TR SIDESLIP HT 0	TR SIDESLIP MACH .8	TR SIDESLIP MACH .9	TR SIDESLIP MACH 1.2	TR SIDESLIP MACH 2.0	NASA CR-158922 FIGURE NUMBERS
Z22	W3	401F-5			x					x	x					x	x							x	x																1-1,1-2,3-40,3-41
Z22A	W3	401F-5			x					x	x																														1-1,1-2
Z23	W3	401F-5														x	x							x	x																3-40,3-41
Z24	W3	401F-10A														x	x	x						x	x	x					x						x	x	x	x	3-42,3-43,3-44,3-45,3-46,4-36,4-37,4-38
Z25	W3	401F-10A														x	x	x						x	x	x					x						x	x	x	x	3-42,3-43,3-44,3-45,3-46,4-36,4-37,4-38
Z26	W3	401F-10A														x	x	x						x	x	x					x						x	x	x	x	3-42,3-43,3-44,3-45,3-46,4-36,4-37,4-38
Z27	W3	401F-10A														x	x	x						x	x	x					x						x	x	x		3-42,3-44,3-45,3-46,4-36,4-37
Z28	W3	401F-16														x	x	x						x	x						x						x	x	x		3-47,3-48,3-49,4-39,4-40
Z29	W3	401F-16			x										x	x	x	x						x	x						x						x	x	x		1-3,3-47,3-48,3-49,3-50,3-51,4-39,4-40,4-41,4-42
Z29A	W3	401F-16			x										x																										1-3
Z30	W3	401F-16														x	x	x						x	x						x						x	x	x		3-47,3-48,3-49,4-39,4-40
Z31	W3	401F-16														x	x	x						x	x						x						x	x	x		3-47,3-48,3-49,3-52,3-53,3-54,4-39,4-40,4-43,4-44
Z32	W3	401F-16															x	x						x	x						x						x	x	x		3-50,3-51,4-41,4-42
Z33	W3	401F-16	x		x	x			x	x	x			x	x	x	x	x						x	x						x						x	x	x		1-5,1-6,1-8,1-9,2-1,3-52,3-53,3-54,4-43,4-44
	W3BB	401F-16E														x	x							x	x	x	x	x													3-55,3-56,3-57,3-58,3-59,3-60
Z33A	W3	401F-16			x					x																															1-5
Z33A'	W3	401F-16			x					x																															1-4
Z33B	W3	401F-16			x					x																															1-5
Z33B'	W3	401F-16			x					x																															1-4
Z33C	W3	401F-16			x					x	x																														1-5,1-7
Z33D	W3	401F-16			x					x																															1-5
Z33E	W3	401F-16			x					x																															1-6
Z33F	W3	401F-16			x					x																															1-6
Z33G	W3	401F-16			x					x																															1-6
Z33H	W3	401F-16			x					x																															1-6
Z33I	W3	401F-16			x							x																													1-7
Z48	W3BB	401F-16E															x									x			x												3-60
Z49	W3BB	401F-16E															x									x			x												3-60
Z50	W3	401F-16	x	x						x				x	x																										1-8,1-9,2-1
	W3BB	401F-16E														x	x							x	x	x	x	x													3-55,3-56,3-57,3-58,3-59,3-60
Z55	W3BB	YF-16		x											x																										1-10

Table 4 (Continued)

STRAKE	WING	CONFIGURATION	LS PITCH LEF 0	15	25	35	OFF	LS PITCH HT -25	-20	-10	0	25	LS SIDESLIP LEF 0	25	LS SIDESLIP HT 0	TR PITCH LEF 0	5	10	15	25	TR PITCH HT -30	-20	-10	0	MACH .6	.8	.9	1.2	1.6	2.0	TR SIDESLIP LEF 0	5	10	15	25	TR SIDESLIP HT 0	MACH .8	.9	1.2	2.0	NASA CR-158922 FIGURE NUMBERS
Z56	W3BB	YF-16	x										x																													1-10
Z57	W3BB	YF-16	x										x																													1-11
Z58	W3BB	YF-16	x										x																													1-11
Z63	W3BB	YF-16+30.5Str	x	x				x	x	x		x	x	x	x	x								x	x	x	x	x	x	x			x	x				x		1-12,1-14,1-15,1-16,1-23,1-24,1-25,1-26,1-27,1-30,1-32,1-33,2-2,3-61,3-62,3-64,3-65,3-66,3-91,3-98,3-69,3-74,3-75,3-76,3-77,4-45,4-46,4-49,4-50,4-51,4-52,2-3,2-4,2-10,2-11,2-13,2-16
		YF-16+30.5Str +N6											x	x	x																											
Z64	W3BB	YF-16+30.5Str	x	x							x	x	x	x	x	x								x	x	x	x	x	x	x			x	x						1-12,1-17,1-18,1-23,1-24,2-2,2-9,3-61,3-62,3-63,3-64,3-65,3-66,4-45,4-46
		YF-16+30.5Str +N6		x									x																													2-3
Z65	W3BB	YF-16+30.5Str.		x									x	x	x	x								x	x	x	x						x				x		x		1-12,2-2,3-61,3-62,3-63,3-64,4-45
Z66	W3BB	YF-16+30.5Str.	x	x				x	x	x		x	x	x	x	x								x	x	x	x						x				x		x		1-12,1-14,1-15,1-16,2-2,3-61,3-62,3-63,3-64,4-45,4-46
		YF-16+30.5Str. +N6											x	x																												2-4,2-6
Z67	W3BB	YF-16+44.5Str.	x	x							x	x	x	x																												1-13,1-19,1-20,2-7
		YF-16+44.5Str. +N6											x	x																												2-8
Z68	W3BB	YF-16+44.5Str.	x	x							x	x	x	x																												1-13,1-17,1-18,2-7,2-9
Z69	W3BB	YF-16+44.5Str.		x							x		x	x																												1-13,2-7
Z70	W3BB	YF-16+44.5Str.	x	x							x	x	x	x																												1-13,1-19,1-20,2-7
		YF-16+44.5Str +N6											x	x																												2-8
Z71	W3BB	YF-16+30.5Str														x								x		x	x	x					x	x				x		3-61,3-62,3-63,3-64,4-45,4-46
Z72	W3BB	YF-16+30.5Str		x							x	x	x	x	x	x								x		x	x	x					x	x				x		1-23,1-24,2-3,3-70,3-71,3-72,3-73,4-47,4-48
Z73	W3BB	YF-16+30.5Str														x								x		x	x	x					x	x				x		3-67,3-68,3-69,4-49,4-50
Z74	W3BB	YF-16+30.5Str	x	x							x		x	x	x	x								x		x	x	x					x	x				x		1-25,1-26,2-10,2-11,3-67,3-68,3-69,4-49,4-50
Z75	W3BB	YF-16+30.5Str		x							x	x	x	x	x	x								x		x	x	x					x	x				x		1-28,1-29,2-12,3-70,3-71,3-72,3-73,4-47,4-48
Z76	W3BB	YF-16		x							x	x	x	x																												1-21,1-22,2-14
Z77	W3BB	YF-16											x	x																												2-15
Z79	W3BB	YF-16											x	x																												2-15

Table 4 (Continued)

50

Column groups — LOW SPEED: PITCH [LEF: 0,15,25,35 · OFF · HT: -25,-20,-10,0,25] · SIDESLIP [LEF: 0,25 · HT: 0]. TRANSONIC: PITCH [LEF: 0,5,10,15,25 · HT: -30,-20,-10,0 · MACH: .6,.8,.9,1.2,1.6,2.0] · SIDESLIP [LEF: 0,5,10,15,25 · HT: 0 · MACH: .8,.9,1.2,2.0].

STRAKE	WING	CONFIGURATION	LS P LEF 0	LS P LEF 15	LS P LEF 25	LS P LEF 35	LS P OFF	LS P HT -25	LS P HT -20	LS P HT -10	LS P HT 0	LS P HT 25	LS S LEF 0	LS S LEF 25	LS S HT 0	TR P LEF 0	TR P LEF 5	TR P LEF 10	TR P LEF 15	TR P LEF 25	TR P HT -30	TR P HT -20	TR P HT -10	TR P HT 0	TR P M .6	TR P M .8	TR P M .9	TR P M 1.2	TR P M 1.6	TR P M 2.0	TR S LEF 0	TR S LEF 5	TR S LEF 10	TR S LEF 15	TR S LEF 25	TR S HT 0	TR S M .8	TR S M .9	TR S M 1.2	TR S M 2.0	NASA CR-158922 FIGURE NUMBERS
Z80	W3BB	YF-16+30.5Str.		x							x	x	x		x	x				x				x	x	x	x				x			x		x			x		1-28,1-29,2-12,3-70,3-71, 3-72,3-73,4-47,4-48
Z81	W3BB	YF-16+30.5Str.														x				x				x	x	x	x				x			x		x			x		3-74,3-75,3-76,3-77,4-51, 4-52
Z82	W3BB	YF-16											x		x																										2-15
Z84	W3BB	YF-16+30.5Str.		x							x	x	x		x																										1-26,1-27,2-11
Z86	W3BB	YF-16		x									x		x																										1-21,2-14
Z87	W3BB	YF-16+30.5Str.	x	x							x	x	x	x	x	x								x				x	x												1-28,1-29,1-30,1-32,1-33, 2-12,2-13,2-16,3-65,3-66
Z88	W3BB	YF-16+30.5Str.			x										x	x								x				x	x												1-31,1-57,3-65,3-66
Z89	W3BB	YF-16+30.5Str.			x										x																										1-31
Z100	W3BB	YF-16		x									x		x																										1-34,2-17
Z100	W24	F-16														x								x		x										x	x		x		3-78,4-53
Z101	W3BB	YF-16+30.5Str.		x									x		x																										1-32,1-33,2-16
Z102	W3BB	YF-16											x		x																										2-17
Z103	W3BB	F-16	x	x							x	x	x	x	x	x								x				x	x												1-35,1-36,1-37,2-18,2-20, 2-21,3-78,3-79,3-80,3-81, 3-82,4-53
Z103	W24	F-16	x	x							x	x	x	x	x																										1-38,1-39,1-40,1-41,1-44, 2-19,2-20,2-22
Z103		F-16+Z112		x									x		x																										1-42,1-43,2-23
Z104	W3BB	F-16		x							x	x	x		x																										1-36,1-37,2-18
Z104	W24	F-16		x							x	x	x		x																										1-39,1-40,2-19
Z105	W3BB	F-16		x							x	x	x		x																										1-36,1-37,2-18
Z105	W24	F-16		x							x	x	x		x																										1-39,1-40,2-19
Z106	W3BB	F-16+30.5Str.		x							x	x	x		x																										1-32,1-33,2-16
Z107	W24	F-16		x								x	x		x																										1-41,2-22
Z107		F-16+Z112		x								x																													1-43
Z108	W24	F-16		x								x	x		x	x								x				x	x												1-41,2-22,3-79,3-80
Z108		F-16+Z112		x								x																													1-43
Z109	W24	F-16		x								x				x								x				x	x												1-41,1-45,3-81,3-82
Z109		F-16+Z112		x								x																													1-42,1-43
Z110	W24	F-16											x		x																										2-24,2-25
Z111	W24	F-16											x		x																										2-24
Z112	W24	F-16		**x**								x	x		x																										1-44,1-45,2-24
Z113	W24	F-16											x		x																										2-24
Z114	W24	F-16											x		x																										2-24
Z115	W24	F-16											x		x																										2-24
Z117	W24	F-16											x		x																										2-25
Z120	W24 W25	F-16		x						x	x	x	x	x	x																										1-46,1-47,1-48,1-49,1-50, 1-51,1-52,2-26,2-27,2-28, 2-29,2-30,2-31

Table 4 (Continued)

Page 51

Low-speed (LS) and Transonic (T) test matrix. P = PITCH, SS = SIDESLIP. LEF / HT angle values and MACH numbers are given in each column header.

STRAKE	WING	CONFIGURATION	LS P LEF 0	LS P LEF 15	LS P LEF 25	LS P LEF 35	LS P LEF OFF	LS P HT -25	LS P HT -20	LS P HT -10	LS P HT 0	LS P HT 25	LS SS LEF 0	LS SS LEF 25	LS SS HT 0	T P LEF 0	T P LEF 5	T P LEF 10	T P LEF 15	T P LEF 25	T P HT -30	T P HT -20	T P HT -10	T P HT 0	T MACH .6	T MACH .8	T MACH .9	T MACH 1.2	T MACH 1.6	T MACH 2.0	T SS LEF 0	T SS LEF 5	T SS LEF 10	T SS LEF 15	T SS LEF 25	T SS HT 0	T SS MACH .8	T SS MACH .9	T SS MACH 1.2	T SS MACH 2.0	NASA CR-158922 FIGURE NUMBERS
Z121	W25	F-16											x		x																											2-26
Z123	W25	F-16		x									x		x																											1-51,2-31
Z124	W24 W25	F-16		x								x	x	x	x	x									x						x	x				x				x	x	1-47,1-48,1-49,1-50,1-52, 2-27,2-28,2-29,2-30,4-54, 4-55
Z125	W25	F-16		x									x		x																											1-51,2-31
Z126	W25	F-16		x									x		x																											1-51,2-31
Z127	W25	F-16		x									x		x																											1-51,2-31
Z128	W25	F-16		x									x		x																	x				x				x		1-52,2-30,4-56
Z131	W25	F-16		x									x		x																											1-53,1-54,2-32,2-33,2-36
Z131A	W25	F-16											x		x																											2-32
Z131B	W25	F-16											x		x																											2-32
Z132	W25	F-16		x									x		x																											1-54,2-33
Z133	W25	F-16		x									x		x																											1-55,2-34

NOTES:

(1) Configurations have single vertical tail unless noted as twin vertical (TV)

(2) The YF-16 fuselage was stretched 25.4 cm (10 in) for the F-16

Table 5   STRAKE GEOMETRY FOR $C_{L_{\alpha_S}}$ and ℓ_S CALCULATION

STRAKE	AR_{EFF}	b_{EFF} m (ft)	c_r m (ft)	c_t m (ft)	Λ_{LE_i} Degrees	A_{EFF} m^2 (ft^2)
Z7	.308	1.57 (5.17)	6.78 (22.25)	3.45 (11.33)	77.0	8.06 (86.75)
Z8	.287	1.37 (4.5)	6.10 (20.0)	3.45 (11.33)	75.0	6.55 (70.49)
Z9	.257	1.27 (4.17)	6.30 (20.67)	3.58 (11.76)	77.0	6.28 (67.56)
Z10	.157	.71 (2.33)	5.31 (17.42)	3.76 (12.33)	77.0	3.22 (34.66)
Z4	.293	1.68 (5.5)	7.19 (23.58)	4.27 (14.0)	73.5	9.60 (103.35)
Z5	.262	1.68 (5.5)	7.62 (25.0)	5.21 (17.08)	71.0	10.73 (115.50)
Z16	.192	1.17 (3.83)	7.06 (23.17)	5.13 (16.83)	73.5	7.12 (76.65)
Z17	.436	2.79 (7.5)	6.48 (21.25)	4.01 (13.17)	65.5	11.99 (129.08)
Z18	.297	1.68 (5.5)	6.65 (21.83)	4.65 (15.25)	67.5	9.47 (101.98)

Table 6   CALCULATIONS FOR AERODYNAMIC CENTER CORRELATIONS

STRAKE	A_{EFF} m^2 (ft^2)	M = 0.80						M = 1.20				
		$\ell_S/\bar{c}$	$C_{L\alpha_S}$ per radian	$\dfrac{\ell_S\,A_{EFF}}{\bar{c}\,S_{REF}}$	$\dfrac{\ell_S\,A_{EFF}}{\bar{c}\,S_{REF}}C_{L\alpha_S}$ per radian	AC_1	AC_2	$\ell_S/\bar{c}$	$C_{L\alpha_S}$ per radian	$\dfrac{\ell_S\,A_{EFF}}{\bar{c}\,S_{REF}}$	$\dfrac{\ell_S\,A_{EFF}}{\bar{c}\,S_{REF}}C_{L\alpha_S}$ per radian	AC_1
Z7	8.06 (86.75)	.69.	.468	.214	.100	.049	.34	.81	.530	.25	.133	.045
Z8	6.55 (70.49)	.642	.443	.162	.072	.041	.29	.772	.486	.194	.094	.03
Z9	6.28 (67.6)	.670	.395	.161	.064	.029	.28	.80	.432	.193	.083	.02
Z10	3.22 (34.7)	.596	.244	.074	.018	.014	.24	.76	.248	.094	.023	.01
Z4	9.60 (103.3)	.815	.452	.220	.099	.048	.24	.945	.491	.349	.171	.04
Z5	10.73 (115.5)	.998	.407	.412	.168	.088	.34	1.139	.422	.470	.198	.06
Z16	7.12 (76.65)	.932	.299	.255	.076	.035	.11	1.086	.302	.297	.09	–
Z17	11.99 (129.08)	.65	.671	.300	.201	.06	.12	.760	.741	.35	.26	–
Z18	9.47 (101.98)	.786	.461	.286	.132	.05	.14	.923	.476	.336	.16	–
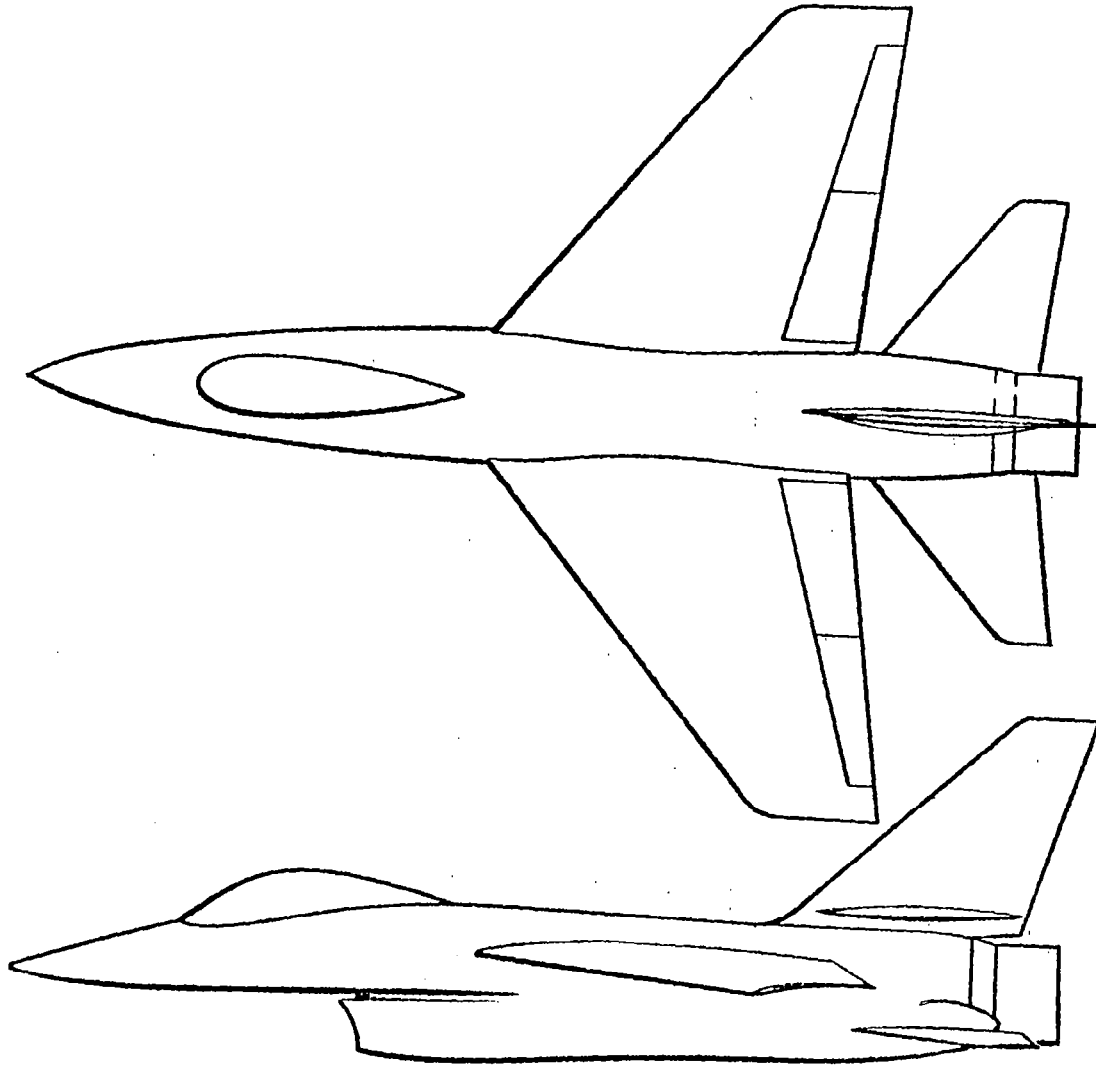
Figure 1   Sketch of Configuration 785
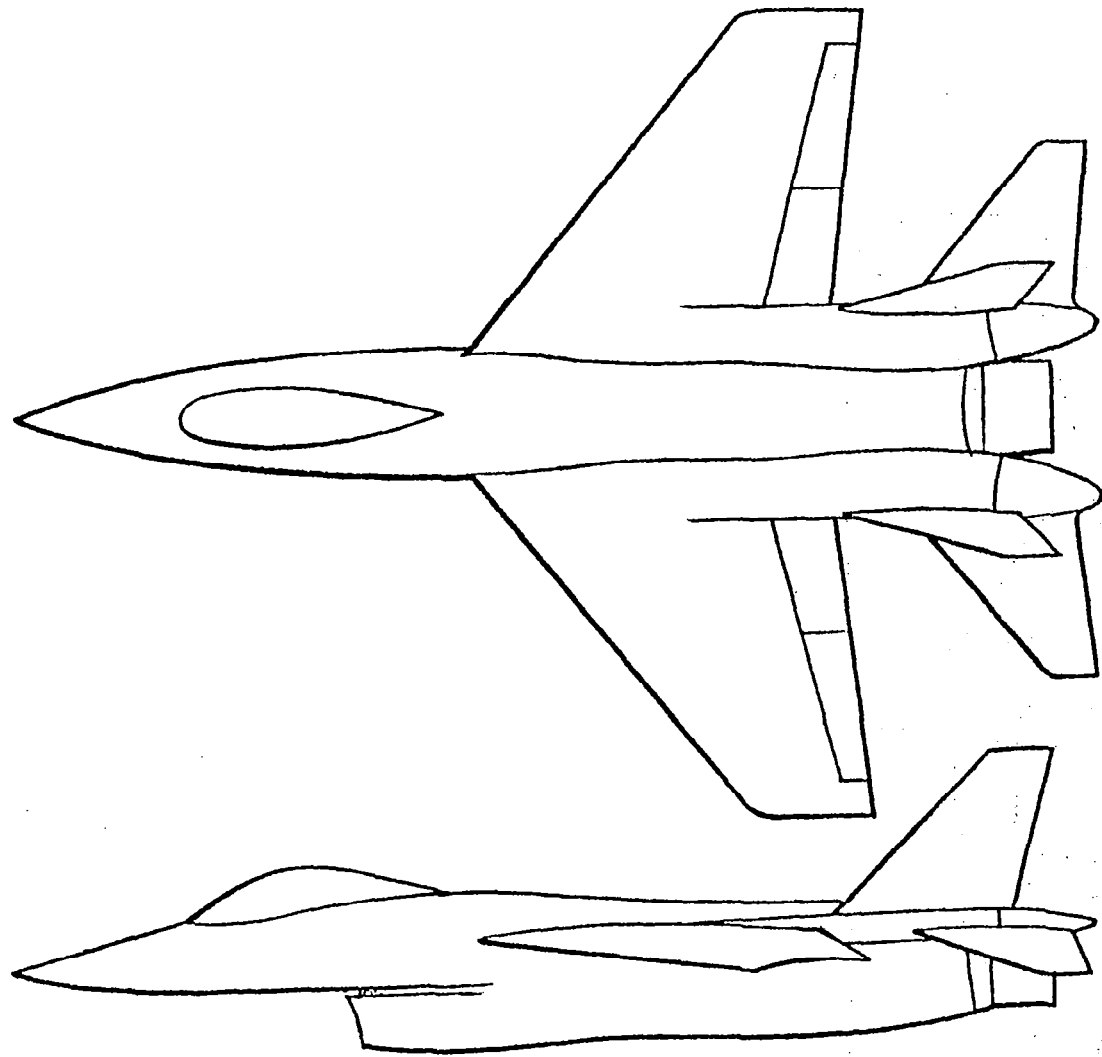
Figure 2   Sketch of Configuration 786
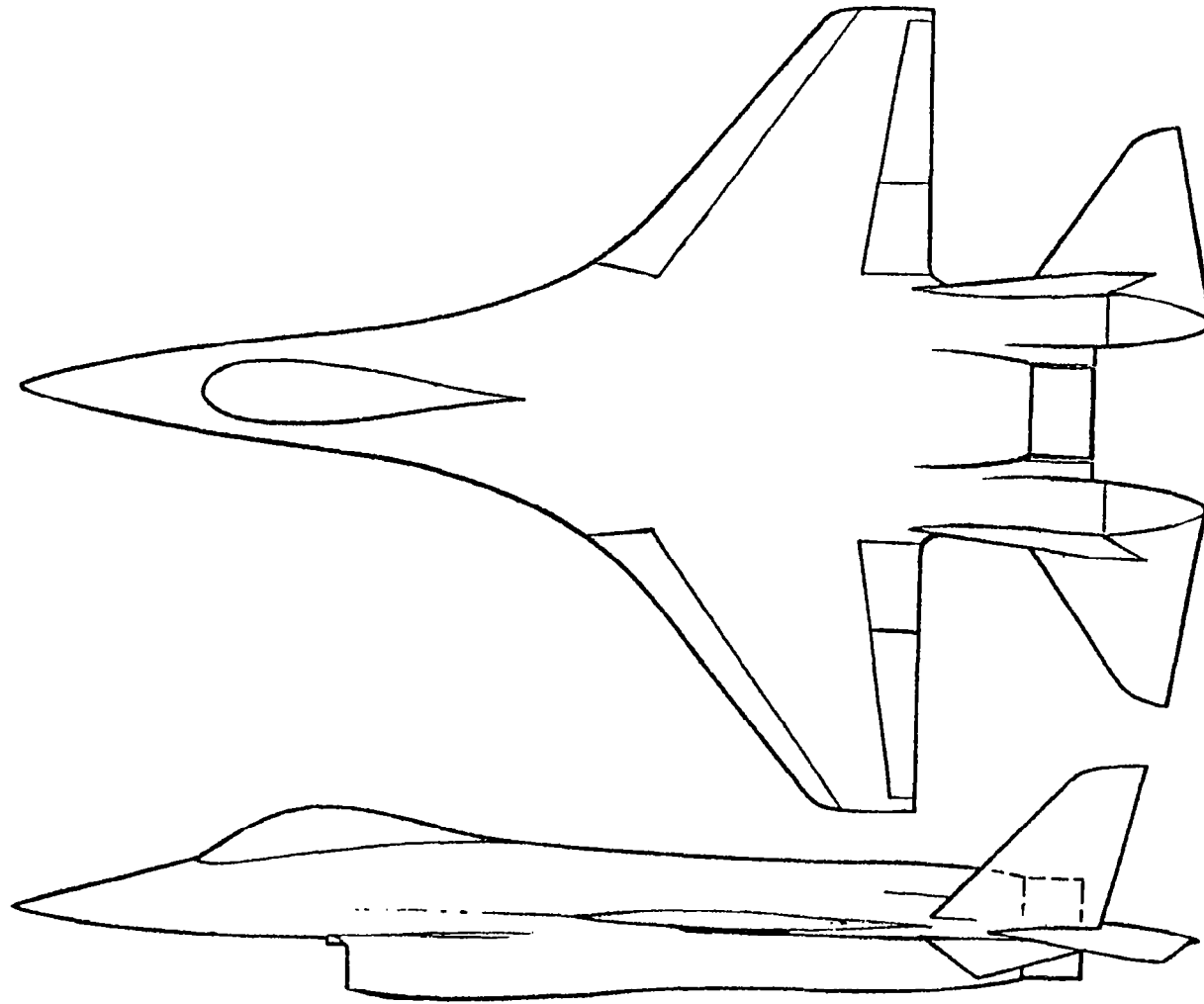
Figure 3   Sketch of Configuration 401F-2
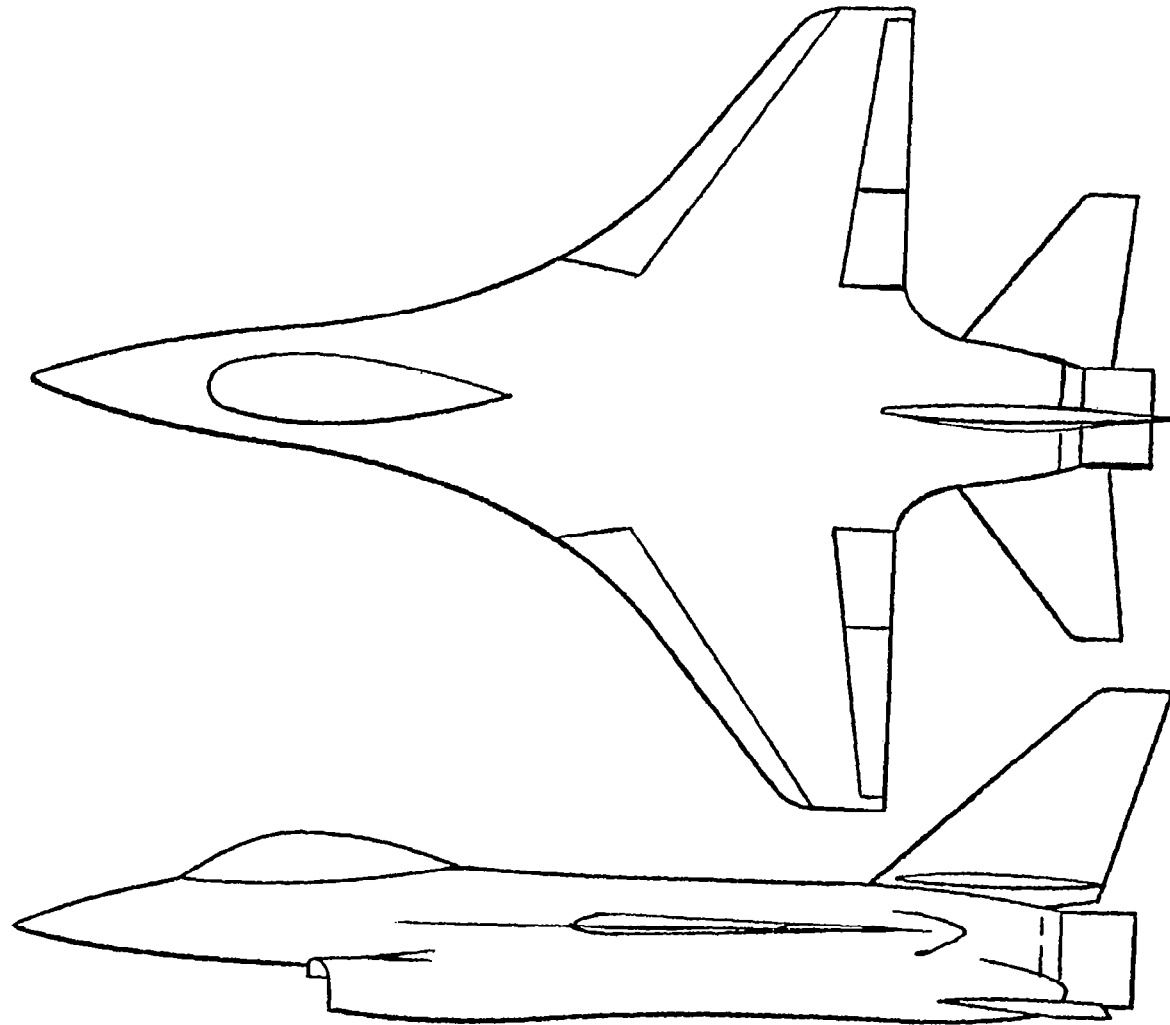
Figure 4   Sketch of Configuration 401F-5
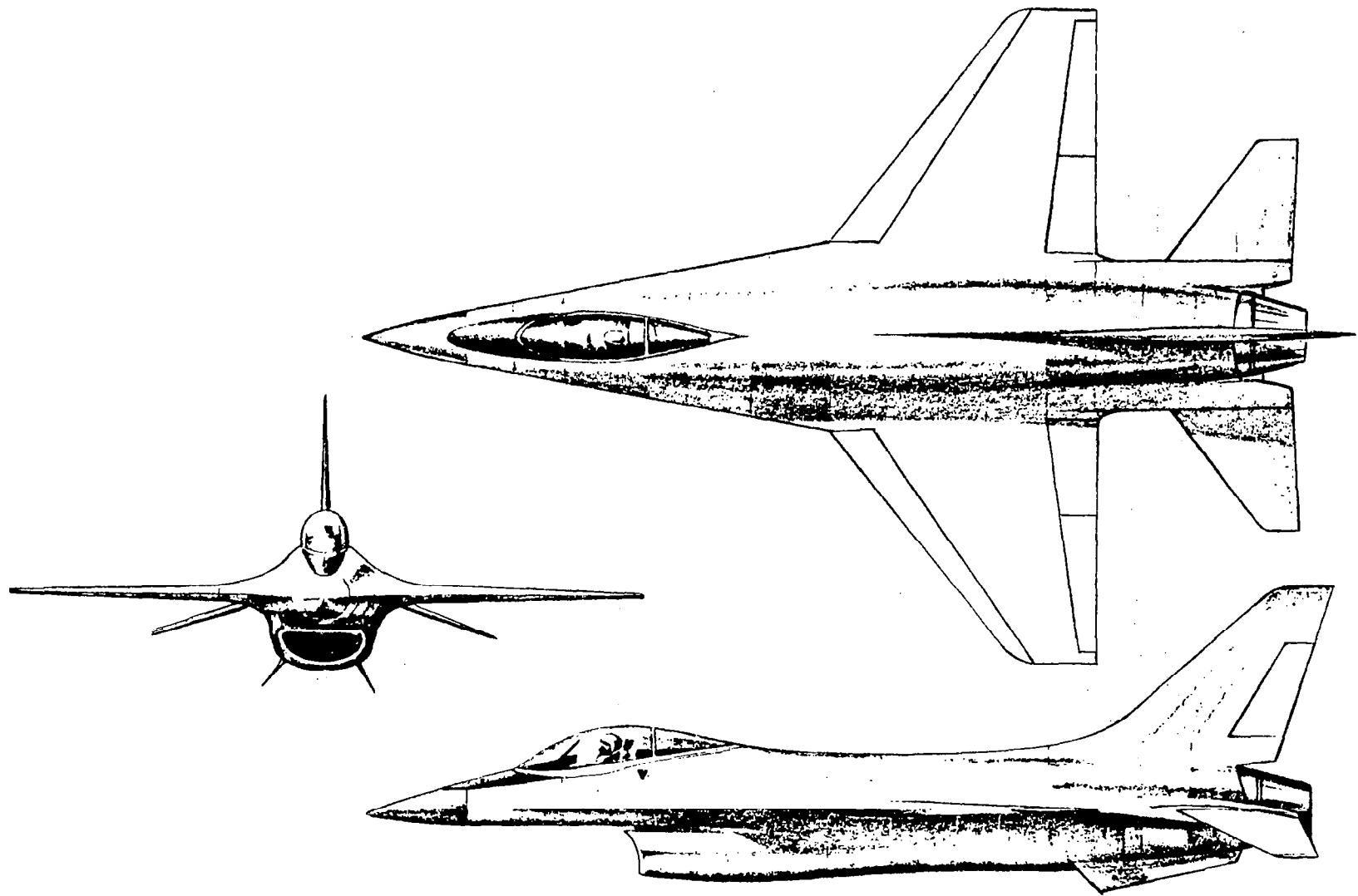
Figure 5   Sketch of Configuration 401F-10A

WING	$S_w \sim m^2 (ft^2)$	AR	λ	$\Lambda_{LE} \sim$ DEG	$\Lambda_{TE} \sim$ DEG
W3	26.01 (280.0)	3.00	.227	40	0
W3BB	26.10 (280.9)	3.05	.220	40	0
W6	26.01 (280.0)	3.00	.30	40	6.9
W24	27.58 (296.9)	3.03	.222	40	0
W25	27.87 (300)	3.00	.227	40	0

Figure 6   Wing Planforms

59

FS 158.8 (62.5)

433.1(170.5)

311.2(122.5)

622.3(245.0)

99.8(253.5)

656.6(258.5)

BL 0.0

77° For Z7, Z9, Z10
75° For Z8

BL 108.6(42.8)

BL 133.4(52.5)

BL 147.3(58.0)

FS 68.6(27.0)

Z10

Z9

Z8

Z7

Wing L.E.

WL 232.9(91.7)

$4^o01'$

WL

$7^o40'$

Typ all strakes

541.0(213.0)
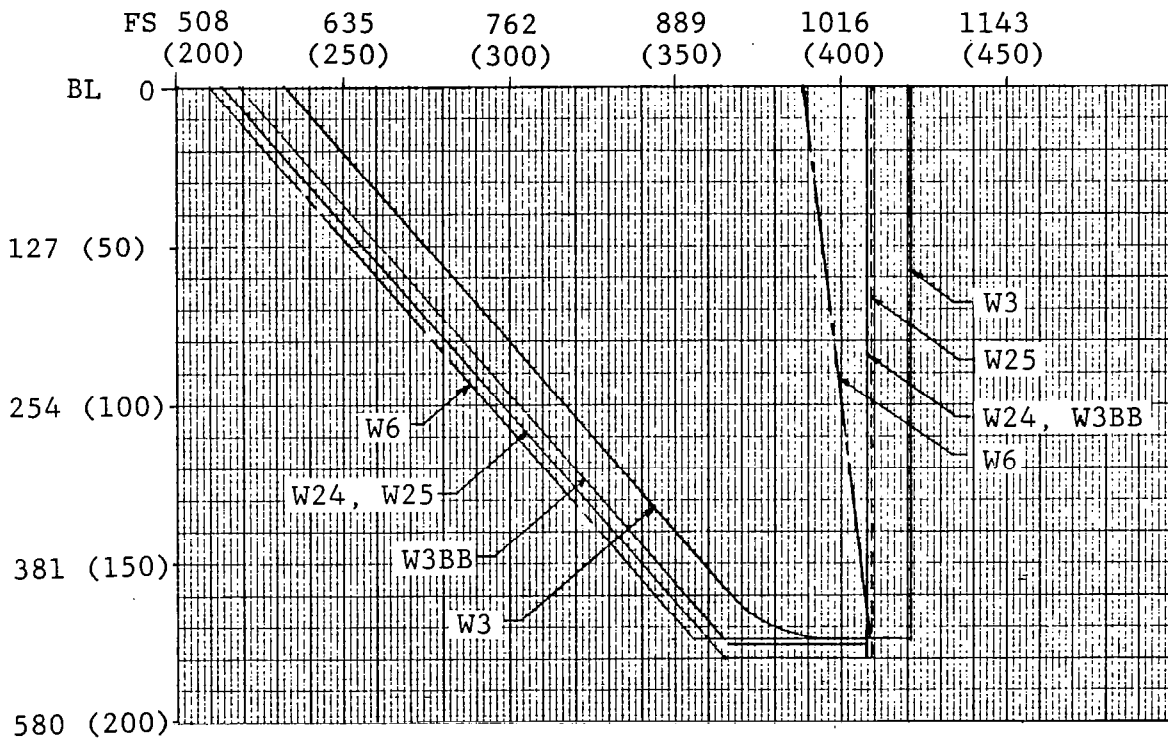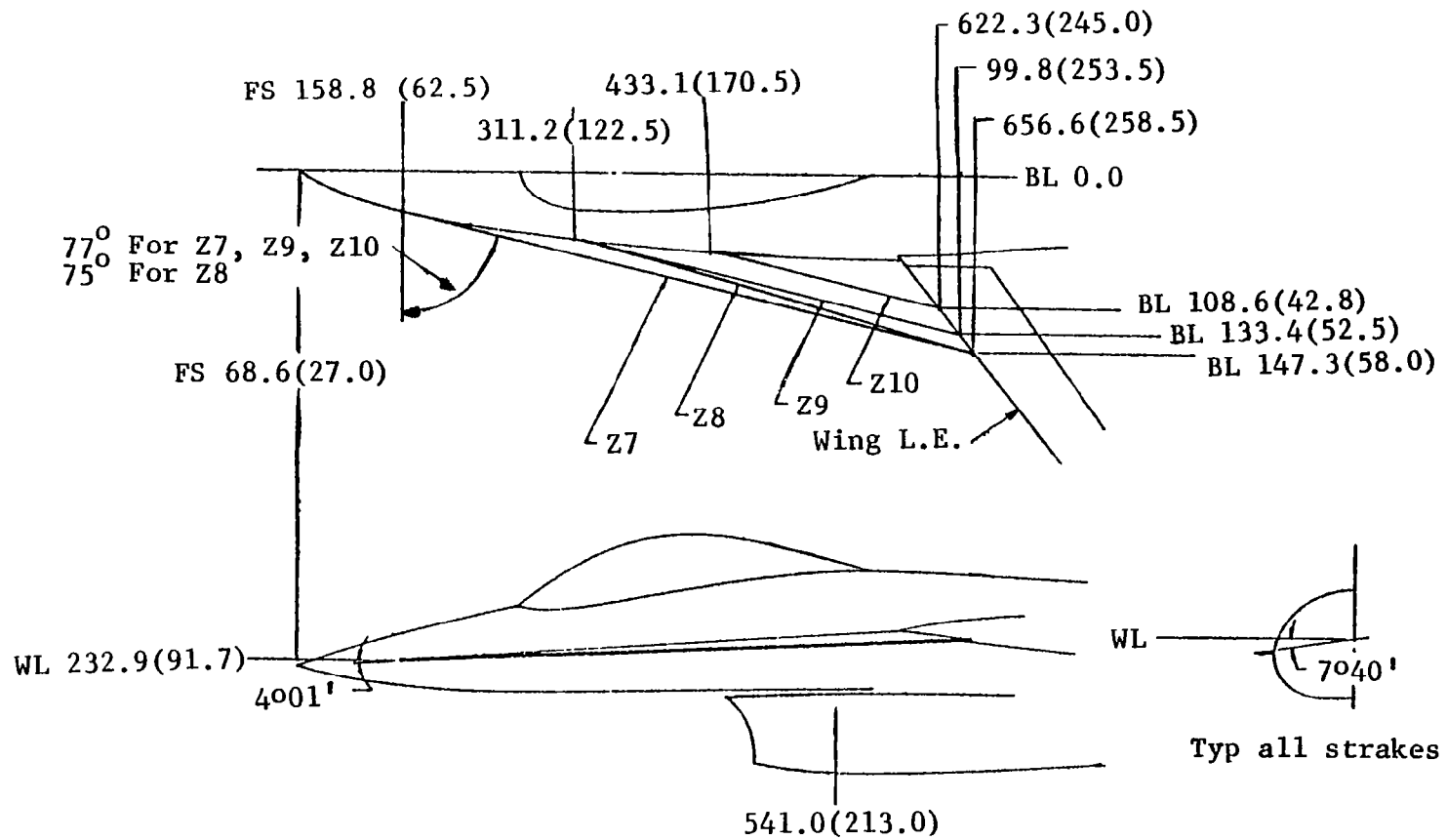
Figure 7   Configuration 785 and 786 Strakes

Hingeline

Z1 Z1A Z2

A

WL 269.3(106.0)

WL 236.2(93.0)

WL 256.8(101.1)

3°15'

292.1(115.0)

A

FS 52.1(20.5)   381.0(150.0)

472.4(186.0)

Z1A REF
Z2 REF
Z1 REF

Section A-A
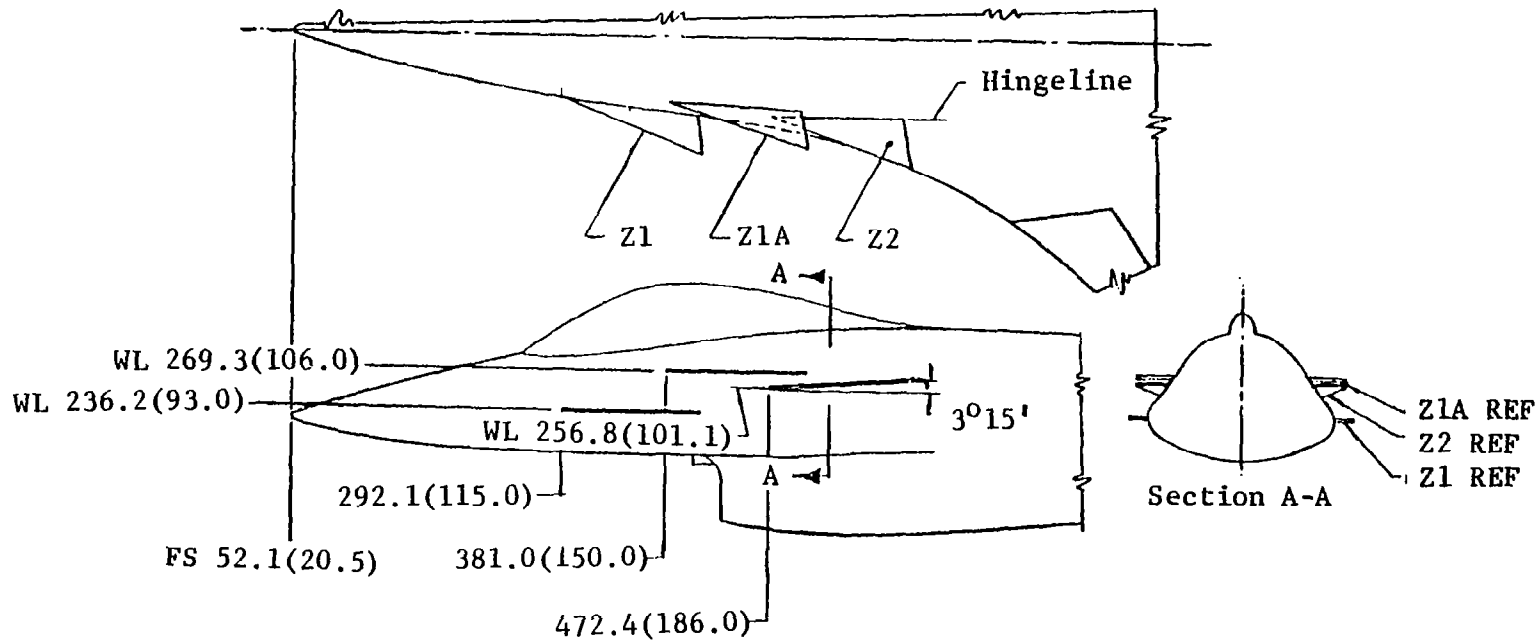
Figure 8   Configuration 401F-2 Strakes

381.0(150.0)

292.1(115.0)

254.0(100.0)

BL 0.0

FS 76.2(30.0)

684.5(269.5)

Z3

Z1B

Z5

Z4

BL 151.1(59.5)

A

190.5(75.0)

WL 237.5(93.5)

1°55'

A

Section A-A
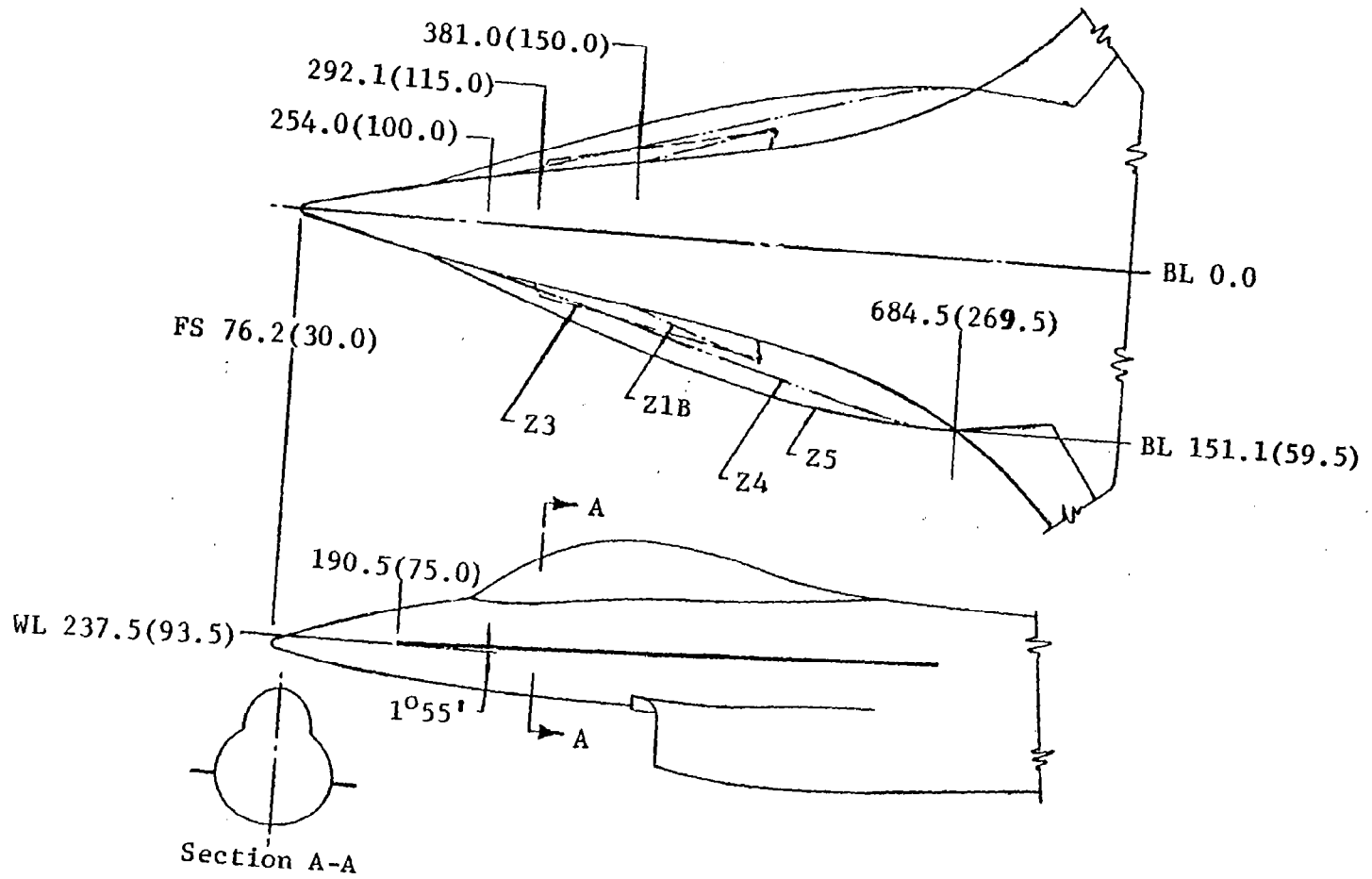
Figure 9   Configuration 401F-4 Strakes
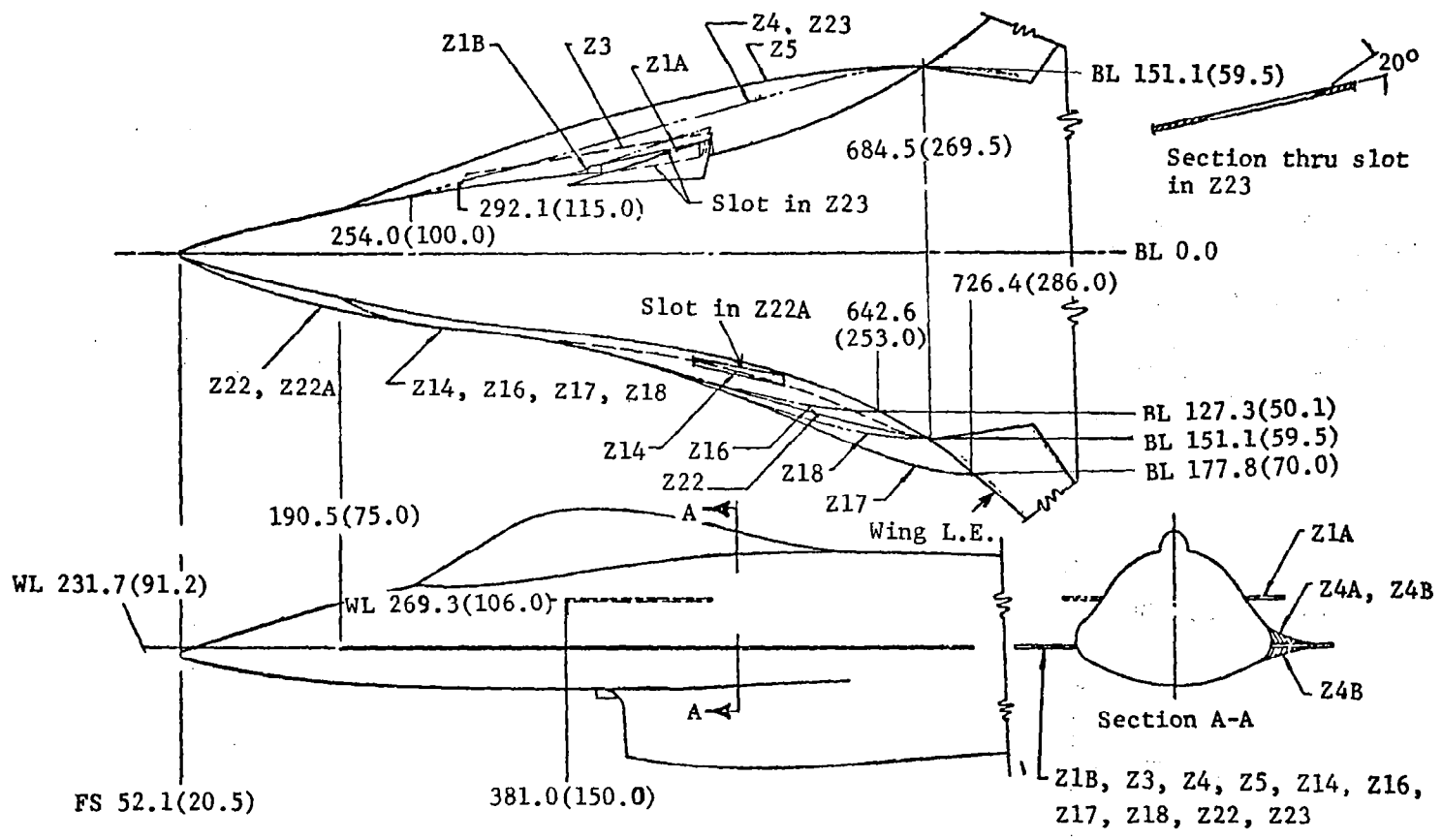
Figure 10   Configuration 401F-5 Strakes

63

L.E. Z21
Z20, Z21
off
BL 0.0
190.5(75.0)
696.2(274.0)
Z1A
BL 127.0(50.0)
Wing L.E.

Z1A
A
WL269.3(106.0)
WL 254.0(100.0)
Z1A
Z20
Z21
Section A-A
A
FS 55.9(22.0)
381.0(150.0)
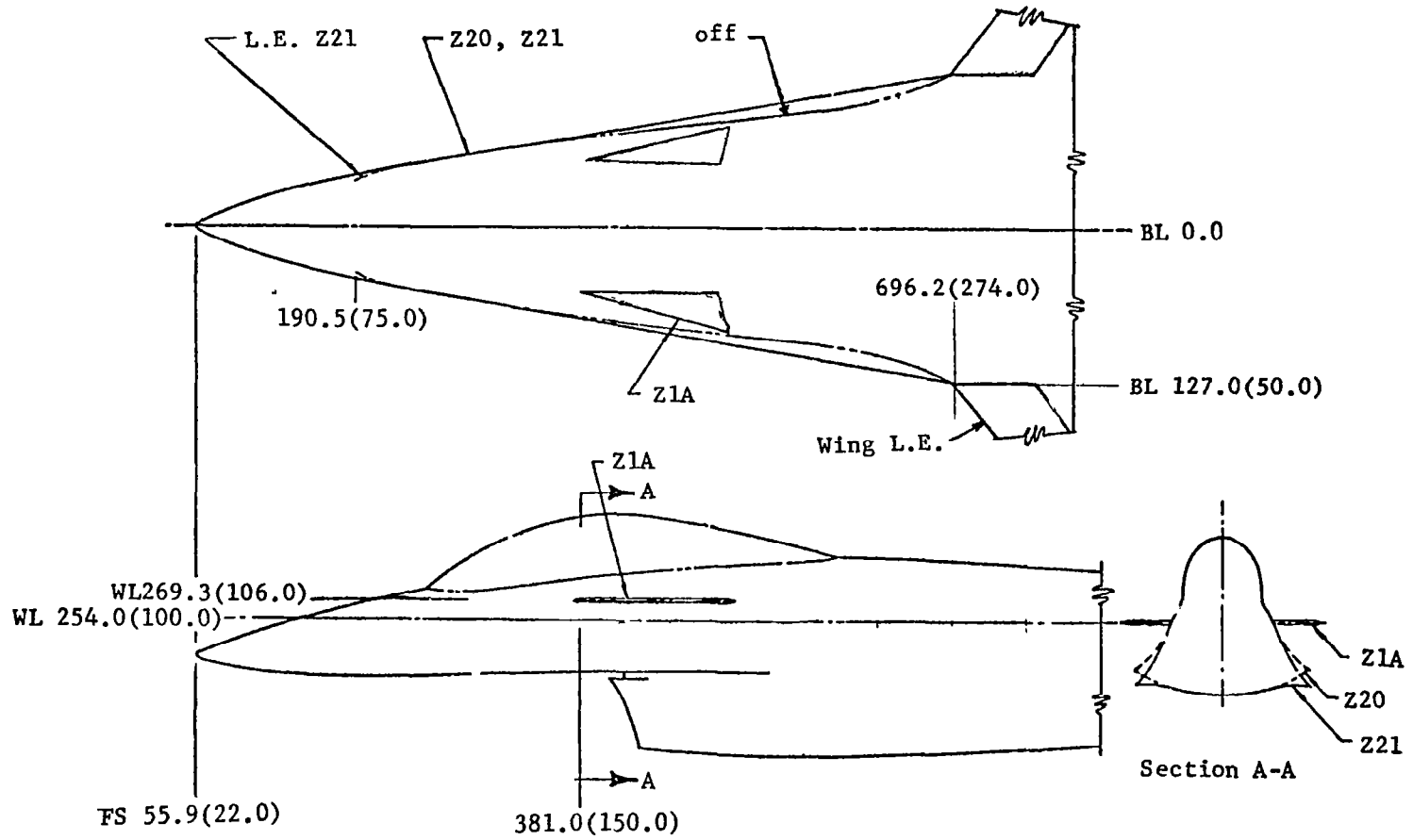
Figure 11a   Configuration 401F-10A Strakes

64

FS 55.9(22.0)

BL 0.0

190.5(75.0)

381.0(150.0)

Off

BL 127.0(50.0)

Z25

Z24,Z26

A

Z24, Z25

Z20

Z26

A

B
Wing L.E.

BL 0.0

696.0(274.0)

Z27

BL 0.0

A

Z20

BL 127.0(50.0)

Z27

Z27

Z24, Z25, Z26

Z27

BL 147.3
(58.0)

Z20

Wing L.E.

Section B-B

Section A-A

Note: All strakes on maximum half breadth
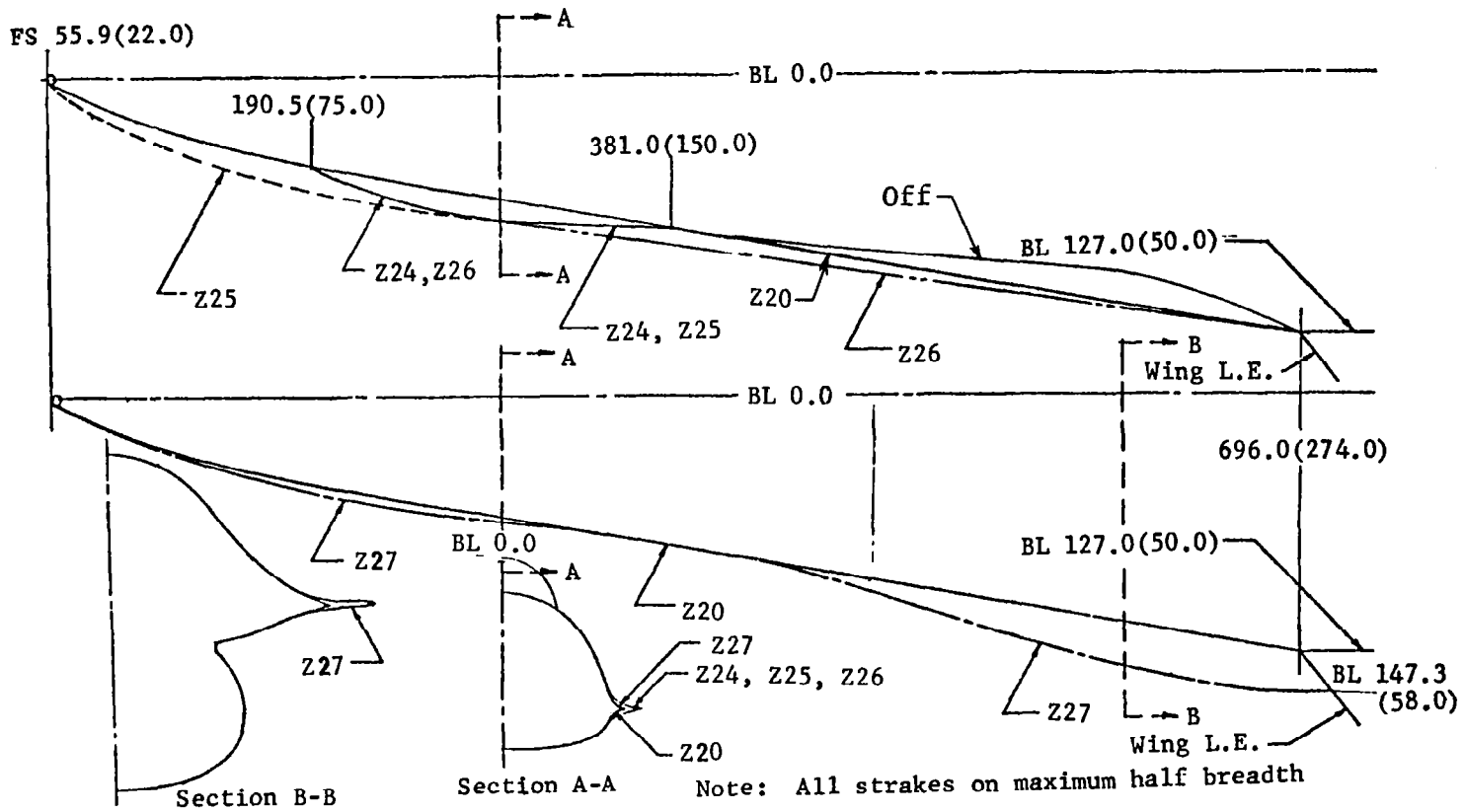
Figure 11b Additional Configuration 401F-10A Strakes

698.5(275.0)

BL 0.0

254.0(100.0)

Z31

Z32

Z33

Z28, Z29

FS 55.9(22.0)

BL 127.0(50.0)

B.L. 137.2 (54.0)

BL 147.3(58.0)

Z28   Z29A

Z29, Z33   Slot

Wing LE

BL 0.0

254.0(100.0)

190.5(75.0)

BL 127.0(50.0)

Z30

Z31   BL 147.3(58.0)

Wing L.E.
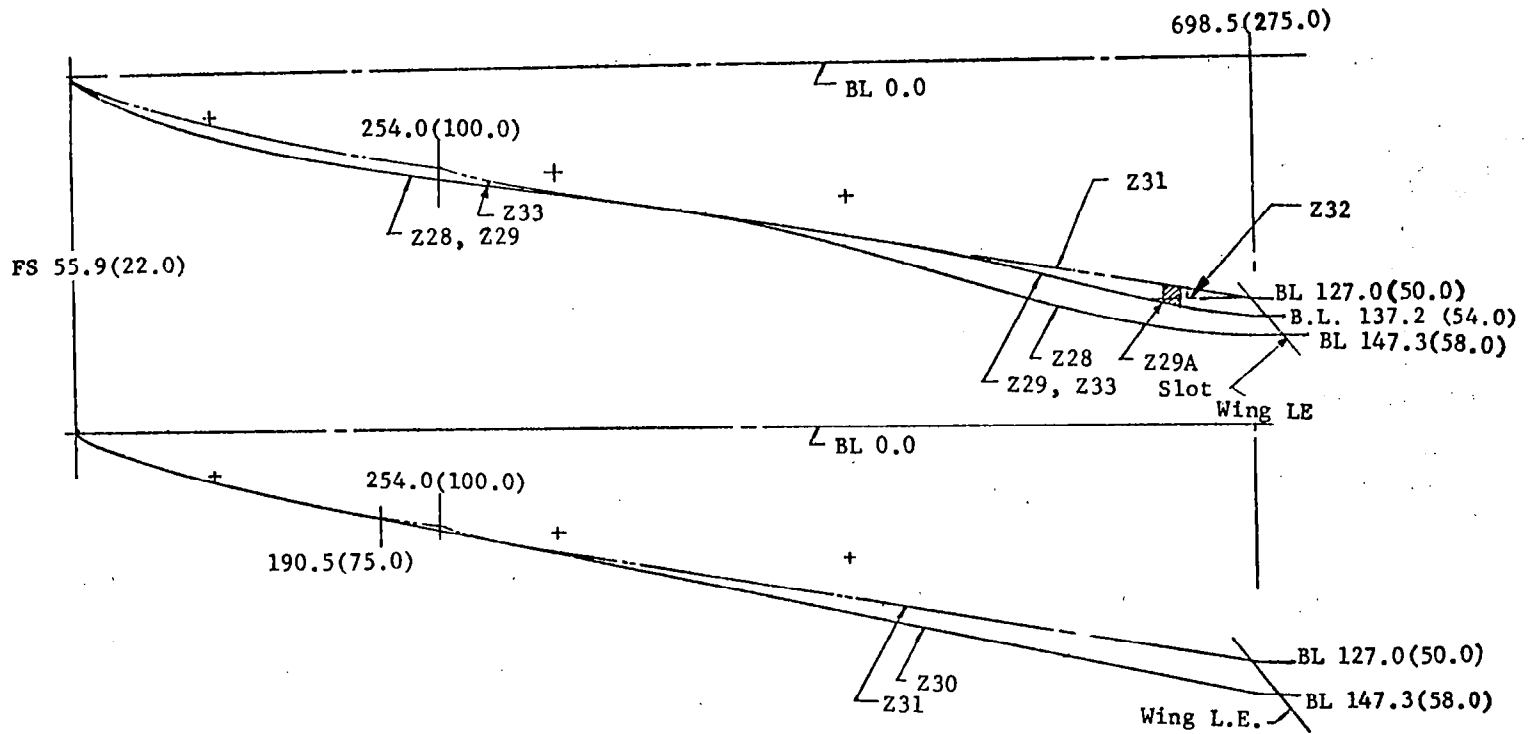
Figure 12   Configuration 401F-16 Strakes

99

FS 158.8(62.5)

221.0(87.0)

555.8(218.8)

BL 0.0

Z48

207.0(81.5)

Z50 Straight line L.E.

BL 137.2(54.0)

Z49

635.0 (250.0)

670.6 (264.0)

Wing L.E.

67
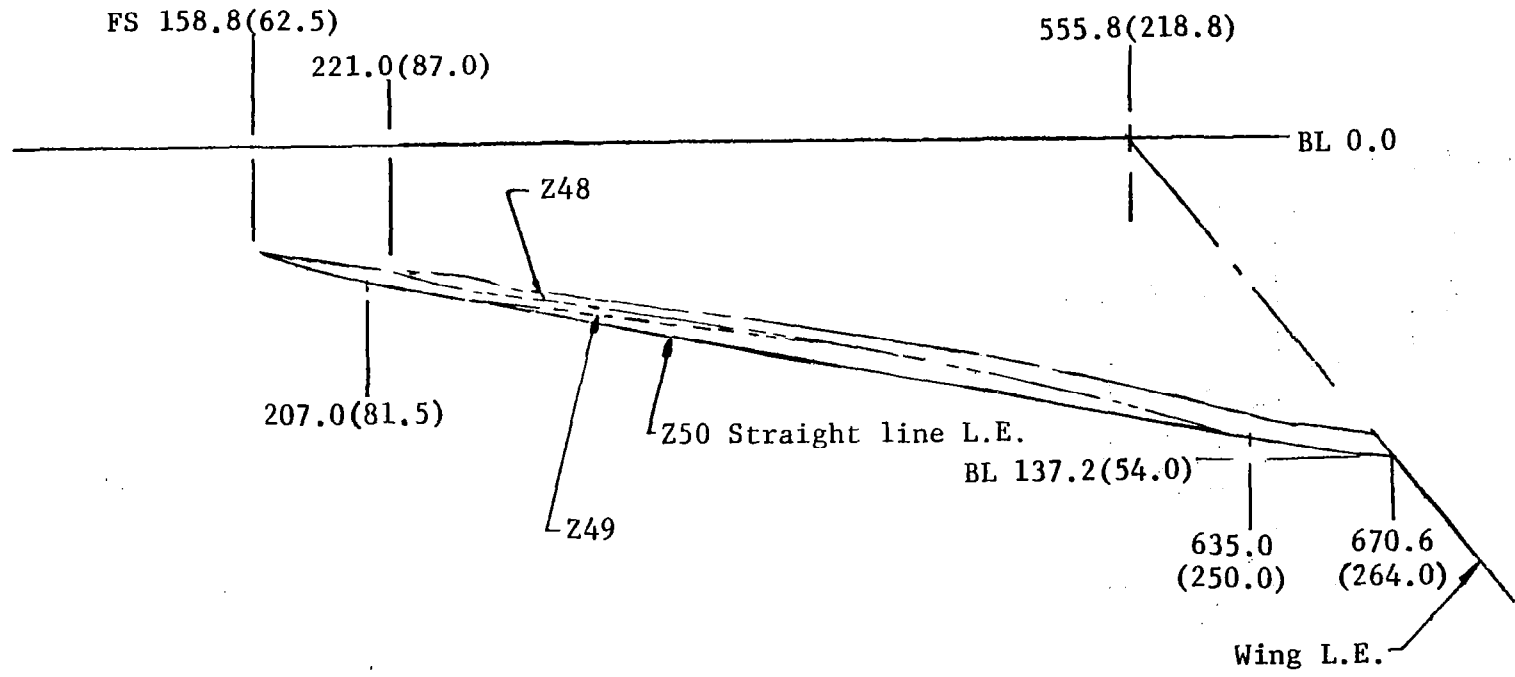
Figure 13   Configuration 401F-16E Strakes

521.5(205.3)

BL 0.0

396.7
(156.2)

Tan Pt

FS 254.0(100.0)

34.3
(13.5)

Z55   Z56

401F-16   539.5(212.4)

Tan Pt

Wing L.E.

FS 637.5 (251.0)
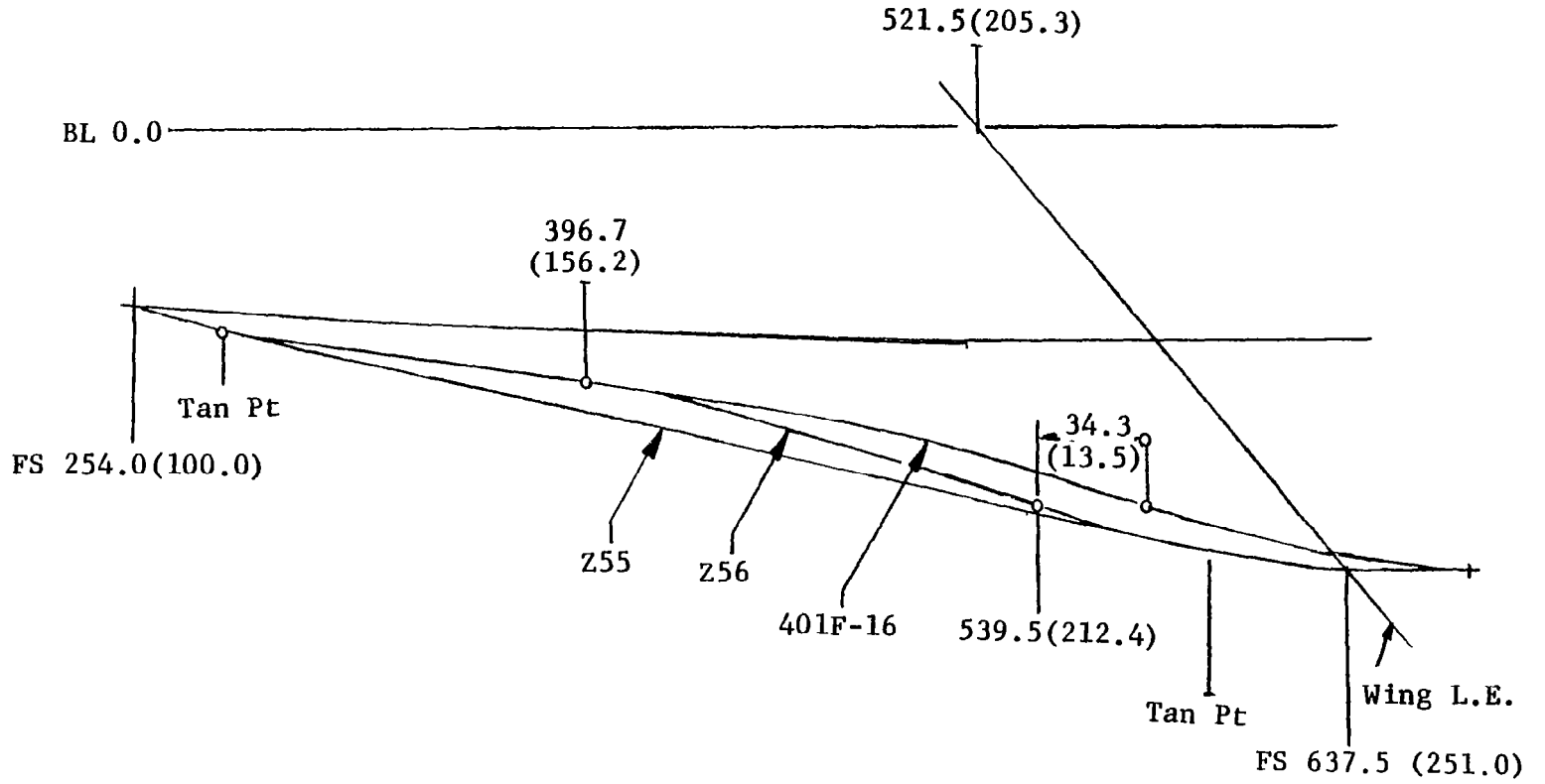
Figure 14   YF-16 Strakes with Wing Forward

Z33

Z33H

Z33B,Z33C

B.L. 94.7(37.3)

B.L. 103.4(40.7)

B.L. 98.3(38.7)

Z33A

521.5(205.3)

662.9
(261.0)

Note:
(1) All strakes are in contour except Z33A'
    and Z33B' which are flat plates.
(2) Z33A' and Z33B' have the same planform as
    Z33A and Z33B respectively
(3) Z33I is Z33C removed
(4) Z29A' is same as Z33A'

565.2(222.5)
Z33H HL

597.7(235.3)

616.0(242.5)
Z33A,Z33B HL

598.2(235.5)
Z33C HL

Wing L.E.
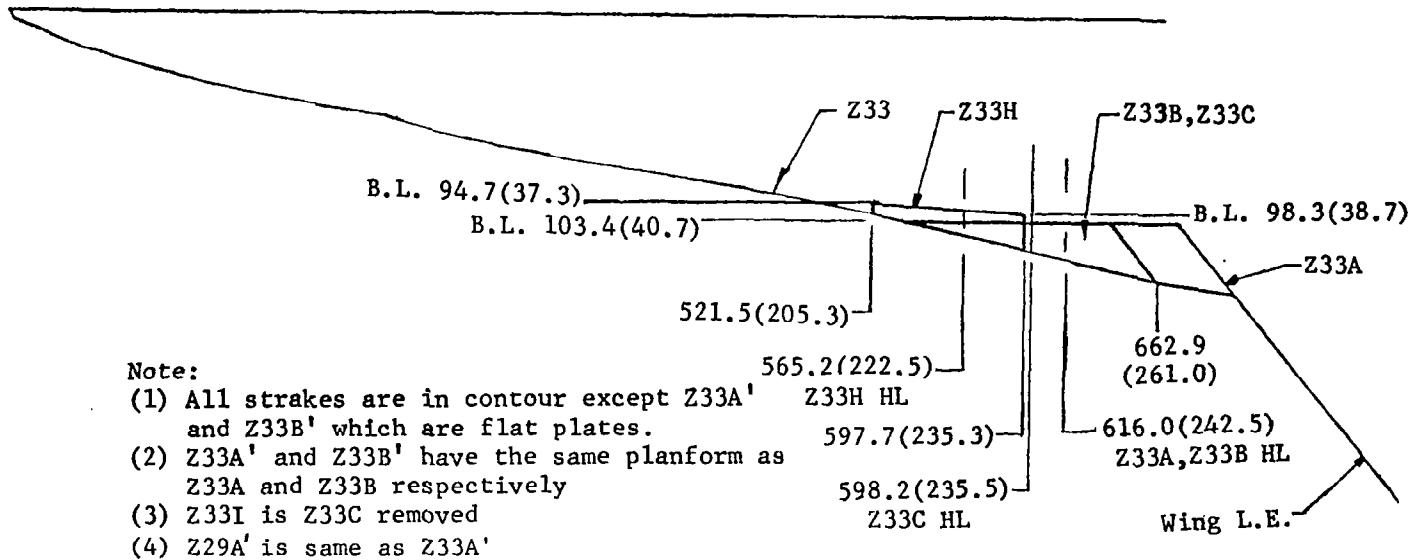
Figure 15a   Configuration 401F-16 Small Rotating Strakes
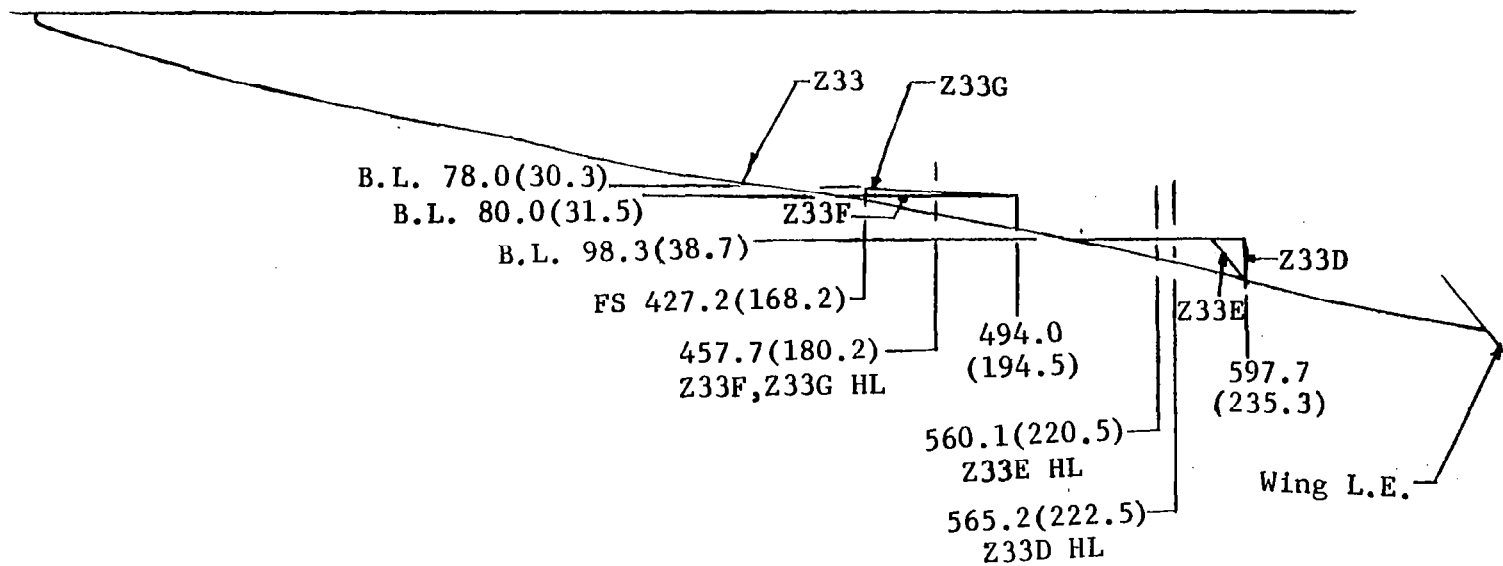
Figure 15b   Additional Configuration 401F-16 Small Rotating Strakes

555.8(218.8)

401F-16

Parting
Plane

H.L. 671.1(264.2)

B.L. 86.4(34.0)

FS 254.0(100.0)

Z57

368.3
(145.0)

436.9
(172.0)

Z58

Wing L.E.
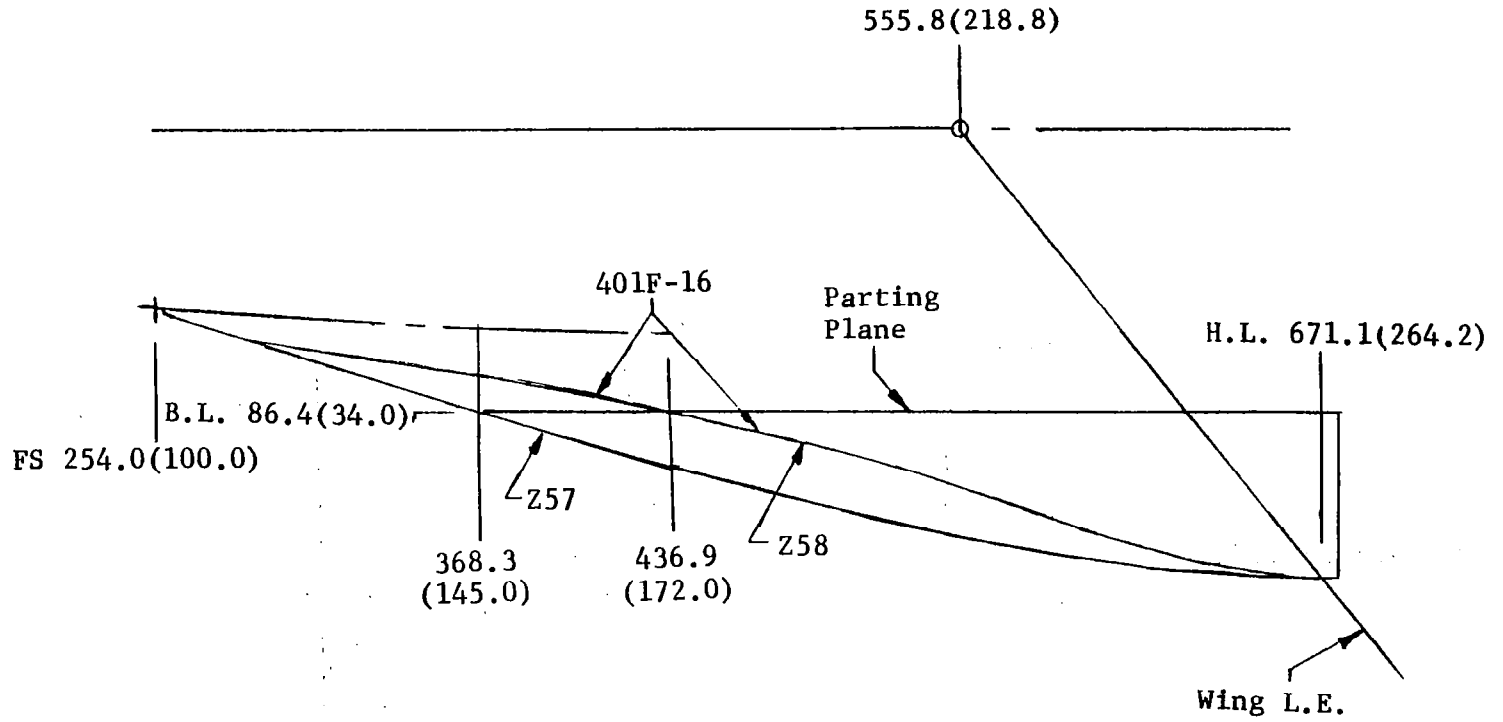
Figure 16   Large YF-16 Rotating Strakes

77.5(30.5)

144.0(56.7)

152.1(59.9)

198.1(78.0)

254.0(100.0)

BL 0.0

Z76

Z77

Z82

FS 20.32(8.0)

Z79

Z86

260.1 (102.4)

BL 137.2(54.0)

WL 225.3
(88.7)

WL 227.3
(89.5)

WL 217.7(85.7)

3°30'

1°00'

Strake Line (TYP)

254.0
(100.0)

152.2
(59.9)
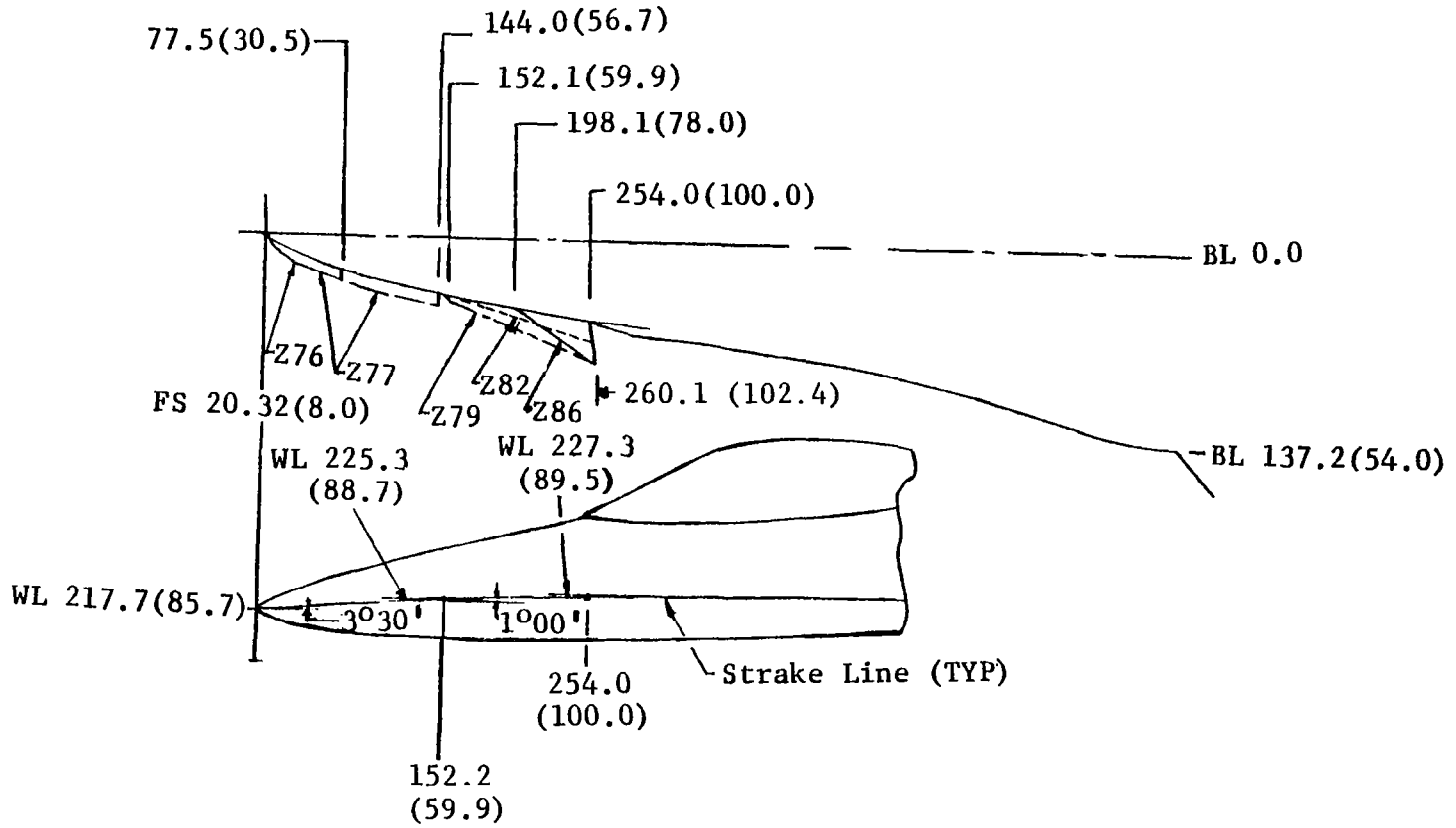
Figure 17   YF-16 Nose and Canard Strakes

YF-16 + 77.5(30.5) Stretch

FS 99.6(39.2)

176.5(69.5)

254.0(100.0)

381.0(150.0)

508.0(200.0)

635.0(250.0)

670.8(264.1)

141.0
(55.5)

BL 0.0

Z72,Z75,Z80
Z68, Z69, Z70*
Z64, Z65, Z66, Z71

Z63, Z67*

Z66,Z80
Z65,Z71,Z75

Z63,Z64,Z72

Z80

Z65

Z71,Z75

Z66

Wing LE

BL 137.2
(54.0)
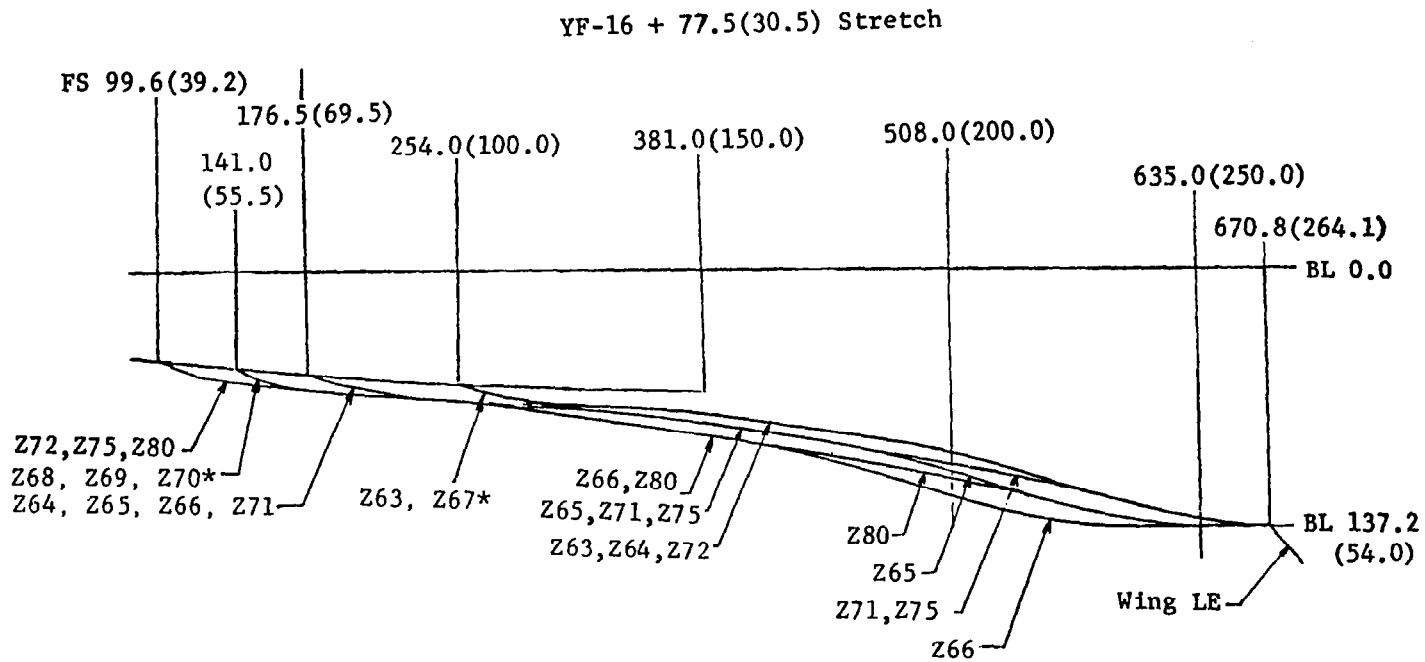
*Z67-Z70 are with 113.0 (44.5) Stretch

Figure 18a   Strakes for Stretched YF-16

YF-16 + 77.5(30.5) Stretch
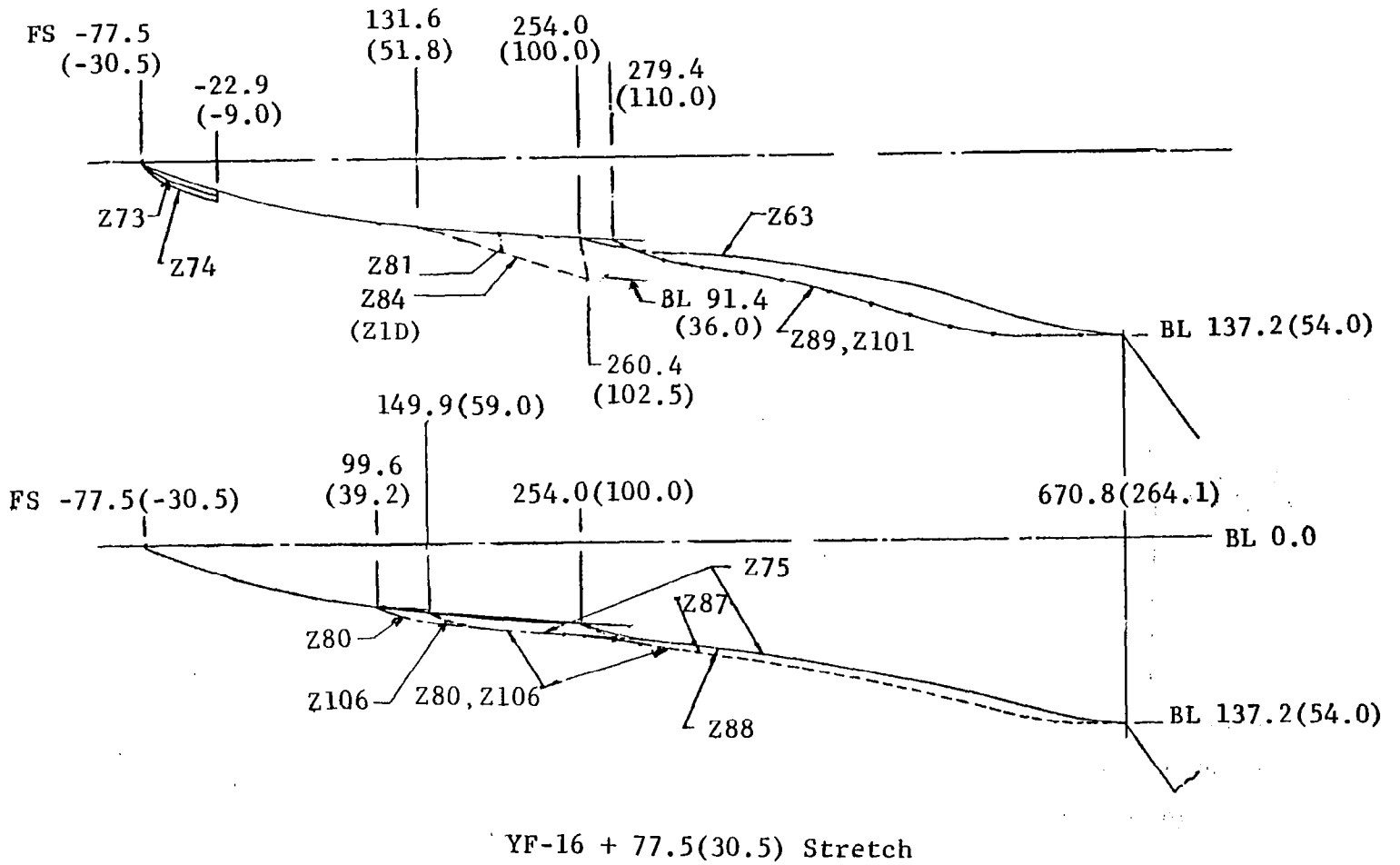
Figure 18b   Additional Strakes for Stretched YF-16

FS 228.6
(90.0)

240.54(94.7)

254.0(100.0)

292.1(115.0)

330.2(130.0)

444.5(175.0)

673.0(265.0)

BL 0.0

Z109

Z108

Z105

Z104,Z120

Z103

Z107,Z121

BL 137.2
(54.0)

Note:
Z107=Z104 cut to FS 292.1(115.0)
Z108=Z105 cut to FS 330.2(130.0)
Z109=Z103 cut to FS 330.2(130.0)

L.E. S_w = 762.0 (300.0)

L.E. S_w = 711.2 (280.0)
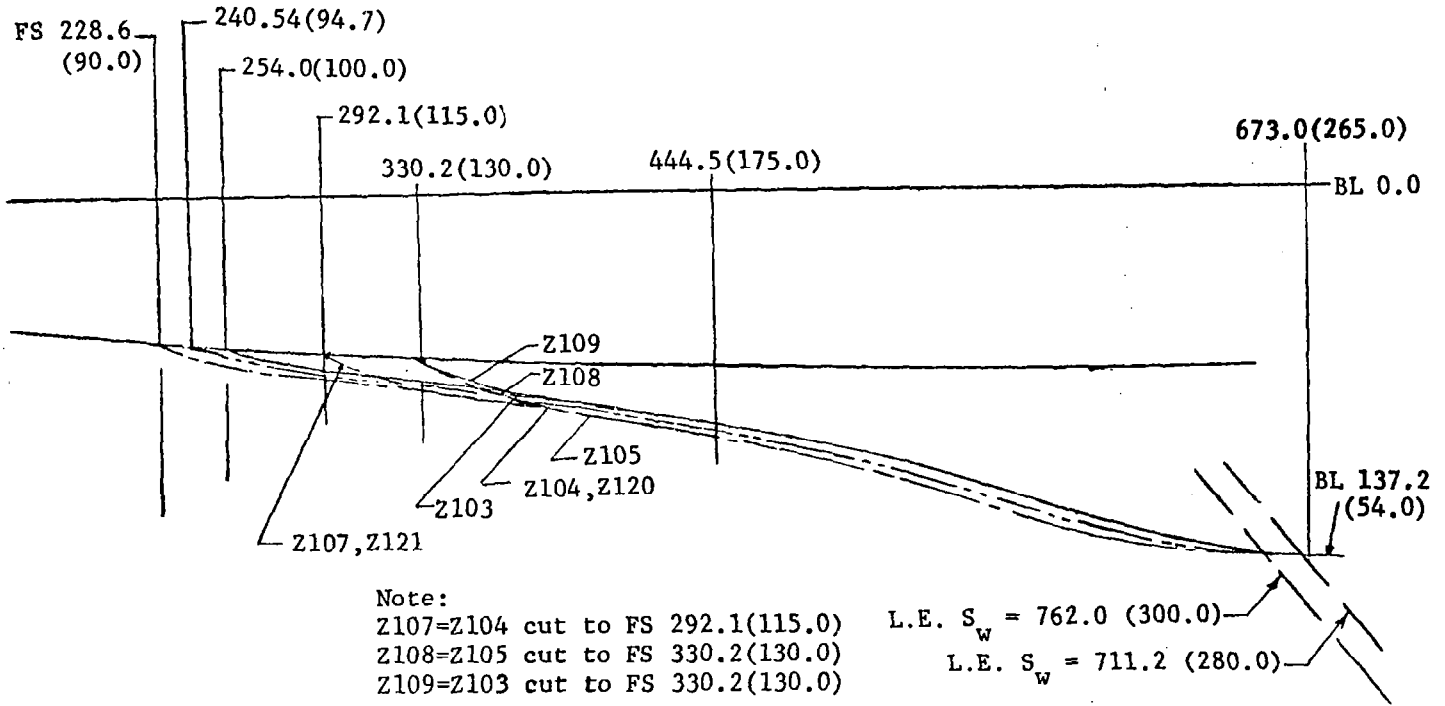
Figure 19   F-16 Forebody Strakes

FS -67.3
(-26.5)

29.2(11.5)

Z110,Z112

Z112

Z100,Z117

Z110

170.7
(67.2)

-25.4
(-10.0)

-52.1
(-20.5)

31.8(12.5)

Z114

Z115

Z113,Z114

Z111

Z113

173.2
(68.2)

-25.4
(-10.0)

44.5 (17.5)

142.2
(56.0)

C.L. nose probe all strakes
except Z117, 2.5° from W.L.

W.L.
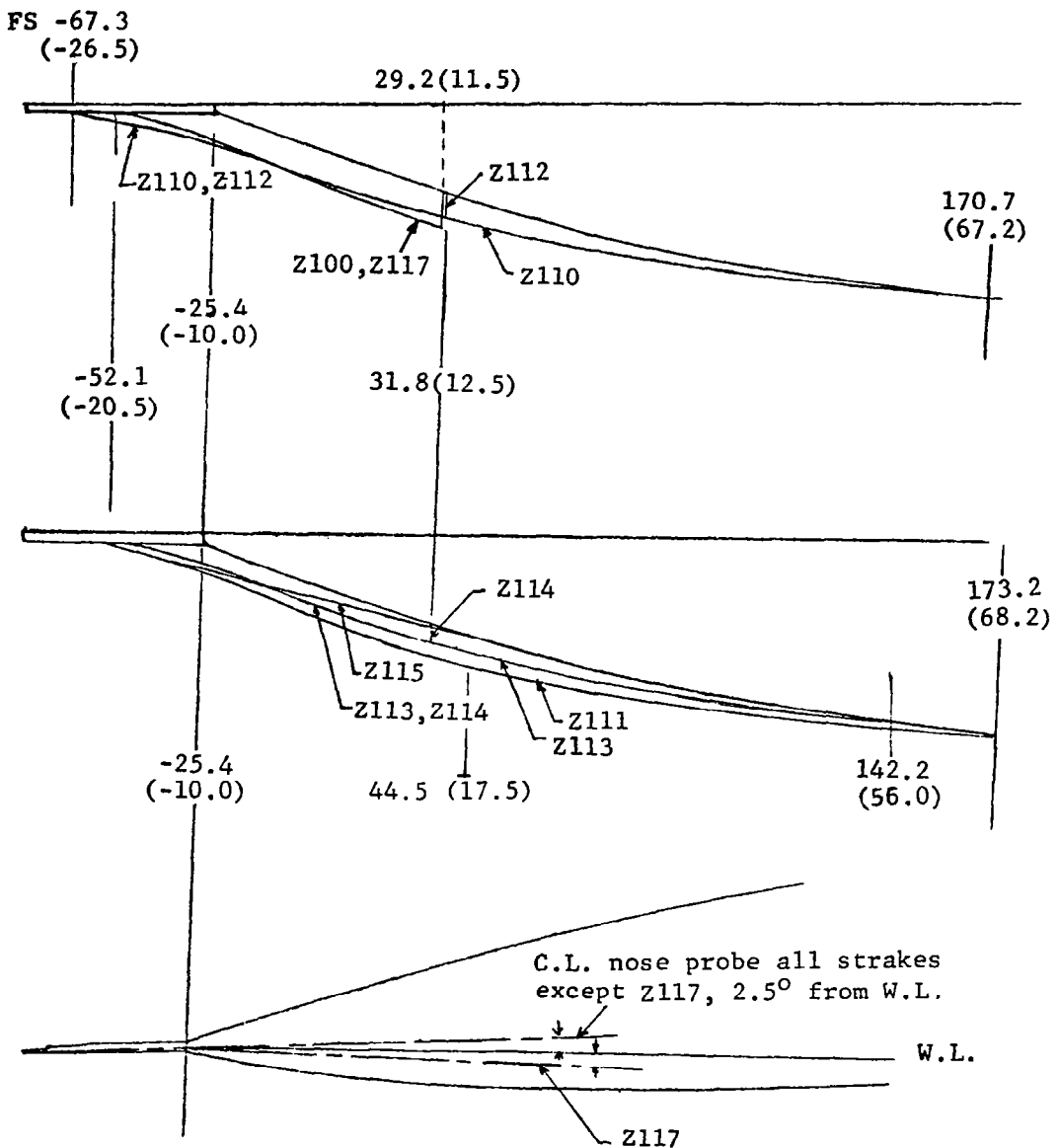
Z117

Note:
All strakes are parallel to the probe
except Z117 which is bent down 5°,i.e., 2½°
below waterline

Figure 20a   F-16 Nose Strakes

Note:
Z128 same as Z124 but rotated up 5° about FS -12.7(-5.0)

Nose probe

Z124,Z128

FS -54.1(-21.3)

Nose

Z123

B.L. 0.0

B.L. 31.2 (12.3)

-12.7(-5.0)

44.5(17.5)

16.0(6.3)

-21.6(-8.5)

-40.6(-16.0)

Nose

BL 0.0

Nose probe

Z126

Z125

Z127

B.L. 31.2 (12.3)
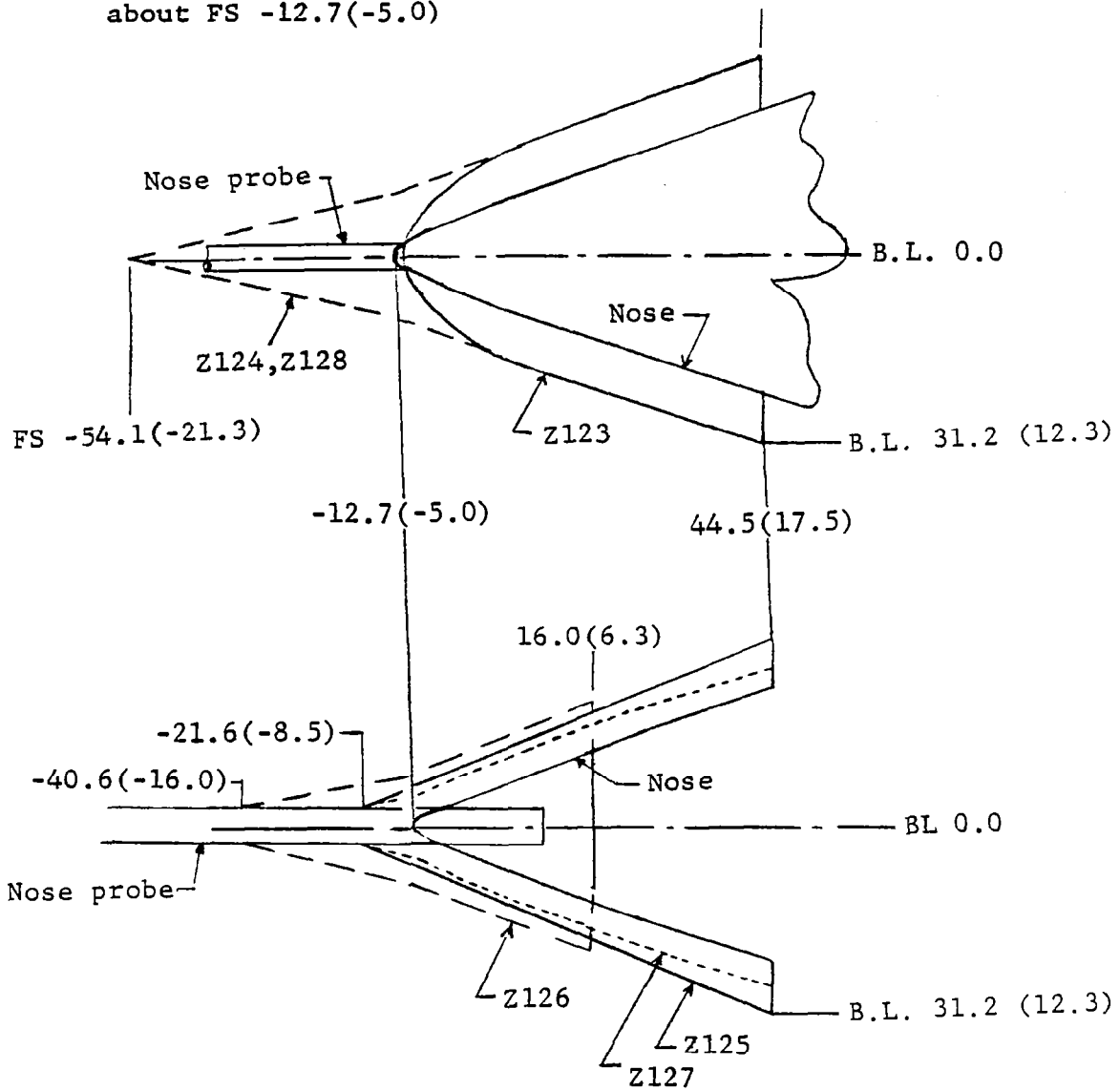
Figure 20b   Additional F-16 Nose Strakes

FS -39.9(-15.7)

BL 0.0

Nose probe

Z131,Z131A,Z131B

Z131B

Nose

Z131A

B.L. 30.5 (12.0)

0.0

31.8
(12.5)

44.5
(17.5)

-12.7
(-5.0)

B.L. 0.0

Nose probe

-33.5
(-13.2)

Z132

B.L. 13.2(5.2)

Nose

-12.7
(-5.0)

0.0

-33.0
(-13.0)

Nose

B.L. 29.2
(11.5)

Z133

44.5(17.5)
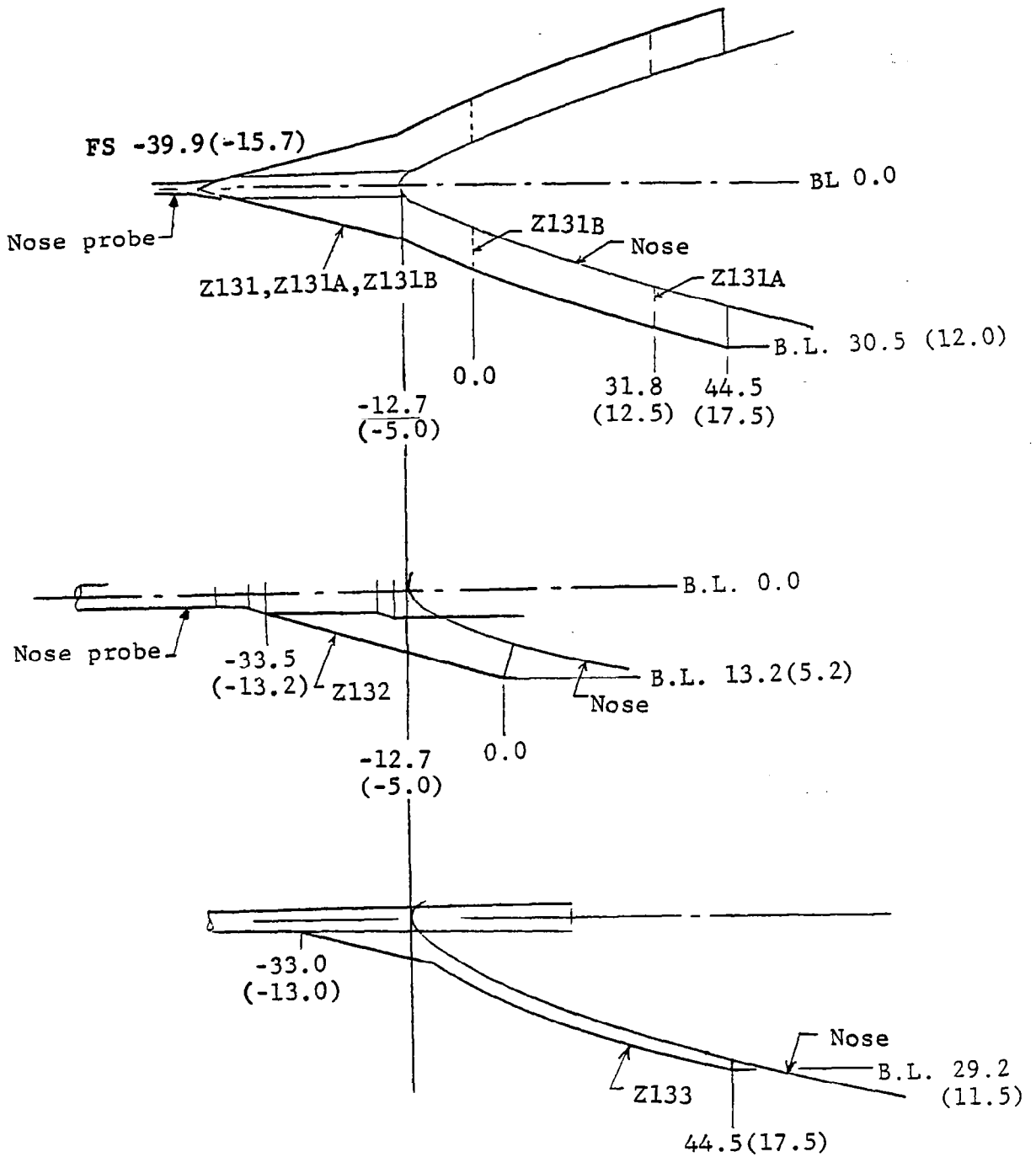
Figure 20c   Additional F-16 Nose Strakes

78

BL 0.0

BASIC F-16
N6
N7
N12

FS 217-2
(85.5)

FS -25.4
(-10.0)

FS   0.0

N6

N12

BASIC F-16

FS -12.7
(-5.0)

N7

WL 211.5 (83.25)
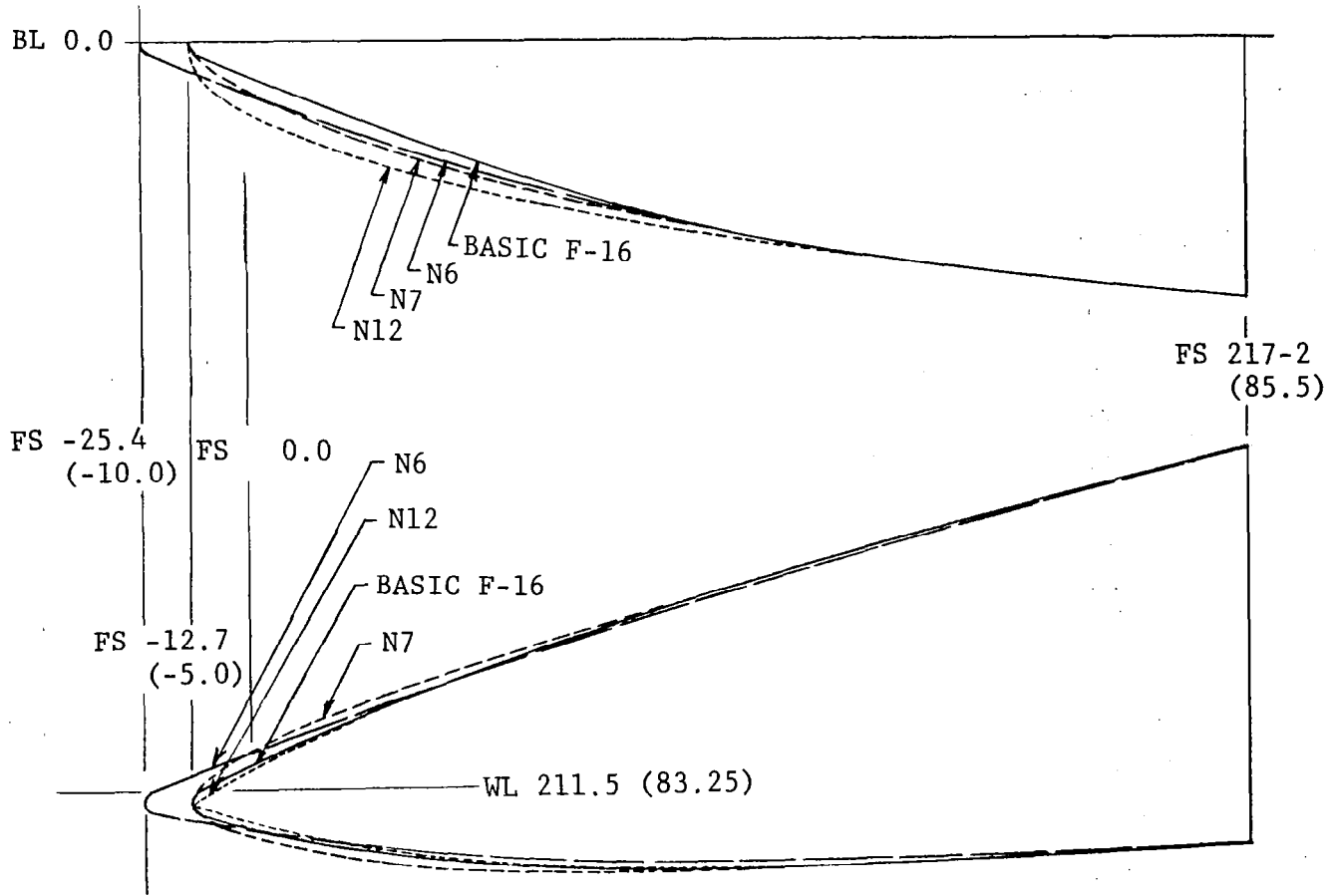
Figure 21   Nose Shapes Tested on the F-16

SYM	TEST	RUN	LEF	TEF	HT	MACH	CONFIG
△	1931	163	0	0	0	0.80	OFF
⊕	1931	171	0	0	0	0.80	Z7
⊞	1931	183	0	0	0	0.90	Z8
⬦	1931	196	0	0	0	0.80	Z9
✳	1931	188	0	0	0	0.80	Z10
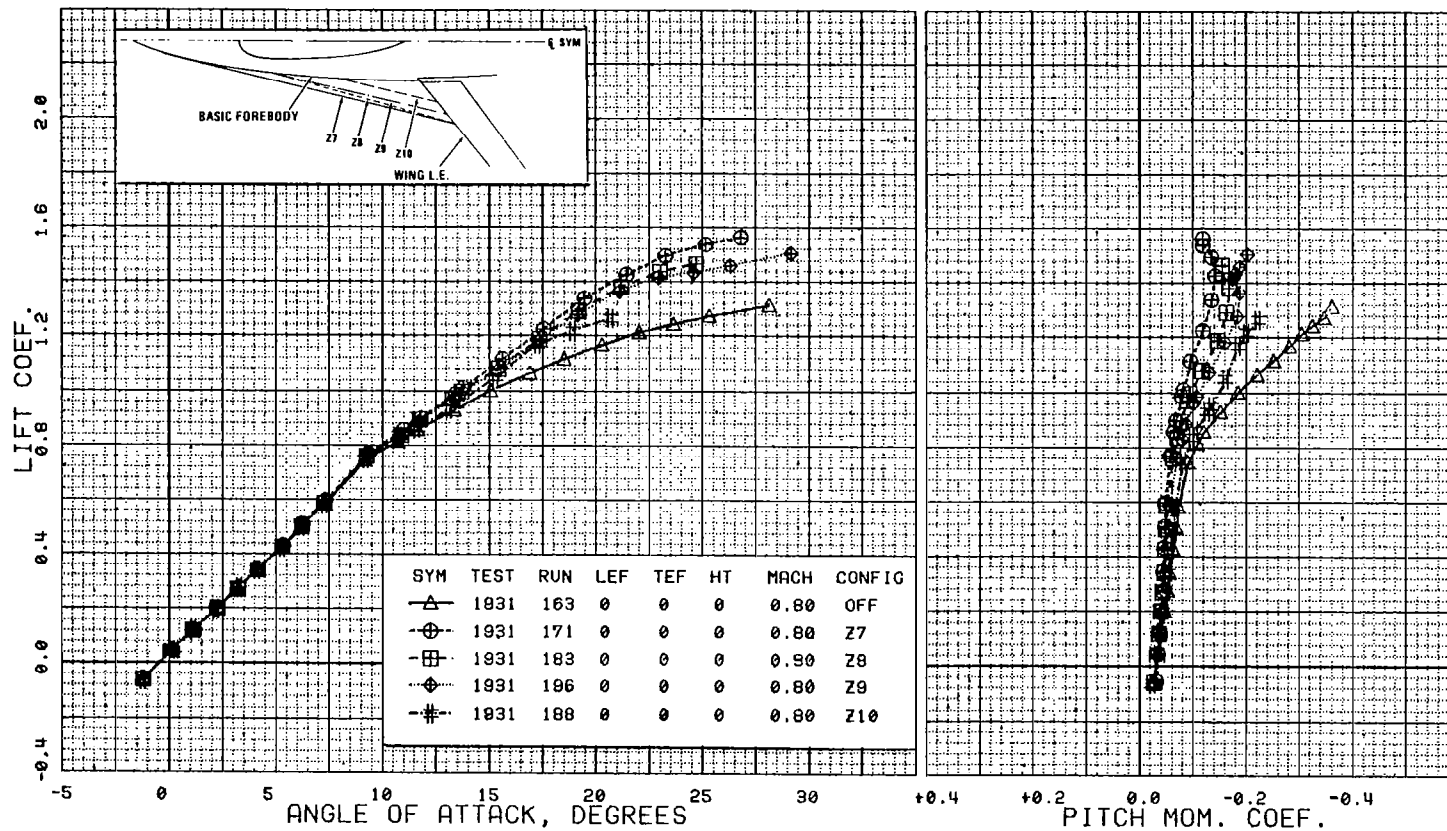
Figure 22a   Lift Effects of a Family of Delta Planform Forebody Strakes on Configuration 785
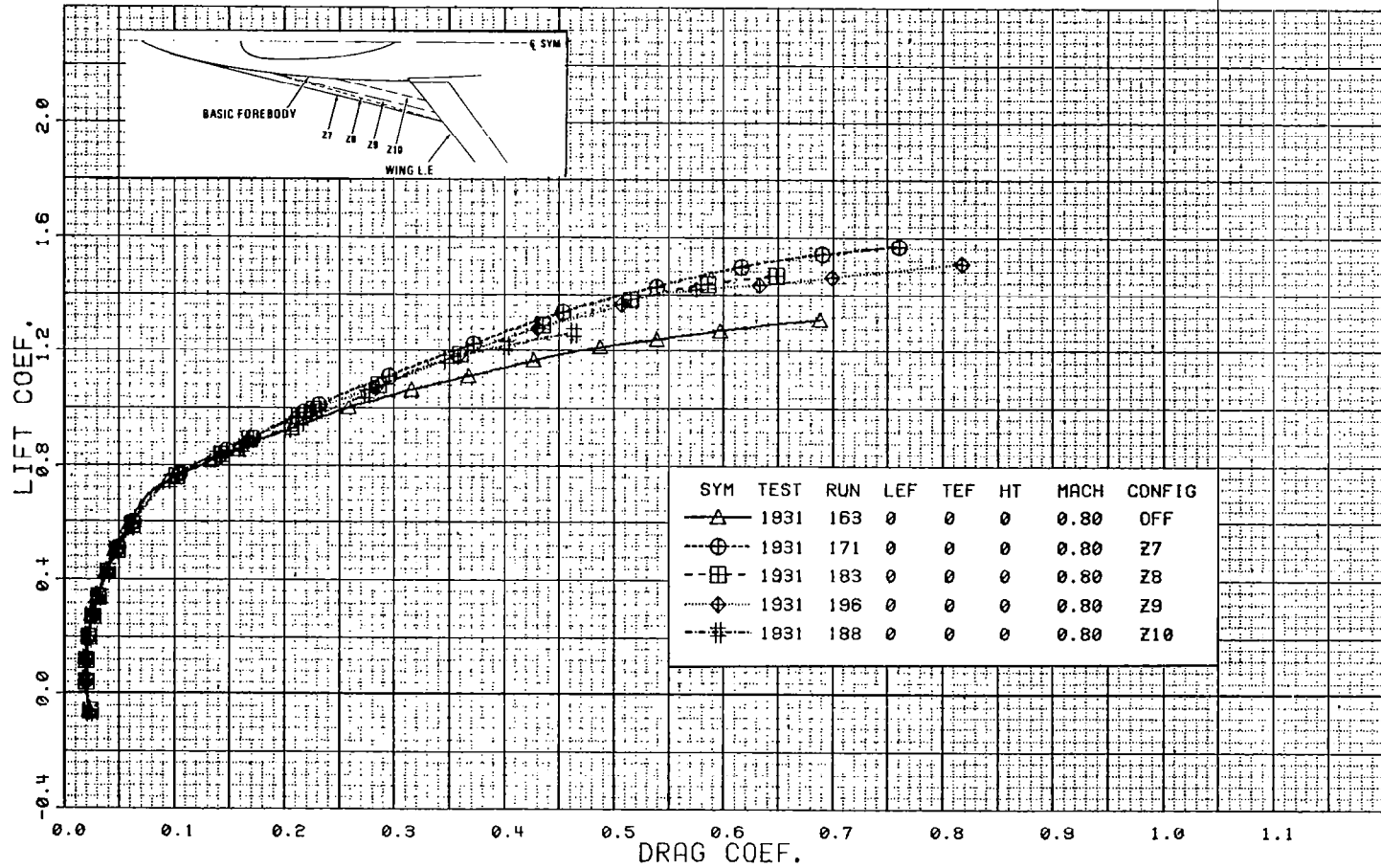
Figure 22b   Drag Effects of a Family of Delta Planform Forebody Strakes on Configuration 785

SYM	TEST	RUN	LEF	TEF	HT	MACH	CONFIG
△	3630	104	0	0	0	0.80	Z63
⊕	3630	153	0	0	0	0.80	Z64
⊞	3630	251	0	0	0	0.80	Z65
◇	3630	255	0	0	0	0.80	Z66
⌗	3630	149	0	0	0	0.80	Z71
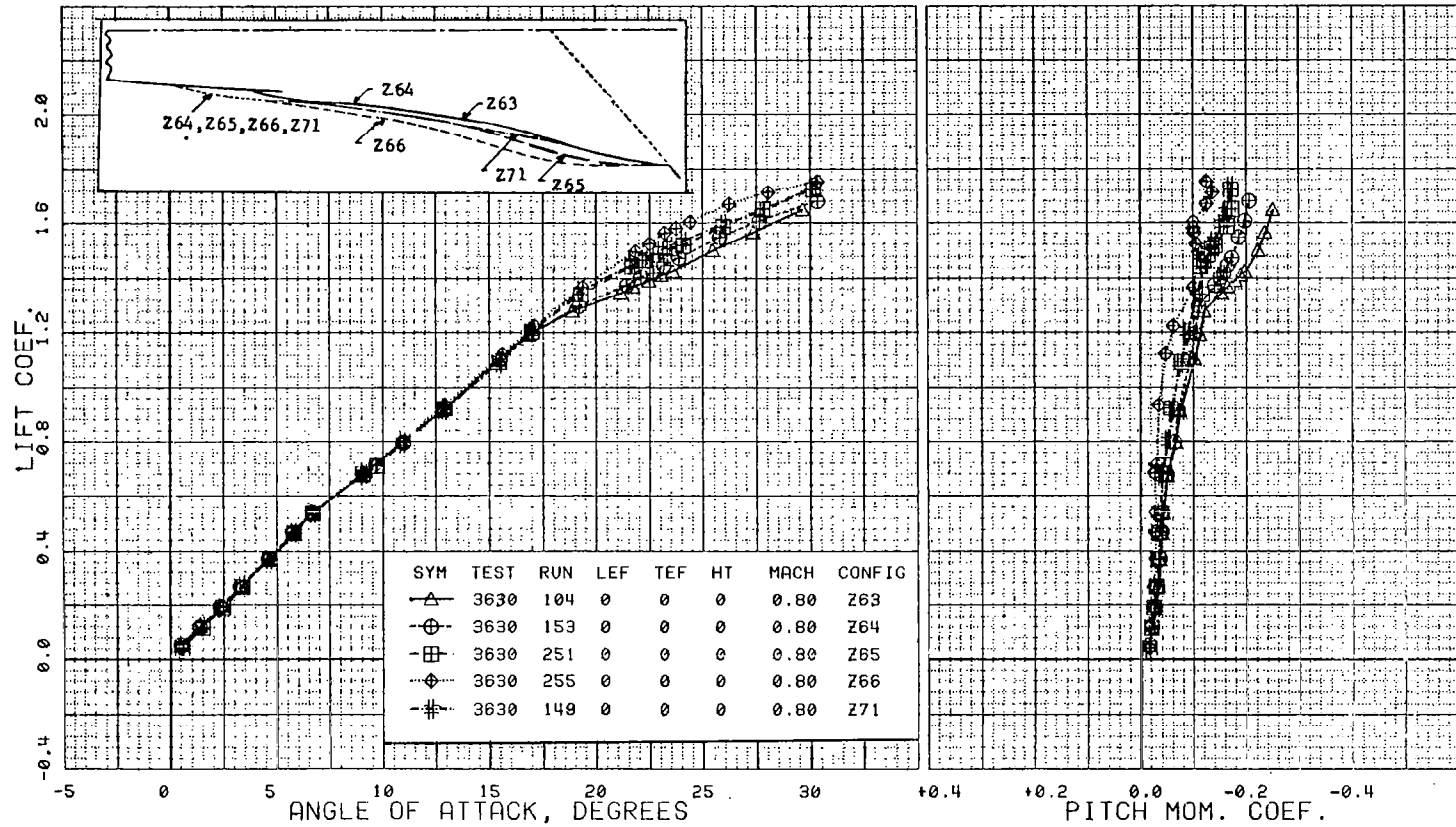
Figure 23a   Lift Effects of a Family of Ogee Planform Forebody Strakes on a Stretched YF-16
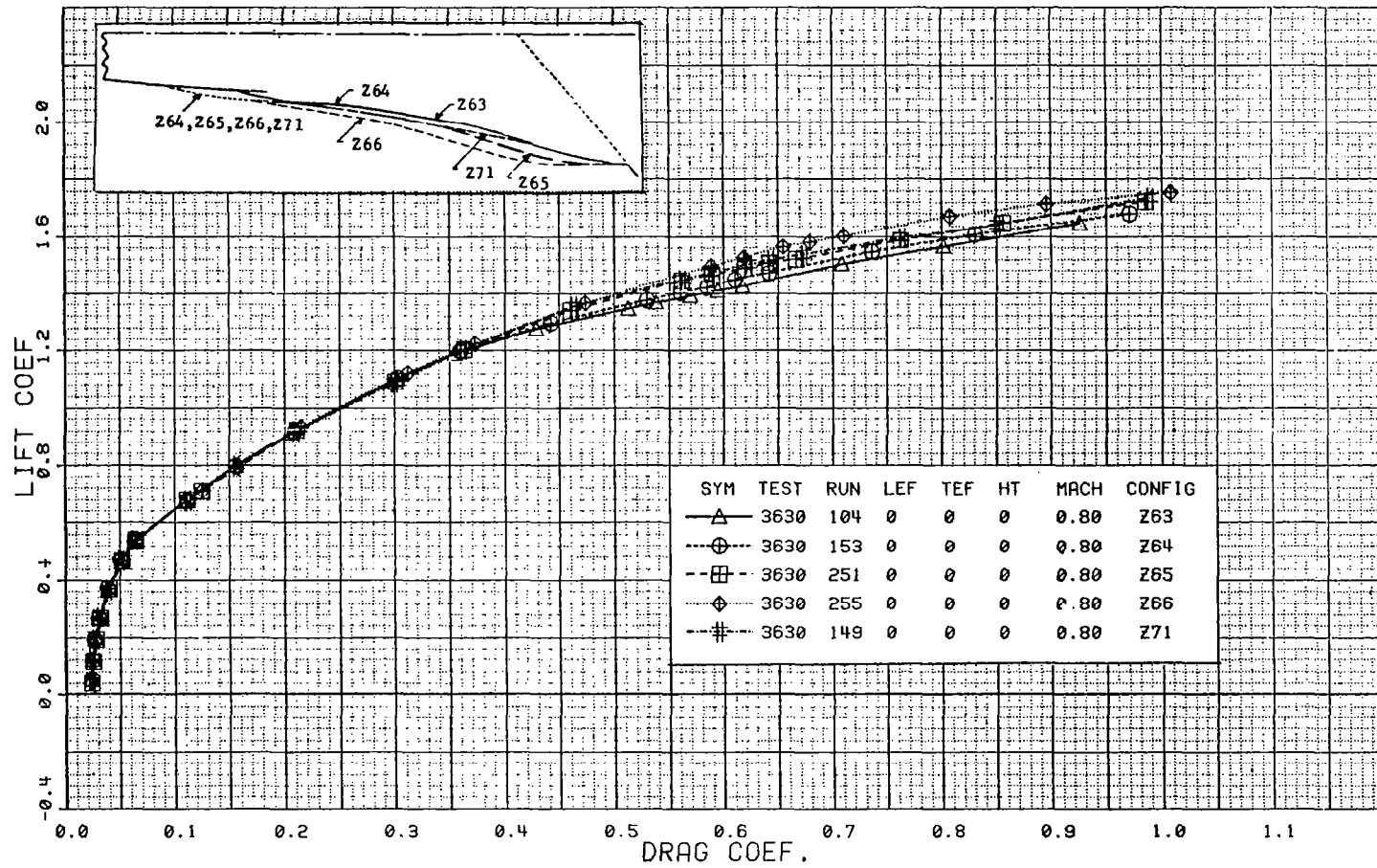
Figure 23b   Drag Effects of a Family of Ogee Planform Forebody Strakes
on a Stretched YF-16
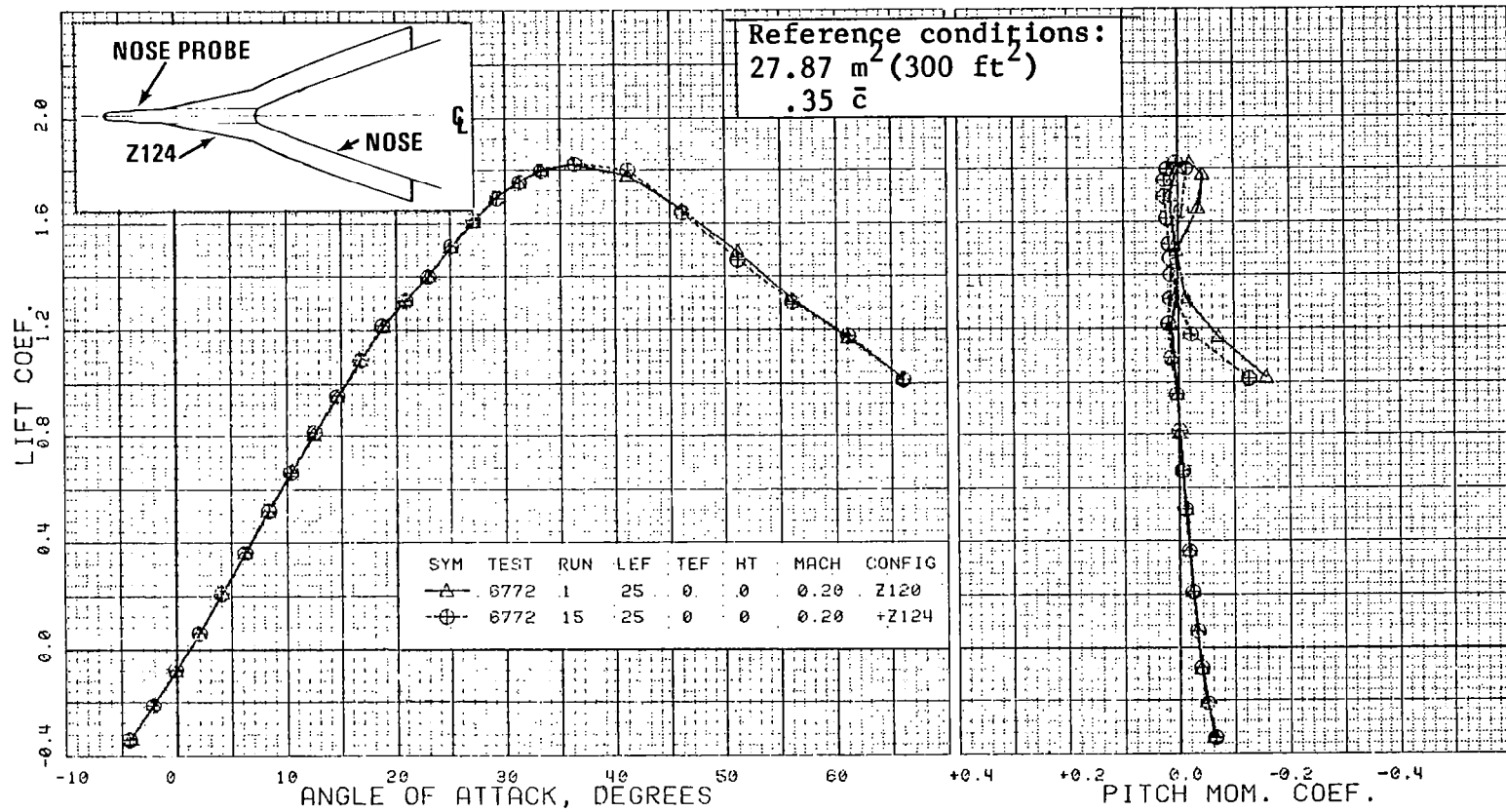
Figure 24   Effects of a Nose Strake on the F-16 Lift
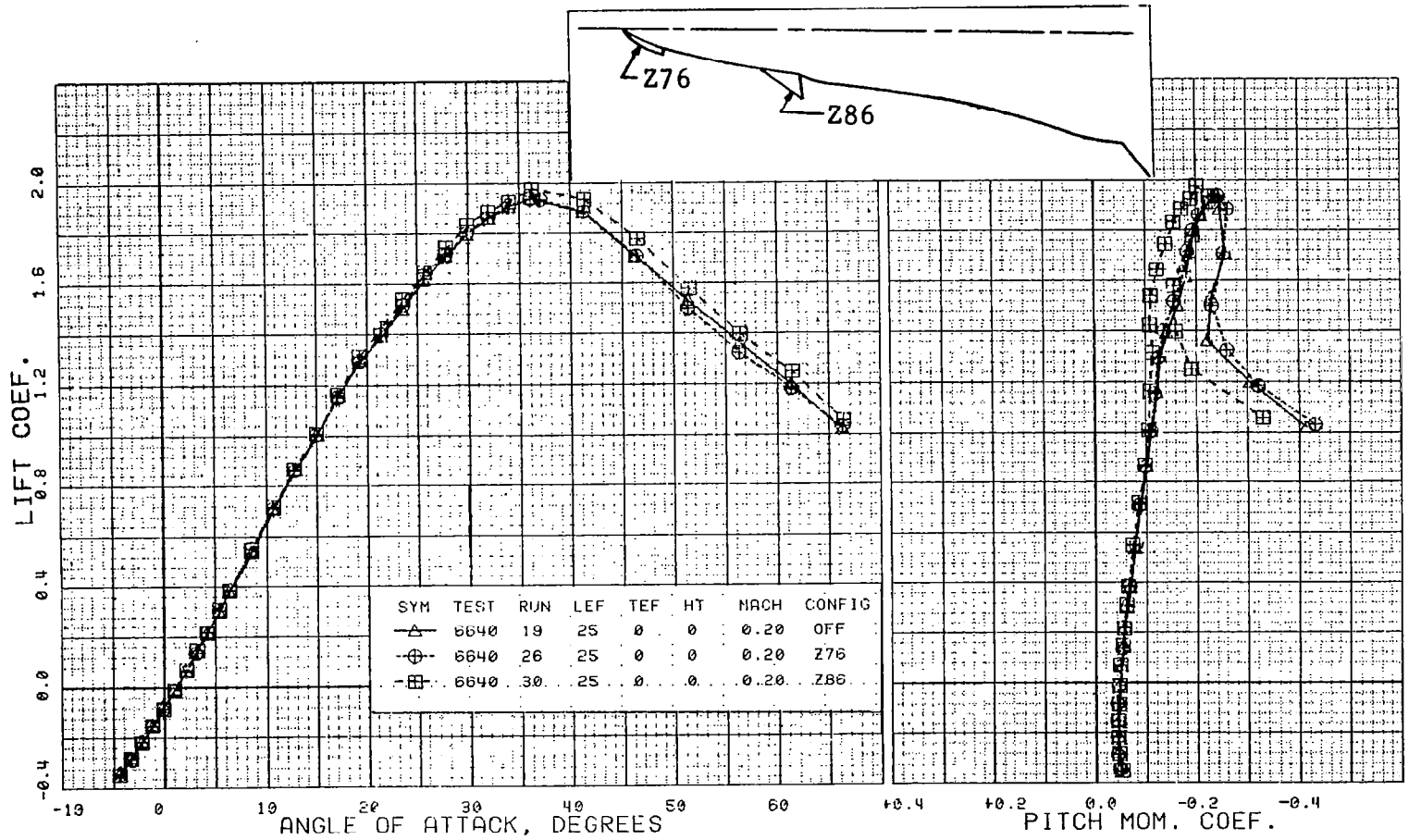
Figure 25a   Lift Effects of a Nose and Canard Strake on the YF-16

The chart contains the following data legend:

SYM	TEST	RUN	LEF	TEF	HT	MACH	CONFIG
△	6640	19	25	0	0	0.20	OFF
⊕	6640	26	25	0	0	0.20	Z76
⊞	6640	30	25	0	0	0.20	Z86

LIFT COEF.

DRAG COEF.

Z76

Z86

98
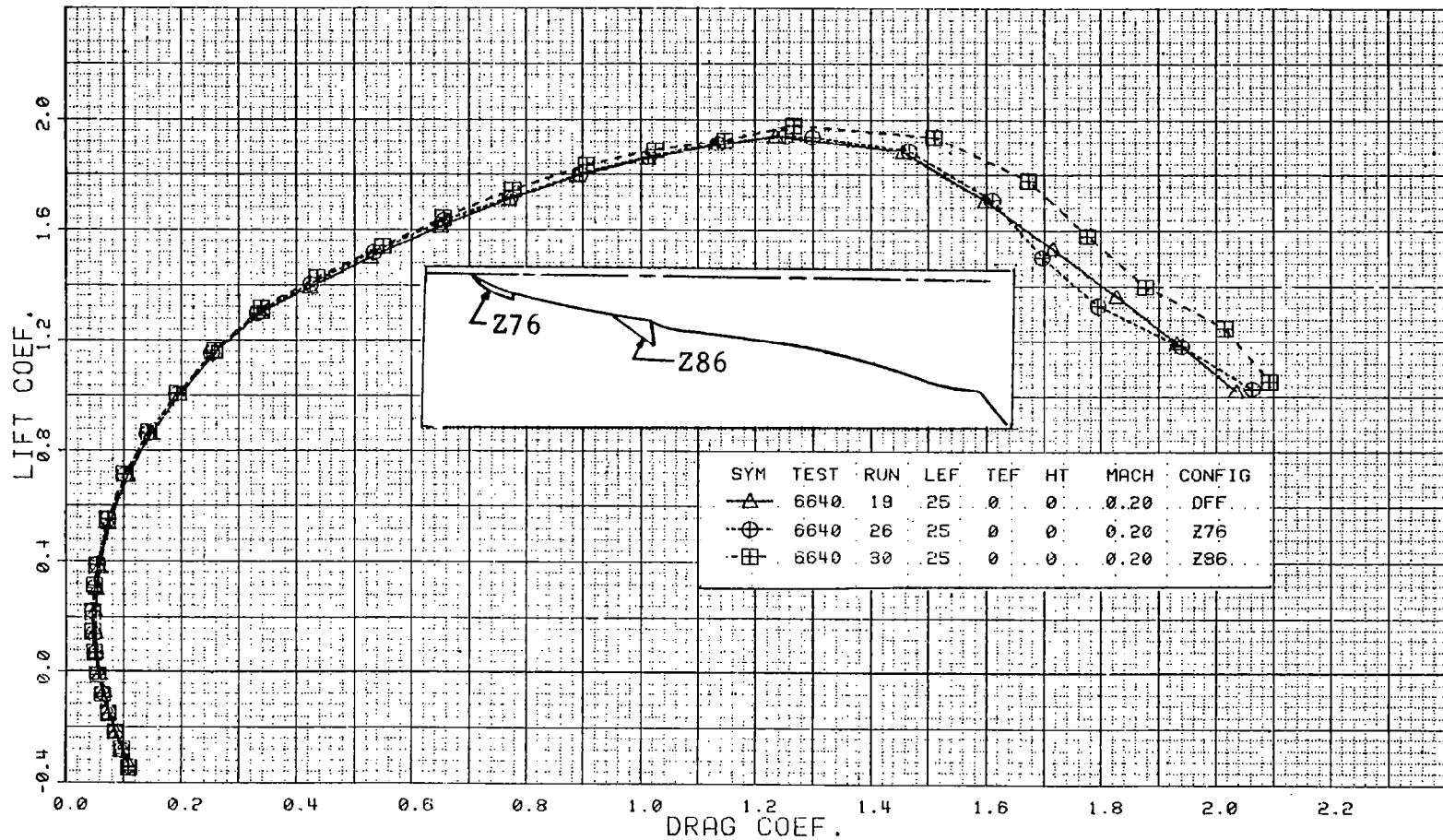
Figure 25b   Drag Effects of a Nose and Canard Strake on the YF-16

SYM	TEST	RUN	LEF	TEF	HT	MACH	CONFIG
△	1932	437	0	0	0	0.80	OFF
⊕	1932	428	10	0	0	0.80	OFF
⊞	1932	573	15	0	0	0.80	OFF
◇	1932	448	25	0	0	0.80	OFF
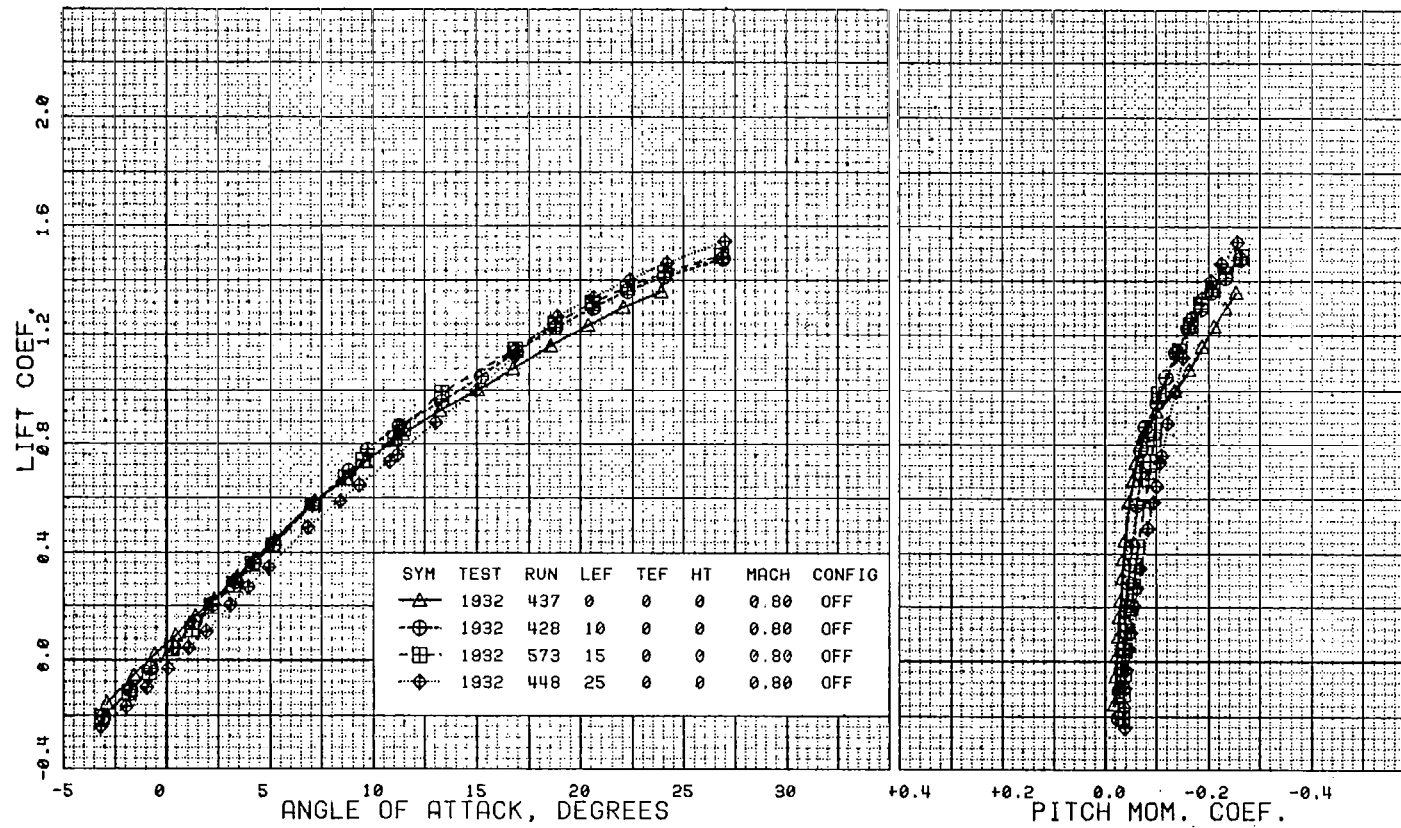
Figure 26a   Lift Effects of a Leading-Edge Flap on Configuration 401F-5 with No Strake

SYM TEST RUN LEF TEF HT MACH CONFIG
△ 1932 437 0 0 0 0.80 OFF
⊕ 1932 428 10 0 0 0.80 OFF
⊞ 1932 573 15 0 0 0.80 OFF
◈ 1932 448 25 0 0 0.80 OFF
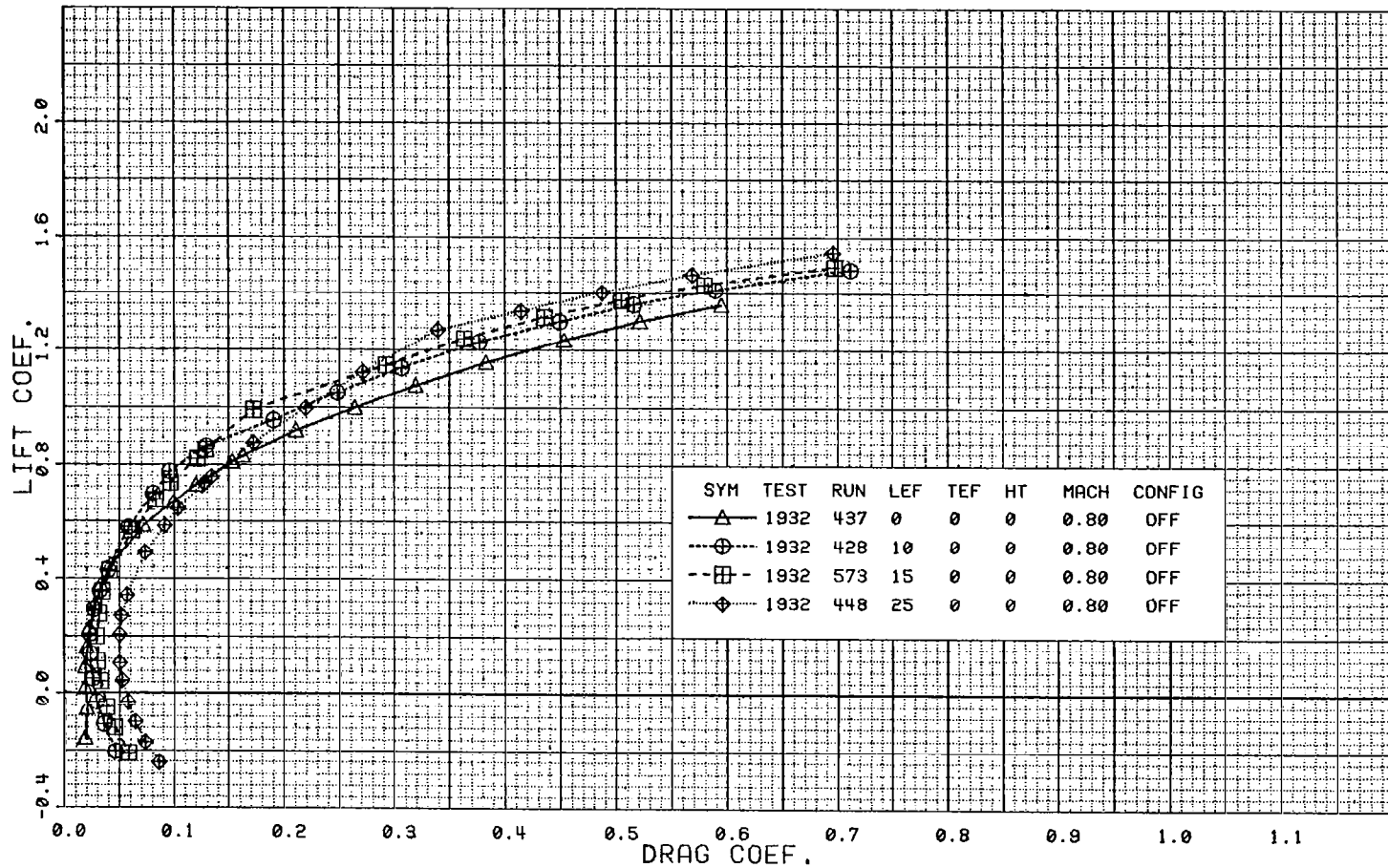
Figure 26b   Drag Effects of a Leading-Edge Flap on Configuration 401F-5
with No Strake

SYM	TEST	RUN	LEF	TEF	HT	MACH	CONFIG
—△—	1932	437	0	0	0	0.80	OFF
—⊕—	1932	471	0	0	0	0.80	Z4
—⊞—	1932	483	10	0	0	0.80	Z4
—◇—	1932	577	15	0	0	0.80	Z4
—✳—	1932	580	25	0	0	0.80	Z4

LIFT COEF.

ANGLE OF ATTACK, DEGREES

PITCH MOM. COEF.
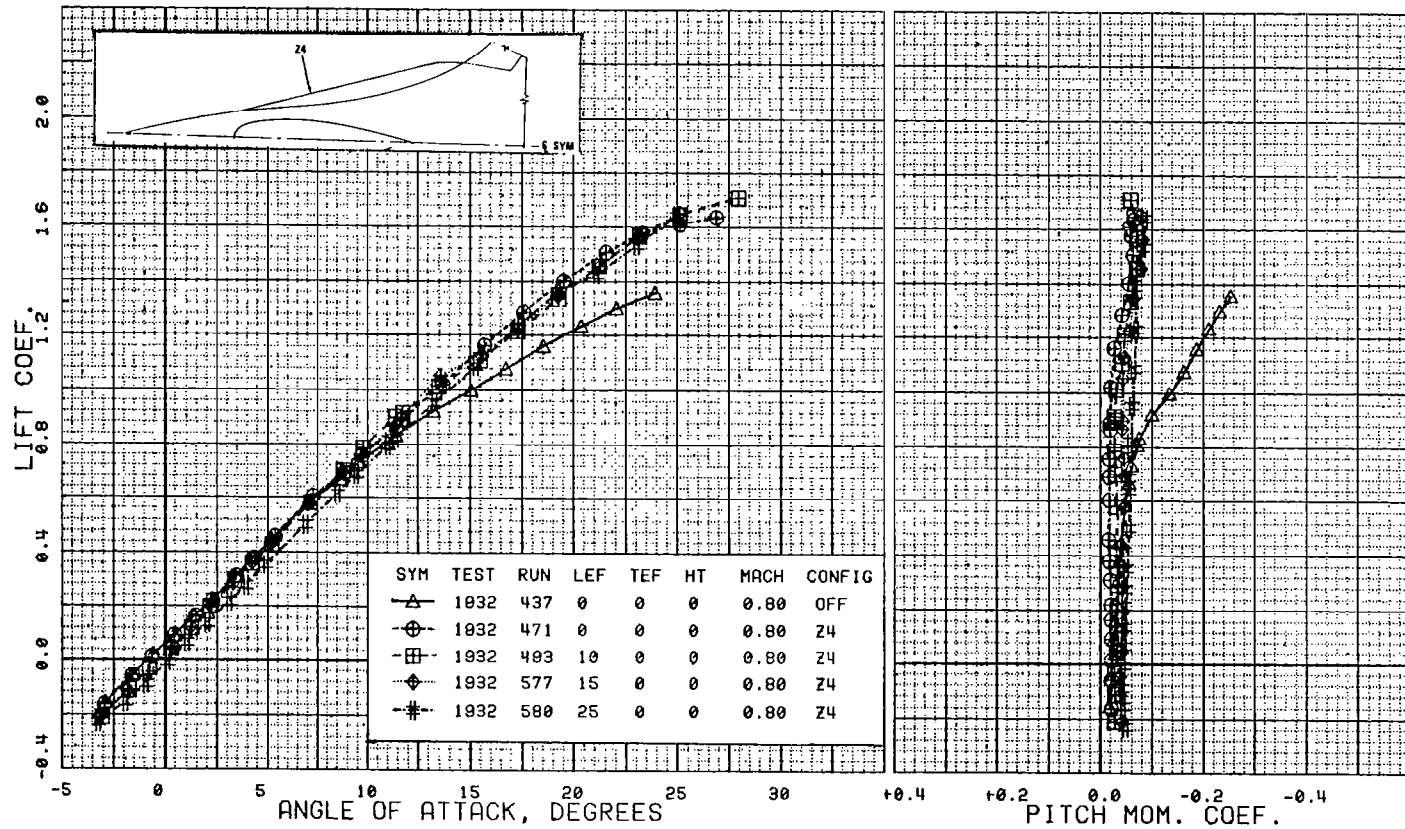
Figure 27a   Lift Effects of a Leading-Edge Flap on Configuration 401F-5 with a Forebody Strake

SYM	TEST	RUN	LEF	TEF	HT	MACH	CONFIG
△	1932	437	0	0	0	0.80	OFF
⊕	1932	471	0	0	0	0.80	Z4
⊞	1932	493	10	0	0	0.80	Z4
◈	1932	577	15	0	0	0.80	Z4
▦	1932	580	25	0	0	0.80	Z4

LIFT COEF.

DRAG COEF.
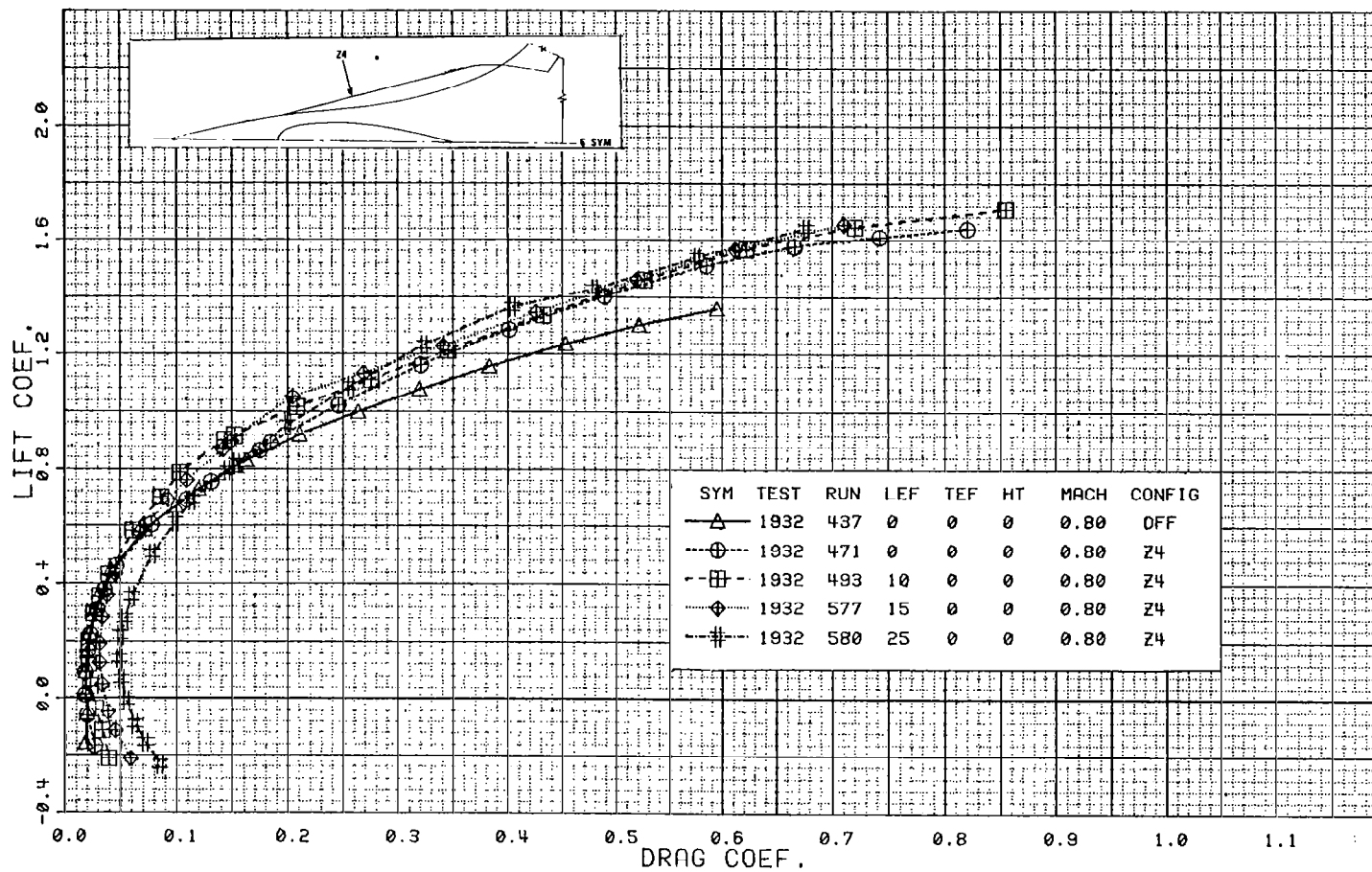
Figure 27b   Drag Effect of a Leading-Edge Flap on Configuration 401F-5
with a Forebody Strake
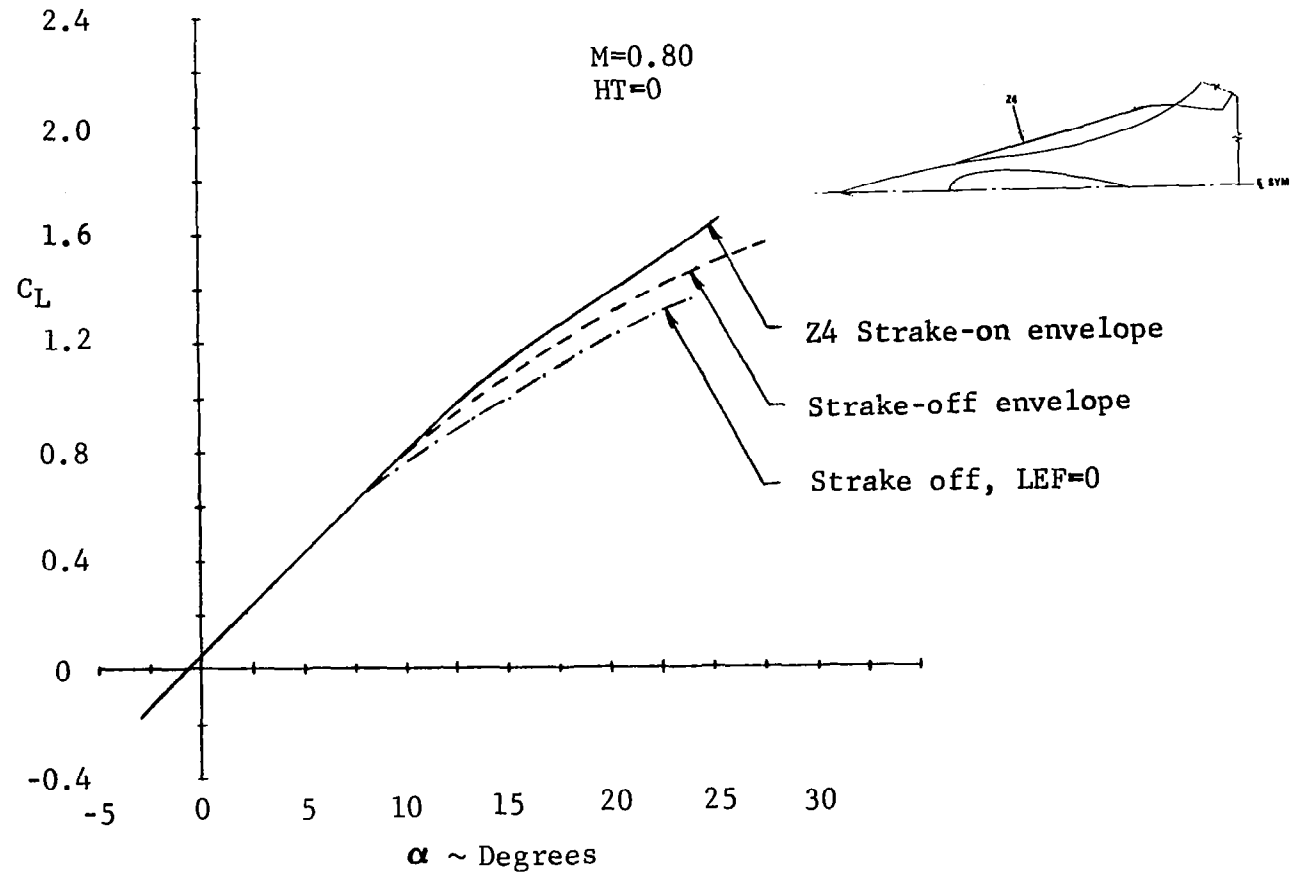
Figure 28a   Effect of a Forebody Strake on the Envelope Lift Curve
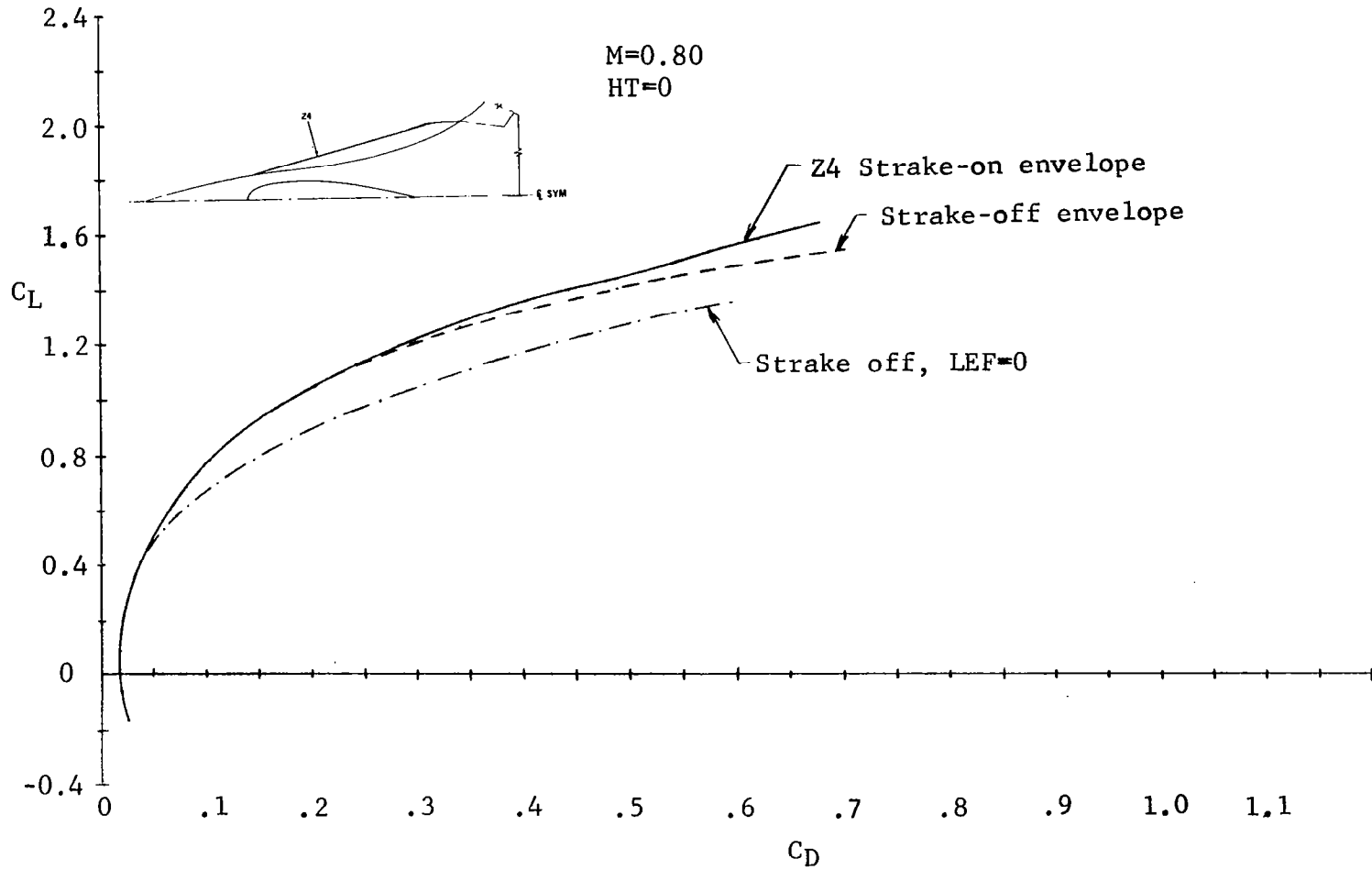
Figure 28b   Effect of a Forebody Strake on the Envelope Drag Polar
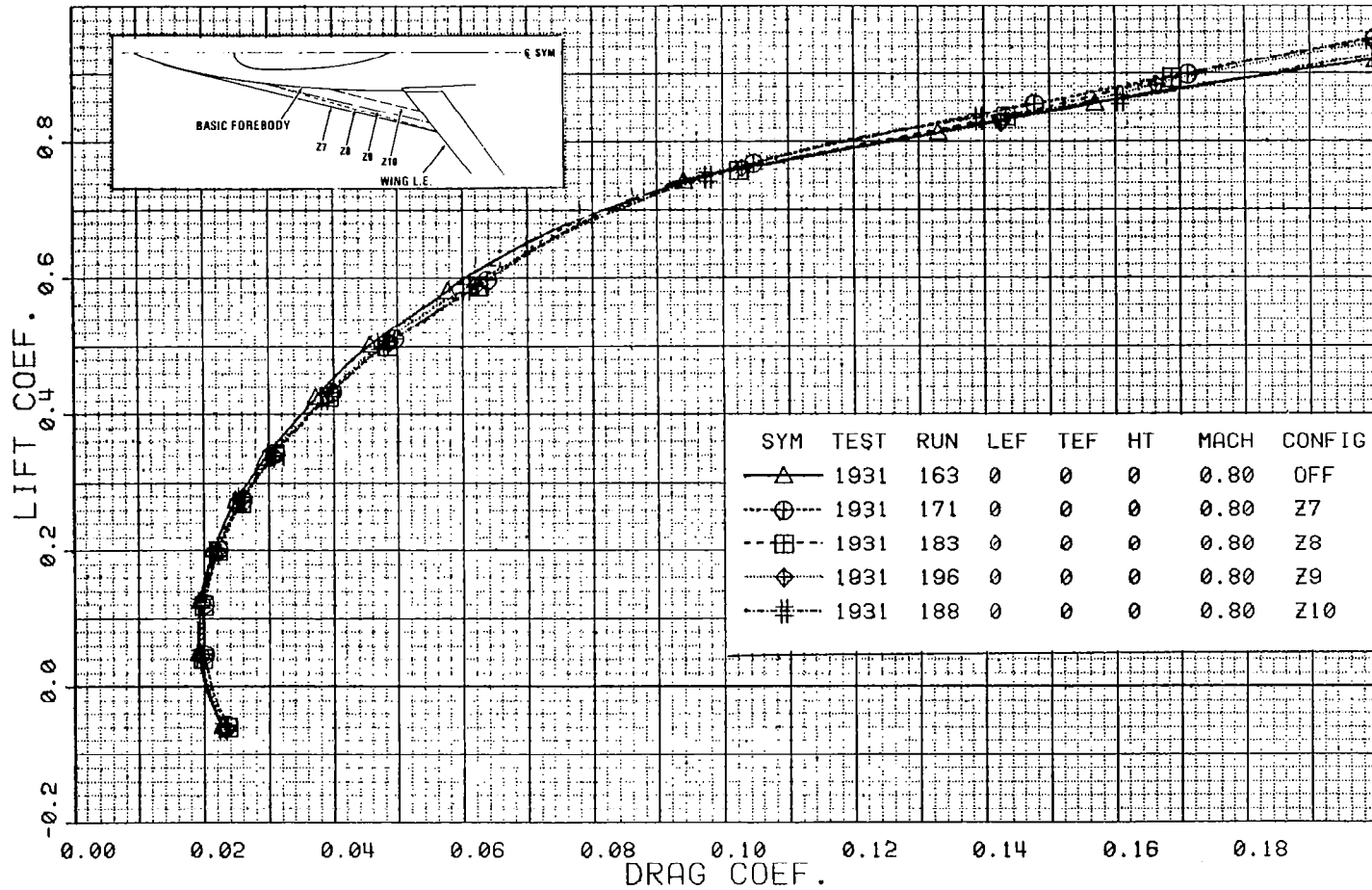
Figure 29   Effects of a Family of Delta Planform Forebody Strakes on
the Low-Lift Drag at .80 Mach Number

The chart is a plot of LIFT COEF. versus DRAG COEF. with the following legend:

SYM	TEST	RUN	LEF	TEF	HT	MACH	CONFIG
△	1931	161	0	0	0	1.20	OFF
⊕	1931	168	0	0	0	1.20	Z7
⊞	1931	177	0	0	0	1.20	Z8
◇	1931	199	0	0	0	1.20	Z9
⧪	1931	187	0	0	0	1.20	Z10
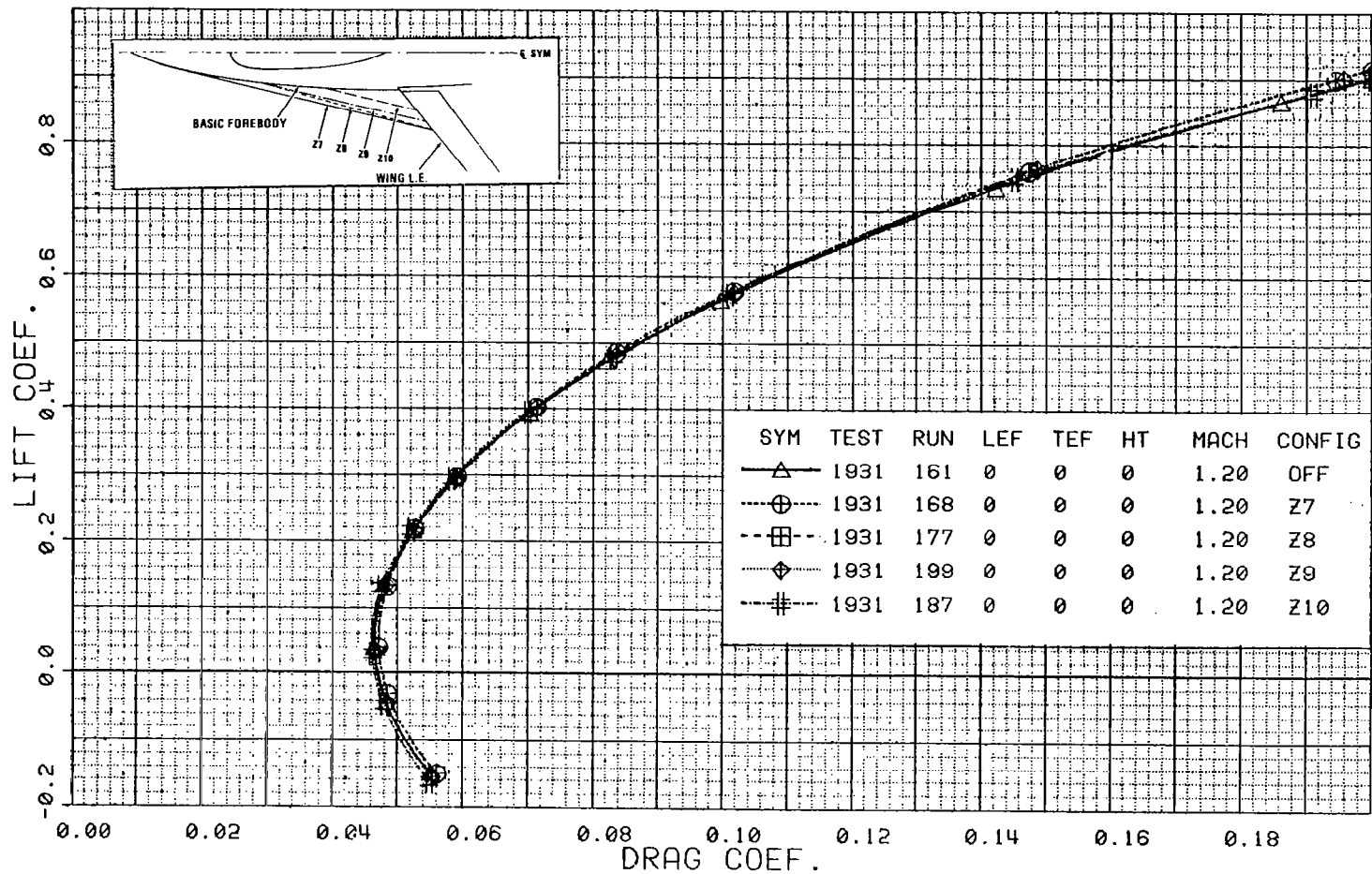
Figure 30   Effects of a Family of Delta Planform Forebody Strakes on the Low-Lift Drag at 1.20 Mach Number
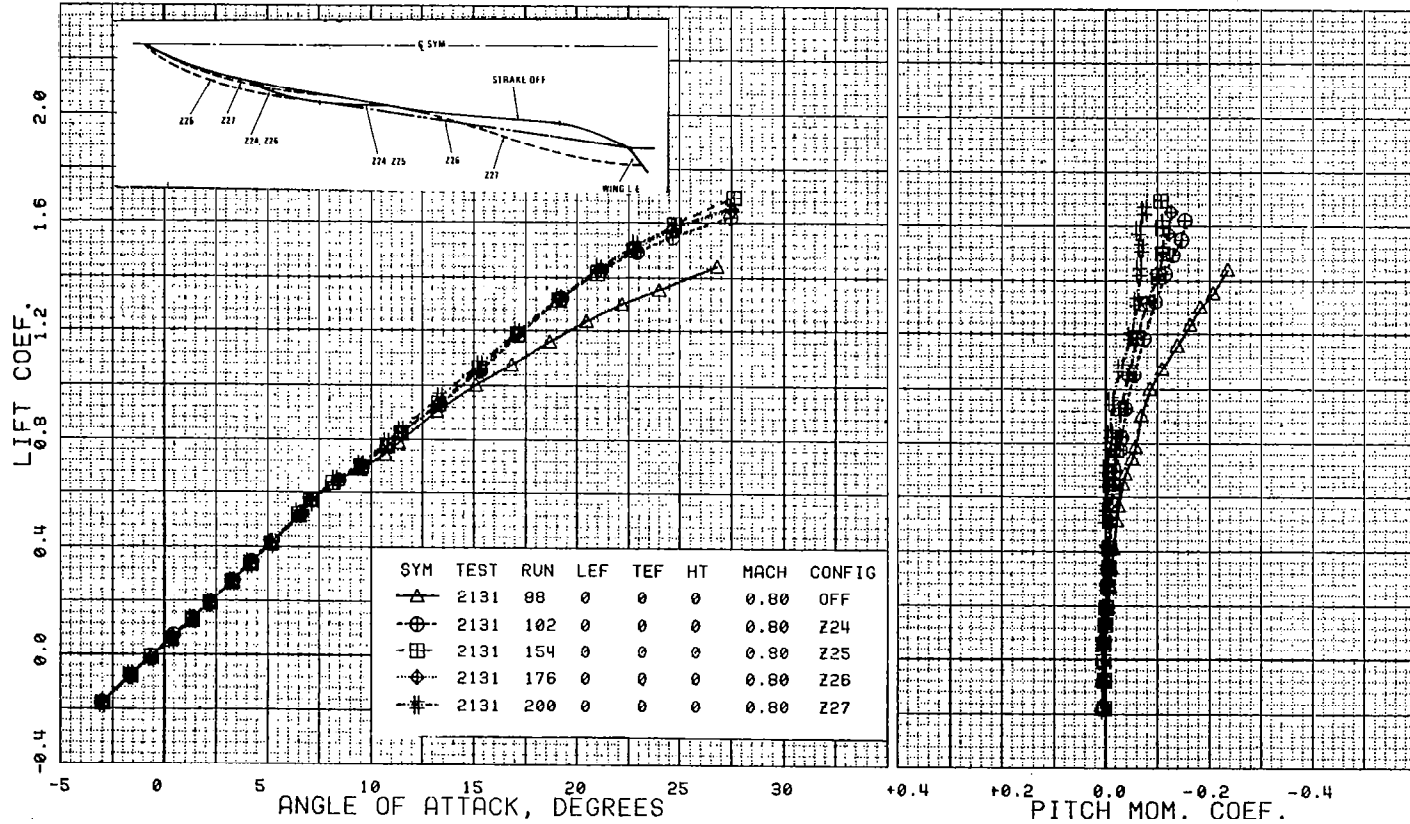
Figure 31   Lift Effects of a Family of Forebody Strakes on Configuration 401F-10A at .80 Mach Number

SYM	TEST	RUN	LEF	TEF	HT	MACH	CONFIG
—△—	2131	06	0	0	0	0.80	OFF
--⊕--	2131	101	0	0	0	0.90	Z24
-⊞-	2131	153	0	0	0	0.90	Z25
--⊕--	2131	175	0	0	0	0.90	Z26
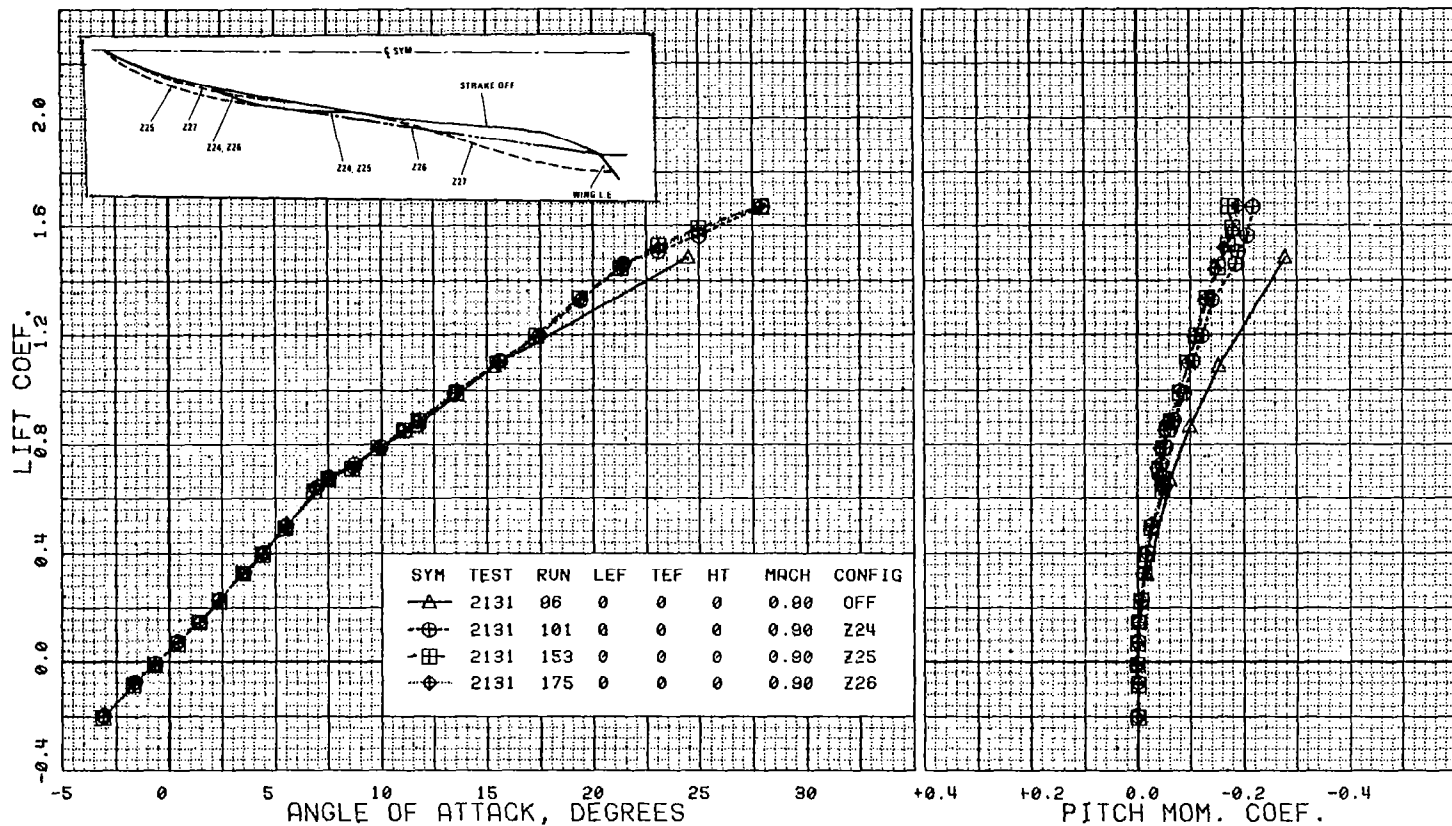
Figure 32   Lift Effects of a Family of Forebody Strakes on Configuration 401F-10A at .90 Mach Number
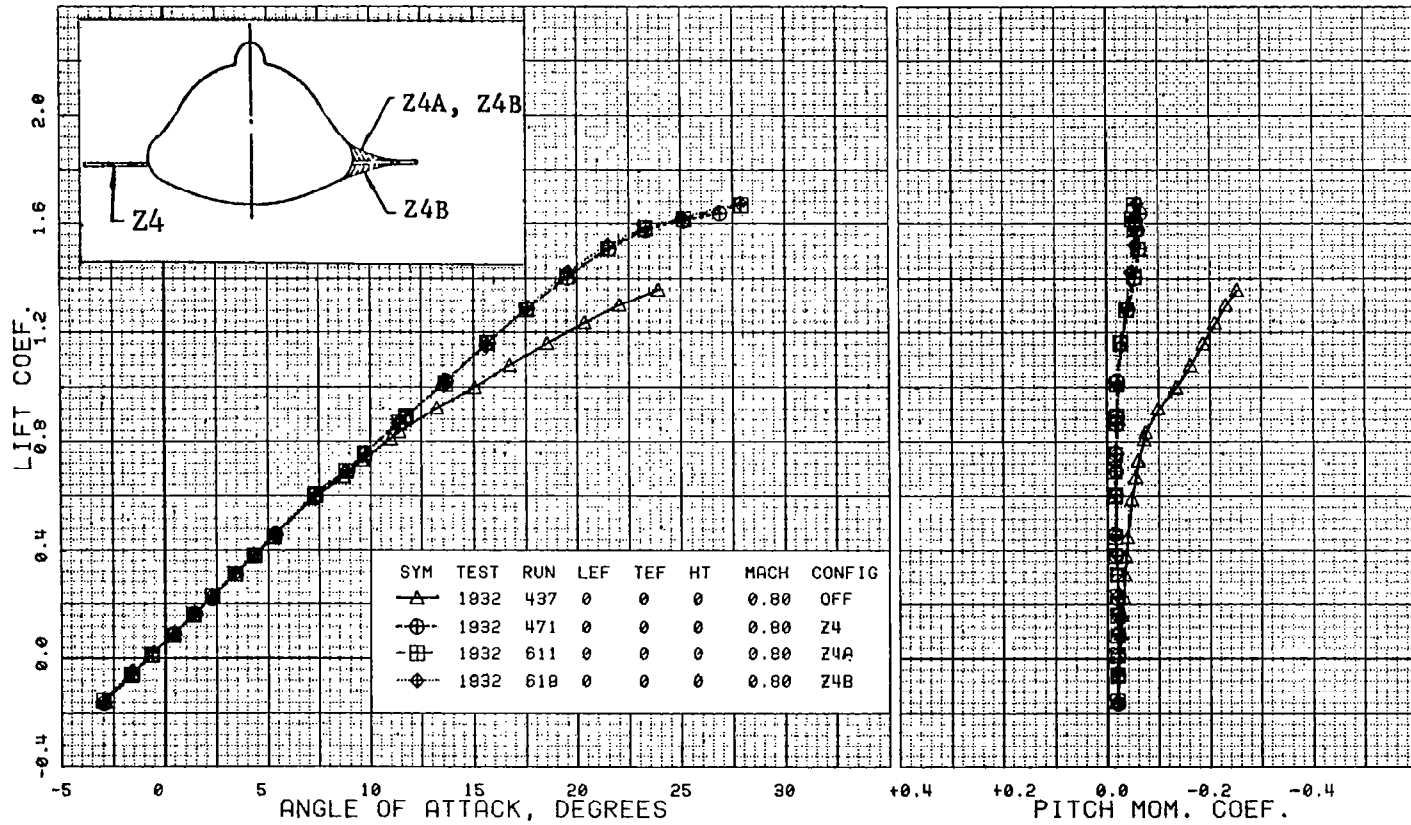
Figure 33a   Effects of Forebody-Strake Blending on Lift
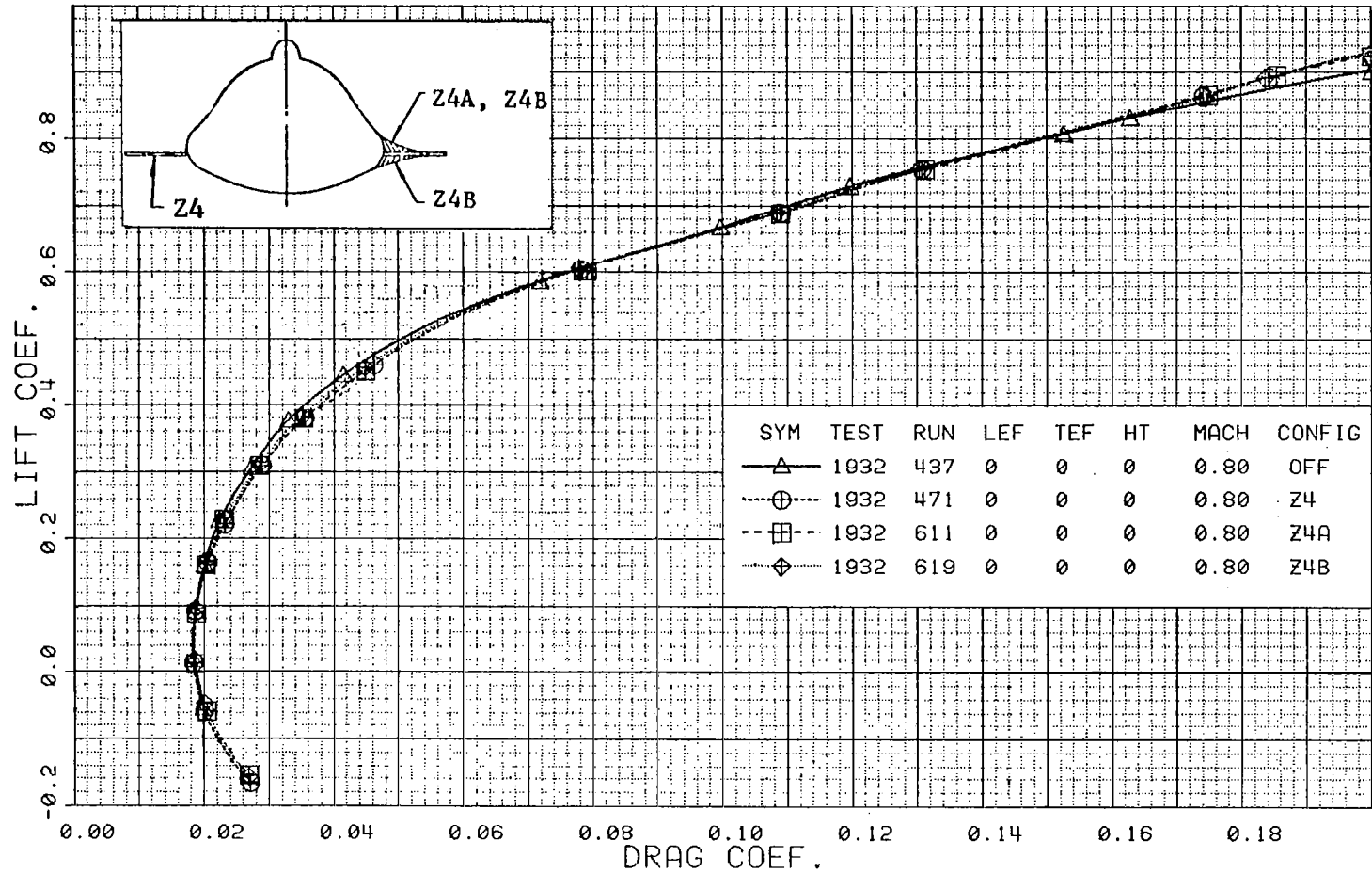
Figure 33b   Effects of Forebody-Strake Blending on Drag
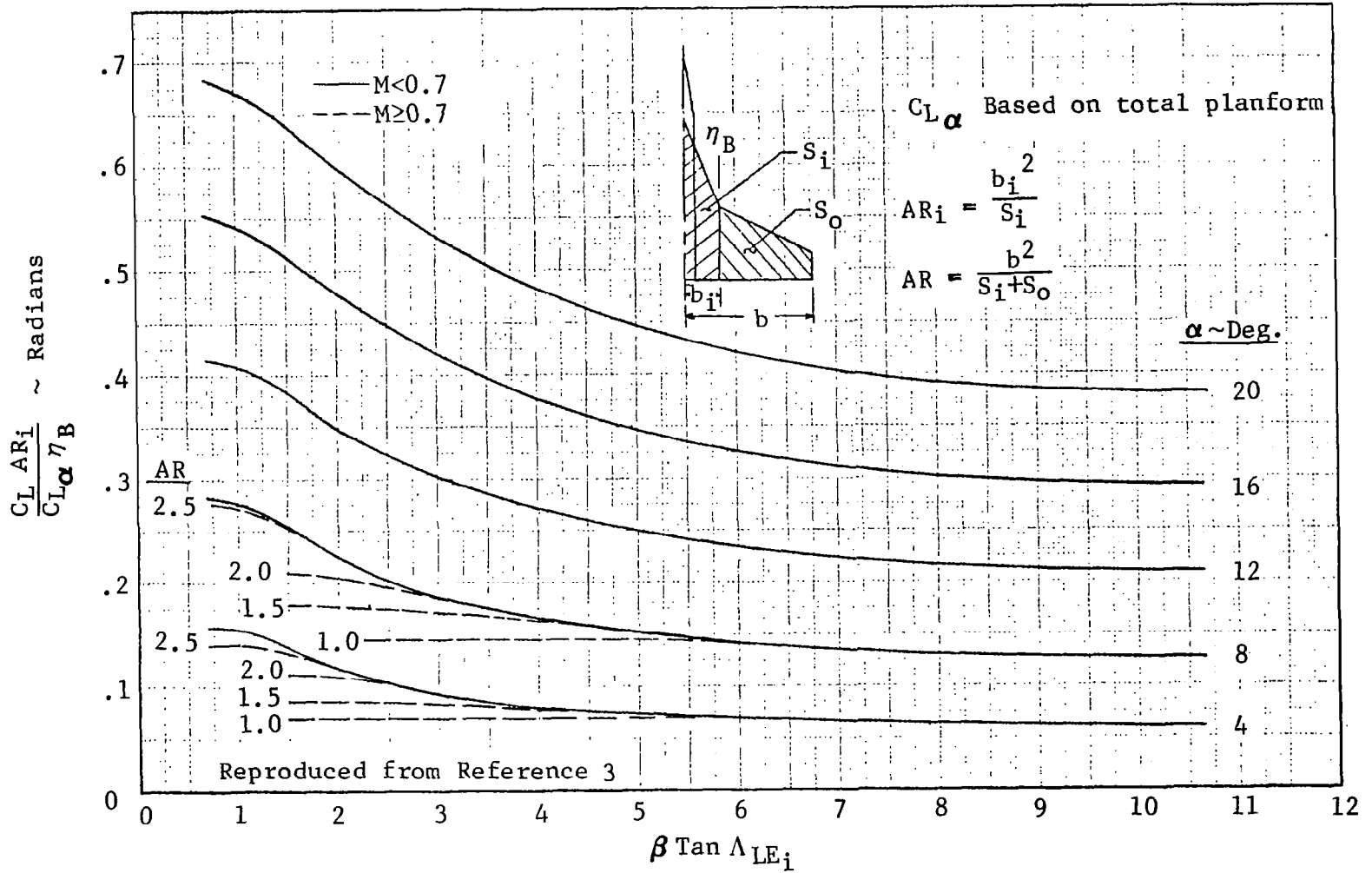
Figure 34   Calculation Chart for Prediction of Non-Linear Lift of Double-Delta Planforms at Subsonic Speeds.
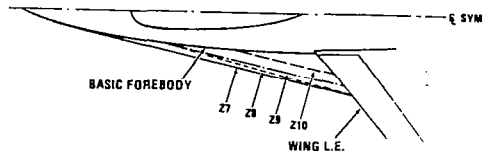
SYM	TEST	RUN	LEF	TEF	HT	MACH	CONFIG
•••	1931	163	0	0	0	0.90	OFF
——	1931	171	0	0	0	0.80	Z7
——	1931	183	0	0	0	0.80	Z8
—•—	1931	196	0	0	0	0.80	Z9
——	1931	188	0	0	0	0.80	Z10

••• BASELINE RUN
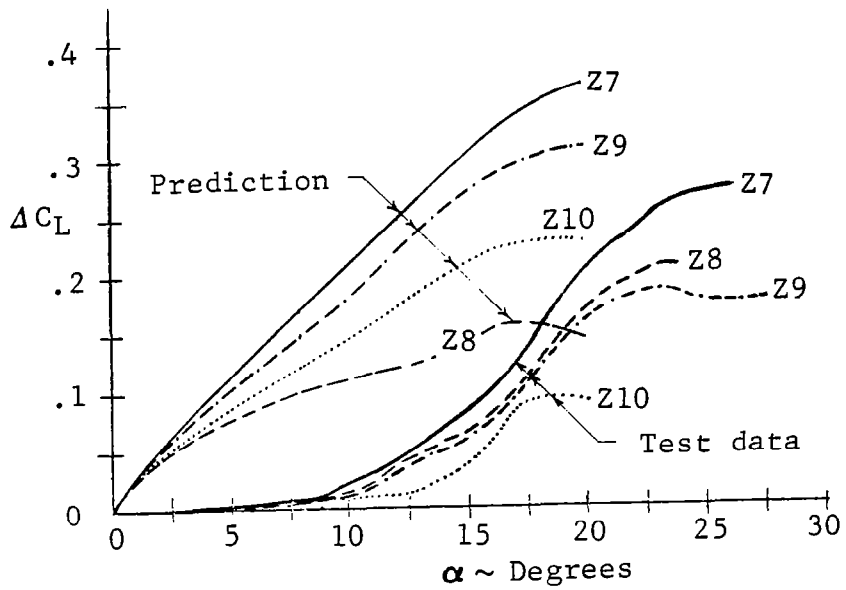
Figure 35   Evaluation of WINSTAN Lift Prediction Technique
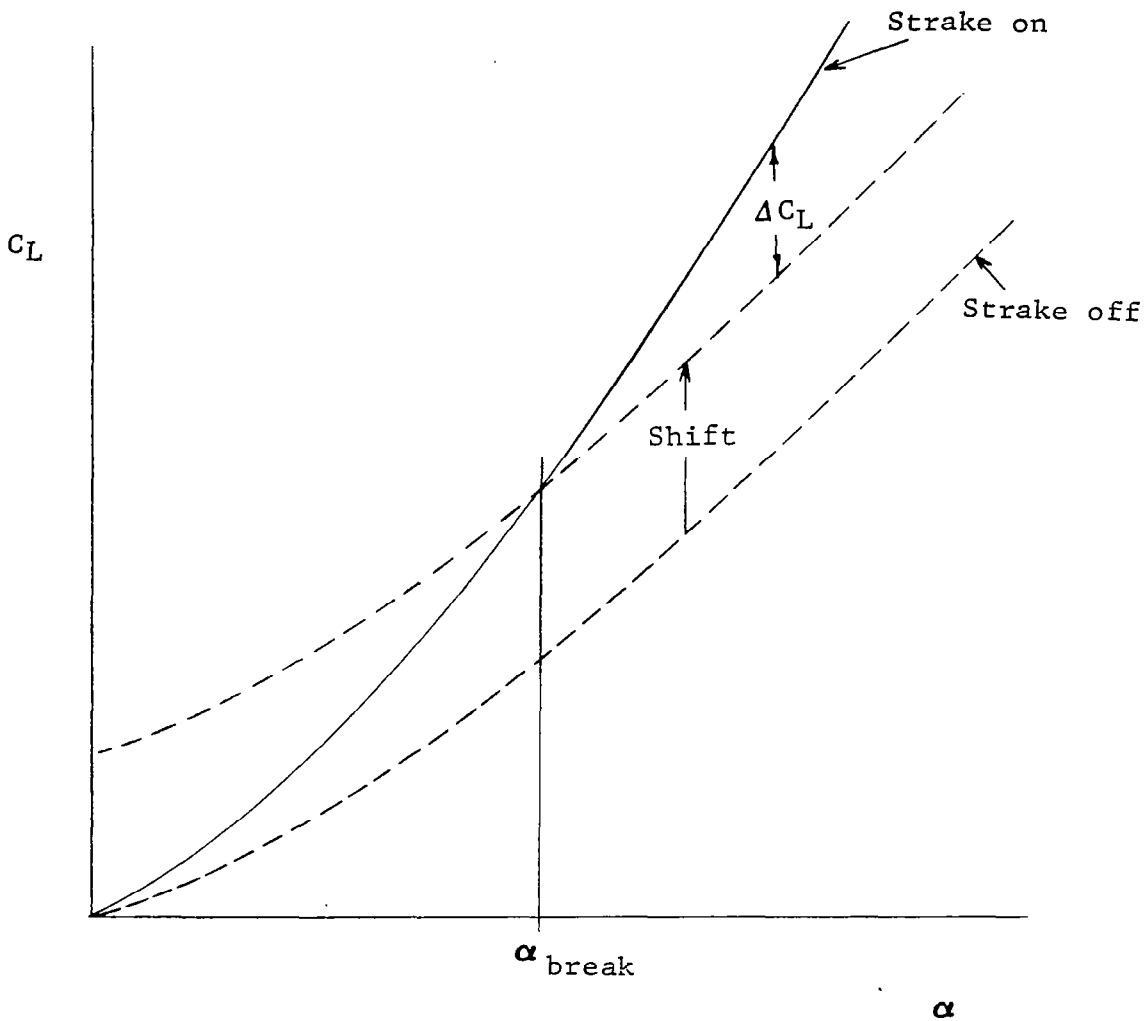
Figure 36   Modified WINSTAN Lift Prediction Technique
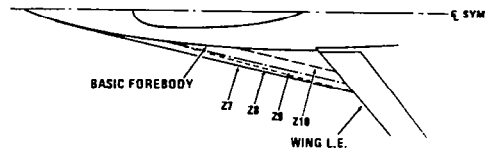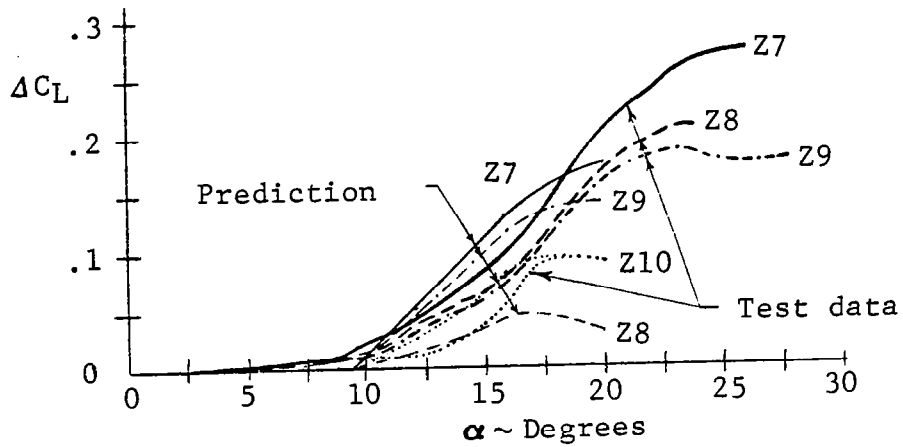
Figure 37   Evaluation of Modified WINSTAN Lift
             Prediction Technique

A

A

A_{EFF}

Section A-A
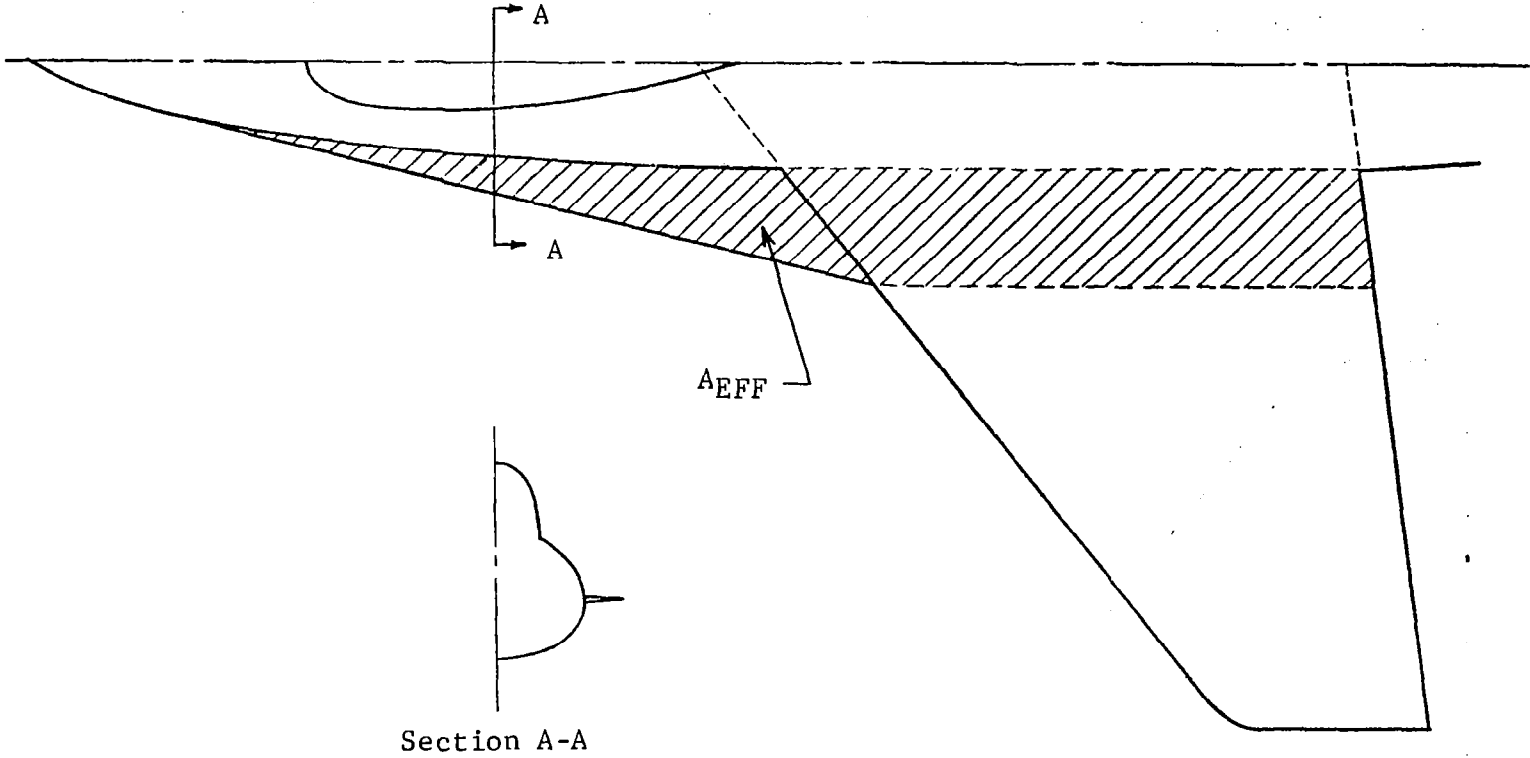
Figure 38   Definition of Effective Strake Area for a Simple Wing Body Configuration

Section A-A
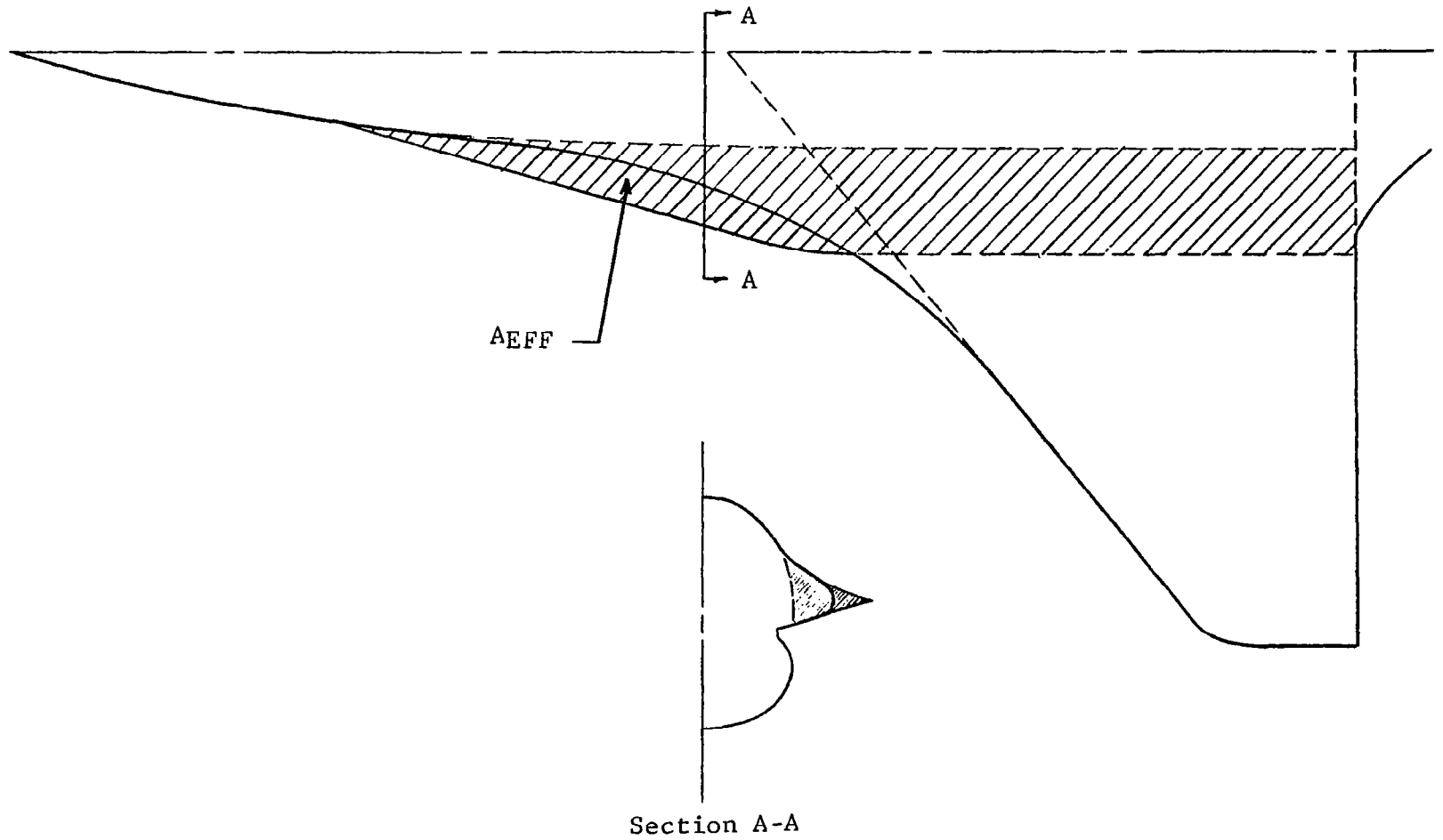
Figure 39   Definition of Effective Strake Area for a Blended Configuration

SYM	TEST	RUN	LEF	TEF	HT	MACH	CONFIG
***	1931	163	0	0	0	0.80	OFF
—	1931	171	0	0	0	0.80	Z7
-·-·-	1931	183	0	0	0	0.80	Z8
- - -	1931	196	0	0	0	0.80	Z9
········	1931	188	0	0	0	0.80	Z10

*** BASELINE RUN

SYM	TEST	RUN	LEF	TEF	HT	MACH	CONFIG
***	1730	95	5	0	0	0.80	OFF
—	1931	202	5	0	0	0.80	Z7
-------	1931	207	5	0	0	0.80	Z10

*** BASELINE RUN

SYM	TEST	RUN	LEF	TEF	HT	MACH	CONFIG
***	1730	39	15	0	0	0.80	OFF
—	1931	219	15	0	0	0.80	Z7
-------	1931	223	15	0	0	0.80	Z10

*** BASELINE RUN
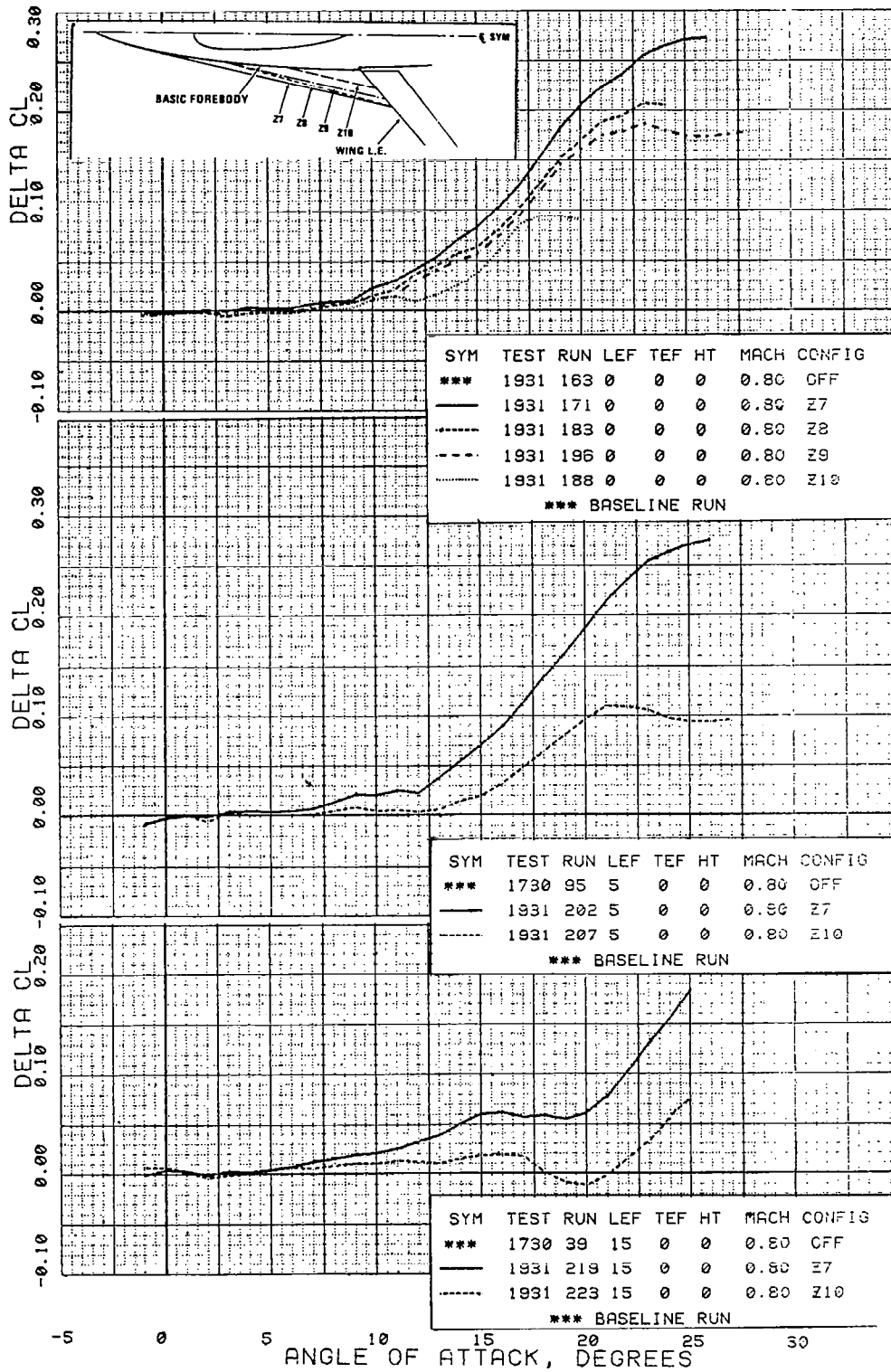
Figure 40   Incremental Strake Lift for a Family of Delta
Planform Strakes on Configuration 785
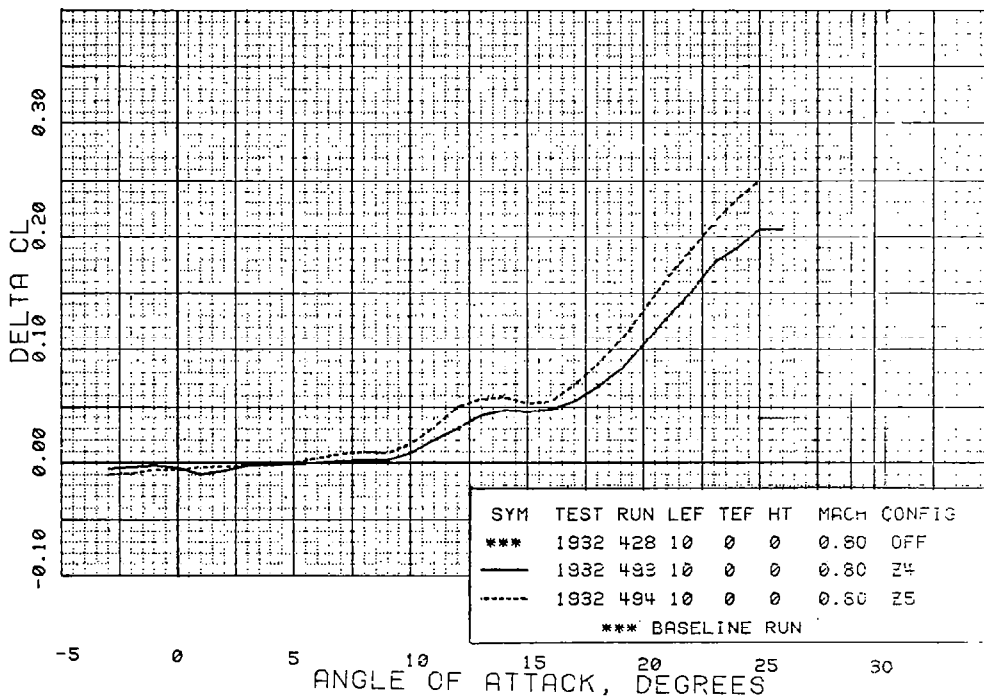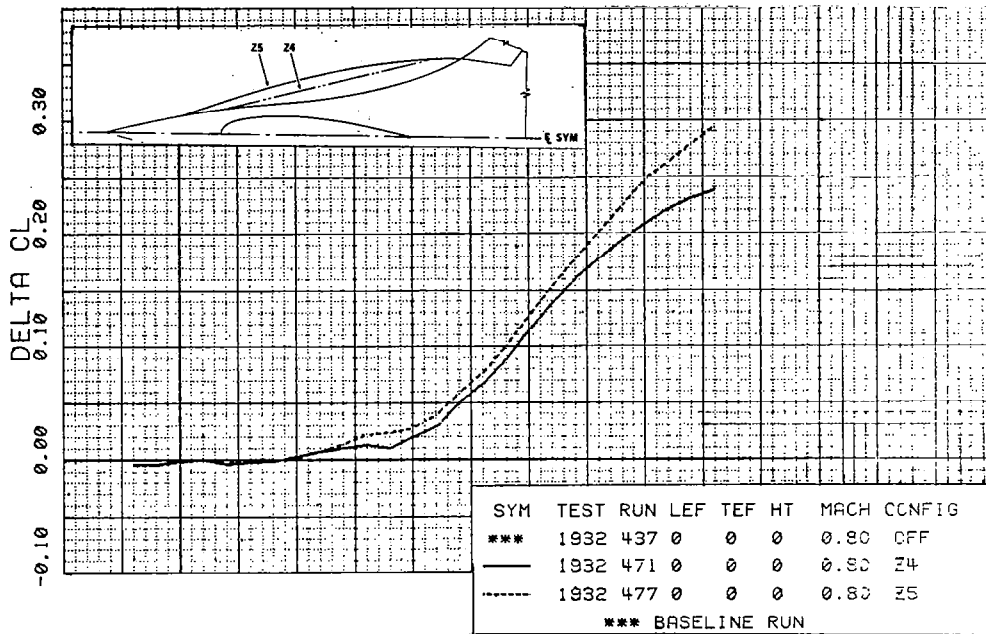
Figure 41   Incremental Strake Lift for a Delta and Gothic
Planform Strake on Configuration 401F-5

SYM	TEST	RUN	LEF	TEF	HT	MACH	CONFIG
∗∗∗	1932	428	10	0	0	0.80	OFF
——	1932	603	10	0	0	0.80	Z14
------	1932	597	10	0	0	0.80	Z16
– – –	1932	594	10	0	0	0.80	Z17
··········	1932	600	10	0	0	0.80	Z18
		∗∗∗	BASELINE	RUN			
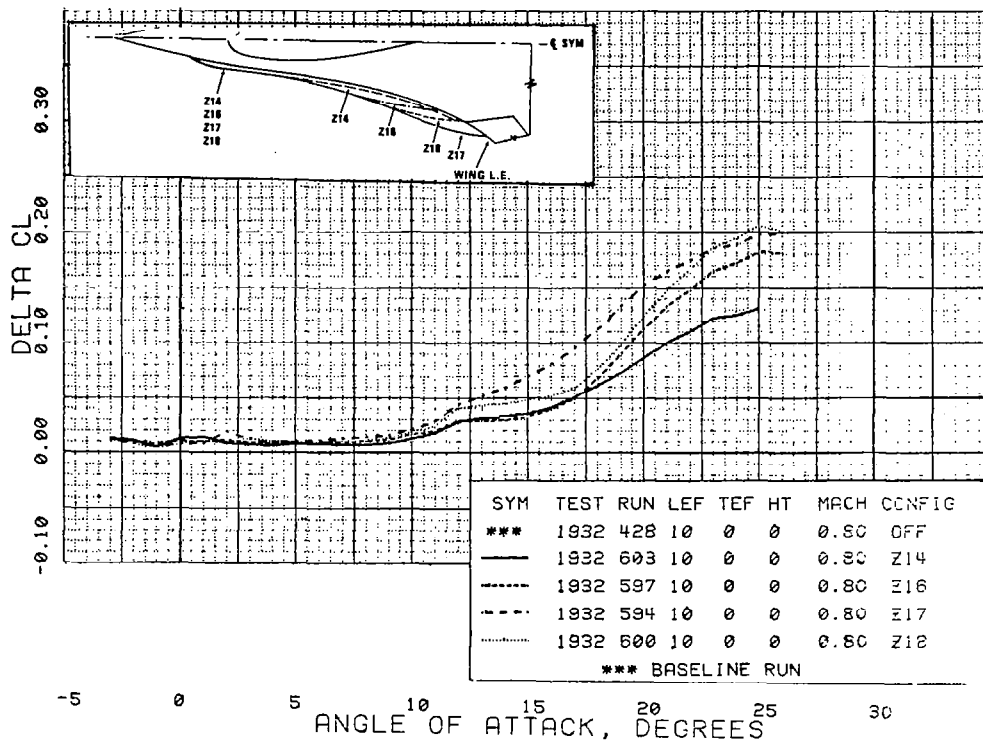
Figure 42   Incremental Strake Lift for a Family of Ogee
Planform Strakes on Configuration 401F-5

107
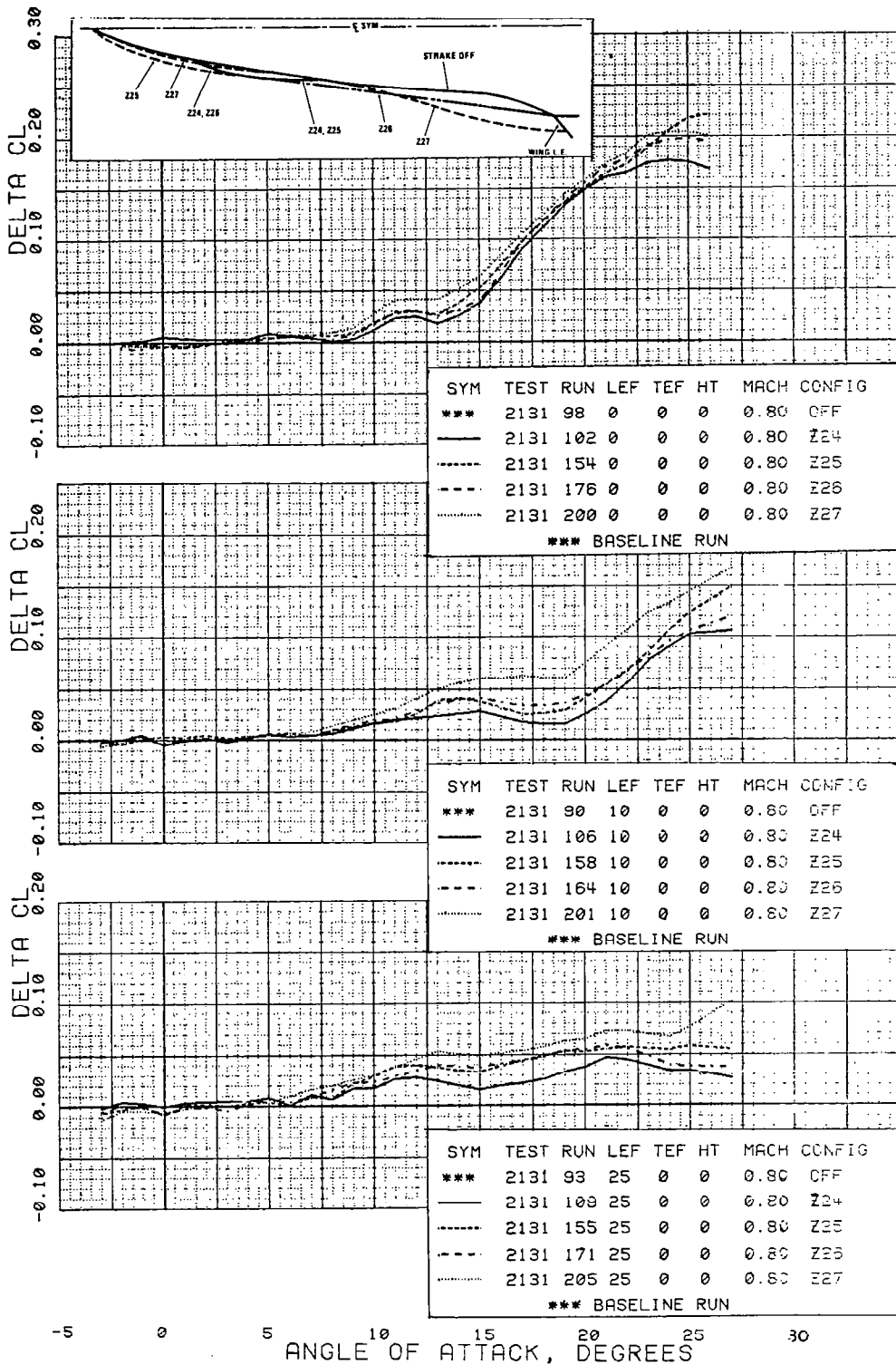
Figure 43   Incremental Strake Lift for a Family of Ogee
                 Planform Strakes on Configuration 401F-10A

108
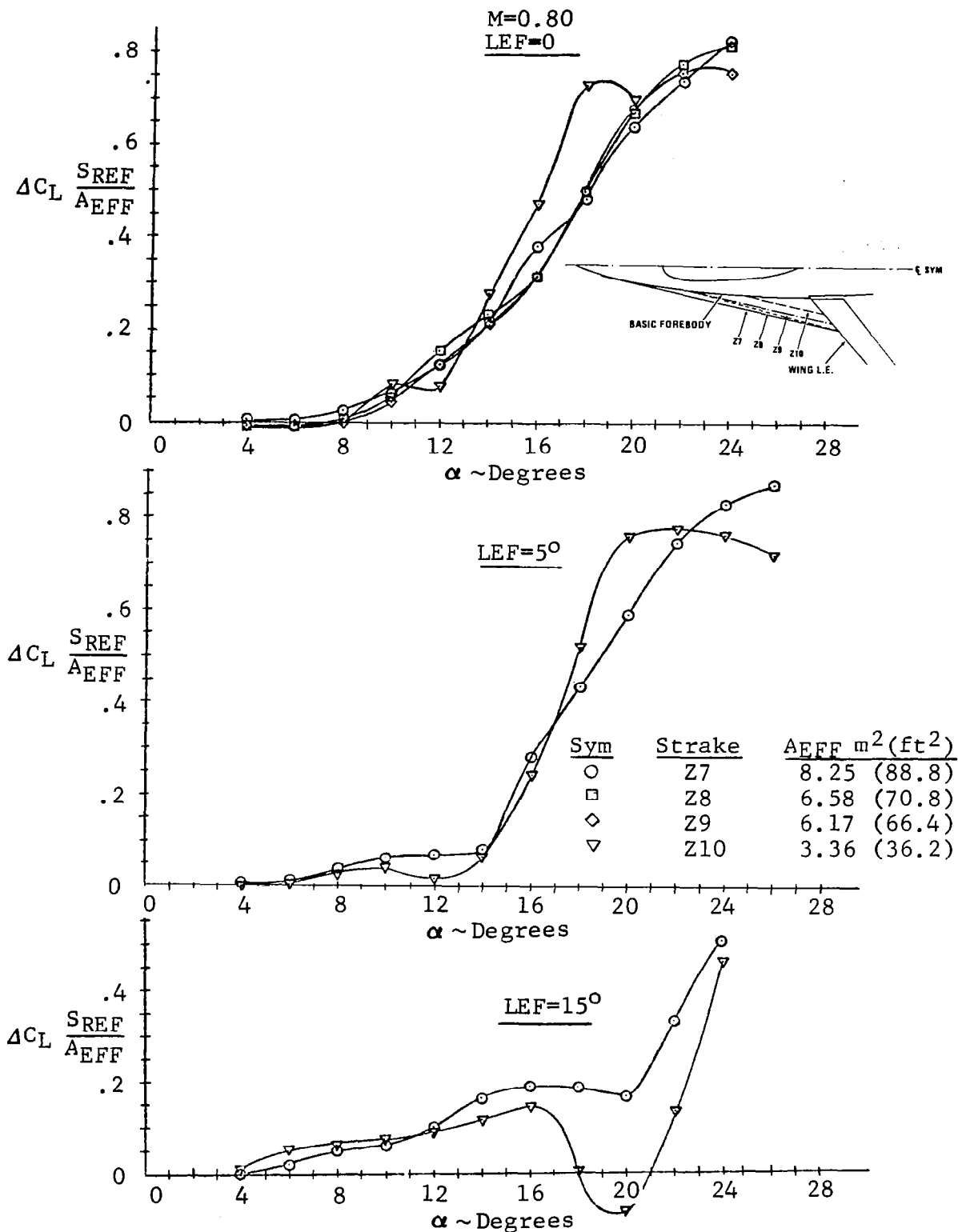
Figure 44 Incremental Strake Lift for a Family of Delta
Planform Strakes on Configuration 785 (Based on A_{EFF})
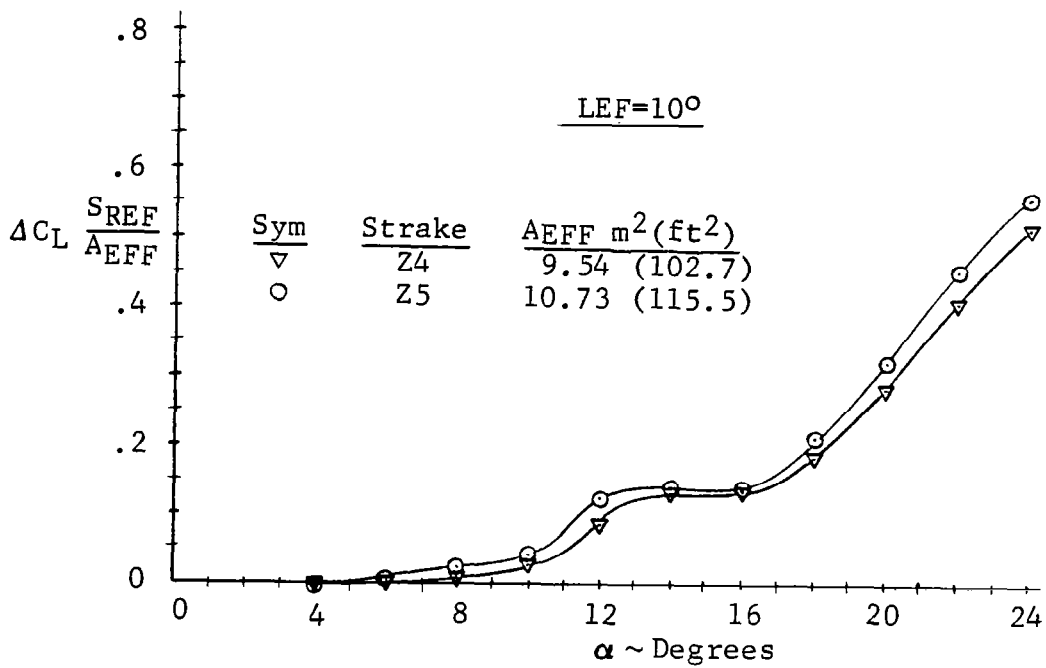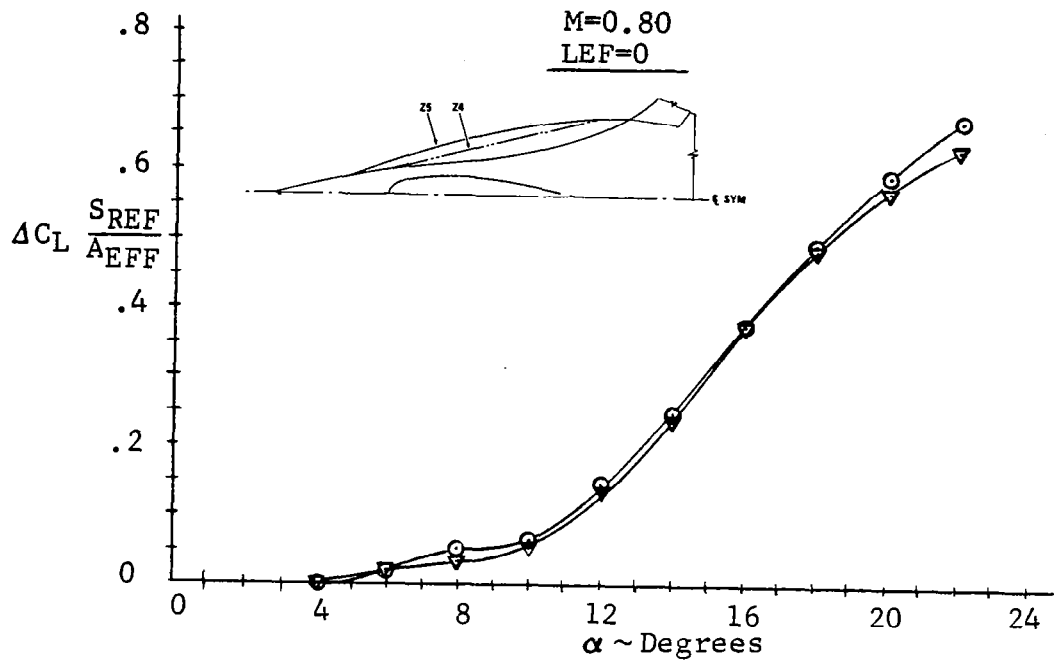
Figure 45   Incremental Strake Lift for a Delta and Gothic Planform Strake on Configuration 401F-5 (Based on A_{EFF})

M = 0.8

LEF = 10°

Sym	Strake	A_{EFF} m^2 (ft^2)
▽	Z14	8.70 (93.6)
○	Z16	7.26 (78.1)
□	Z17	11.98 (129.0)
◇	Z18	9.52 (102.5)

$\Delta C_L \dfrac{S_{REF}}{A_{EFF}}$

$\alpha \sim$ Degrees
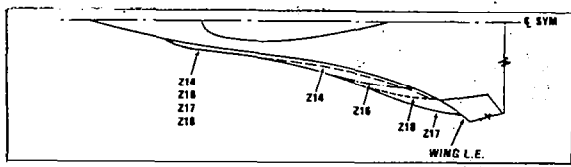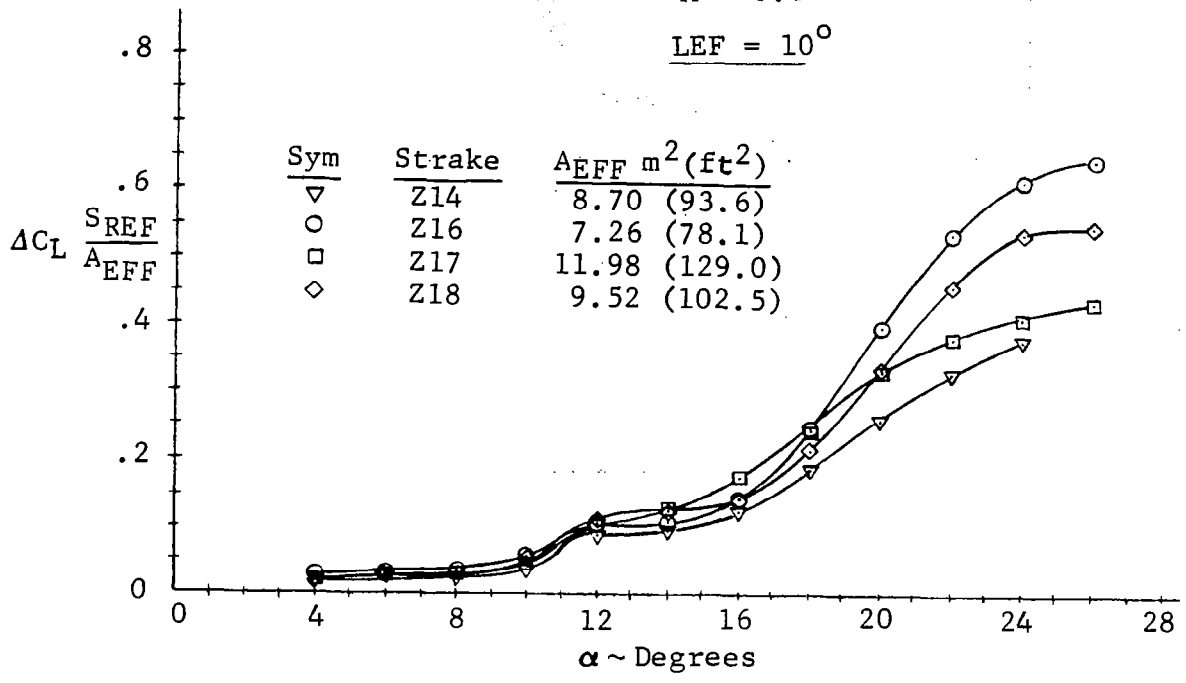
Figure 46   Incremental Strake Lift for a Family of Ogee
Planform Strakes on Configuration 401F-5
(Based on A_{EFF})

111
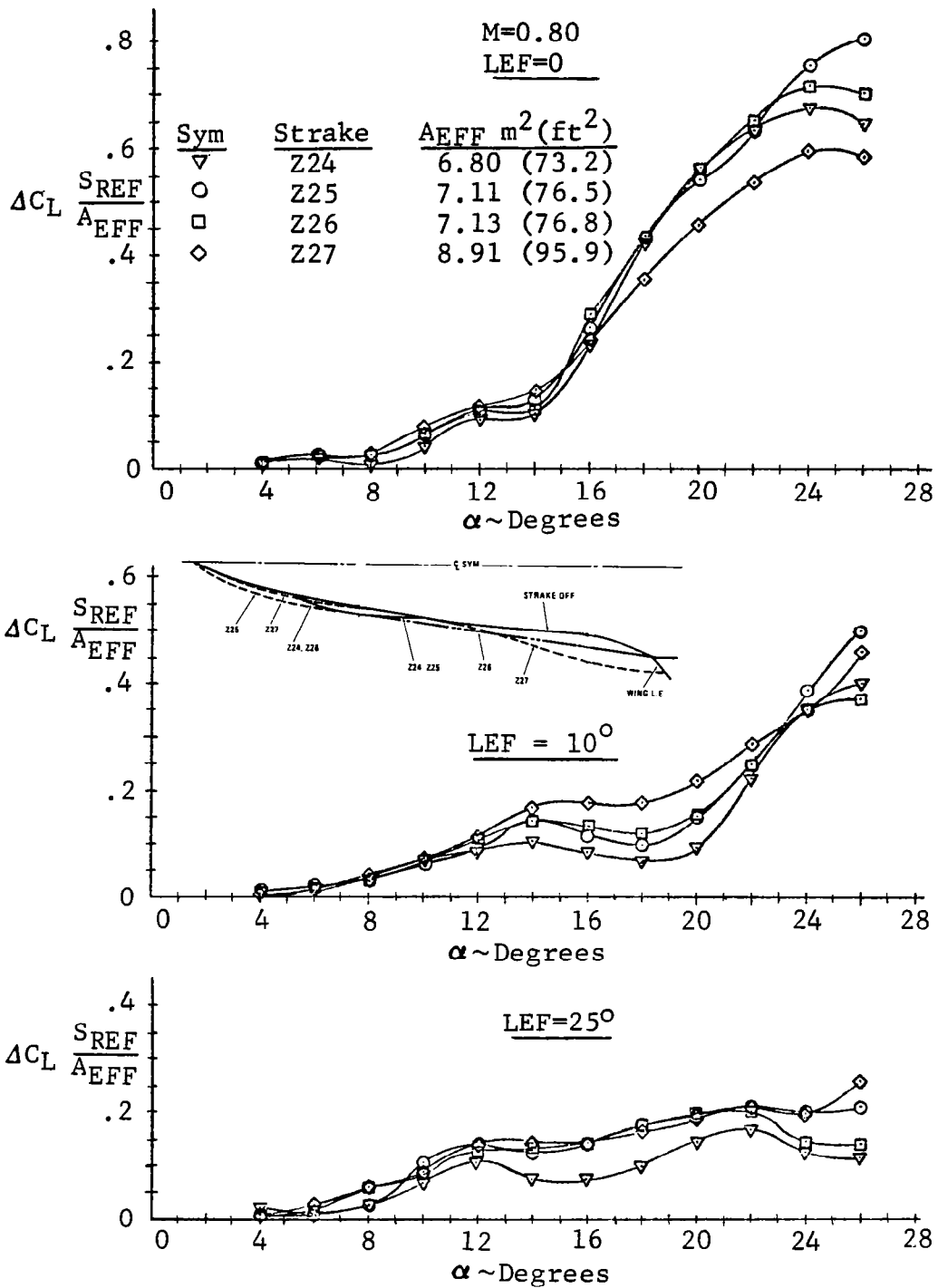
Figure 47   Incremental Strake Lift for a Family of Ogee
             Planform Strakes on Configuration 401F-10A
             (Based on A_{EFF})

Current definition

Probable area for large span strakes
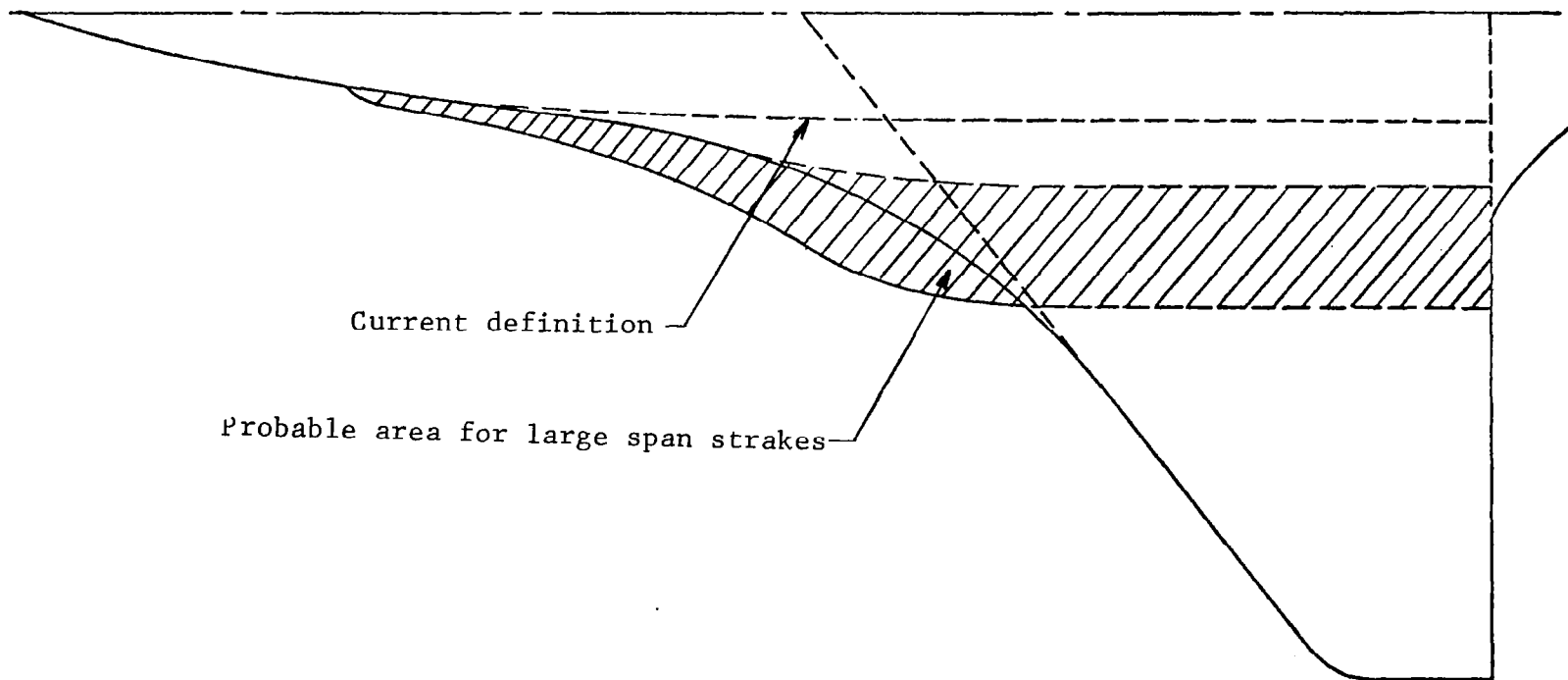
Figure 48   Definition of Effective Strake Area for Large Span Strakes
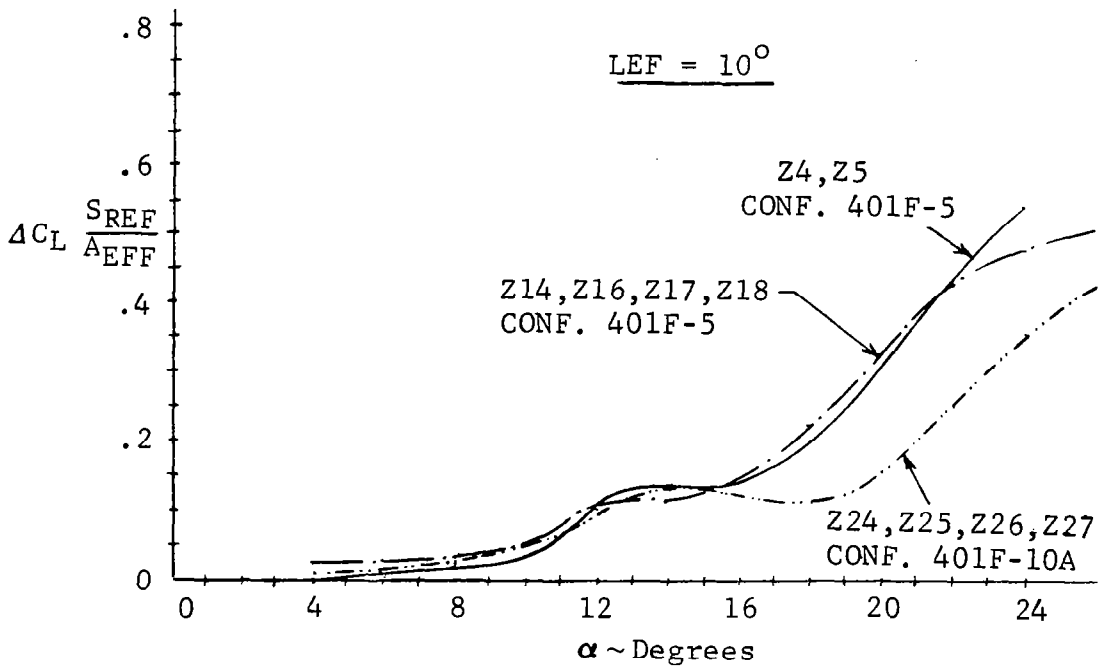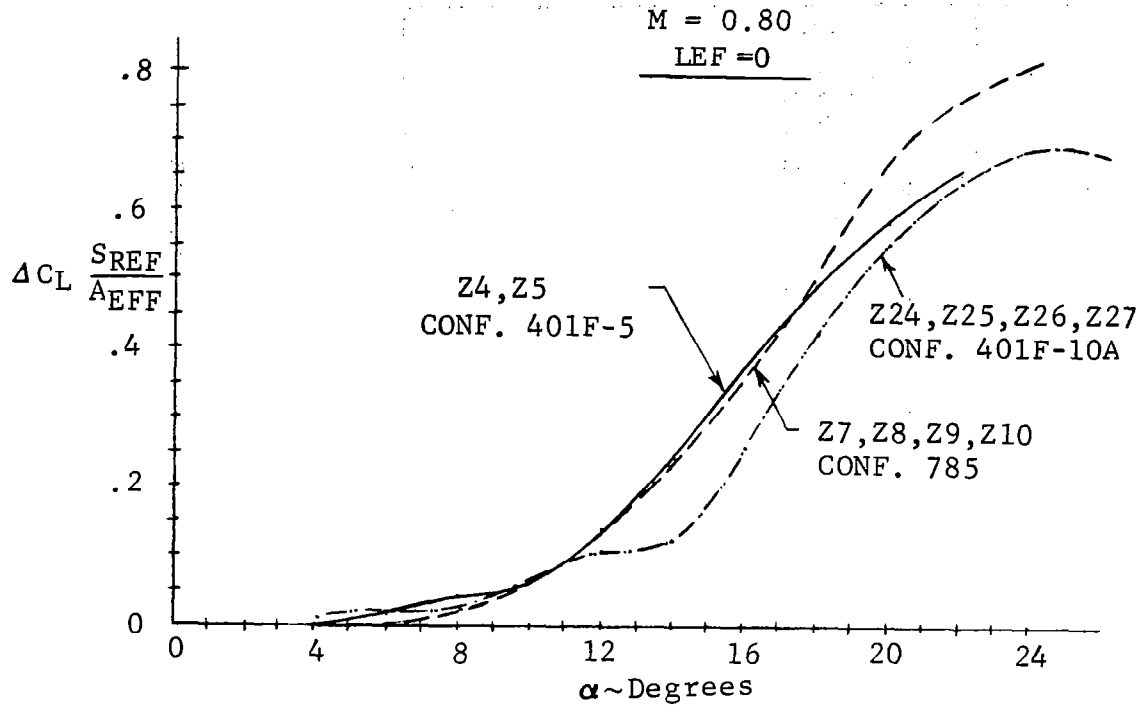
Figure 49   Effects of Configuration and Strake Geometry
             on Incremental Lift
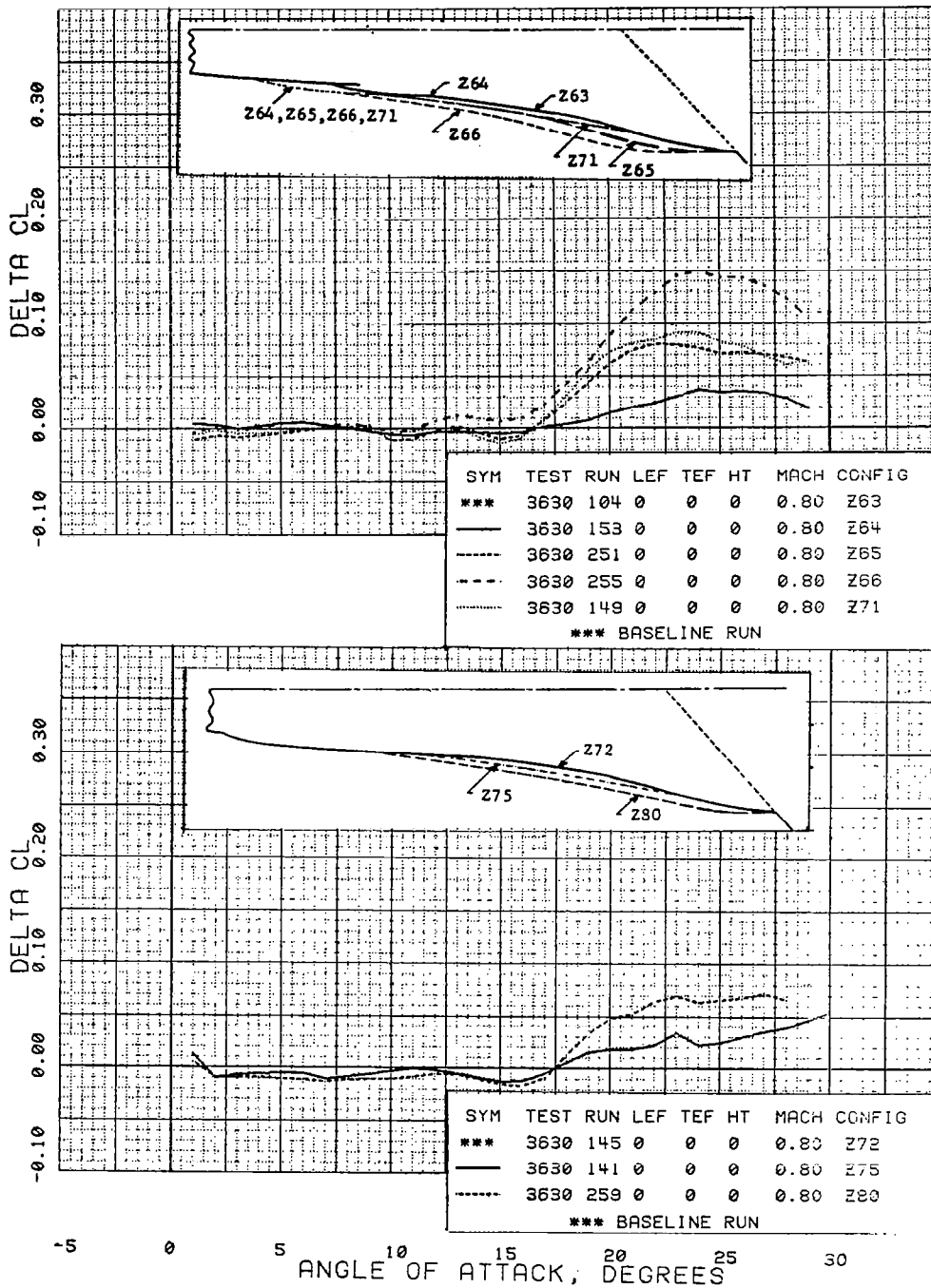
Figure 50   Incremental Strake Lift for a Family of Ogee
Planform Strakes on the Stretched YF-16

115
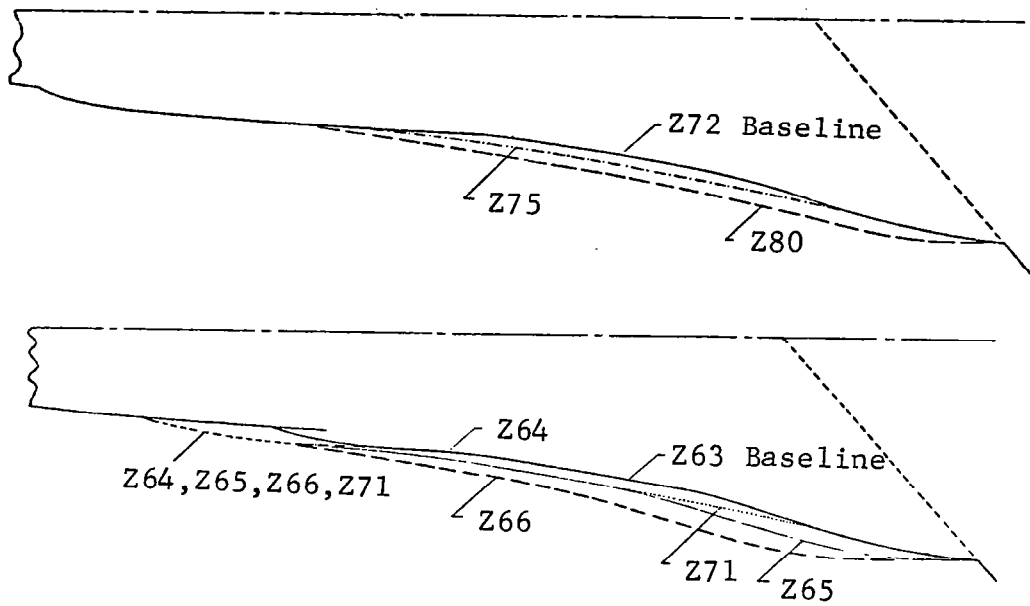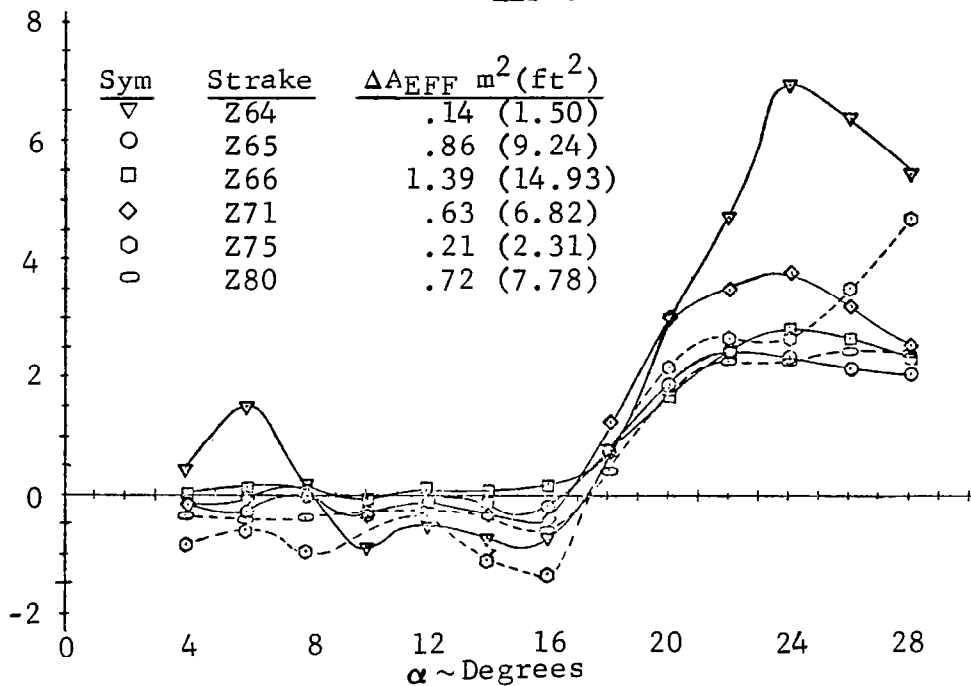
Figure 51   Incremental Strake Lift for a Family of Ogee
             Planform Strakes on the Stretched YF-16
             (Based on ΔA_{EFF})
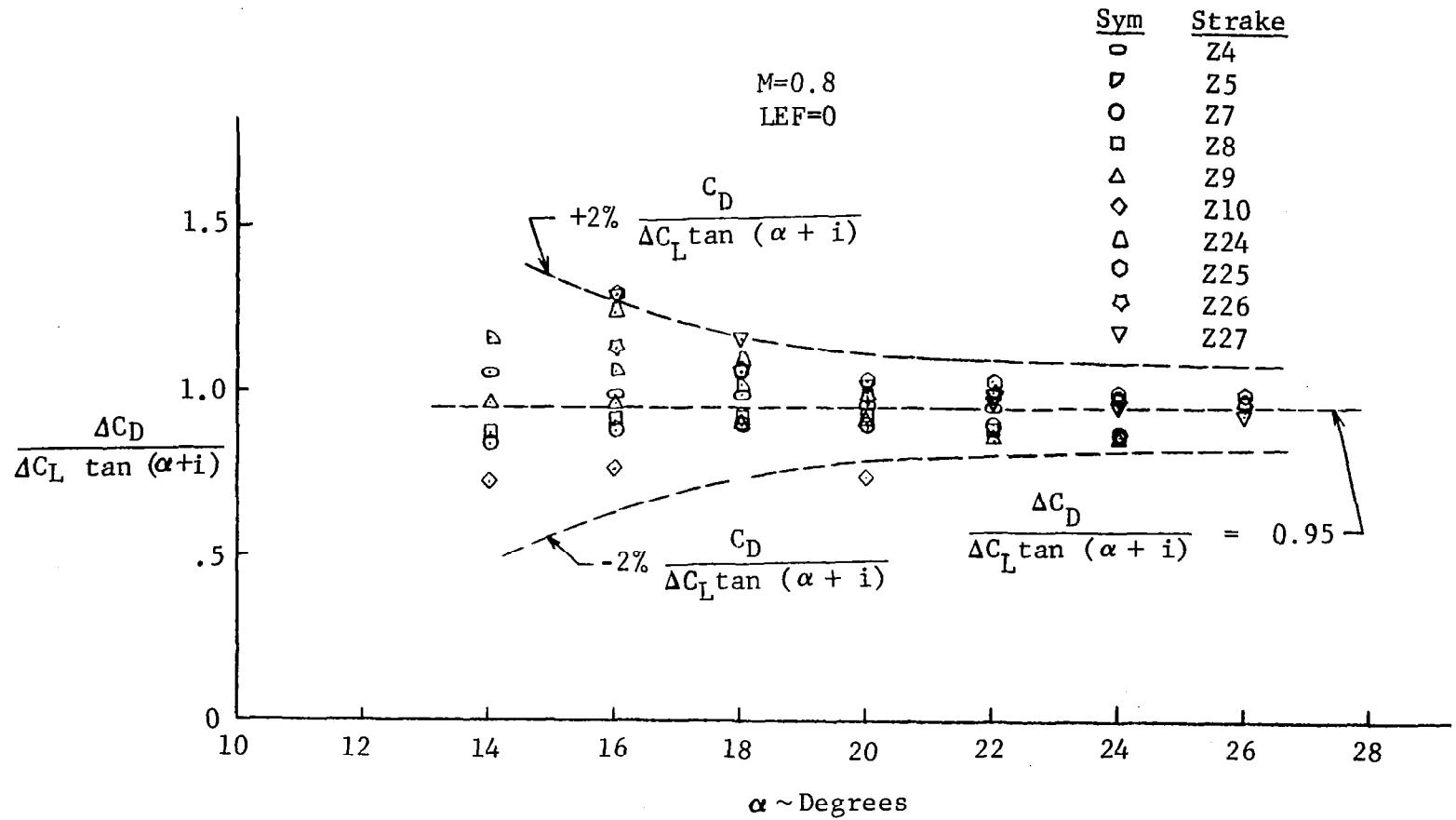
Figure 52   Incremental Drag Correlation for Forebody Strakes
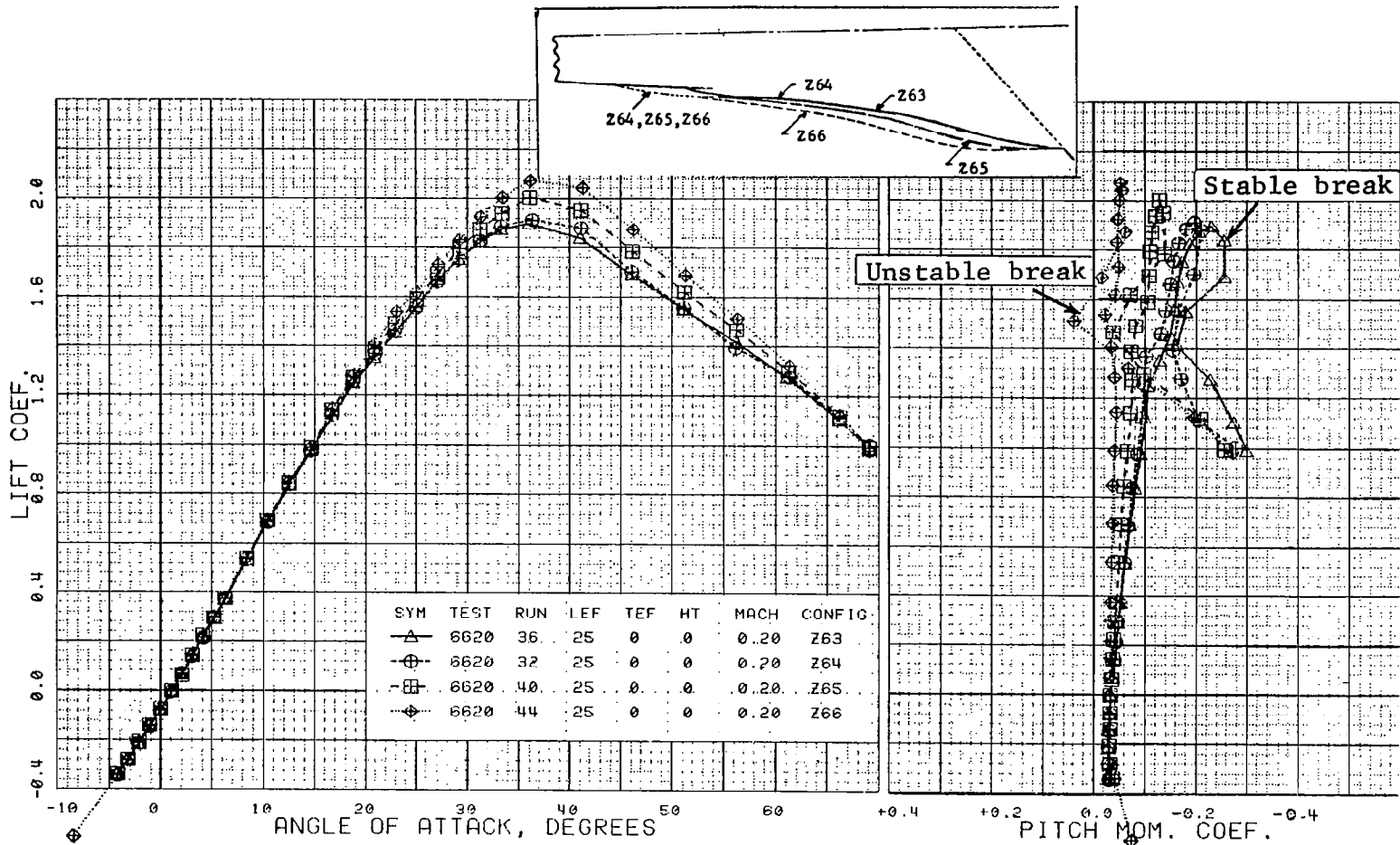
Figure 53   Pitch Effects of a Family of Ogee Planform
Forebody Strakes on the YF-16 + 30.5 Stretch
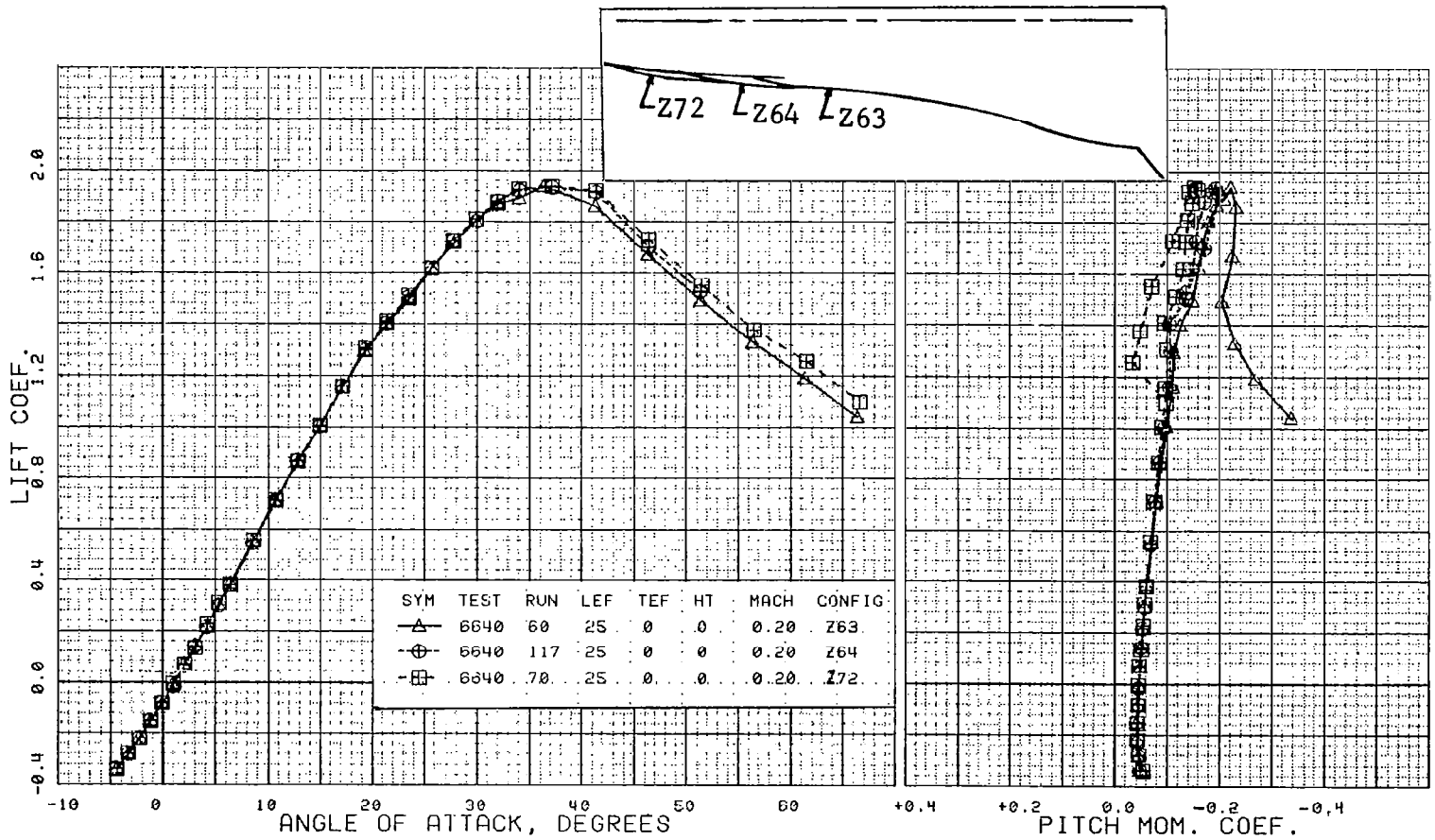
Figure 54   Pitch Effects of Forebody Strake Forward
             Extent on the YF-16 + 30.5 Stretch
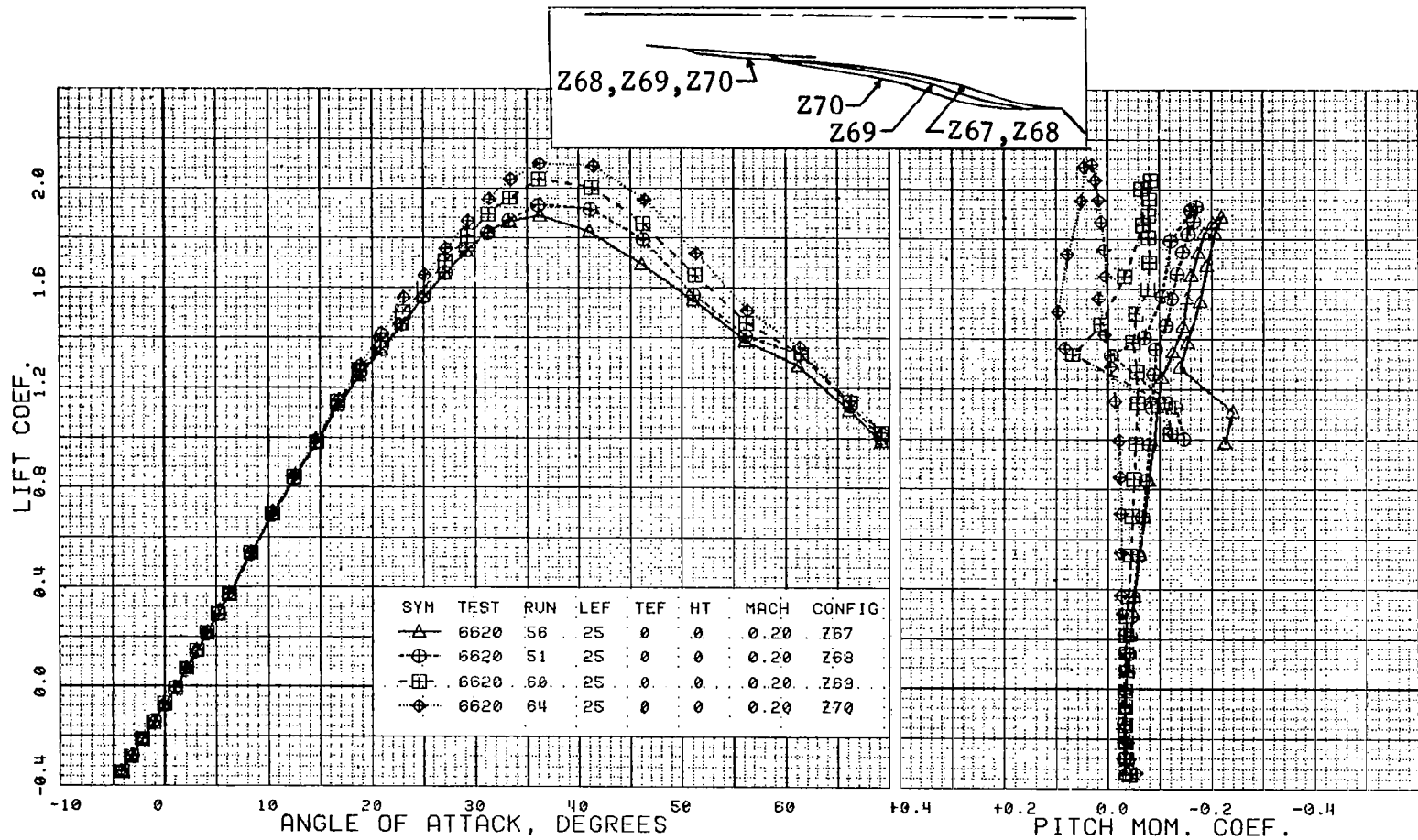
Figure 55   Pitch Effects of a Family of Ogee Planform
             Forebody Strakes on the YF-16 + 44.5 Stretch
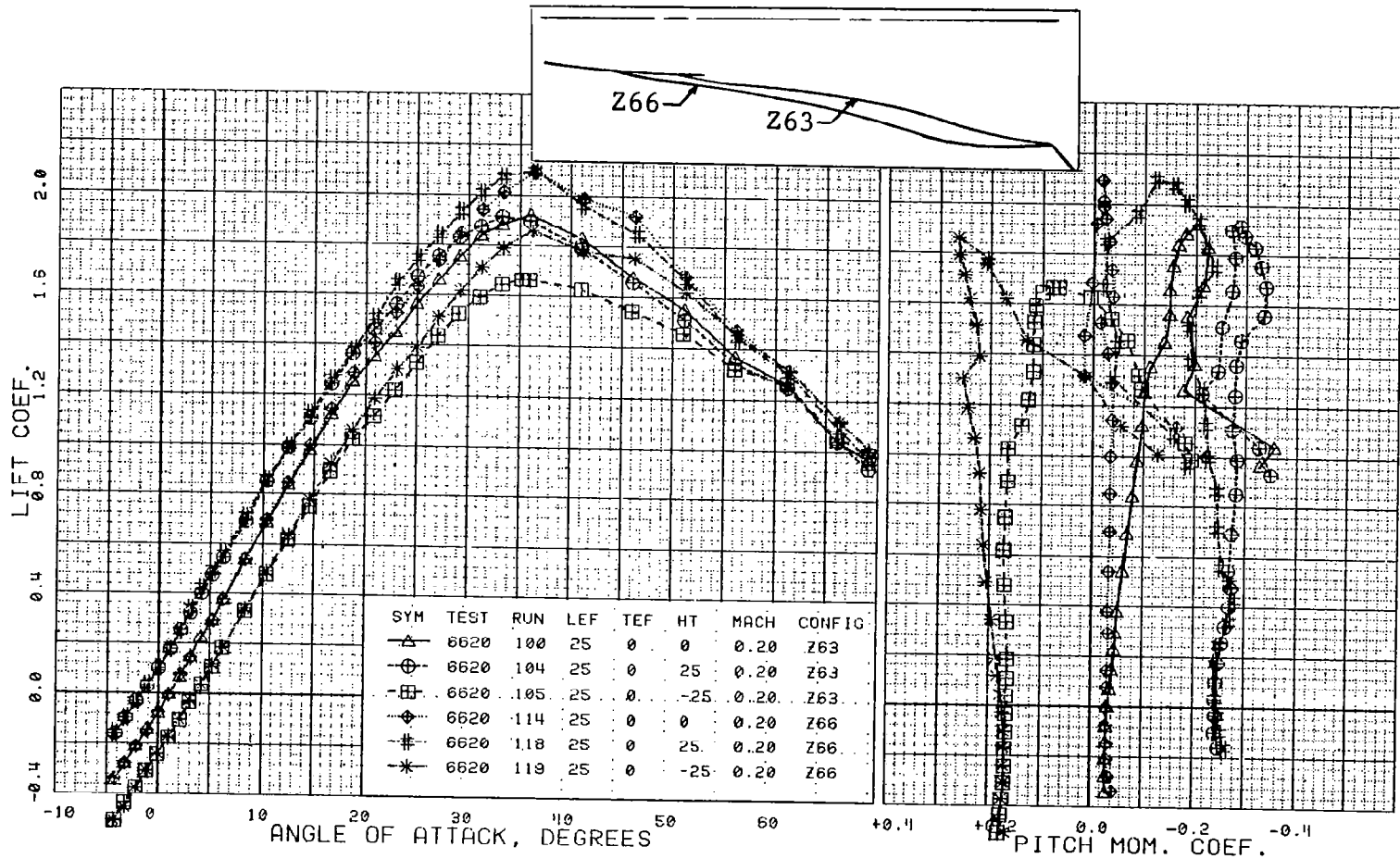
Figure 56   Effect of Horizontal Tail Deflection on the
                   Pitch Effects of Ogee Planform Forebody Strakes,
                   YF-16 + 30.5 Stretch

121

approximate α range
$\alpha < 10^{\circ}$

O STRAKES Z7 - Z10
□ STRAKES Z4 & Z5
△ STRAKES Z16 - Z18

$\dfrac{\ell_s A_{EFF}}{\bar{c} S_{REF}} \, C_{L_{\alpha s}}$

ΔA.C $_1$
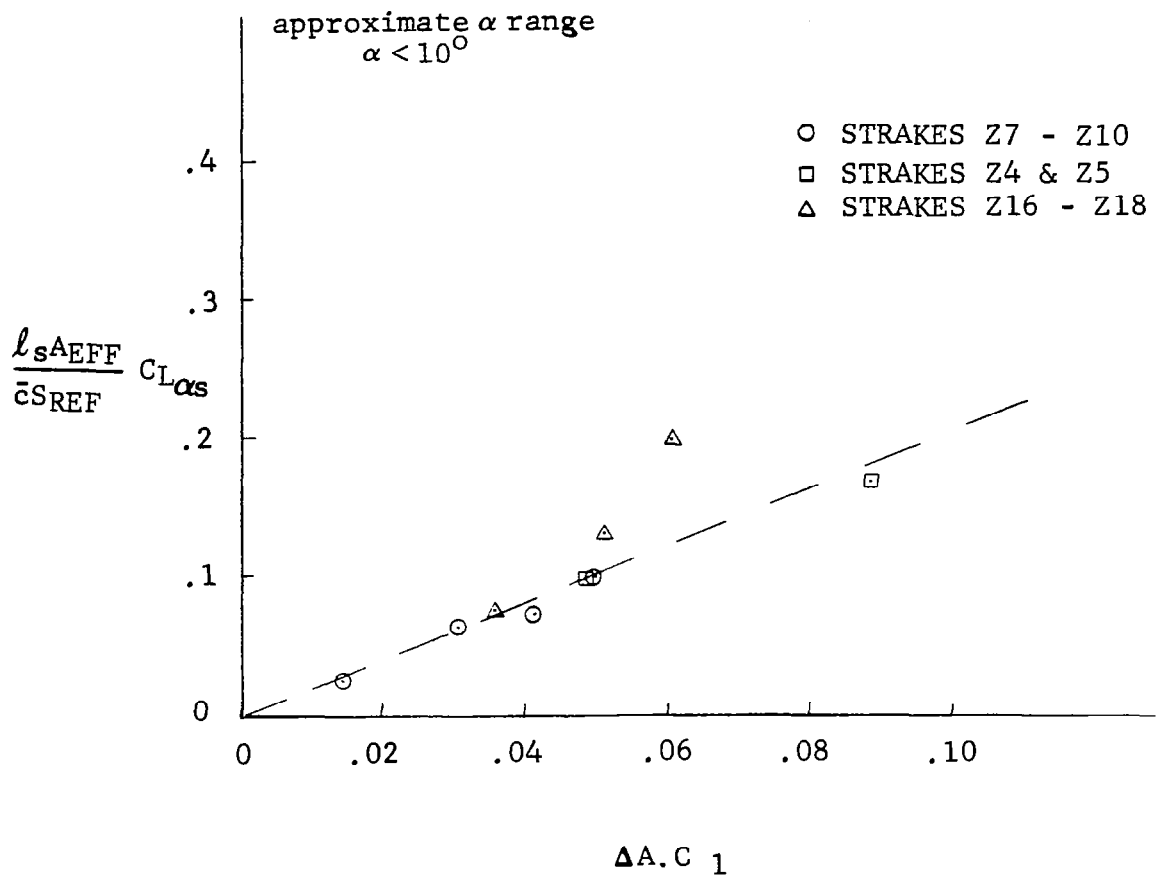
Figure 57   Linear Region Stability Shift Due to Forebody
             Strakes, M = 0.80
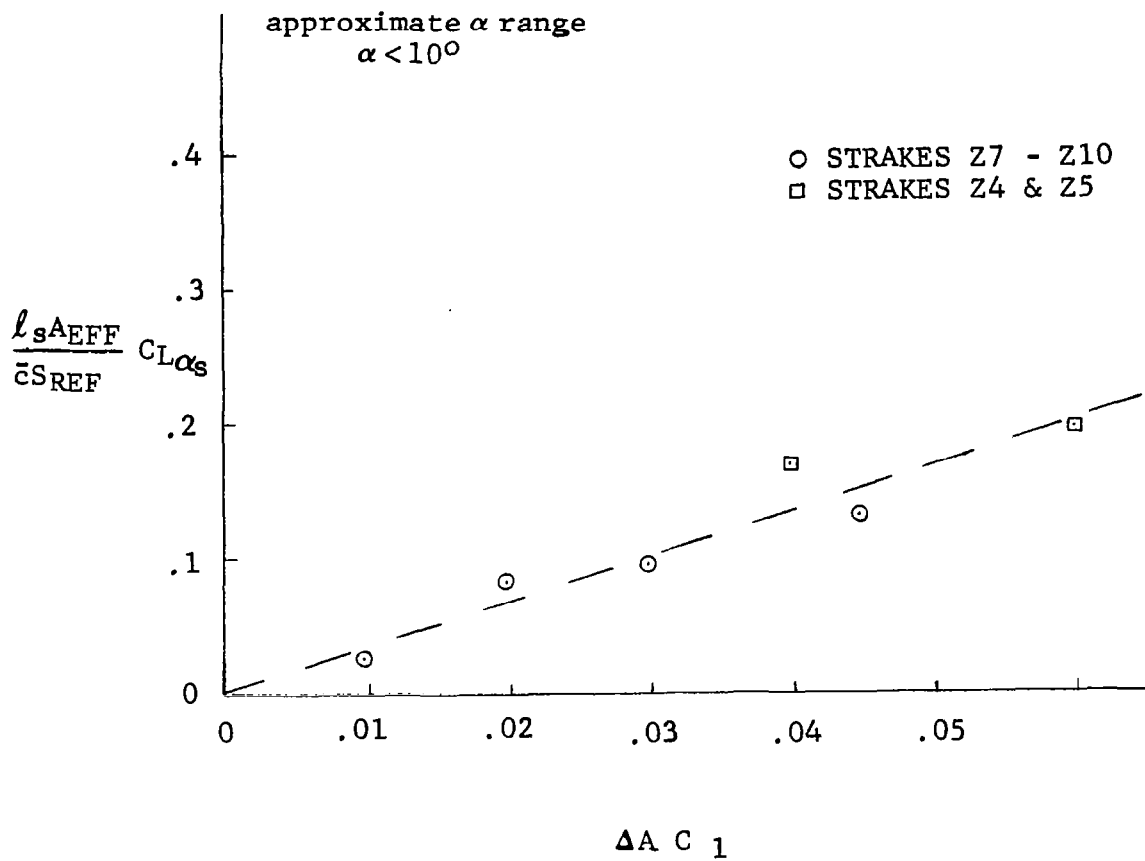
Figure 58   Linear Region Stability Shift Due to Forebody Strakes,
            M = 1.20
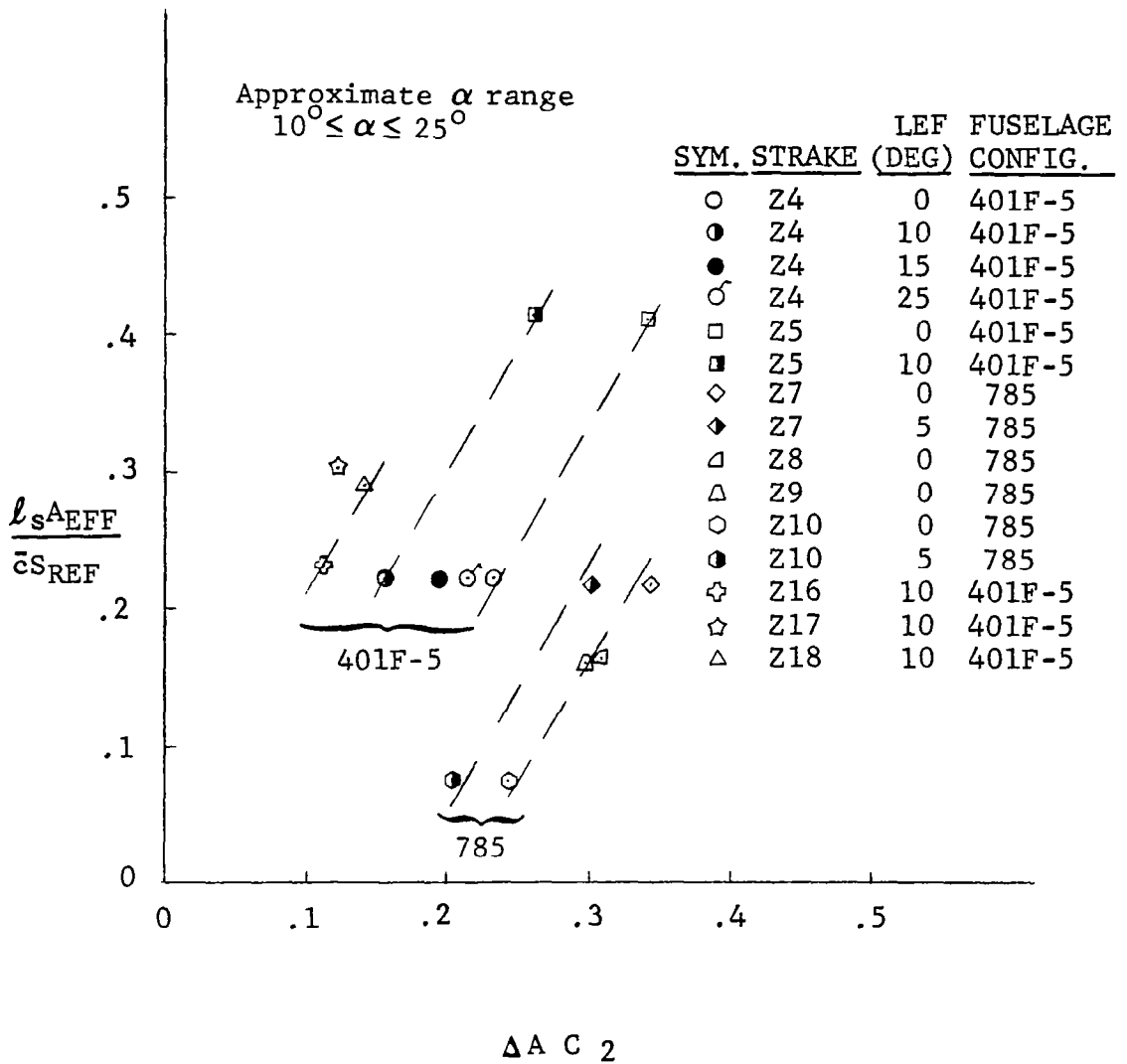
Figure 59   High Angle of Attack Stability Shift Due to Forebody
             Strakes, M = 0.80
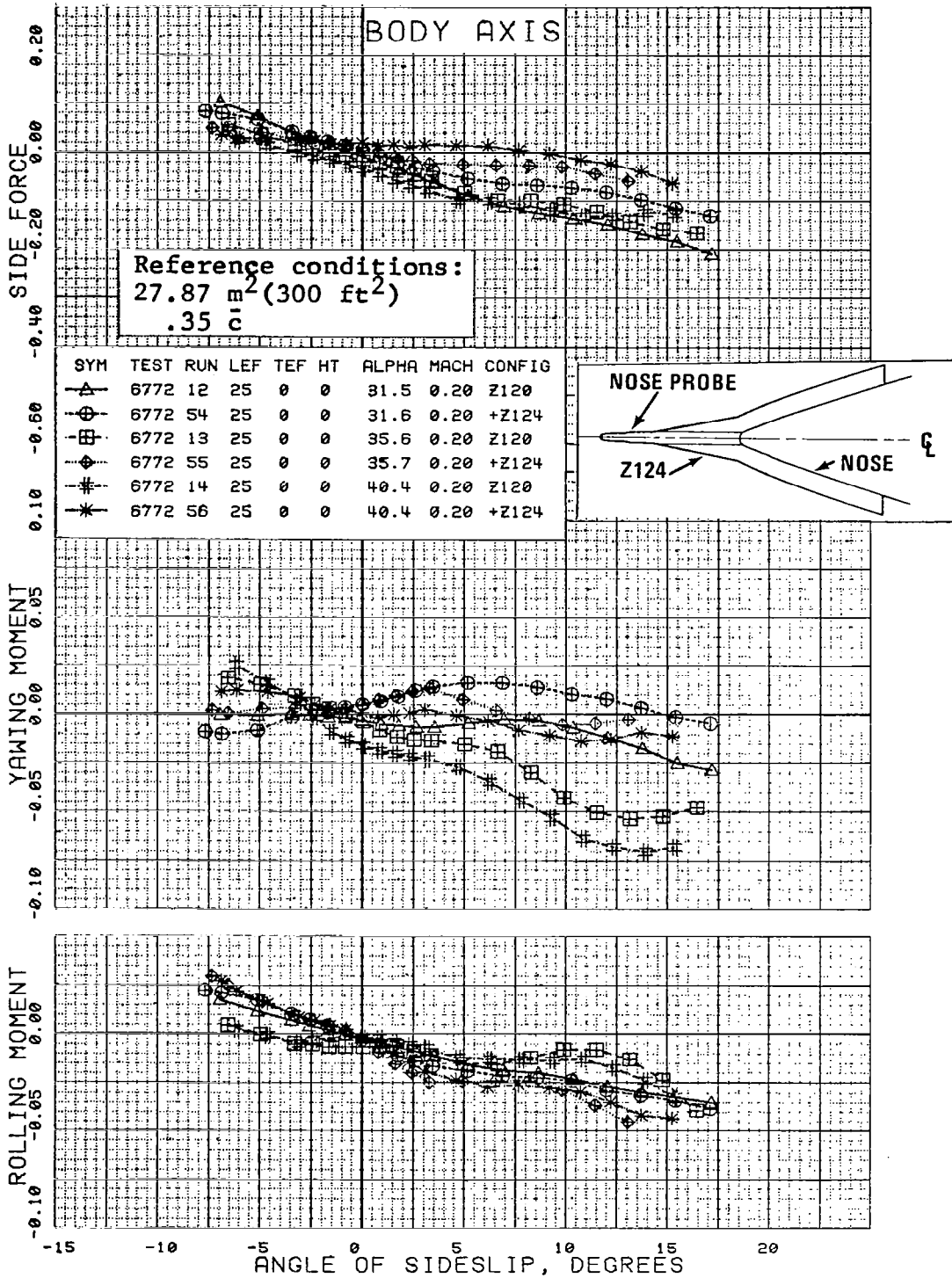
Figure 60   Sideslip Characteristics of Nose Strake Z124 on the F-16
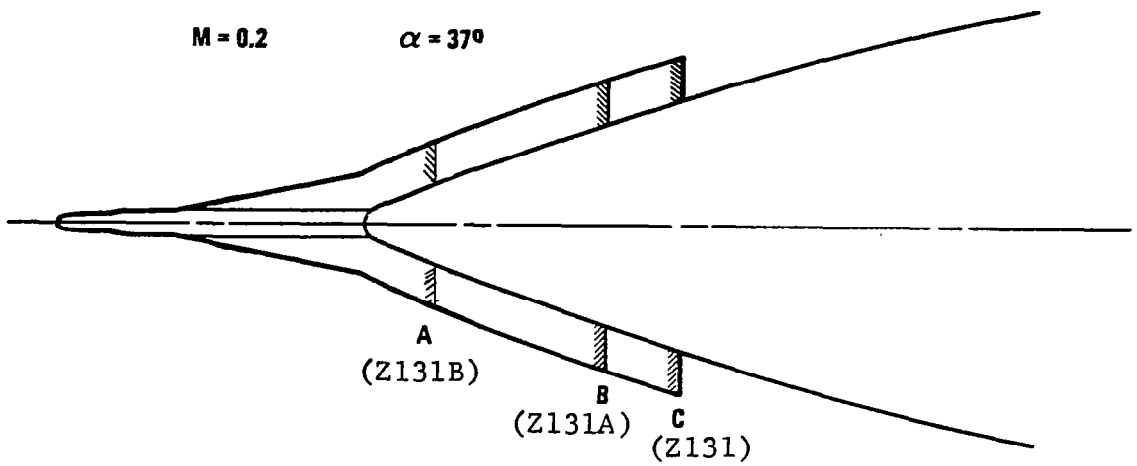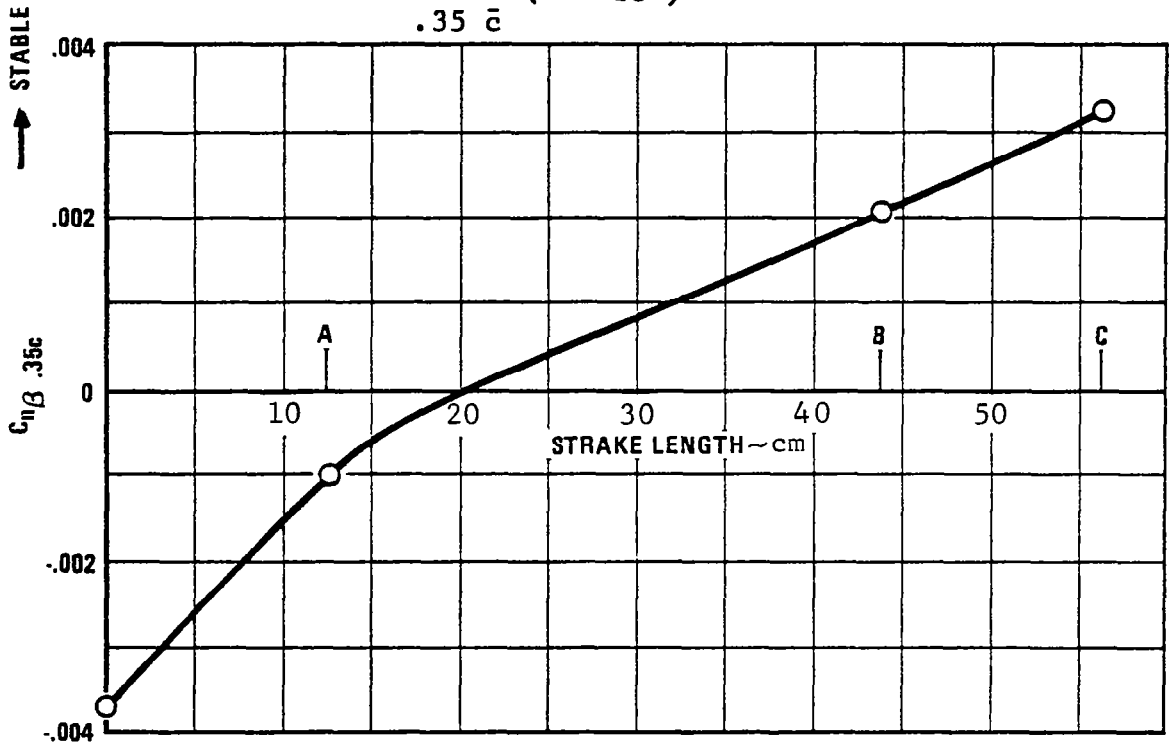
Figure 61   Effect of Nose Strake Length on Directional Stability
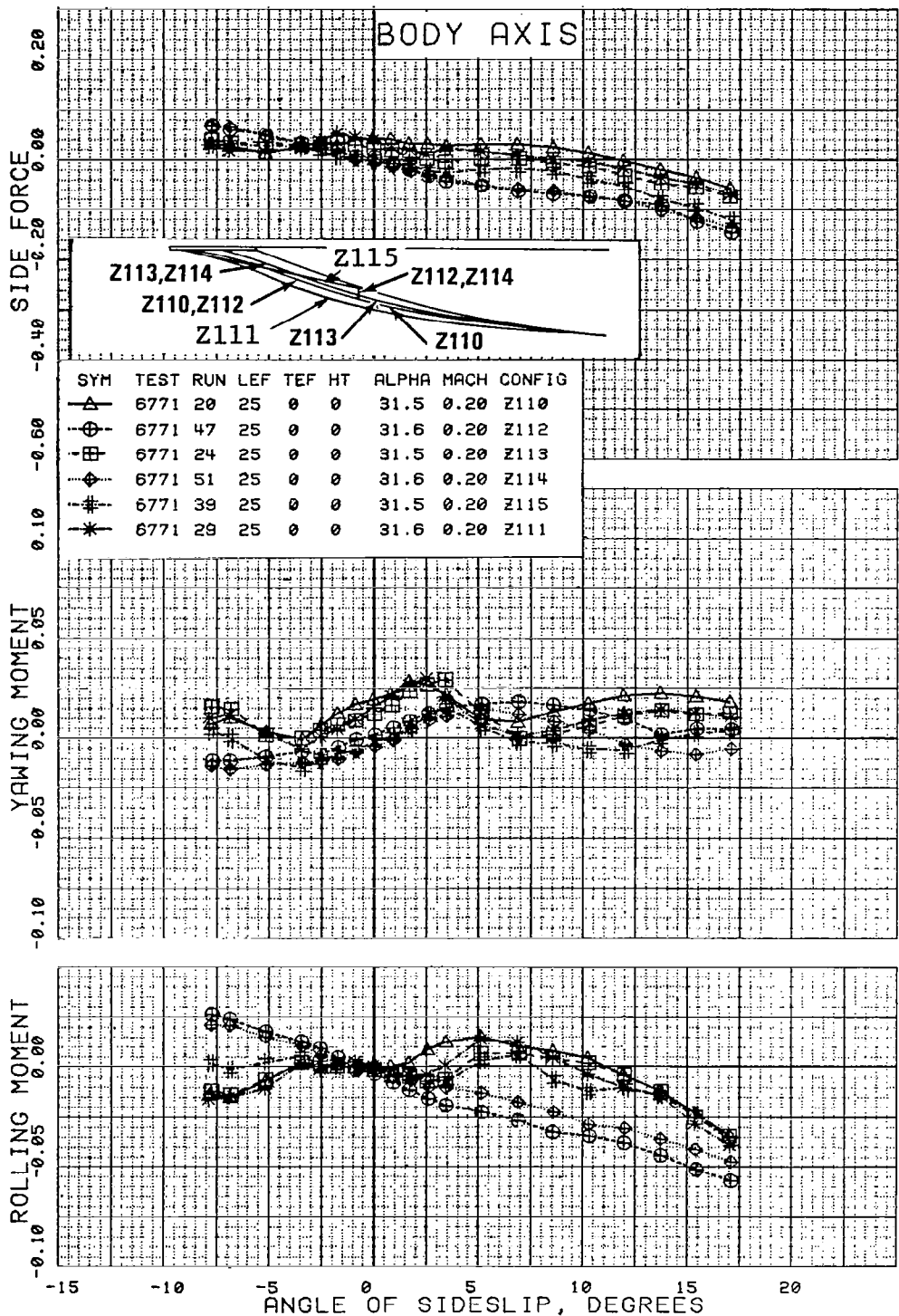
Figure 62   Effect of Nose Strake Shape on the F-16
             Sideslip Characteristics

127
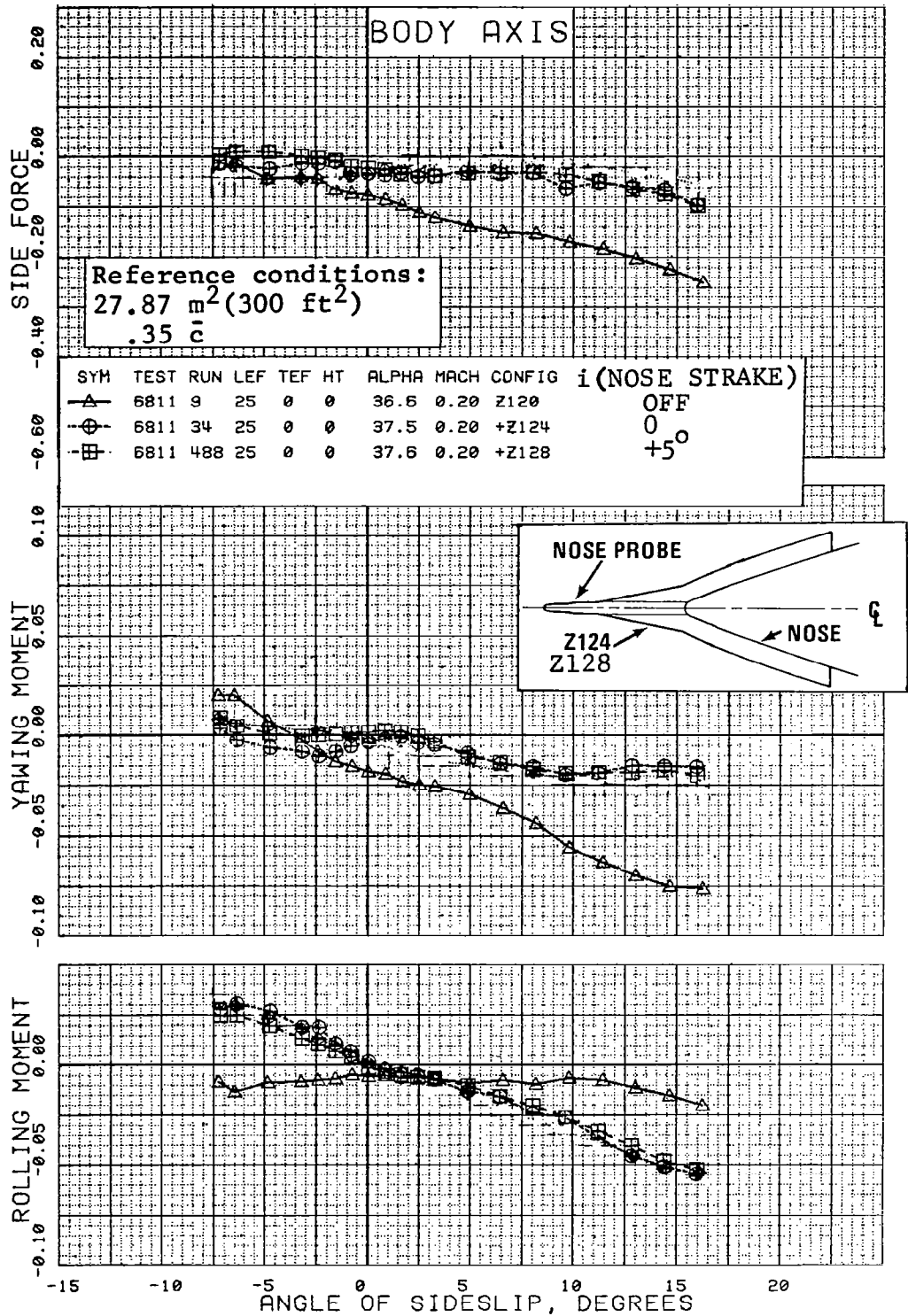
Figure 63   Effect of Nose Strake Inclination on the F-16 Sideslip
Characteristics
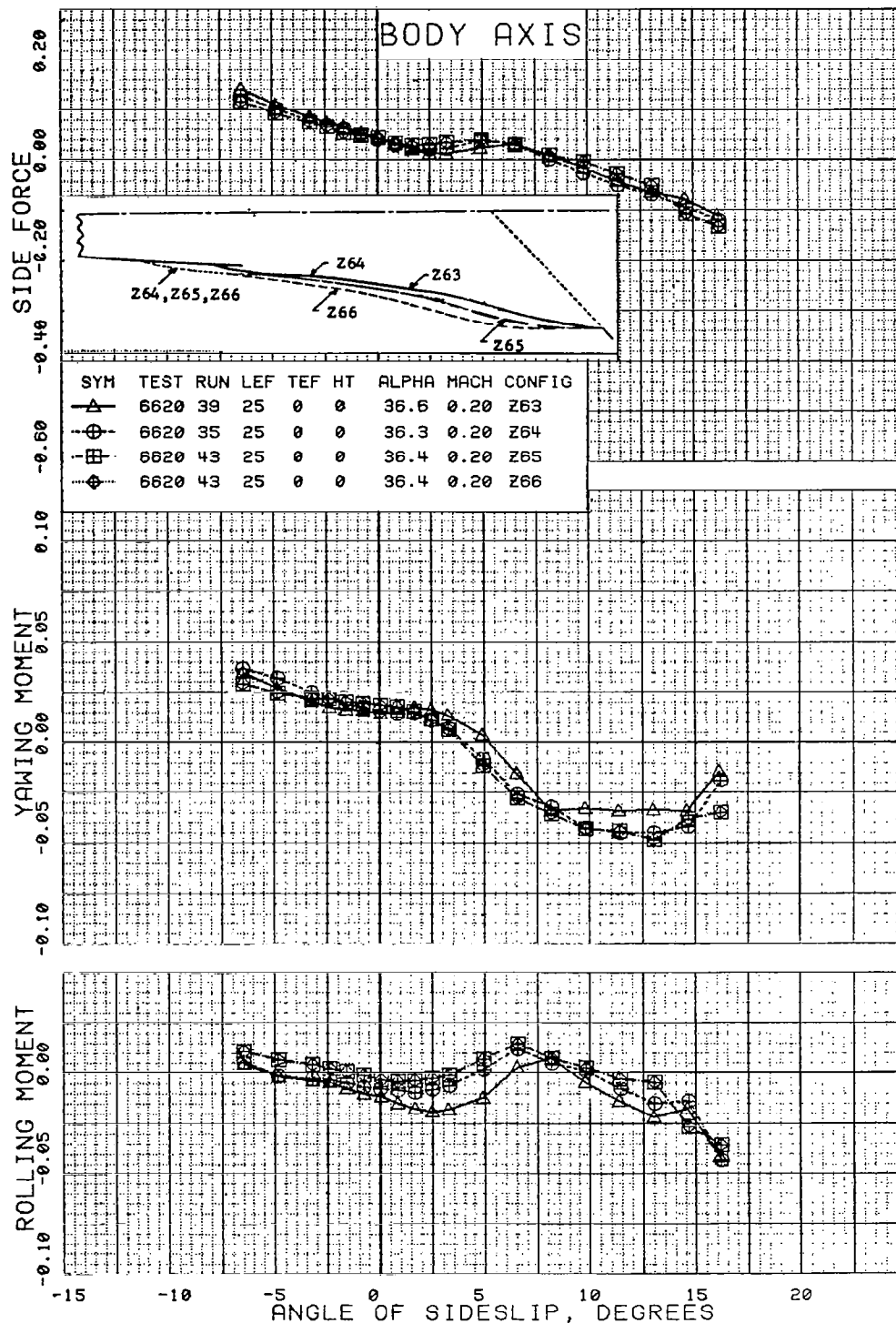
Figure 64   Sideslip Characteristics of a Family of Ogee Planform
             Forebody Strakes, YF-16 + 30.5 Stretch
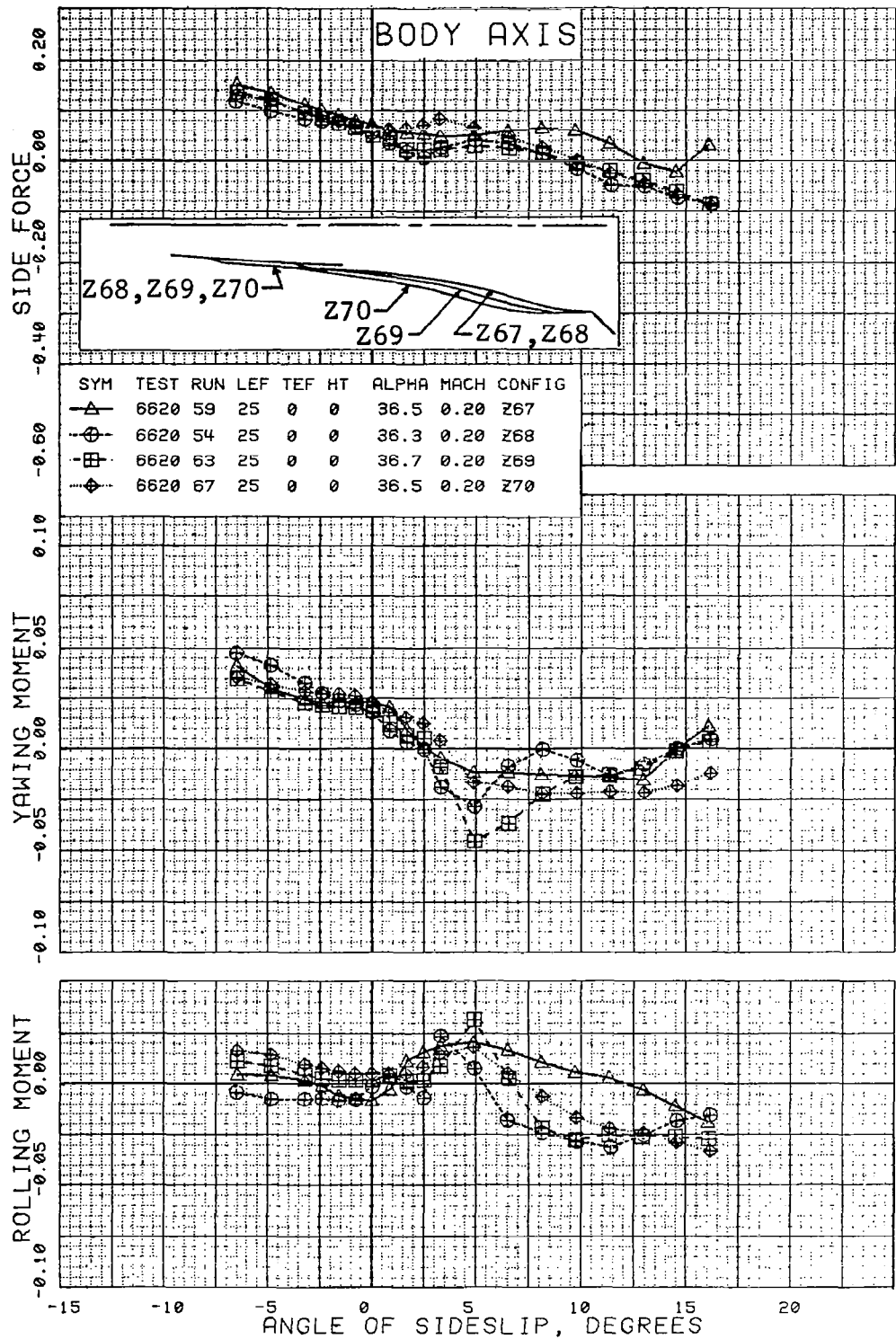
Figure 65   Sideslip Characteristics of a Family of Ogee Planform
Forebody Strakes, YF-16 + 44.5 Stretch

130
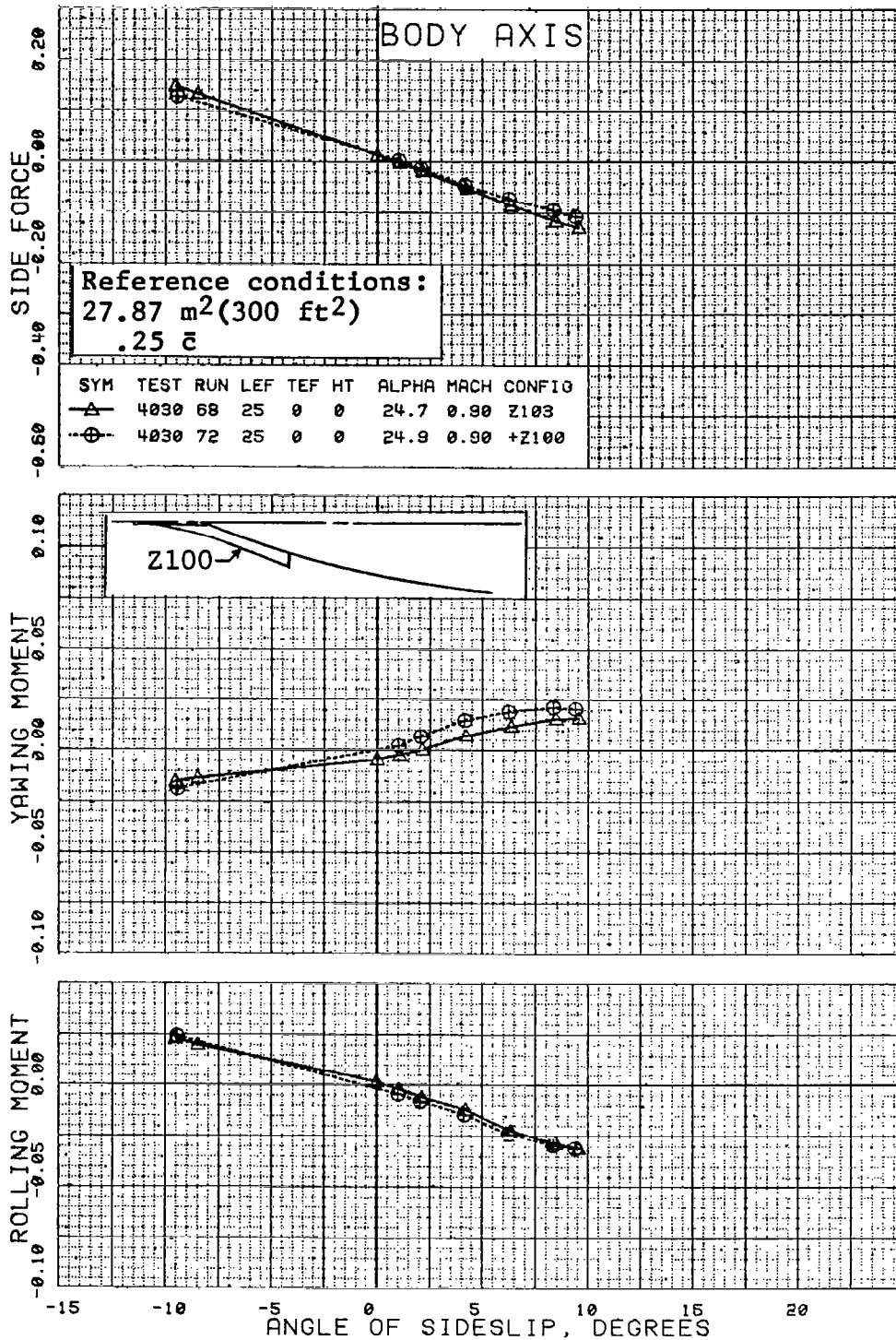
Figure 66   Sideslip Characteristics of Nose Strake Z100 on the F-16
             at 0.9 Mach Number

SYM	TEST	RUN	LEF	TEF	HT	ALPHA	MACH	CONFIG
△	1730	18	0	0	0	25.7	0.80	OFF
⊕	1931	164	0	0	0	21.7	0.80	OFF
⊞	1831	174	0	0	0	24.3	0.80	Z7
⬦	1931	182	0	0	0	23.9	0.80	Z8
✳	1931	195	0	0	0	22.6	0.80	Z9
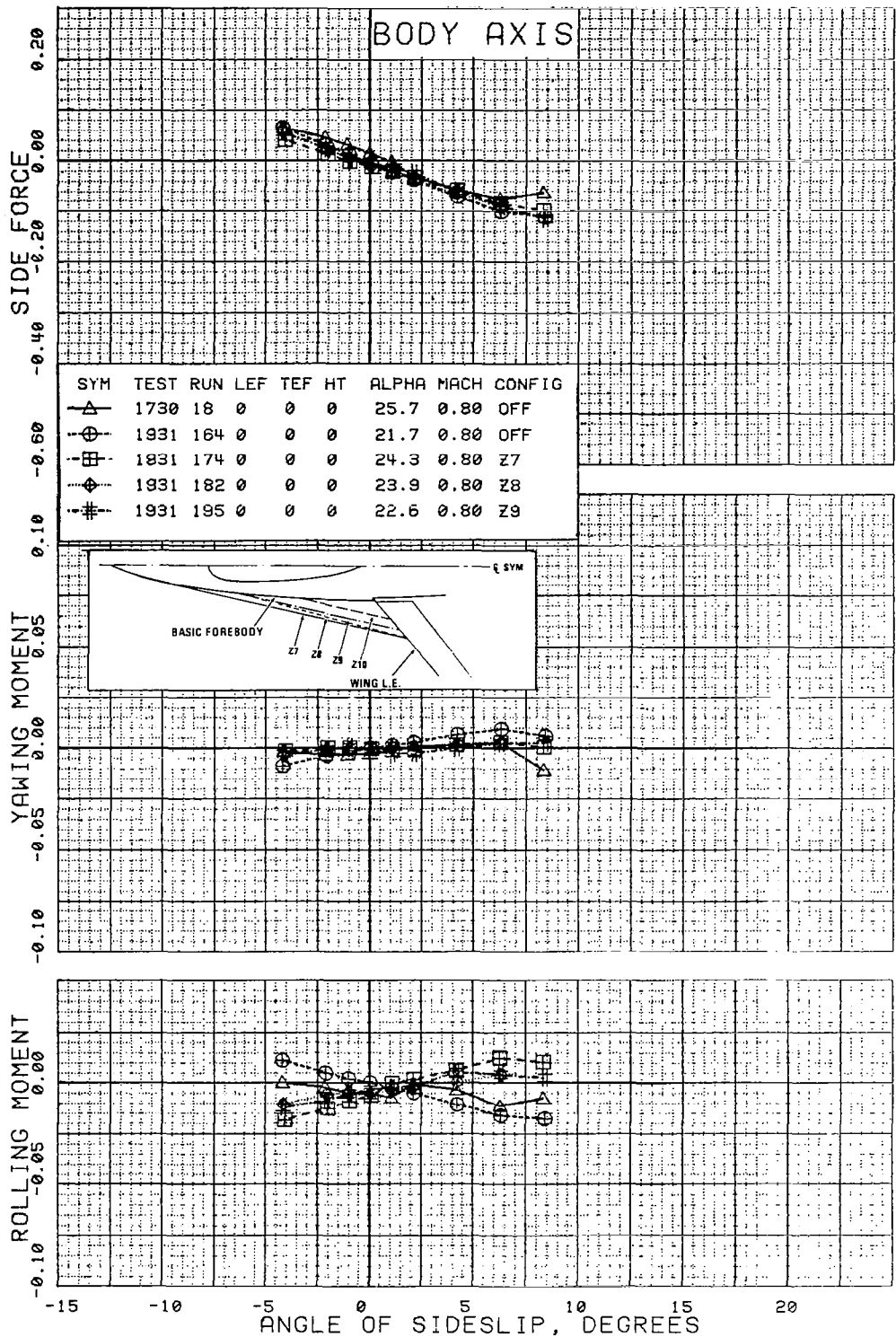
Figure 67   Sideslip Characteristics of a Family of Delta Planform
Forebody Strakes on Configuration 785, LEF = 0

132
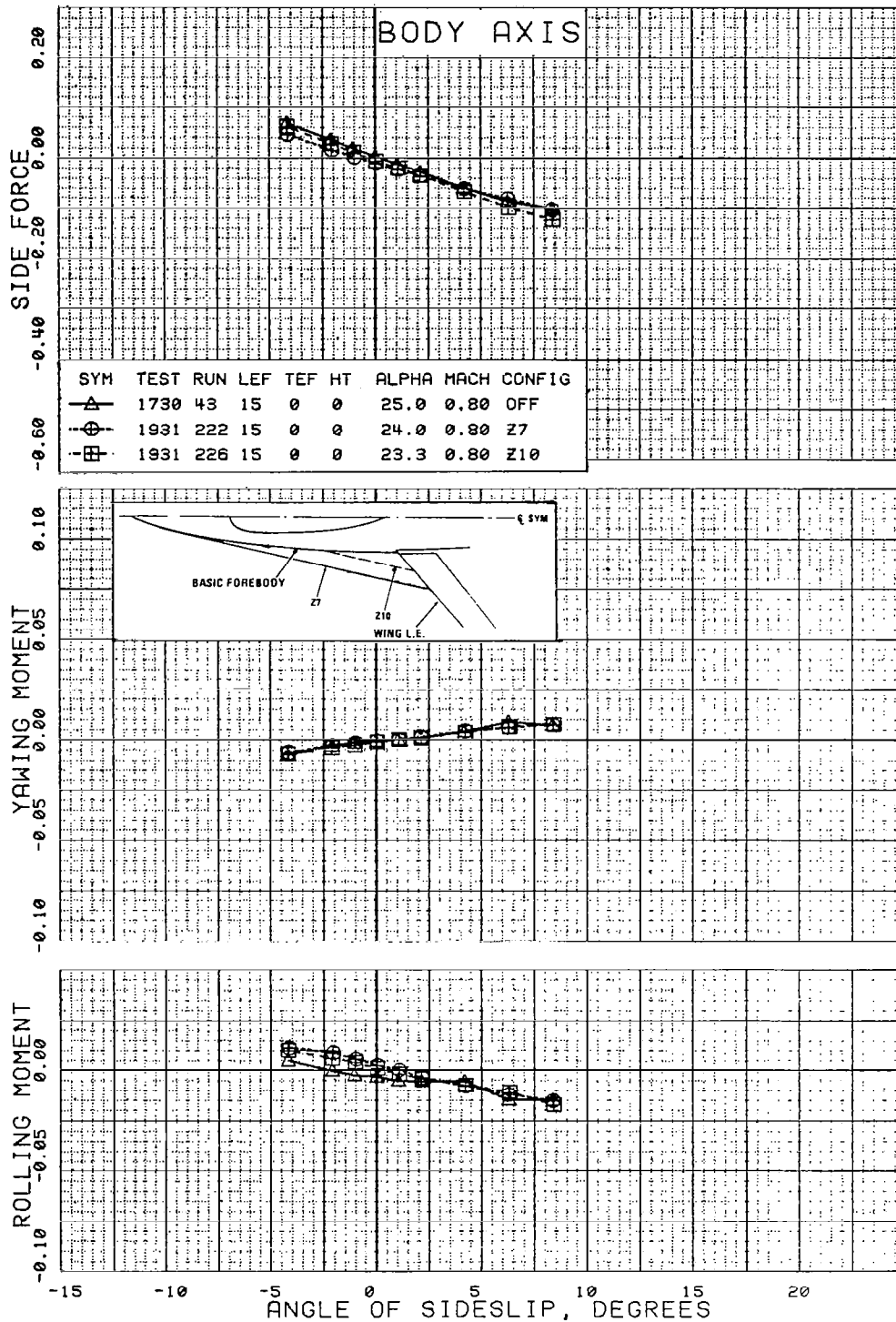
Figure 68   Sideslip Characteristics of Delta Planform Forebody
             Strakes Z7 and Z10 on Configuration 785, LEF = 15°

133
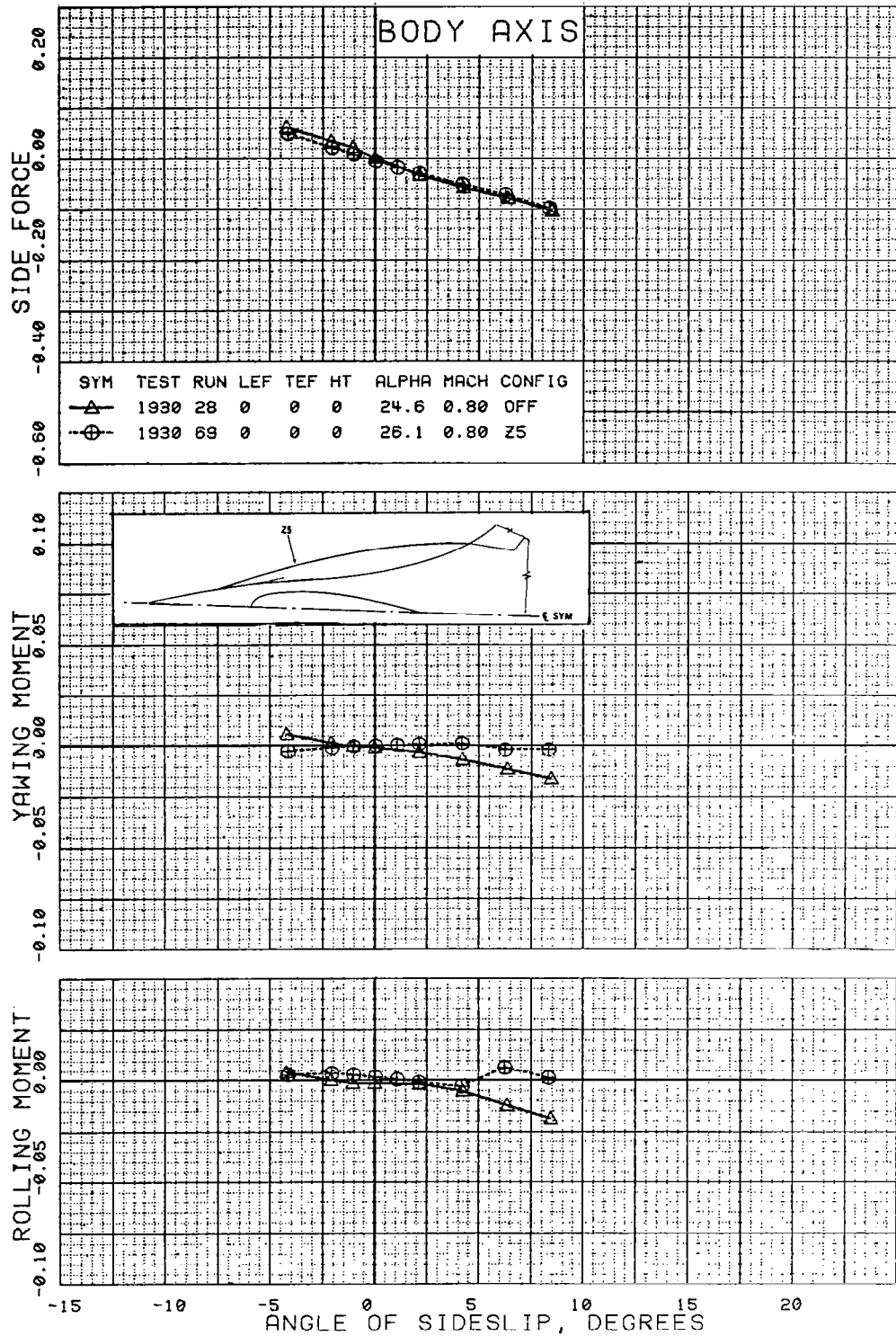
Figure 69   Sideslip Characteristics of Gothic Planform Forebody
Strake Z5 on Configuration 401F-5, LEF = 0
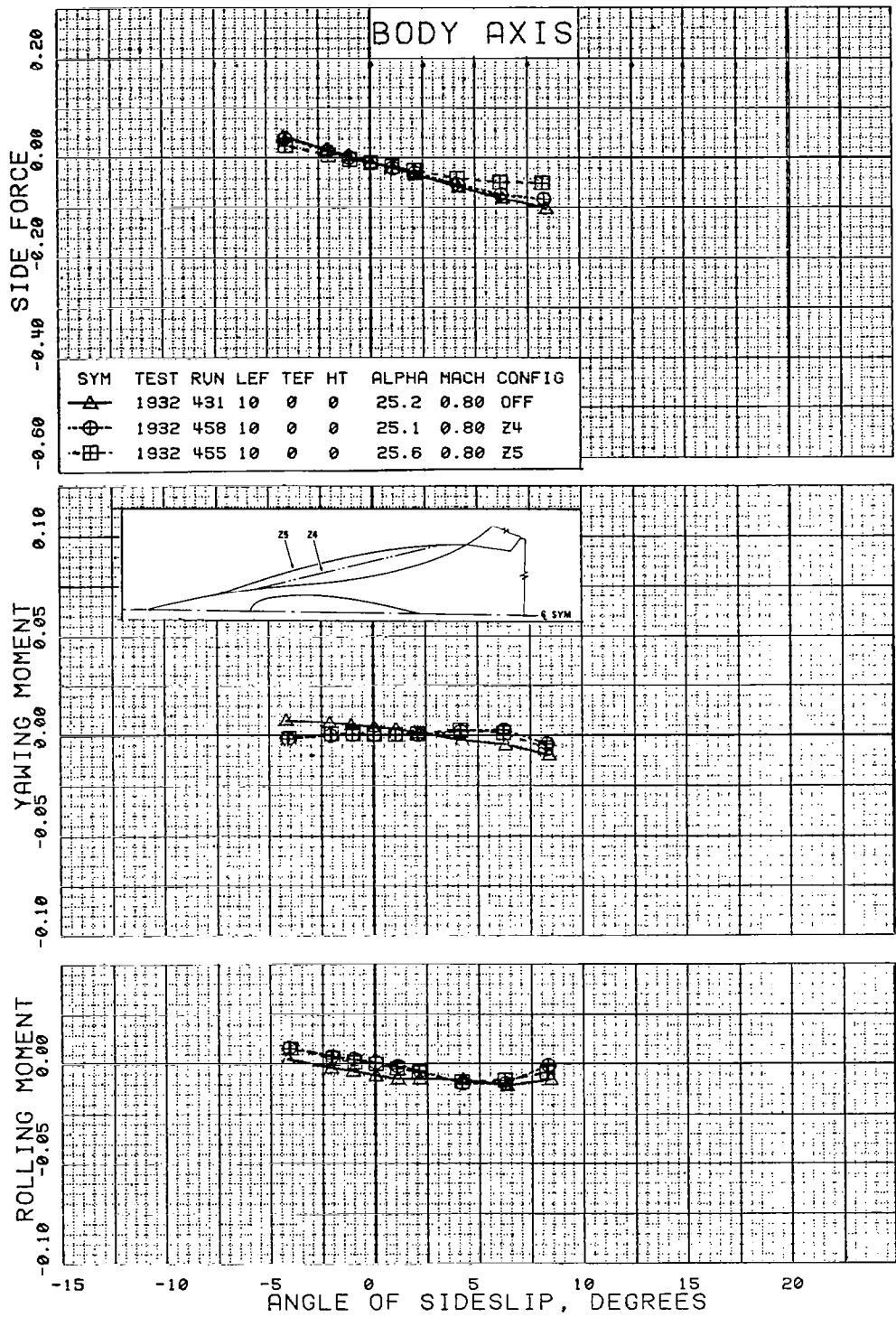
Figure 70   Sideslip Characteristics of Delta and Gothic Planform
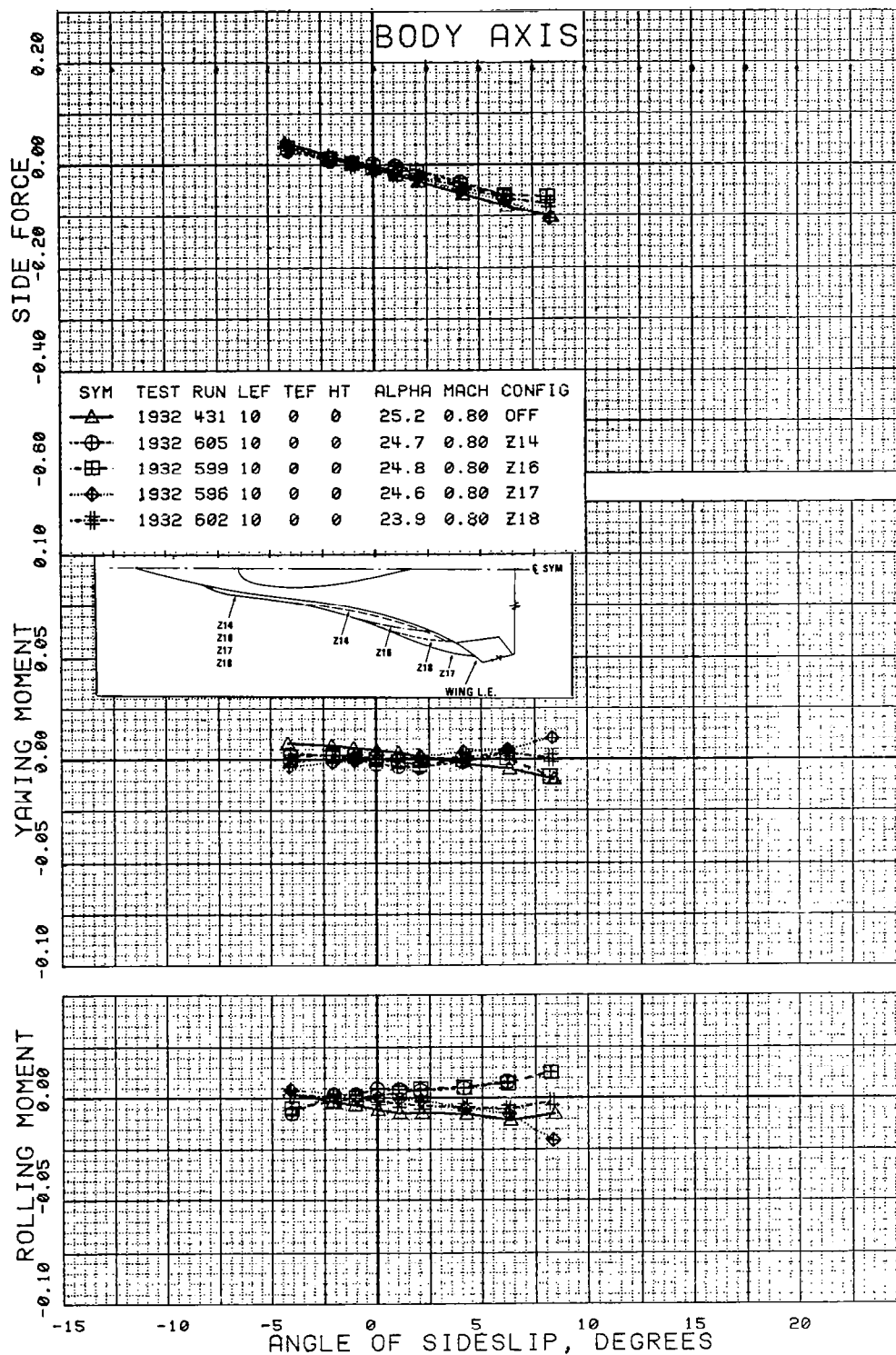Forebody Strakes Z4 and Z5 on Configuration 401F-5,
LEF = 10°

135

Figure 71   Sideslip Characteristics of a Family of Ogee Planform
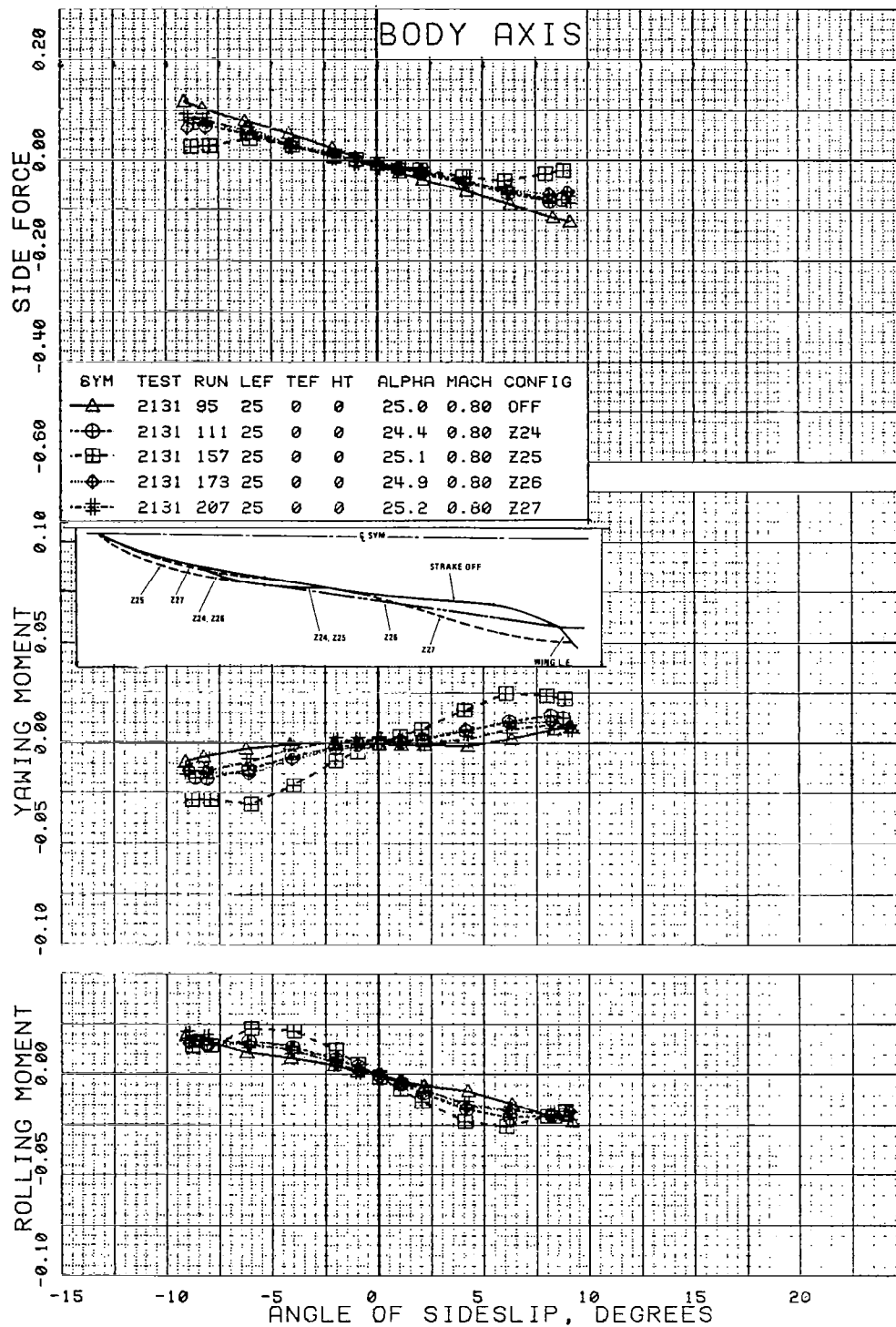Forebody Strakes on Configuration 401F-5

136

Figure 72   Sideslip Characteristics of a Family of Ogee Planform
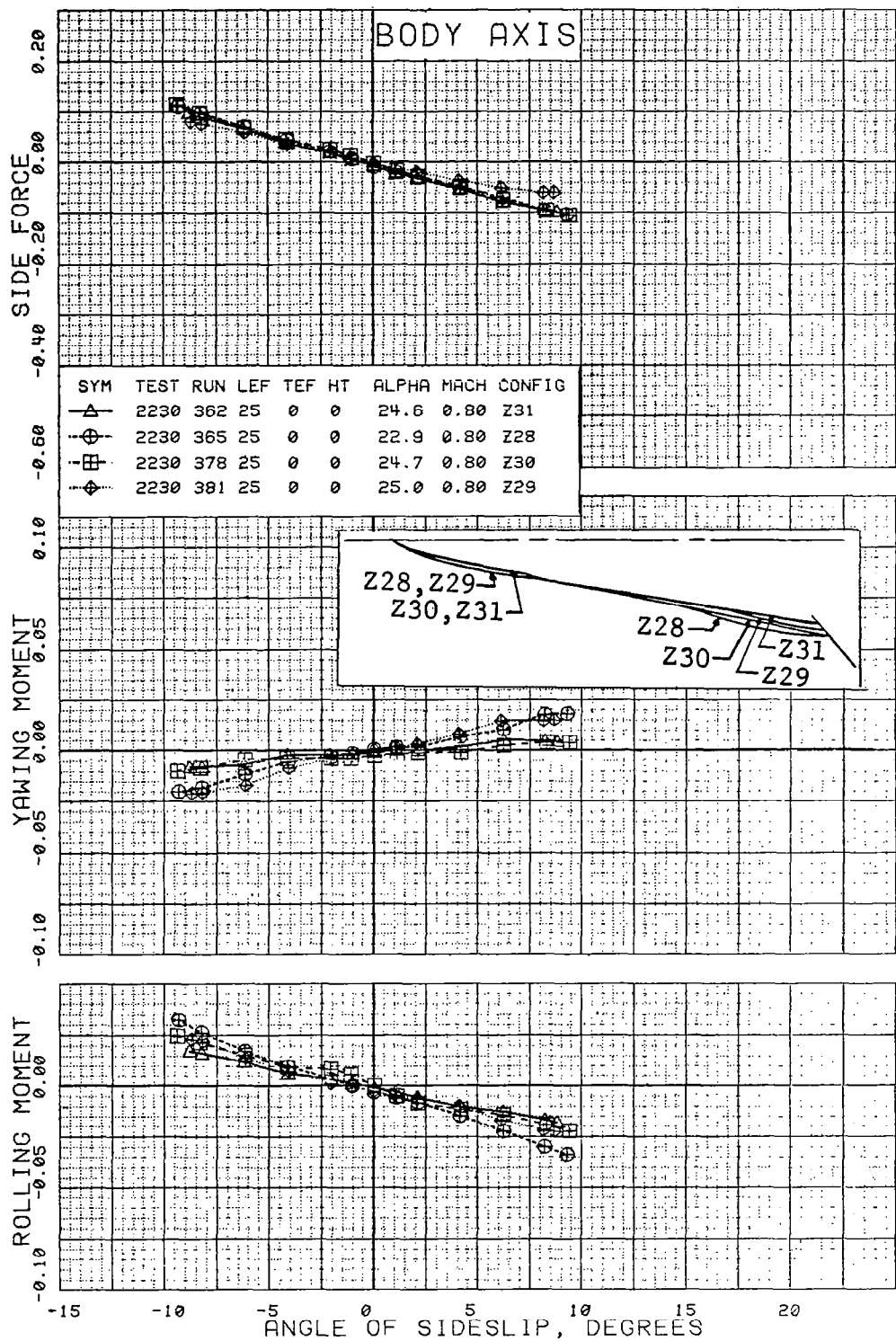Forebody Strakes on Configuration 401F-10A

137

Figure 73   Sideslip Characteristics of a Family of Ogee Planform
             Forebody Strakes on Configuration 401F-16

138

1. Report No. NASA CR-3053	2. Government Accession No.	3. Recipient's Catalog No.
4. Title and Subtitle AERODYNAMIC CHARACTERISTICS OF FOREBODY AND NOSE STRAKES BASED ON F-16 WIND TUNNEL TEST EXPERIENCE: VOLUME I Summary & Analysis		5. Report Date July 1979
		6. Performing Organization Code
7. Author(s) C.W. Smith J.N. Ralston H.W. Mann		8. Performing Organization Report No.
		10. Work Unit No.
9. Performing Organization Name and Address GENERAL DYNAMICS/Fort Worth Division P.O. Box 748 Fort Worth, Texas 76101		11. Contract or Grant No. NAS1-15006
		13 Type of Report and Period Covered Contractor Report Sept 1,77-Sept 30,78
12. Sponsoring Agency Name and Address National Aeronautics and Space Administration Washington, D.C. 20546		14. Sponsoring Agency Code

15. Supplementary Notes

Langley Technical Monitor: James M. Luckring
Final Report

16. Abstract

The YF-16 and F-16 developmental wind tunnel test program has been reviewed and all force data pertinent to the design of forebody and nose strakes extracted. Volume I contains geometrical descriptions, general comments, representative data, and the initial efforts toward the development of design guides for the application of strakes to future aircraft. Volume II, NASA CR-158922, contains a complete set of these data without analysis.

17. Key Words (Suggested by Author(s)) Forebody Strakes,Nose Strakes, Vortex Lift, High-Angle-of-Attack Aerodynamics		18. Distribution Statement Unlimited - Unclassified Subject Category 02		
19. Security Classif. (of this report) Unclassified	20. Security Classif. (of this page) Unclassified	21. No. of Pages 142	22. Price* $7.25	